High-throughput proteomic analysis of the Dengue virus replication complex.

James Bazire

MSc by Research in Cellular and Molecular Medicine

Supervisor: Professor Andrew D. Davidson

Start date: 22nd September 2019

A dissertation submitted to the University of Bristol in accordance with the requirements for the award of the degree of Cellular and Molecular Medicine MScR in the Faculty of Life Sciences

School of Cellular and Molecular Medicine

August 2023

Word count: 34595

ABSTRACT

Dengue virus (DENV) is the causative agent of Dengue, a subtropical disease affecting up to 390 million people per year. Dengue can progress to a severe form, and there are no licensed treatments. DENV-2 infected Huh-7 cells, Huh-7 cells stably maintaining a self-replicating DENV-2 sub-genomic RNA (termed the replicon) and mock infected cells were used to prepare cellular lysates from which a heavy membrane fraction (16K) containing the replication complex was isolated. Proteins in the fraction were analysed by Tandem Mass Tagging (TMT) combined with mass spectrometry. Bioinformatic analysis of the data revealed a strong enrichment of proteins associated with mitochondrial terms in DENV-2 infected cells, but more secretory pathway proteins in the replicon containing cells compared to mock infected cells. Using the data, potential host factors (HFs) were selected and a silencing RNA (siRNA) screen was attempted to validate their involvement in DENV-2 infection, but ultimately this failed as there was not time to optimise the conditions fully. Overall, the mass spectrometry and bioinformatic techniques used showed greater power than previous studies making them a good way to identify potential HFs.

ACKNOWLEDGMENTS

This piece has been a very long time coming and was a major part of who I was over the last four years. To finish this is to put a line under my life at Bristol – for the time being.

I must first thank my supervisor, Prof. Andrew Davidson, for his patience and guidance. Then I must thank and acknowledge all those who worked in E50, but especially Max Erdmann and Dr Maia Kavanagh Williamson for their constant efforts and their happiness to be sounding boards – a big thank you to Max for helping me stay sane throughout the process. Another thank you to Dr Kate Heesom and Dr Phil Lewis for the mass spectrometry data and the help with bioinformatics respectively.

Additionally, I would like to thank my friends in Bristol for never getting bored of me wittering on about my project (especially Dan, Maddie, and Charlie), and to those not living in Bristol for showing interest over the four years. Likewise, my family for always being there to listen to me moan about the difficulties of a master's thesis (imagine if this was a PhD!) – thank you for your patience.

Finally, I would like to thank my Casio wristwatch for never letting me down and always keeping me on time (in the lab at least).

AUTHOR DECLARATION

I declare that the work in this dissertation was carried out in accordance with the requirements of the University's Regulations and Code of Practice for Research Degree Programmes and that it has not been submitted for any other academic award. Except where indicated by specific reference in the text, the work is the candidate's own work. Work done in collaboration with, or with the assistance of, others, is indicated as such. Any views expressed in the dissertation are those of the author.

SIGNED: ..... DATE: .....

Table of Contents

1. Introduction and Aims

1.1. Introduction

Dengue virus (DENV) is the causative agent of Dengue, a disease spread in tropical and sub-tropical regions by a mosquito vector – typically *Aedes aegypti.* DENV is estimated to infect up to 390 million people per year, causing a range of clinical outcomes, from a mild febrile illness to a potentially fatal condition termed severe Dengue (SD) (Bhatt et al., 2013; Brady et al., 2012; Murray et al., 2013).

DENV belongs to the family *Flaviviridae*, and the genus *Flavivirus,* which also includes Zika virus (ZIKV), West Nile virus (WNV), yellow fever virus (YFV) and Japanese encephalitis virus (JEV) (Chong et al., 2019). DENV is a positive sense RNA virus and has four serotypes (DENV-1 to 4) which share between 65 and 70% homology at the nucleic acid level. DENV-2 is the most common serotype (Zeng et al., 2018) and was investigated in this study.

There are two vaccines available, but both come with limitations. Firstly, Dengvaxia, a tetravalent live-attenuated vaccine that is only licenced for use in individuals between the ages of 9 and 45 who are seropositive i.e. those who have previously contracted Dengue, as seronegative patients can develop more serious disease if infected with DENV post-vaccination (Izmirly et al., 2020). Secondly, there is a two-dose vaccine from Takeda called TAK-003. This has been approved by Indonesian and Brazilian regulators, as well as the European Commission, for individuals four years and older regardless of serostatus (Thomas, 2023).

Recently however, there have been complementary developments to prevent DENV infection. The avirulent *w*Mel strain of the *Wolbachia pipientis* bacteria was transinfected into *Aedes aegypti* mosquitos – which has been known to have the potential to inhibit DENV survival in mosquitos for some time (Walker et al., 2011) – and the mosquitos released into different locations of Yogyakarta, Indonesia. The number of residents contracting Dengue were reduced by 77% and hospitalisations decreased by 86% (Utarini et al., 2021). This method of DENV control has its positives and negatives. The *w*Mel *A. aegypti* is self-sustaining and remains in the wild, providing protection to humans living in the area. However, although the risk of *w*Mel resistant DENV developing is small, it is still possible – in which case additional inhibitory *Wolbachia* strains may have to be developed and released (Utarini et al., 2021; H. Zhang & Lui, 2020).

1.2. DENV Genome, Viral Particle, and Viral Proteins

The DENV genome is a positive sense, single strand of RNA ~ 11 kilobase (kb) in length. The genome is translated as a polyprotein which is inserted into the endoplasmic reticulum (ER) membrane and cleaved co- and post-translationally to produce three structural and seven non-structural (NS) proteins (Zeng et al., 2018). Figure 1.1 shows the membrane topology and the cleavage sites of the DENV polyprotein.

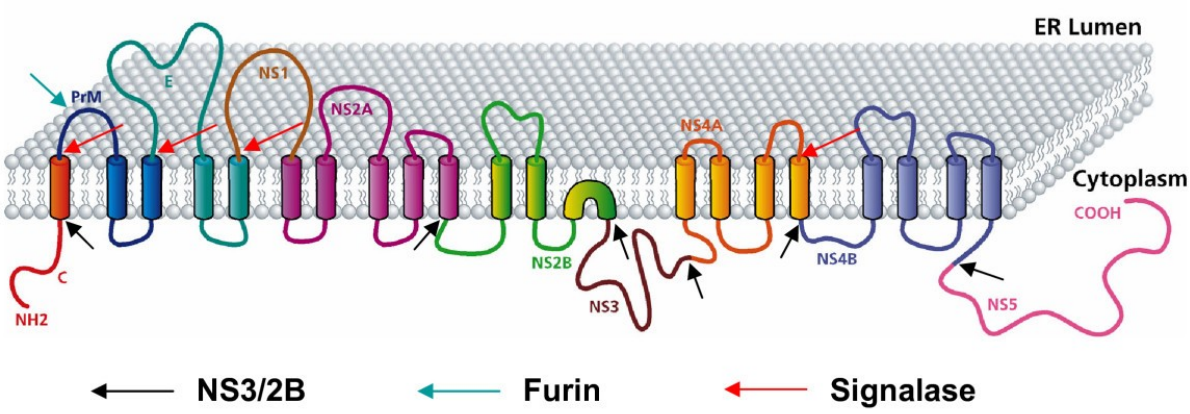

Figure 1. 1. Membrane topology of the DENV polyprotein after insertion into the ER membrane. Cleavage sites shown with coloured arrows (Black - DENV NS2B/3 protease, blue – host furin, red – host signalase). Taken from Umareddy et al., (2007).

The NS proteins of DENV have varied roles and range from multifunctional enzymes to small protein co-factors (Kaufmann & Rossmann, 2011). These are discussed in the context of the viral replication cycle in section 1.3. The structural proteins in the mature virion are the capsid (C), envelope (E), and the membrane (M) proteins. The viral genome is packaged by multiple copies of the C protein – this is termed the nucleocapsid – and is surrounded by a host-derived lipid bilayer. The DENV M protein is expressed as a precursor – termed prM – which forms heterodimers with E as the immature virion passes through the secretory pathway – this is discussed in more detail in section 1.3 (Carbaugh & Lazear, 2020; Cruz-Oliveira et al., 2015; Reyes-del Valle et al., 2014; Wong et al., 2012).

In the mature virion, this bilayer is studded with M proteins, along with 180 copies of E – arranged in homodimers (Carbaugh & Lazear, 2020; Norazharuddin & Lai, 2018; Wong et al., 2012). The mature virus is icosahedral in shape and approximately 50 nm in diameter (Kaufmann & Rossmann, 2011).

Brief information on the DENV NS proteins is described below in Table 1.1.

NON-STRUCTURAL PROTEINS

NS1	A 48 kilodalton (kDa) glycoprotein, the only DENV secreted NS protein. Forms an intracellular dimer which is essential for replication. Found in the blood in a hexameric form. Causes vascular leakage. Serum concentration is positively correlated with disease severity in humans (Chen, Lai and Yeh, 2018).
NS2A	Modulates host immune responses, and forms part of the replication complex. NS2A also has a role in processing the C terminus of NS1 (Gopala Reddy, Chin and Shivananju, 2018).
NS2B	Forms a heterodimer with the protease domain of NS3 to create the fully functional protease complex, NS2B/3 (Gopala Reddy, Chin and Shivananju, 2018).
NS3	Multifunctional protein; has protease, helicase, adenosine triphosphatase (ATPase), and ribonucleic triphosphatase (RTPase) activities (Swarbrick et al., 2017).
NS4A	Small hydrophobic membrane protein. Can bind to highly curved membranes, NS4A also reshapes the ER (Gopala Reddy, Chin and Shivananju, 2018).
NS4B	After cleavage from NS4A, NS4B relocates to ER lumen and localises with NS3, E and double stranded RNA (dsRNA) in the replication complex (Gopala Reddy, Chin and Shivananju, 2018).
2K	23 residue region of NS4, found between NS4A and NS4B, cleaved by NS2B/3 and signalase. Works as a signal sequence to relocate NS4B to the ER lumen (Gopala Reddy, Chin and Shivananju, 2018).
NS5	Largest DENV protein; contains a methyltransferase domain (which caps viral RNA to mediate translation and prevent degradation) and an RNA dependant RNA polymerase (RdRp) domain. Forms a complex with NS3 in the ER (Bhatnagar et al., 2021).

Table 1. 1. List and functions of DENV NS proteins. Information taken from various sources and shown in text.

1.3. Replication Cycle

The replication cycle of DENV in an infected human can be broken down into four major steps: attachment and internalization, genome expression and replication, assembly, and release, which are shown below in Figure 1.2.

Firstly, DENV virions bind to the target cell through the E protein interacting with an extracellular receptor and are internalized *via* receptor-mediated clathrin-dependent endocytosis (Figure 1.2.i.) (Wang & Zhang, 2017). In natural infection this is predominantly immune cells located close to the location of the mosquito bite, such as dendritic cells, monocytes, and macrophages, but DENV can infect a range of cells including hepatic cells (Fischl & Bartenschlager, 2011; Reyes-del Valle et al., 2014). The E protein can bind a wide range of molecules and there is no one specific receptor – reflected in the gwide range of cells permissive to DENV infection (Norazharuddin & Lai, 2018).

DENV can also enter Fc receptor expressing cells, such as monocytes, if opsonised in an immune complex during a secondary infection with a different DENV serotype. This is termed antibody dependent enhancement (ADE) and can lead to a more serious infection (Kaufmann & Rossmann, 2011). ADE normally occurs in individuals who have been previously infected with another serotype of DENV such that their antibodies are at a sub-neutralising level in their blood (Katzelnick et al., 2017).

Once inside the cell, the mildly acidic endosome induces an irreversible conformational change of the DENV E dimers into E trimers, causing the virion membrane to fuse with the endosomal membrane (Klein, Choi, and Harrison, 2013). The single stranded viral RNA is released and transported to the rough ER (rER) (Norazharuddin & Lai, 2018), shown in Figure 1.2.ii. The rER is the site of virus induced membrane alteration, where the replication complex (RC) is created. The RC has multiple roles; it allows fixed theefficient separation of translation and replication of viral RNA; high local concentrations of metabolites and replication complexes which facilitates an efficient replication cycle; and also protects the replicating virus from intracellular immune responses – discussed in more detail in section 1.5 (Lescar et al., 2018; Paul & Bartenschlager, 2015; Van Den Elsen et al., 2021).

At the rER, the positive sense RNA genome is translated directly into the viral polyprotein (Figure 1.2.iii.), which is cleaved co- and post-translationally by host proteases and the viral protease NS2B/3. NS4A and NS4B act as scaffolds for RC reformation (Norazharuddin & Lai, 2018), which is shown in greater detail in Figure 1.2.iv. The NS proteins of DENV induce membrane curvature of the ER and generate the RC.

Once the RC is formed, translation switches off. The RNA template is transcribed from positive to negative sense by the NS5 RdRp, which in turn functions as a template for *de novo* genomic RNA synthesis (Norazharuddin & Lai, 2018). Once copies of the genome are made and the structural proteins are expressed, they bud into the lumen of the ER, and are packaged into non-infectious, immature virions, aided by NS1 and NS2A (Byk & Gamarnik, 2016; Ma et al., 2004; Nasar et al., 2020).

The immature virions travel through the secretory pathway (Figure 1.2.v.). In the trans-Golgi, prM is cleaved by furin protease to leave M, this generates the mature DENV particle, which is subsequently released by exocytosis. Once released, the precursor portion of prM dissociates as a result of the pH change – this renders the DENV particle infectious (Byk & Gamarnik, 2016; Markoff et al., 1997; Samsa et al., 2009; Screaton et al., 2015).

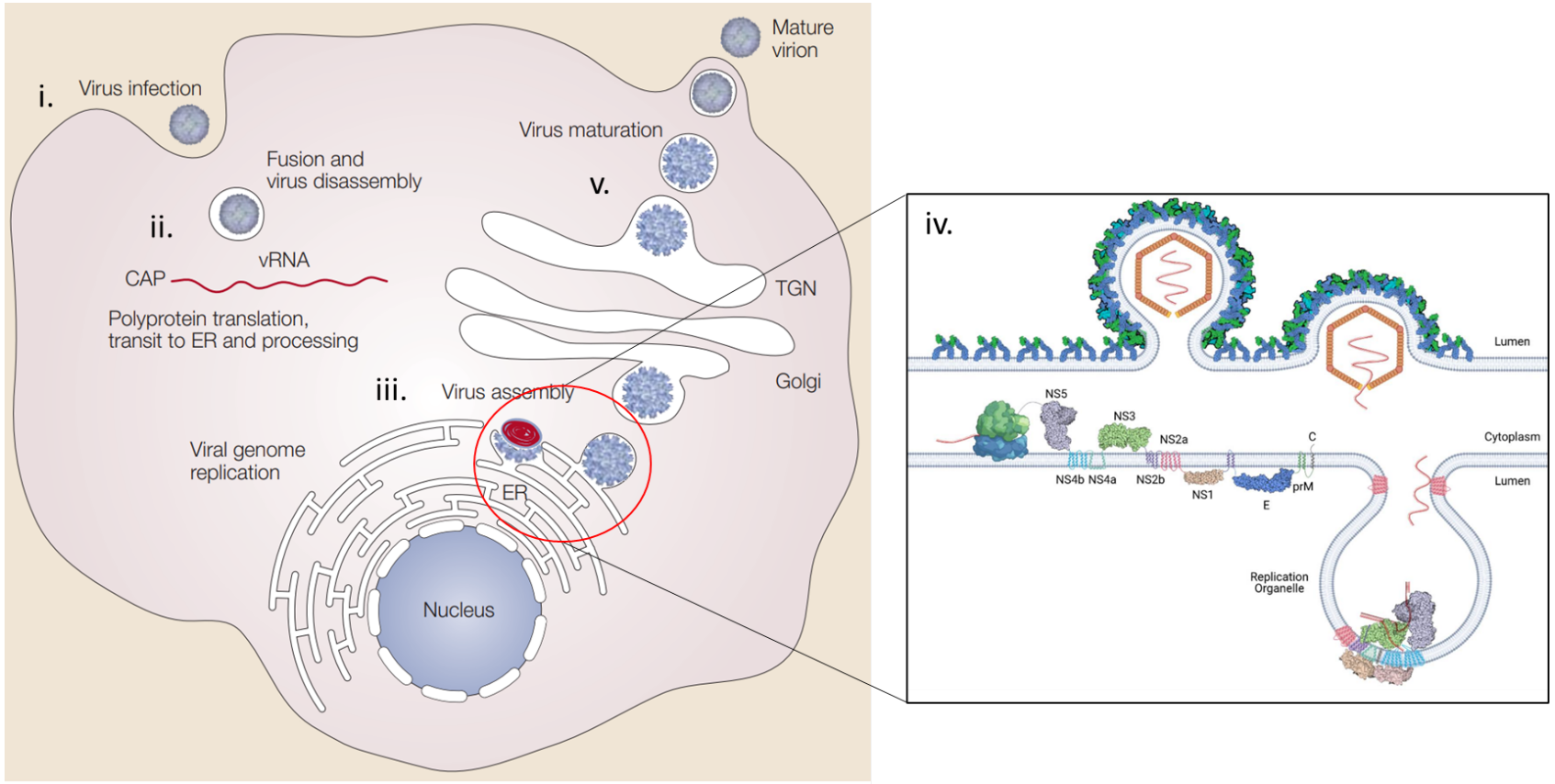

*Figure 1. 2. Diagram of the DENV replication cycle. **(i)** DENV virion binds to the host cell via a range of receptors, and the virion is internalised via clathrin-mediated endocytosis. **(ii)** Once inside the cell, the low pH of the endosome causes a conformational change of the DENV E dimers to trimers. The E trimer is now primed and fuses to the membrane of the endosome and releases the RNA genome. The genome is transported to the ER where it is translated into a single polyprotein that undergoes co- and post-translational cleavage. The DENV NS proteins remodel the ER and create RCs, where DENV RNA can be produced. **(iii)** DENV virions are assembled using lipids and membranes gathered in the replication complex. The RNA genome is packed in the immature virion with C proteins, the outer layer of membrane studded with heterodimers of E and prM. **(iv)** shows the enlarged replication organelle, which is highlighted by the red circle, containing the RC and the constituent NS proteins. Shown additionally, is the viral particle assembly and budding from the ER. **(v)** The immature virions are released from the ER and travel through the secretory pathway. Travelling through the Golgi apparatus, the host protease furin cleaves the pr- portion from the M protein (where it stays associated due to the low pH). The DENV virions are released and the pr- dissociates, rendering the virion mature and ready to infect another permissive cell. Figure taken and adapted from Mukhopadhyay et al. (2005); Pan et al. (2019); Van Den Elsen et al. (2021); Q. Zhang et al. (2012).*

1.4 The Replicon

A DENV replicon is a non-infectious, self-replicating sub-genomic RNA encoding the DENV NS proteins. To allow visualisation and potentially selection of cells maintaining an introduced replicon, the structural genes are typically replaced by sequences encoding fluorescent proteins and drug selectable markers. In this study a human Huh-7 liver cell line, stably maintaining a DENV-2 replicon encoding a fusion protein comprised of eGFP and puromycin N-acetyltransferase (PAC; conferring resistance to puromycin) (Massé et al., 2010) was used. The replicon is stable through passage and selection (as shown in Chapter 4.1.3). A schematic of the replicon genome compared to the DENV genome is shown below in Figure 1.3.

Even though the replicon does not encode the structural proteins, and as such cannot complete the full DENV life cycle, it is a useful tool for research investigations. Not only is it categorised at biosafety level 2 (BSL2) – one level lower than for DENV – and so can be handled more easily; but the replicon is a useful surrogate for investigating DENV replication. DENV replicons have been shown to be inhibited by known anti-flavivirus agents such 2'-C-methyladenosine and ribavirin and siRNA against NS3 (Ng et al., 2007a) thus providing a suitable platform for knockdown or screening experiments. A DENV-2 replicon maintained in baby hamster kidney (BHK-21) cells has also been shown to produce similar ultrastructural changes to the ER (like the RC) as caused during infection with the parental DENV-2. As such it can be expected that the replicon used in the present study would also cause these changes in Huh-7 cells.

Nevertheless, proteomic analysis using mass spectrometry to identify host factors has not been performed using cells maintaining a DENV replicon and as such the full effectiveness of the replicon remains to be uncovered.

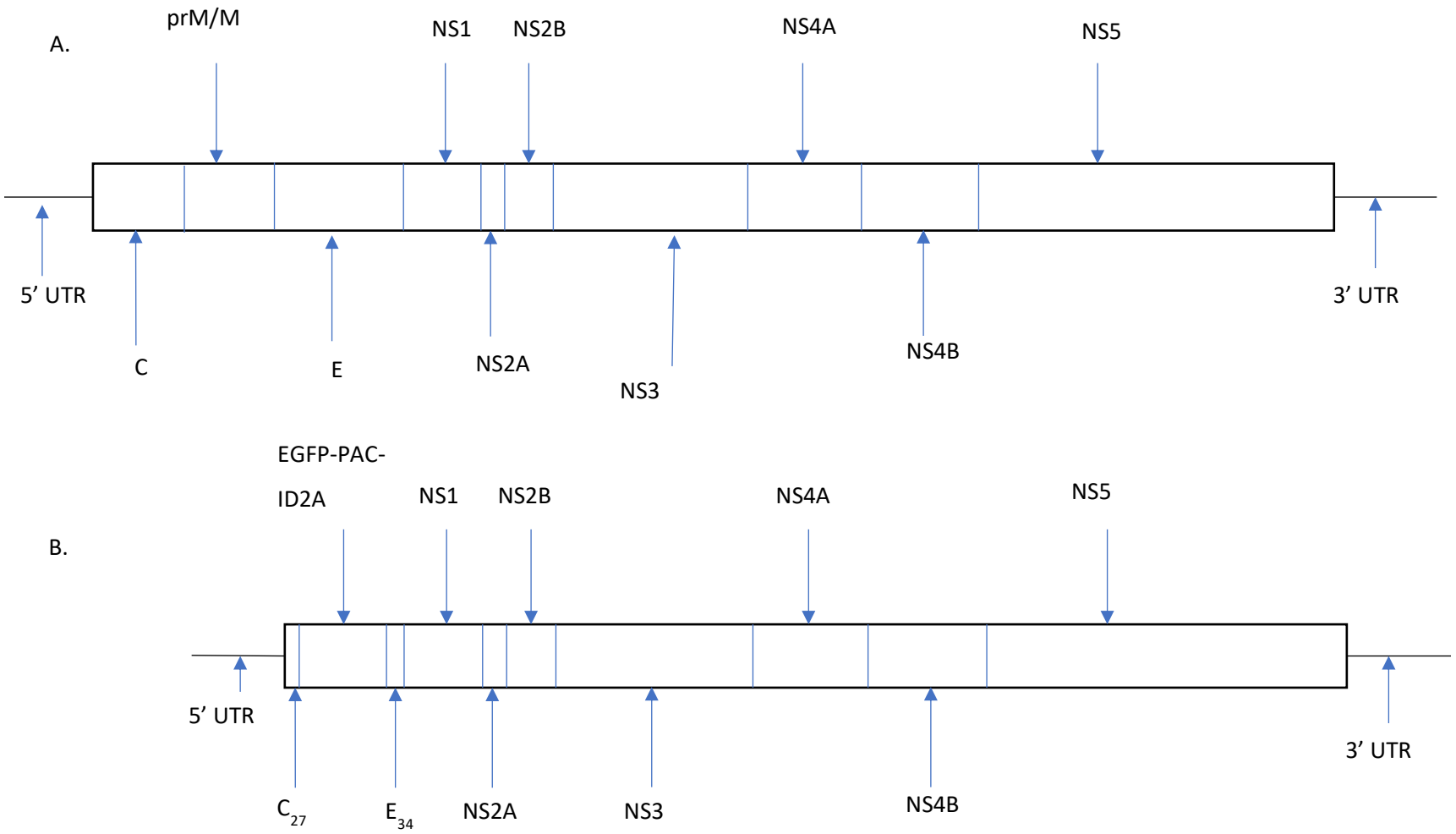

Figure 1. 3. A. Schematic of the DENV-2 genome, adapted from Harapan et al. (2020). B. Replicon schematic showing that all NS genes are present, but the structural genes have been modified. Sequence encoding the first 27 amino acids of the C protein and last 34 amino acids of the E protein are retained, but most of the C and E genes and the prM/M gene has been replaced with an eGFP-PAC gene. Adapted from Massé et al. (2010).

1.5 Host Factors in Dengue Infection

The DENV genome only codes ten proteins, three of which provide the structure of the virion (Harapan et al., 2020) and so for DENV to fully execute its life cycle it must rely on host proteins, complexes, and molecules – these are termed host sensitivity factors (HSFs) (Krishnan et al., 2008). In contrast, host resistance factors (HRFs) are host proteins, molecules, or complexes that inhibit DENV infection in some way (Krishnan et al., 2008). Together, they are termed host factors (HFs).

Host factors are important for all stages of a virus' life cycle, for example entry of SARS-CoV-2 is governed by the ACE2 receptor (Baggen et al., 2021) and influenza virus is detected by Toll-like receptors (TLR) 3 and 7, which initiate an antiviral response (Husain, 2020).

DENV is no different. HSFs of DENV infection could be thought to start with cell surface receptors that render the cell permissive to DENV infection; factors that facilitate the binding and entry of a viral particle into the cell. EGFR Protein tyrosine kinase Substrate 15 (Esp15), a member of the accessory protein 2 (AP2) complex, is relied on in clathrin-mediated endocytosis (Van Bergen En Henegouwen, 2009), and infection of cells with DENV virus (Carnec et al., 2016). RNA mediated knockdown and expression of Esp15 dominant negative isoforms reduce DENV-2 infection in HeLa cells (Krishnan et al., 2007).

Following entry, the virion is uncoated in the late endosomal system and the infection is established. During this process there are many proteins and complexes that are hijacked, annexed, and inhibited that promote or facilitate the infection, some of which are discussed below. Ras analog in brain 5 (Rab5) guanidine triphosphatase (GTPase) plays a role in early endosomal transport from the plasma membrane (Haas et al., 2005). When a dominant-negative version of Rab5 was overexpressed, it inhibited the infection of HeLa cells with DENV-2 (Krishnan et al., 2007) showing the importance of the endosomal transport system in DENV-2 infection.

Subsequent manipulation of the micro-environment of an infected cell enables replication of the viral genome and expression of the viral proteins. Production of the nascent viral particle follows. After the DENV proteins are expressed, the exploitation of different pathways, such as lipid metabolism and glycolysis, can begin.

DENV infected Huh-7 cells switch to primarily use fatty acids as an energy source (via β-oxidation) and use the glycolytic pathway as a source of oxaloacetate for the tricarboxylic acid (TCA) cycle. If β-oxidation is inhibited, DENV replication is reduced (Fernandes-Siqueira et al., 2018). To liberate the fatty acids needed, lipophagy is stimulated – which if inhibited, reduces DENV replication (Heaton et al., 2010a; Heaton & Randall, 2010). These include two actin polymerisation genes, two fatty acid

synthesis genes, three ER stress and autophagy genes, a trans-Golgi to late endosome gene and a scaffold protein (Heaton et al., 2010a). Pharmacological inhibition of 3-hydroxy-3-methylglutaryl-CoA reductase and siRNA knockdown of mevalonate diphosphodecarboxylase – both key enzymes in cholesterol synthesis – inhibits replication of both a DENV-2 replicon (introduced in section 1.8 below) and DENV-2 in infected A549 cells (Rothwell et al., 2009).

This is not an exhaustive list of HSFs utilised during DENV infection, but a snapshot of the broad range of proteins required by DENV during infection of a variety of cell types.

HRFs are mainly proteins involved in innate immune response and type I interferon (IFN) production pathways. These include tumour necrosis factor- α (TNF-α) and interferons (IFNs) secreted by dendritic cells to restrict replication immediately after infection, and intracellular recognition proteins such as TLR3, interferon regulatory factor (IRF) -3 and IRF-7 which sense dsRNA and activate the JAK/STAT pathway (Nanaware et al., 2021). However, these antiviral responses can be subverted by the NS proteins of DENV. NS2B targets cyclic GMP-AMP synthase (cGAS) for lysosomal degradation, facilitating DENV replication (Aguirre et al., 2017). DENV also inhibits the activation of TANK-binding kinase 1 (TBK1) and Inhibitor of nuclear factor kappa-B kinase subunit epsilon (IKBKE) which in turn inhibits the activation of the IRF3 transcription factor (Tremblay et al., 2019).

Tetherin, or bone marrow stromal cell antigen 2 (BST2), is known to inhibit the replication of a wide range of virus types by preventing the release of the virus – by restricting the release from the cell surface membrane or arresting its travel through the trans-Golgi network (TGN) (Fishburn et al., 2022). Expression of tetherin (BST2) in Huh-7 cells reduces the yield of DENV viruses (Ben Pan et al., 2012), but possibly this protein is actively targeted by DENV to allow greater release because during JEV infection *in vitro*, E interacts with BST2 and targets it for lysosomal degradation – thereby negating its antiviral effect (Li et al., 2017).

1.6 Changes to Cellular Environment

Like all viruses, DENV exploits multiple pathways and alters the morphology of the cell. Metabolic and innate immune response pathways are perturbed by DENV infection, and so too are the morphologies of mitochondria and the ER (Chatel-Chaix et al., 2016; Chatel-Chaix & Bartenschlager, 2014; Du Toit, 2016; El-Bacha et al., 2007; Fernandes-Siqueira et al., 2018).

Unsurprisingly, DENV infection alters the metabolic balance of cells – a clinical study (Cui et al., 2013) has shown that lipid metabolism is affected in patients infected with DENV, they were found to have elevated levels of acyl-carnitines and free fatty acids in their blood. Another clinical study showed

similar results, but also showed a depletion in the TCA cycle metabolites citrate and succinic acid (Shahfiza et al., 2017).

The ATP:ADP ratio of HepG2 cells is decreased during infection compared to uninfected controls, showing DENV infected cells are more active than normal (El-Bacha et al., 2007). Glycolysis was shown to be altered in that early pathway metabolites are increased in abundance at 48 hours post infection (hpi) and late metabolites are decreased in abundance 48 hpi, including phosphoenolpyruvate, inhibition of this central carbon metabolism reduced DENV replication in human foreskin fibroblast (HFF) cells (Fontaine et al., 2015). Lipid droplet (LD) autophagy and fatty acid β-oxidation are both increased and necessary for DENV replication (Heaton & Randall, 2010), and *de novo* fatty acid synthesis is also increased by DENV NS3 (Heaton et al., 2010a). Work by Fernandes-Siqueira et al. in 2018 demonstrated that fatty acid β-oxidation is the primary source of energy in DENV infected Huh-7 cells and the authors hypothesised that the glycolytic pathway provides not the metabolites of the TCA cycle, but the pentose-phosphate pathway (Fernandes-Siqueira et al., 2018).

Pharmacological inhibition of β-oxidation using etomoxir *in vitro* decreased DENV E production and significantly reduced the amount of infectious virus produced in liver cells (Heaton & Randall, 2010). Furthermore, activation of AMP-activated protein kinase (AMPK) inhibits flavivirus replication and inhibition of acetyl-coenzyme A carboxylase through pharmacological modulation also reduces viral infection in flavivirus mouse models, providing evidence that β-oxidation is necessary for DENV survival (Jiménez de Oya et al., 2018, Jiménez de Oya et al., 2019).

DENV activates autophagy as a pro-viral strategy (Lee et al., 2008). If autophagy is blocked, DENV replication is reduced in Huh-7 cells; if stimulated by rapamycin, DENV replication is increased – also demonstrated in Huh-7 cells (Lee et al., 2008).

Furthermore, the morphology of mitochondria changes along with the metabolic equilibrium. Mitochondria lengthen, and associate with the ER via an interaction between glucose regulated protein 78 (GRP78), E, and the outer mitochondrial membrane (OMM) voltage-dependent anion channel (VDAC) channels (Jitobaom et al., 2016). Mitochondrial associated membranes (MAMs) are also disrupted which interferes with their role in the innate immune system (Chatel-Chaix & Bartenschlager, 2014).

DENV infection also changes the morphology of the ER (Chatel-Chaix & Bartenschlager, 2014; Paul & Bartenschlager, 2015). The ER is modified to support a pro-viral micro-environment, resulting in morphological changes including the formation of; vesicle packets (VP), invaginations of the ER where the DENV genome is replicated, virus bags – dilated ER-derived membranes where assembled

viruses align in paracrystalline arrays – and convoluted membranes (CM), which are poorly understood but are possible sources of lipids for viral assembly (Anton et al., 2021; Chatel-Chaix & Bartenschlager, 2014; Paul & Bartenschlager, 2015; Płaszczyca et al., 2019). As the RNA genome is translated into the polyprotein, it is inserted into the membrane of the ER and is cleaved into its component proteins by NS3 and host proteases (Van Den Elsen et al., 2021). The NS proteins, along with host proteins such as reticulon 3.1A, are recruited and create the membrane curvature required for RC formation (Aktepe et al., 2017; Diaz & Ahlquist, 2012; Van Den Elsen et al., 2021). The viral components are protected from the cellular environment, and the DENV virions can be produced, unperturbed by immune responses.

1.7 Cellular Fractionation

DENV-2 infection, as described in sections 1.5 and 1.6, relies on host proteins and processes and causes physical alterations in the cellular environment, of which the most prominent physical change induced is the formation of the RC. To understand more about the host proteome response to DENV-2 and replicon replication in Huh-7 cells, the RC (which is found adjacent to the ER) was extracted by sequentially centrifuging cell lysates, finishing by pelleting at $1.6x10^4$ x g (Yousef, 2016). This is called the 16K fraction, and the method by which it is obtained is found in section 2.5.1.

The 16K fraction will include perinuclear membranes, the ER, and mitochondria, as well as the RC and DENV induced membrane alterations. The 16K fraction was analysed by using tandem mass-tagging (TMT) spectroscopy and downstream analysis programs (sections 2.52, 2.5.3, 2.5.4, and 2.5.5). The results of which are presented in chapter 3. The whole cell lysates (WCL) of DENV-2 infected and replicon containing Huh-7 cells were also analysed, but the 16K fraction was the main focus of this study. Fractionation of samples such as this can reduce complexity and can allow for a comparison between two regions of a cell to demonstrate differences in subcellular localisation of a protein, for example.

1.8 Solute Carrier Family 25

Multiple solute carrier family 25 (SLC25A) members were identified as potential DENV host factors. SLC25A family members are inner mitochondrial membrane transporters responsible for the shuttling of molecules required for metabolic processes in the mitochondria (Gutiérrez-Aguilar & Baines, 2013).

This 53-member family displays high levels of structural conservation; they all possess a tripartite structure consisting of six transmembrane α-helices (in anti-parallel pairs) with a signature motif made of three repeats found on the odd number helices (Palmieri, 2013). SLC25A family members

can transport a very wide range of distinct molecules including, but not limited to ADP and ATP, carnitine and acyl-carnitine, carboxylates, and amino acids with high levels of specificity which arise from changes to specific residues in the substrate-binding site (Gutiérrez-Aguilar & Baines, 2013; Palmieri, 2013).

Some key SLC25A members and their potential roles in DENV infection are described here. SLC25A1, citrate carrier (CiC), is crucial in the fatty acid synthesis pathway as it transports citrate from the mitochondrial matrix which can then be cleaved to release acetyl-CoA – possibly revealing an importance for DENV infection (Gutiérrez-Aguilar & Baines, 2013). SLC25A3 is a phosphate carrier (known as PiC) and transports inorganic phosphate ions (P_i) and hydrogen ions (H^+) into the matrix for use in ATP generation. ATP generation is enhanced and so the activity of this transporter is required in DENV infection (Gutiérrez-Aguilar & Baines, 2013; Palmieri, 2013). SLC25A4, 5, and 6 are adenine nucleotide transporters (ANT1/2/3) and antiport ADP and ATP in and out of the matrix. Like SLC25A3, this would be necessary to provide the ATP generation blocks in a more metabolically active cell (Gutiérrez-Aguilar & Baines, 2013; Palmieri et al., 2020). Finally, SLC25A20 is a carnitine/acylcarnitine carrier, and provides the route for cytosolic fatty acids to enter the matrix and enter the β-oxidation pathway – which as previously described is crucial for DENV infection hs(Fernandes-Siqueira et al., 2018; Gutiérrez-Aguilar & Baines, 2013).

1.9 The TMED Protein Family

Transmembrane EMP-domain containing proteins (TMED), are small (~24kDa) type 1 transmembrane proteins found predominantly in the secretory pathway (Pastor-Cantizano et al., 2016; Strating et al., 2009; Strating & Martens, 2009). The main roles for the TMED family in the secretory pathway are intracellular transport, coat of protein (COP) I and possibly COPII vesicle biogenesis (Pastor-Cantizano et al., 2016; Strating & Martens, 2009).

TMED2 has documented involvement in DENV infection. Transcriptional analysis of Huh-7 cells infected with DENV showed that depletion or overexpression of TMED2 reduced or increased DENV replication respectively without affecting cell viability (Zanini et al., 2018). TMED2 also strengthens anti-DNA virus signalling through the dimerization of human mediator of IRF3 activation (MITA) and aids its trafficking through the secretory pathway (Sun et al., 2018).

TMED10 has been most widely studied out of the selected TMEDs in this study. A study analysing the changes in miRNAs and mRNAs in patients with osteoarthritis documented an increase in the expression of TMED10 compared to controls (yan Huang et al., 2021). In a paper more relevant to this present study cytomegalovirus protein gp40 has been shown to interact with TMED10 to prevent major histocompatibility complex 1 (MHC1) molecules from being expressed on the cell

surface membrane of infected cells, thus preventing an efficient host immune response (Ramnarayan et al., 2018). Whilst there is no evidence of this occurring in DENV infected cells, it is still interesting to consider the varied roles the TMED family possess.

Donovan-Banfield (2019) showed an increase in abundance of TMEDs 2, 5, 7, 9 and 10 in the 16K fraction of DENV infected Huh-7 cells via Western Blot. siRNA knockdown performed on these TMEDs resulted in a decrease in the amount of NS5 detected via western blot, however these results were not validated (Donovan-Banfield, 2019). This study will aim to more fully understand the role of TMED proteins 2, 5, 7, 9 and 10 in DENV infection.

1.10 Aims and Objectives

1. To perform proteomic analysis of the 16K fraction and whole cell lysate of DENV-2 infected and replicon containing Huh-7 cells.
2. To compare the effectiveness of using a heat inactivated DENV-2 treatment versus a mock infection as a control in a proteomic analysis.
3. To develop an IF based approach to titrate DENV-2 viral stocks.
4. Attempt to develop siRNA-based approach to understand the importance of selected proteins in the DENV lifecycle and validate the proteomic results.

Chapter 2: Materials and Methods

2.1 Cell Culture

All protocols involving cell culture were performed with aseptic techniques, in sterile class two microbiological safety cabinets (MSC2) at biosafety level (BSL) 2. If live DENV-2 was used, those techniques were performed at BSL3.

Human hepatocarcinoma cells (Huh-7) and Huh-7 cells containing a DENV replicon (pDENΔCprME-EGFP-PAC-1D2A (Ng et al., 2007)); termed Huh-7 replicon cells (produced in the laboratory by Dr Maia Kavanagh-Williamson after extracting and purifying replicon RNA, and transfecting Huh-7 cells) were maintained in Dulbecco's modified Eagle's Medium (DMEM) (12-60F, Lonza, Switzerland) supplemented with 0.1 mM non-essential amino acids (Sigma-Aldrich), and 10% (v/v) foetal bovine serum (FBS) (Gibco, Life Technologies, UK), termed cell culture medium (CCM). Huh-7 replicon cells were selected using 3.5 µg/mL of puromycin (Invivogen). The cells were grown in a humidified incubator at 37° C under 5% CO_2. A replicon in a non-infectious, self-replicating sub-genomic RNA construct that usually contains a selection marker, in this case a puromycin resistance gene.

Both cell lines were passaged following a basic adherent cell culture protocol. All reagents were warmed to 37° C before use. The cell culture media was removed from each flask (typically a T75 flask; volumes were scaled appropriately for larger or smaller flasks) and disposed of in 1% Virkon. The cells were then washed once with 10 mL of 1x phosphate buffered saline (PBS) (Lonza, Switzerland) and 2 mL of 0.05% Trypsin/EDTA (Life Sciences) (v/v) in 1x PBS was added to detach the cells. Once detached the cells were resuspended in fresh media. For routine passaging, an appropriate volume of cell suspension was removed and diluted to approximately 15 mL with fresh CCM in a fresh flask. When undertaking assays using a 96-well plate format, the cells were prepared as above, and resuspended to a final volume of 10 mL. If multiple flasks were used, the cells were pooled in a 50 mL falcon tube. The cells were spun at 200 x *g* for 5 minutes, the supernatant discarded, and the cells resuspended in an appropriate volume of fresh media (usually 10 mL per flask used). A haemocytometer was cleaned and 10 µL of the cell suspension added to each chamber. The cells were counted, averaged and then an appropriate dilution was made. The diluted cells were transferred to a sterile reservoir and 80 µL seeded into the wells of a 96-well plate using a multi-channel pipette. Volumes of cell dilutions added was increased appropriately for 24 well format.

Huh-7 cells were frozen using the following procedure. The cells were detached as above and spun at 200 x *g* for 5 minutes and the supernatants discarded. Then, the cells were resuspended in an

appropriate volume (1 mL per 1/3 of a confluent T75) of freezing media. Freezing media contains 70% foetal bovine serum, 20% DMSO (Sigma-Aldrich), and 10% CCM. One millilitre of the cell suspension was added to a cryovial, and the cells frozen slowly in a Mr Frosty in a -80˚ C freezer for at least 24 hours, then transferred to liquid nitrogen for long term storage.

Huh-7 cells were removed from the liquid nitrogen storage and defrosted in a 37˚ C water bath before being moved to the MSC2 hood. The thawed cell mixture was added dropwise to a falcon containing 9 mL pre-warmed media, then spun at 150 x *g* for 5 minutes. The supernatant was removed, and the cells resuspended in 3 mL fresh media, before being added to a T25 with 3 mL fresh media already present.

2.2 Dengue Infection

2.2.1 Dengue Titrations

Twenty-four hours prior to infection $5x10^4$ Huh-7 cells in 150 µL CCM were seeded per well into the middle 60 wells of a µClear 96-well microplate (Greiner Bio-one). A two-fold serial dilution of DENV-2 stocks (recombinant DENV-2 strain New Guinea C (Gualano et al., 1998); GenBank accession number AF038403) was carried out in triplicate wells of a round bottomed 96-well cell culture plate with 75 µL minimum essential medium (MEM) (Gibco), supplemented with 2% FBS (v/v) (Gibco) and 0.1 mM non-essential amino acids (Gibco), termed viral assay medium (VAM). The CCM of the Huh-7 cells was removed and replaced with 60 µL inoculum. The cells were incubated at 37˚ C for 90 minutes, the inoculum removed and disposed of in 5% Virkon, and replaced with 100 µL VAM per well. The cells were incubated for a further 18 hours. The cells were fixed following the procedure at the beginning of section 2.2.3.

2.2.2 Virus Infection

Five thousand Huh-7 cells were seeded per well in 80 µL, with or without siRNAs into the middle 60 wells of a µClear 96-well microplate (Greiner Bio-one). After 72 hours the CCM was replaced with 100 µL of VAM before infection. Once titred, the DENV-2 stock was diluted in VAM to give a multiplicity of infection (MOI) of 5.

All infections were carried out using DENV-2 strain in the BSL3 laboratory. The cell culture media was removed, and a DENV-2 stock diluted suitably in VAM was added to the appropriate wells and the plates incubated at 37° C for 90 minutes, then the inoculum was removed and replaced with 100 µL VAM, and the cells incubated at 37° C for 24 hours. The plates were fixed following the procedure described at the beginning of section 2.3.1.

2.3 Assays

2.3.1 Immunofluorescence Staining

At an appropriate time post-infection, 8% (w/v) paraformaldehyde (PFA) was added 1:1 to the media in the wells and the entire plates and lids submerged in 4% PFA for one hour, after which time the PFA was drained as much as possible, and the plates gently submerged in sterile 1x PBS. The decontaminated plates were removed from the tub, without excessive draining, and removed from the BSL3 laboratory for assay.

Non-infectious Huh-7 replicon cells were fixed by addition of 8% (w/v) PFA 1:1 to the CCM in the wells for 15 minutes. The PFA was removed, and the cells washed once with sterile PBS.

Fixed cells were stained following a protocol developed by Dr Maia Kavanagh Williamson for high-throughput SARS-CoV-2 assays and adapted for this study.

The fluid from the wells was removed and the plate left upside down and left to drain for one minute. Fifty microlitres of 0.1% Triton-X100 (v/v) (Sigma-Aldrich) in filtered PBS (0.22 µm filter) was then added and left for 10 minutes. The solution was removed, and the plate left to drain for one minute, the wells were then washed with 100 µL filtered PBS, which was in turn removed and the plates left to drain for one minute. The fixed cells were blocked with 50 µL of 1% (w/v) bovine serum albumin (BSA) (Sigma-Aldrich) in PBS for 30 minutes at room temperature.

The blocking solution was removed, and a primary antibody added (Table 2.1). Huh-7 cells infected with DENV-2 were stained with 40 µL of anti-E protein antibody or anti-prM antibody diluted 1:50 or 1:1000, respectively in blocking agent for 45 minutes at room temperature. Huh-7 replicon cells were stained with 40 µL of anti-dsRNA antibody diluted 1:250 in blocking agent for 45 minutes at room temperature. After the incubation was complete, the primary antibodies were removed, and the fixed cells washed three times with filtered PBS. Forty microlitres of secondary antibody containing solution was then added to each well. To the infected Huh-7 cells, a goat anti-mouse Alexa-Fluor 555 IgG (H+L) (Invitrogen) diluted 1:3000 in blocking agent and 1mg/mL DAPI (Thermo Scientific) at 1:2000 was added per well and left to incubate for 30 minutes at room temperature. To the Huh-7 replicon cells goat anti-mouse Alexa-Fluor 555 IgG (H+L) (Invitrogen), Goat anti-Rabbit IgG (H+L) Highly Cross-Adsorbed Secondary Antibody, Alexa Fluor™ Plus 647 (Invitrogen) both at 1:3000 and 1mg/mL DAPI (Thermo Fisher) at 1:2000 in blocking agent and left to incubate for 30 minutes. After such time the secondary antibodies were removed, the plates drained and washed three times with filtered PBS and a final 100 µL aliquot of filtered PBS added per well.

Name	Produced in	Working dilution	Catalogue number	Source
Anti-GFP	Goat	1:250	Ab0020200	SicGen
Anti-E	Rabbit	1:500	NBP2-52666	Novus Biologicals
Anti-NS1	Rabbit	1:500	GTX103346	GeneTex
Anti-NS5	Rabbit	1:500	In house mix, 1011, 1012, 1013	Prof A Davidson
Anti-dsRNA	Mouse	1:250	Scicons	Scicons
Anti-prM	Rabbit	1:1000	GTX128092	Genetex

Table 2. 1. Primary antibodies used in IFA

Name	Produced in	Working dilution	Catalogue number	Source
Goat anti-Mouse IgG (H+L) Highly Cross-Adsorbed Secondary Antibody, Alexa Fluor™ Plus 555	Goat	1:3000	A32727	Invitrogen
Goat anti-Rabbit IgG (H+L) Highly Cross-Adsorbed Secondary Antibody, Alexa Fluor™ Plus 647	Goat	1:3000	A32733	Invitrogen
Donkey anti-Goat IgG (H+L) Highly Cross-Adsorbed Secondary Antibody, Alexa Fluor™ Plus 488	Donkey	1:2000	A32814	Invitrogen

Table 2. 2. Secondary antibodies used in IFA

Name	Working dilution	Catalogue number	Source
DAPI 1mg/mL	1:2000	62248	Thermo Scientific

Table 2. 3. Stains used in IFA

2.3.2 Immunofluorescence Assay

To determine the number of virus infected cells, images were acquired on an ImageXpress Pico Automated Cell Imaging System (Molecular Devices) using the 10X objective. Stitched images of 9 fields covering the central 50% of the well were analysed for virus infected cells using Cell Reporter Xpress software (Molecular Devices). The cell number was determined by automated counting of DAPI stained nuclei and infected cells were identified as those cells in which positive E/prM staining or GFP fluorescence was detected associated with nuclear DNA staining.

2.3.3 Cell Viability Assay

A 5 mg/mL thiazolyl blue tetrazolium bromide (MTT) (Sigma-Aldrich) stock solution in sterile PBS (Lonza) was made and diluted to 1 mg/mL when needed for the assay. Five thousand Huh-7 or Huh-7 replicon cells were seeded into each well of a 96-well culture plate containing various volumes of Dharmafect (DF) 4 (Dharmacon) transfection reagent and left for 24 hours. The media was removed and 100 µL of 1mg/mL MTT reagent was added per well. The cells were incubated at 37 °C in the dark for 3 hours, at which point the MTT reagent was removed. 100 µL of molecular biology grade ethanol (Fisher Scientific, UK) was then added to each well. The plates were wrapped in foil and rocked for 30 minutes. The absorbance at 600 nm was measured using a built-in protocol on a Promega GloMax plate reader (Promega).

2.4 Silencing RNAs

2.4.1 Preparation of Cherry-Picked siRNA Library

Custom siRNA libraries chosen based on proteomic analysis (Chapter 3) were ordered from Dharmacon (Horizon Discovery, USA) in a 96-well plate format. Each plate contained 0.1 nmol of siRNA per well, Table 2.5.

The custom libraries were taken out of the freezer and left to thaw on ice for 30 minutes, then spun at 300 x *g* for 3 minutes. Two millilitres of 5x RNA resuspension buffer (Horizon Discovery) was diluted with 8 mL UltraPure Water (Gibco) and 100 µL of 1x RNA resuspension buffer was added per well and mixed by pipetting 3 times to make a 1 µM solution. The plates were put on a shaking platform for 45 minutes and spun again at 300 x *g* for 45 minutes. The 100 µL siRNA solutions were

split between five 96-well round bottomed cell culture plates with 20 µL per plate. The plates were sealed with aluminium foil and the edges wrapped in parafilm, and frozen at -20˚ C until needed. When needed they were defrosted on ice for 30 minutes and spun at 300 x *g* for 3 minutes.

This procedure was performed in sterile and RNase-free conditions.

2.4.2 Preparation of Additional siRNA Aliquots

Additional control siRNAs were also ordered individually and prepared when required. One millilitre of 5x Resuspension Buffer (Horizon Discovery) was diluted with 4 mL of UltraPure Water (Gibco) and 1 mL was added to the siRNA. This was split into 10 x 100 µL aliquots, which when needed were diluted with 400 µL fresh 1x Resuspension Buffer (Horizon Discovery) to make a 1 µM siRNA solution.

2.4.3 siRNA Reverse Transfection

Transfection mixes were made using serum-free OPTI-MEM (Life Technologies) and the appropriate concentrations of siRNA (Dharmacon) and transfection reagents DF1, DF4, or Lipofectamine RNAiMAX (Thermo-Scientific) to a total volume of 20 µL per condition (Table 2.4). These were left to complex for 45 minutes, following the manufacturer's instructions.

During this time Huh-7 and Huh-7 replicon cells were detached using trypsin, counted, and diluted in fresh media to a final cell density of 6.0 x 10^5 cells per mL. Eighty microlitres of cell suspension was seeded per well of a 96-well plate into the 20 µL of transfection mix. The cells and incubated for 24 hours. The transfection media was then removed and replaced with 150 µL of CCM.

After 72 hours, the Huh-7 cells were infected with DENV (as described above), and the Huh-7 replicon cells were fixed by the addition of a 1:1 volume of 8% (w/v) PFA to the CCM followed by a 15-minute incubation. After the 24-hour infection the Huh-7 cells were fixed using the method described previously. Once decontaminated the plates were used for IFA using the method described previously.

Final Concentration siRNA (nM)	**Volume of 1 µM siRNA (µL)**	**Volume of DF4 (µL)**	**Volume of OPTI-MEM (µL)**	**Total Volume of Transfection Mix per Well (µL)**
50	5	0.2	14.8	20

Table 2. 4. Tables of volumes of reagents used for siRNA reverse transfection

Pool Catalogue Number	Duplex Catalogue Number	Gene Symbol	GENE ID	Gene Accession	GI Number	Sequence
L-004037-00	J-004037-06	AGA	175	NM_000027	32313568	CCAAUGUGACUGGAAGUUA
L-004037-00	J-004037-07	AGA	175	NM_000027	32313568	CCAUAAGACAGGACAUAUU
L-004037-00	J-004037-08	AGA	175	NM_000027	32313568	UAGGAGAUCUCAGACGAAU
L-004037-00	J-004037-09	AGA	175	NM_000027	32313568	UGACGGCUCUGUAGGCUUU
L-006812-00	J-006812-09	AK2	204	NM_001625	26665889	GAACCCGAGUAUCCUAAAG
L-006812-00	J-006812-10	AK2	204	NM_001625	26665889	GUGAUGAAAUGGUAGUGGA
L-006812-00	J-006812-11	AK2	204	NM_001625	26665889	GCUGAAAACUUCUGUGUCU
L-006812-00	J-006812-12	AK2	204	NM_001625	26665889	CAUAGAGUACUACAGGAAA
L-009239-01	J-009239-09	ARSD	414	NM_009589	71852585	CGAGAGCAGUCACCGGCAU
L-009239-01	J-009239-10	ARSD	414	NM_009589	71852585	ACACUGAGAACGCCGAAUA
L-009239-01	J-009239-11	ARSD	414	NM_009589	71852585	UUGACUAUUUCUACGGCAU
L-009239-01	J-009239-12	ARSD	414	NM_009589	71852585	GUGCGACGCUGGAACUGUA
L-008197-00	J-008197-06	CALR	811	NM_004343	5921996	CCUAUGAGGUGAAGAUUGA
L-008197-00	J-008197-07	CALR	811	NM_004343	5921996	GCACGGAGACUCAGAAUAC
L-008197-00	J-008197-08	CALR	811	NM_004343	5921996	GAAGCUGUUUCCUAAUAGU

L-008197-00	J-008197-09	CALR	811	NM_004343	5921996	GCAAGGAUGAUGAGUUUAC
L-003481-00	J-003481-05	CTH	1491	NM_153742	34328938	GUACAGGGAUGGUCACCUU
L-003481-00	J-003481-06	CTH	1491	NM_153742	34328938	GCACUCGGGUUUUGAAUAU
L-003481-00	J-003481-07	CTH	1491	NM_153742	34328938	CUACAUGUCCGAAUGGAAA
L-003481-00	J-003481-08	CTH	1491	NM_153742	34328938	GAGCUUGGGAGGAUUCGAA
L-005854-00	J-005854-05	DPP7	29952	NM_013379	62420887	GGACGUCACGGCGGACUUU
L-005854-00	J-005854-06	DPP7	29952	NM_013379	62420887	CAAUGUGACCGAUAUGUUC
L-005854-00	J-005854-07	DPP7	29952	NM_013379	62420887	GUGAUCGGCUGCUGAGUGA
L-005854-00	J-005854-08	DPP7	29952	NM_013379	62420887	UGGCAGGGCUGGUCUACAA
L-020493-00	J-020493-05	ERO1A	30001	NM_014584	7657068	GGACCAAGCAUGAUGAUUC
L-020493-00	J-020493-06	ERO1A	30001	NM_014584	7657068	GUGACUACUUUAGGUAUUA
L-020493-00	J-020493-07	ERO1A	30001	NM_014584	7657068	GAAUUAAAUCUGCGAGCUA
L-020493-00	J-020493-08	ERO1A	30001	NM_014584	7657068	UAUCCAAAGUGUUACCAUU
L-008127-00	J-008127-06	ETFDH	2110	NM_004453	4758311	GGAUUUCGGUUACAGAUAA
L-008127-00	J-008127-07	ETFDH	2110	NM_004453	4758311	CUGAAGGAGUUAUGGGUUA
L-008127-00	J-008127-08	ETFDH	2110	NM_004453	4758311	GACUGGAACUACAUGCUAA

L-008127-00	J-008127-09	ETFDH	2110	NM_004453	4758311	UUGAAGAACUCAUGGGUAU
L-011030-00	J-011030-05	EXT1	2131	NM_000127	46370065	CAAAGUGGACGAACGACUA
L-011030-00	J-011030-06	EXT1	2131	NM_000127	46370065	GAACCAAGCUGCCGUCAUA
L-011030-00	J-011030-07	EXT1	2131	NM_000127	46370065	CGACAGAGCUGCAUGAAUA
L-011030-00	J-011030-08	EXT1	2131	NM_000127	46370065	GAUGAGAGAUUGUUAUUAC
L-007902-00	J-007902-07	FGB	2244	NM_005141	70906434	ACACAGAUGGGAAGAAUUA
L-007902-00	J-007902-08	FGB	2244	NM_005141	70906434	GGUGUAGUAUGGAUGAAUU
L-007902-00	J-007902-09	FGB	2244	NM_005141	70906434	UGUCAAACCGUAUAGAGUA
L-007902-00	J-007902-10	FGB	2244	NM_005141	70906434	GGAUGGUGGUAUAAUAGAU
L-007903-00	J-007903-09	FGG	2266	NM_000509	70906436	GAAAUAUGAAGCAUCGAUU
L-007903-00	J-007903-10	FGG	2266	NM_000509	70906436	GCUGACAAGUACCGCCUAA
L-007903-00	J-007903-11	FGG	2266	NM_000509	70906436	GAAAGAUUCGGUAGUUAUU
L-007903-00	J-007903-12	FGG	2266	NM_000509	70906436	GGAUCUGGUUGGUGGAUGA
L-009683-00	J-009683-06	FKBP14	55033	NM_017946	51593093	AGACAAAGAUGGGUUUAUA
L-009683-00	J-009683-07	FKBP14	55033	NM_017946	51593093	ACGAUGAGUUAUAGAGAUA
L-009683-00	J-009683-08	FKBP14	55033	NM_017946	51593093	GGACCAAGAUCCCAUGAAU

L-009683-00	J-009683-09	FKBP14	55033	NM_017946	51593093	AAGAUGAGGUUAAAGCAUA
L-019634-00	J-019634-09	FTH1	2495	NM_002032	56682958	UCAGAUAGAACUAAGGGUU
L-019634-00	J-019634-10	FTH1	2495	NM_002032	56682958	UCUUUGAGGUCUUGGGAUG
L-019634-00	J-019634-11	FTH1	2495	NM_002032	56682958	GAGUCUGAGUUAAAUGUUU
L-019634-00	J-019634-12	FTH1	2495	NM_002032	56682958	GAAAUUUGGUACCCAGGUG
L-008700-01	J-008700-09	HPGD	3248	NM_000860	52851450	UUGCACAGCAGCCGGUUUA
L-008700-01	J-008700-10	HPGD	3248	NM_000860	52851450	CAGUAAAUGAUGUCGGUUU
L-008700-01	J-008700-11	HPGD	3248	NM_000860	52851450	GCGGCAUCAUUAUCAAUAU
L-008700-01	J-008700-12	HPGD	3248	NM_000860	52851450	GGCAUAAGCUUGUUUGUAU
L-008198-00	J-008198-06	HSPA5	3309	NM_005347	21361242	GCGCAUUGAUACUAGAAAU
L-008198-00	J-008198-07	HSPA5	3309	NM_005347	21361242	GAACCAUCCCGUGGCAUAA
L-008198-00	J-008198-08	HSPA5	3309	NM_005347	21361242	GAAAGAAGGUUACCCAUGC
L-008198-00	J-008198-09	HSPA5	3309	NM_005347	21361242	AGAUGAAGCUGUAGCGUAU
L-003678-00	J-003678-06	HYOU1	10525	NM_006389	13699861	CAGCAAGCAUGGCGAUUAA
L-003678-00	J-003678-07	HYOU1	10525	NM_006389	13699861	GGGCAUGGUUCUCAAUUAU
L-003678-00	J-003678-08	HYOU1	10525	NM_006389	13699861	ACACUGAGCCUUUGGAGUU

L-003678-00	J-003678-09	HYOU1	10525	NM_006389	13699861	GGAGAAUGGUACUGAUACU
L-020202-00	J-020202-05	KNG1	3827	NM_000893	38455404	GUACAAGGAUGCUGCAAAA
L-020202-00	J-020202-06	KNG1	3827	NM_000893	38455404	CCGAGGAAAUUGACUGCAA
L-020202-00	J-020202-07	KNG1	3827	NM_000893	38455404	GAAUGGUGAUACCGGUGAA
L-020202-00	J-020202-08	KNG1	3827	NM_000893	38455404	GGUUGGCUCUGACACGUUU
L-019549-00	J-019549-05	LETM1	3954	NM_012318	6912481	CCAAAGACUUCUCUGUGUU
L-019549-00	J-019549-06	LETM1	3954	NM_012318	6912481	UCGCAGAGGUGAAGAGCUA
L-019549-00	J-019549-07	LETM1	3954	NM_012318	6912481	GCGAGCAGGUGGACAACAA
L-019549-00	J-019549-08	LETM1	3954	NM_012318	6912481	ACGACAAGCUGAUUGCUGA
L-005924-00	J-005924-05	LGMN	5641	NM_005606	56682961	GGGCAUAGGAUCCGGCAAA
L-005924-00	J-005924-06	LGMN	5641	NM_005606	56682961	CCAUGGAUCUACUGGAAUA
L-005924-00	J-005924-07	LGMN	5641	NM_005606	56682961	GAACAGAUCGUUGUGAUGA
L-005924-00	J-005924-08	LGMN	5641	NM_005606	56682961	GAUCGUGGCAGGUUCAAAU
L-012158-00	J-012158-06	MANF	7873	NM_006010	54873599	UGAAGAAGCUCCGAGUUAA
L-012158-00	J-012158-07	MANF	7873	NM_006010	54873599	GAGAAUCGGUUGUGCUACU
L-012158-00	J-012158-08	MANF	7873	NM_006010	54873599	GACUACAUCCGGAAGAUAA

L-012158-00	J-012158-09	MANF	7873	NM_006010	54873599	CGACUGCGAAGUUUGUAUU
L-015519-02	J-015519-17	MCU	90550	NM_138357	24308399	GAUCAGGCAUUGUGGAAUA
L-015519-02	J-015519-18	MCU	90550	NM_138357	24308399	GUUUUGACCUAGAGAAAUA
L-015519-02	J-015519-19	MCU	90550	NM_138357	24308399	ACUGAGAGACCCAUUACAA
L-015519-02	J-015519-20	MCU	90550	NM_138357	24308399	GUAAUGACACGCCAGGAAU
L-020233-02	J-020233-17	MPC2	25874	NM_015415	142350140	GGGUUUAUUUGGUCAAGAU
L-020233-02	J-020233-18	MPC2	25874	NM_015415	142350140	CCACCGGCUCCUCGAUAAA
L-020233-02	J-020233-19	MPC2	25874	NM_015415	142350140	CCAUUGGGACCUAGUUUAU
L-020233-02	J-020233-20	MPC2	25874	NM_015415	142350140	AGAAAUUGAGGCCGUUGUA
L-020748-01	J-020748-09	MRS2	57380	NM_020662	93204868	GACAAACAGGGAAACGUUA
L-020748-01	J-020748-10	MRS2	57380	NM_020662	93204868	AGGGUCAACUCGUUACAUA
L-020748-01	J-020748-11	MRS2	57380	NM_020662	93204868	CUGCUAAUCUAUAUGCCUA
L-020748-01	J-020748-12	MRS2	57380	NM_020662	93204868	CAAAGUAGUGUGCAUGGAA
L-008301-00	J-008301-05	MTTP	4547	NM_000253	4557762	GCAAUGGAGUUUAGCUUGU
L-008301-00	J-008301-06	MTTP	4547	NM_000253	4557762	GAGAAACUGUUAUGAUCAU
L-008301-00	J-008301-07	MTTP	4547	NM_000253	4557762	GUUCAAAGGUUCUAUUGGU

L-008301-00	J-008301-08	MTTP	4547	NM_000253	4557762	CAACGGAUACAGUGAUUUG
L-009809-00	J-009809-05	NNT	23530	NM_182977	33695085	CAGGAACGCUGAUUAGUUU
L-009809-00	J-009809-06	NNT	23530	NM_182977	33695085	CAUCGUGGGUGCACUCAUA
L-009809-00	J-009809-07	NNT	23530	NM_182977	33695085	GCACACAUACGGAAAUCAA
L-009809-00	J-009809-08	NNT	23530	NM_182977	33695085	AAUCCAGAGUUGCUAAAUA
L-017216-00	J-017216-05	NPC2	10577	NM_006432	29171756	GCGAAUAUCCCUCUAUAAA
L-017216-00	J-017216-06	NPC2	10577	NM_006432	29171756	GUACAGAUCGUUUCUCAUC
L-017216-00	J-017216-07	NPC2	10577	NM_006432	29171756	AAGACAAGACCUAUAGCUA
L-017216-00	J-017216-08	NPC2	10577	NM_006432	29171756	GGAUGGAGUUAUAAAGGAA
L-012696-02	J-012696-17	OXA1L	5018	NM_005015	4826879	GUGAACAACGCAUGCGGAA
L-012696-02	J-012696-18	OXA1L	5018	NM_005015	4826879	GCACGACACACUUGGCUGA
L-012696-02	J-012696-19	OXA1L	5018	NM_005015	4826879	GUUCCAGGAUCUCACGGUA
L-012696-02	J-012696-20	OXA1L	5018	NM_005015	4826879	CAGAAGUUUUCCAGUCGAA
L-003690-00	J-003690-05	P4HB	5034	NM_000918	20070124	CCAAGAGUGUGUCUGACUA
L-003690-00	J-003690-06	P4HB	5034	NM_000918	20070124	GUGACGUGUUCUCCAAAUA
L-003690-00	J-003690-07	P4HB	5034	NM_000918	20070124	GAACGCACGCUGGAUGGUU

L-003690-00	J-003690-08	P4HB	5034	NM_000918	20070124	UGACAUACCAUUUGGGAUC
L-003674-00	J-003674-09	PDIA3	2923	NM_005313	67083697	GGAAUAGUCCCAUUAGCAA
L-003674-00	J-003674-10	PDIA3	2923	NM_005313	67083697	GGGCAAGGACUUACUUAUU
L-003674-00	J-003674-11	PDIA3	2923	NM_005313	67083697	AGACCCAAAUAUCGUCAUA
L-003674-00	J-003674-12	PDIA3	2923	NM_005313	67083697	GAGGAGUUCUCGCGUGAUG
L-019249-00	J-019249-05	PDIA4	9601	NM_004911	33469983	GCAGUUUGCUCCGGAAUAU
L-019249-00	J-019249-06	PDIA4	9601	NM_004911	33469983	CCUGAGAGAAGAUUACAAA
L-019249-00	J-019249-07	PDIA4	9601	NM_004911	33469983	GCGAGUUUGUCACUGCUUU
L-019249-00	J-019249-08	PDIA4	9601	NM_004911	33469983	GAAGUCACGCUUGUGUUGA
L-005250-00	J-005250-09	PIK3C3	5289	NM_002647	34761063	CACCAAAGCUCAUCGACAA
L-005250-00	J-005250-10	PIK3C3	5289	NM_002647	34761063	AUAGAUAGCUCCCAAAUUA
L-005250-00	J-005250-11	PIK3C3	5289	NM_002647	34761063	GAACAACGGUUUCGCUCUU
L-005250-00	J-005250-12	PIK3C3	5289	NM_002647	34761063	GAGAUGUACUUGAACGUAA
L-012204-00	J-012204-05	PRDX4	10549	NM_006406	5453548	GGACUAUGGUGUAUACCUA
L-012204-00	J-012204-06	PRDX4	10549	NM_006406	5453548	CGUGGGAAAUACUUGGUUU
L-012204-00	J-012204-07	PRDX4	10549	NM_006406	5453548	GGAUUCCACUUCUUUCAGA

L-012204-00	J-012204-08	PRDX4	10549	NM_006406	5453548	GAUGAGACACUACGUUUGG
L-003523-00	J-003523-16	PRKCA	5578	NM_002737	47157319	UAAGGAACCACAAGCAGUA
L-003523-00	J-003523-17	PRKCA	5578	NM_002737	47157319	UUAUAGGGAUCUGAAGUUA
L-003523-00	J-003523-18	PRKCA	5578	NM_002737	47157319	GAAGGGUUCUCGUAUGUCA
L-003523-00	J-003523-19	PRKCA	5578	NM_002737	47157319	UCACUGCUCUAUGGACUUA
L-009569-00	J-009569-06	PYGL	5836	NM_002863	71037378	GAACAAUGACCCUAUGGUU
L-009569-00	J-009569-07	PYGL	5836	NM_002863	71037378	UUACAUGGGCCGAACAUUA
L-009569-00	J-009569-08	PYGL	5836	NM_002863	71037378	CGUGGAACCUUCAGAUCUA
L-009569-00	J-009569-09	PYGL	5836	NM_002863	71037378	UAAGAUUGAAGCAGGAAUA
L-010999-00	J-010999-05	SERPING1	710	NM_001032295	73858569	GGAUAGAGCCUCCUCAAAU
L-010999-00	J-010999-06	SERPING1	710	NM_001032295	73858569	AAAGUGCCCAUGAUGAAUA
L-010999-00	J-010999-07	SERPING1	710	NM_001032295	73858569	GCCAGGAUAUGCUCUCAAU
L-010999-00	J-010999-08	SERPING1	710	NM_001032295	73858569	GCUAUUCGUUGAACCCAUC
L-011230-00	J-011230-05	SERPINH1	871	NM_001235	32454740	CAAAGCGGCUCCCUGCUAU
L-011230-00	J-011230-06	SERPINH1	871	NM_001235	32454740	GCACUGCGGAGAAGUUGAG
L-011230-00	J-011230-07	SERPINH1	871	NM_001235	32454740	AAGAUCAACUUCCGCGACA

L-011230-00	J-011230-08	SERPINH1	871	NM_001235	32454740	AGAAACACCUGGCUGGGCU
L-010686-01	J-010686-09	SFXN1	94081	NM_022754	40255158	CUUCAAUGCCGUCGUCAAU
L-010686-01	J-010686-10	SFXN1	94081	NM_022754	40255158	GAAACAAGCCAUCACGCAA
L-010686-01	J-010686-11	SFXN1	94081	NM_022754	40255158	GUAGAUGUUUAACGUCAUA
L-010686-01	J-010686-12	SFXN1	94081	NM_022754	40255158	GGGAACAGCUUACGUUUCU
L-018729-00	J-018729-05	SFXN3	81855	NM_030971	49472836	GCGUUGAAGUGGUCUACUA
L-018729-00	J-018729-06	SFXN3	81855	NM_030971	49472836	GCUGCAUGCUCACAUUCUA
L-018729-00	J-018729-07	SFXN3	81855	NM_030971	49472836	GCUGGAAGCUUCUCGGAAC
L-018729-00	J-018729-08	SFXN3	81855	NM_030971	49472836	GAAGAGCUCCAUACACAUA
L-007424-02	J-007424-21	SLC19A3	80704	NM_025243	93352566	AAGAAGUCAUCAAGCGUGA
L-007424-02	J-007424-22	SLC19A3	80704	NM_025243	93352566	AAGAUUUGAAGGAGUGCUA
L-007424-02	J-007424-23	SLC19A3	80704	NM_025243	93352566	GAUUGUAGUAGAUCAGAGA
L-007424-02	J-007424-24	SLC19A3	80704	NM_025243	93352566	GCAAUGUGACUGUGGACGU
L-007427-00	J-007427-05	SLC1A3	6507	NM_004172	34222301	GAGCUGUAGUCUAUUAUAU
L-007427-00	J-007427-06	SLC1A3	6507	NM_004172	34222301	GAACUUCGGACAAAUUAUU
L-007427-00	J-007427-07	SLC1A3	6507	NM_004172	34222301	UGAGAGAGUUCUUUGAUUC

L-007427-00	J-007427-08	SLC1A3	6507	NM_004172	34222301	CUAGUUGUCUUCUCCAUGU
L-007468-00	J-007468-07	SLC25A1	6576	NM_005984	21389314	GCGCACAAAUACCGGAACA
L-007468-00	J-007468-08	SLC25A1	6576	NM_005984	21389314	GGAAGACGGACUAAGCCUA
L-007468-00	J-007468-09	SLC25A1	6576	NM_005984	21389314	GCCAUCCGCUUCUUCGUCA
L-007468-00	J-007468-10	SLC25A1	6576	NM_005984	21389314	GGUUUGGAAUGUUCGAGUU
L-007469-01	J-007469-09	SLC25A10	1468	NM_012140	34147605	ACGUCAGGAUGCAGAACGA
L-007469-01	J-007469-10	SLC25A10	1468	NM_012140	34147605	GGGAUGAACAAGCAACGCA
L-007469-01	J-007469-11	SLC25A10	1468	NM_012140	34147605	GAGGUGAAGCUGCGCAUGA
L-007469-01	J-007469-12	SLC25A10	1468	NM_012140	34147605	CUUUAUUGCAGGUGGAUGU
L-007470-00	J-007470-05	SLC25A11	8402	NM_003562	34147649	GGACGUGCUGUUCAAAGUU
L-007470-00	J-007470-06	SLC25A11	8402	NM_003562	34147649	GAUCAGCGGUCUUGUCACC
L-007470-00	J-007470-07	SLC25A11	8402	NM_003562	34147649	GCUCUUAUCCGCAUGACUG
L-007470-00	J-007470-08	SLC25A11	8402	NM_003562	34147649	GGGAUGGGAGCUACAGUUU
L-007471-02	J-007471-18	SLC25A12	8604	NM_003705	21361102	ACAUGGAGCUUGUUCGUAA
L-007471-02	J-007471-19	SLC25A12	8604	NM_003705	21361102	GUAGAAAUGUAAUGCGGUU
L-007471-02	J-007471-20	SLC25A12	8604	NM_003705	21361102	AGGUUGAUGGAGAGCGUUA

L-007471-02	J-007471-21	SLC25A12	8604	NM_003705	21361102	GCCUUUAUCUCCCGAAAUU
L-007472-00	J-007472-05	SLC25A13	10165	NM_014251	7657580	GGAUUUAAUUCGCUCCUUA
L-007472-00	J-007472-06	SLC25A13	10165	NM_014251	7657580	UGGGAGAACUCAUGUAUAA
L-007472-00	J-007472-07	SLC25A13	10165	NM_014251	7657580	UAAGUGGAGUGGUGGAUCA
L-007472-00	J-007472-08	SLC25A13	10165	NM_014251	7657580	ACUCGAUACUUGAACAUUU
L-007474-00	J-007474-06	SLC25A15	10166	NM_014252	7657584	GCCUCUGGCUUGCGGUAUA
L-007474-00	J-007474-07	SLC25A15	10166	NM_014252	7657584	GCACUAAUCGCCAACAUCG
L-007474-00	J-007474-08	SLC25A15	10166	NM_014252	7657584	GAAUUAGGCCCUGUACCUU
L-007474-00	J-007474-09	SLC25A15	10166	NM_014252	7657584	CAGGCAGGAUUUAUCAGAA
L-007480-00	J-007480-06	SLC25A20	788	NM_000387	46276890	GAAAGCAAGUACACUGGUA
L-007480-00	J-007480-07	SLC25A20	788	NM_000387	46276890	GAUGUUAUCUGGCGUAUUC
L-007480-00	J-007480-08	SLC25A20	788	NM_000387	46276890	GCCAUGAAGUUCCUUAAUU
L-007480-00	J-007480-09	SLC25A20	788	NM_000387	46276890	CAACUGGGCUGUGGCAAUC
L-007482-01	J-007482-09	SLC25A22	79751	NM_024698	34222352	CCGAGGAGAAGUCGCCUUU
L-007482-01	J-007482-10	SLC25A22	79751	NM_024698	34222352	GCGUCAACGAGGACACCUA
L-007482-01	J-007482-11	SLC25A22	79751	NM_024698	34222352	GCAUCGCACAGGUGGUCUA

L-007482-01	J-007482-12	SLC25A22	79751	NM_024698	34222352	CCGUCCAGGAACUAACUUA
L-007325-02	J-007325-17	SLC25A24	29957	NM_213651	47458040	CAGAUGAAUUCACGGAAGA
L-007325-02	J-007325-18	SLC25A24	29957	NM_213651	47458040	GCAUAUGAACAGUACAAGA
L-007325-02	J-007325-19	SLC25A24	29957	NM_213651	47458040	GGAAAUGGUACAAACGUCA
L-007325-02	J-007325-20	SLC25A24	29957	NM_213651	47458040	GGUGCUGUCUCUCGAACAA
L-007484-00	J-007484-05	SLC25A3	5250	NM_002635	47132592	GGGCAUAUUUAACGGAUUC
L-007484-00	J-007484-06	SLC25A3	5250	NM_002635	47132592	UGGCGCACAUCACUAUAUU
L-007484-00	J-007484-07	SLC25A3	5250	NM_002635	47132592	GCAAUUGUUUCUCACCCUG
L-007484-00	J-007484-08	SLC25A3	5250	NM_002635	47132592	GCCAACACUUUGAGGGAUG
L-007488-01	J-007488-09	SLC26A1	10861	NM_134425	20336273	GCAUCAUCCUGGUGCCGCA
L-007488-01	J-007488-10	SLC26A1	10861	NM_134425	20336273	GGCAUGUCUCCGUGGGCAU
L-007488-01	J-007488-11	SLC26A1	10861	NM_134425	20336273	CGUGCAGUGUGCUGUGCGU
L-007488-01	J-007488-12	SLC26A1	10861	NM_134425	20336273	AUACGUCCUUCUUCGCCAA
L-007565-02	J-007565-17	SLC39A10	57181	NM_020342	187936947	CCACAAACCUGAUCGUGUA
L-007565-02	J-007565-18	SLC39A10	57181	NM_020342	187936947	UGCAUUAGCUGUAGGAACA
L-007565-02	J-007565-19	SLC39A10	57181	NM_020342	187936947	CAUGAAUGUUUGAACGUCA

L-007565-02	J-007565-20	SLC39A10	57181	NM_020342	187936947	AGAAAUAGAGAUCGAACCA
L-011398-00	J-011398-05	SVIL	6840	NM_003174	11496980	GGACUGAUGUCAAGGCAUA
L-011398-00	J-011398-06	SVIL	6840	NM_003174	11496980	GCCAUAAGGAAUCUAAAUA
L-011398-00	J-011398-07	SVIL	6840	NM_003174	11496980	GAAGAAAGGUUUGGCGUCA
L-011398-00	J-011398-08	SVIL	6840	NM_003174	11496980	UAACAAAGUUGGCGGGAUG
L-003718-00	J-003718-05	TMED10	10972	NM_006827	40255040	CCAAGAAAUUGAUUGAGUA
L-003718-00	J-003718-06	TMED10	10972	NM_006827	40255040	CAAACACUCGGGUCCUAUA
L-003718-00	J-003718-07	TMED10	10972	NM_006827	40255040	GGAAUGAGUUAUGCUGUUA
L-003718-00	J-003718-08	TMED10	10972	NM_006827	40255040	AAUAAUCACUGUAGGAGUA
L-008074-01	J-008074-09	TMED2	10959	NM_006815	21314646	CAGUAUGAAUCUUGACGGU
L-008074-01	J-008074-10	TMED2	10959	NM_006815	21314646	UGACAUUGGGACAGAUCUA
L-008074-01	J-008074-11	TMED2	10959	NM_006815	21314646	CGUGGAGAUUACAGGACCA
L-008074-01	J-008074-12	TMED2	10959	NM_006815	21314646	GCACAAAGCCUGAUAGUAC
L-007854-01	J-007854-09	TMED5	50999	NM_016040	47271455	AUUUGAAGCUCGUGAUCGA
L-007854-01	J-007854-10	TMED5	50999	NM_016040	47271455	CUUCAGGUGUCUAGGGGUA
L-007854-01	J-007854-11	TMED5	50999	NM_016040	47271455	AGUUGUAUGUCUACUCAAA

L-007854-01	J-007854-12	TMED5	50999	NM_016040	47271455	CGUAUUGUGAGUACUGAUA
L-007855-02	J-007855-17	TMED7	51014	NM_181836	208431786	CAGCAUGGGCAUAUGUAAA
L-007855-02	J-007855-18	TMED7	51014	NM_181836	208431786	ACACAUAAGUGCCAUACAU
L-007855-02	J-007855-19	TMED7	51014	NM_181836	208431786	UCGCAGUUGUUUAUAUCUA
L-007855-02	J-007855-20	TMED7	51014	NM_181836	208431786	GAAGUUGUCUUGCGGCUUU
L-007924-02	J-007924-17	TMED9	54732	NM_017510	94721306	GGACGCAGCUGUAUGACAA
L-007924-02	J-007924-18	TMED9	54732	NM_017510	94721306	CGGGCUGGGUAGAGUGAUG
L-007924-02	J-007924-19	TMED9	54732	NM_017510	94721306	AGUGCUUUAUUGAGGAGAU
L-007924-02	J-007924-20	TMED9	54732	NM_017510	94721306	ACAUCGGAGAGACGGAGAA
L-014203-01	J-014203-09	TOR1B	27348	NM_014506	14149652	CAGAAGUGGAUCCGCGGUA
L-014203-01	J-014203-10	TOR1B	27348	NM_014506	14149652	CGGAGUGUCUUACCGCAAA
L-014203-01	J-014203-11	TOR1B	27348	NM_014506	14149652	GUGAAUCUAUUGCGCGCAU
L-014203-01	J-014203-12	TOR1B	27348	NM_014506	14149652	UGGCAGAGGAAAUGACGUU
L-010676-00	J-010676-06	TXNDC5	81567	NM_030810	42794770	GCAGAGACCUUGACUCGUU
L-010676-00	J-010676-07	TXNDC5	81567	NM_030810	42794770	GAGCCAAGCGAAAGACGAA
L-010676-00	J-010676-08	TXNDC5	81567	NM_030810	42794770	CAAGAUCGCCGAAGUAGAC

L-010676-00	J-010676-09	TXNDC5	81567	NM_030810	42794770	GUAAGACUCUGGCUCCUAC
L-006632-00	J-006632-05	UGGT1	56886	NM_020120	71061444	GAGCUGACAUUGCGGAGUU
L-006632-00	J-006632-06	UGGT1	56886	NM_020120	71061444	CCAAGACUCCUGUGAAAUU
L-006632-00	J-006632-07	UGGT1	56886	NM_020120	71061444	GUAAUAAUCCGAUGACCAA
L-006632-00	J-006632-08	UGGT1	56886	NM_020120	71061444	GGGACGCUCUGAAGAUAUU
L-020850-00	J-020850-05	VDAC3	7419	NM_005662	25188178	GCUGAAGGGUUGAAACUGA
L-020850-00	J-020850-06	VDAC3	7419	NM_005662	25188178	GAACGAUGGCACUGAAUUU
L-020850-00	J-020850-07	VDAC3	7419	NM_005662	25188178	GGUCAUGCUUACACUGAUA
L-020850-00	J-020850-08	VDAC3	7419	NM_005662	25188178	GAACUUCUCUCUCUGCUAA
L-022568-02	J-022568-17	ZNF319	57567	NM_020807	55741867	AGGCCAGCUUUAAGACGUA
L-022568-02	J-022568-18	ZNF319	57567	NM_020807	55741867	CUGCUGAACAGGCCGACAA
L-022568-02	J-022568-19	ZNF319	57567	NM_020807	55741867	AAGUAAAGACAUUGACCGU
L-022568-02	J-022568-20	ZNF319	57567	NM_020807	55741867	GCUUCAAGUACGCGUCAGA
D-001206-13	D-001210-01	siGENOME Non-targeting Control	0		0	UAGCGACUAAACACAUCAA
D-001206-13	D-001210-02	siGENOME Non-targeting Control	0		0	UAAGGCUAUGAAGAGAUAC

D-001206-13	D-001210-03	siGENOME Non-targeting Control	0		0	AUGUAUUGGCCUGUAUUAG
D-001206-13	D-001210-04	siGENOME Non-targeting Control	0		0	AUGAACGUGAAUUGCUCAA
D-001206-14	D-001210-02	siGENOME Non-targeting Control	0		0	UAAGGCUAUGAAGAGAUAC
D-001206-14	D-001210-03	siGENOME Non-targeting Control	0		0	AUGUAUUGGCCUGUAUUAG
D-001206-14	D-001210-04	siGENOME Non-targeting Control	0		0	AUGAACGUGAAUUGCUCAA
D-001206-14	D-001210-05	siGENOME Non-targeting Control	0		0	UGGUUUACAUGUCGACUAA
D-001050-01	D-001050-01	siGENOME Lamin A/C Control	0		0	GGUGGUGACGAUCUGGGCU
D-001140-01	D-001140-01	siGENOME GAPD Control	0		0	UGGUUUACAUGUUCCAAUA
M-003317-01-0005	J-003317-13	Kif11	3832	NM_004523	13699823	GAGCCCAGAUCAACCUUUA
M-003317-01-0005	J-003317-14	Kif11	3832	NM_004523	13699823	GGAGAGGUCUAAAGUGGAA

M-003317-01-0005	J-003317-15	Kif11	3832	NM_004523	13699823	UCGGGAAGCUGGAAAUAUA
M-003317-01-0005	J-003317-16	Kif11	3832	NM_004523	13699823	GAAUAGGGUUACAGAGUUG

Table 2. 5. Information on siRNA's used

2.5 *In Silico* Methods

2.5.1 Samples Used for Proteomic Analysis

The samples used to produce the proteomic datasets used for this study were prepared by Dr Maia Kavanagh Williamson as follows. Huh-7 cells were either infected at a MOI of 5 with DENV-2, inactivated DENV-2 (iDV2; inactivation by heating at 56° C for 30 minutes) or mock infected. At 28 hours post-infection the cells were detached with trypsin/EDTA and harvested by centrifugation at 150 x *g* for 5 minutes. The cell pellets were washed twice with ice-cold PBS and the cells finally harvested by centrifugation at 800 x *g* for 5 minutes at 4° C. The cell culture supernatants were removed, and the cell pellets resuspended in ice cold TNMg buffer (containing 20 mM Tris-HCl [pH 8], 150 mM NaCl, 5 mM MgCl2, 10% glycerol) at a density of 1-2 x 10^7 cells/mL. The cells were allowed to swell on ice for 30 minutes with gentle agitation. The cells were then disrupted by passing progressively through 19- and 25-gauge needles 20 times each and 10 times through a 27-gauge needle. Cell lysis was confirmed by microscopy and the cell lysates divided into two aliquots. One aliquot was kept on ice and used as the whole cell lysate (WCL). The other aliquot was centrifuged at 800 x *g* for 12 minutes at 4 °C. The supernatants were removed to fresh tubes whilst the pellet fractions were resuspended in 100 µL of TNMg buffer and kept on ice (termed the "nuclear" fraction). The supernatants were centrifuged at 16,000 x *g* for 15 minutes at 4° C. The supernatants were removed to a fresh tube (termed "cytoplasmic" fraction) and the pellet fractions resuspended in 100 µL of TNMg buffer (termed "16K" fraction). An aliquot of the different fractions was sampled and heated with an equal volume of 2X sample buffer at 95° C for 10 minutes. The protein concentration in each sample was determined by bicinchoninic acid (BCA) assay. For this analysis 100 µg of the WCL and 16K fractions were used for proteomic analysis. The sample preparations were repeated independently in triplicate.

2.5.2 Tandem Mass Tag (TMT) Labelling, High pH Reversed-Phase Chromatography and Nano-LC Mass Spectrometry

Mass Spectrometry based proteomic analysis was undertaken in the University of Bristol Proteomics Facility by Dr Kate Heesom. A description of the methodology is included for completeness, as follows. Aliquots of cell lysates containing 100 µg of protein were digested with trypsin (2.5 µg trypsin per 100 µg protein; 37° C, overnight) and labelled with Tandem Mass Tag (TMT) eleven plex reagents according to the manufacturer's protocol (ThermoFisher Scientific) and the labelled samples pooled. See Tables 2.6 and 2.7 below for details on which tag was added to each condition in the WCL and 16K experiments, respectively. An aliquot of 50 µg of the pooled sample was desalted using a SepPak cartridge according to the manufacturer's instructions (Waters, Milford,

Massachusetts, USA). Eluate from the SepPak cartridge was evaporated to dryness and resuspended in buffer A (20 mM ammonium hydroxide, pH 10) prior to fractionation by high pH reversed-phase chromatography using an Ultimate 3000 liquid chromatography system (Thermo Scientific). The resulting fractions were evaporated to dryness and resuspended in 1% formic acid prior to analysis by nano-LC MS/MS using an Orbitrap Fusion Tribrid mass spectrometer (Thermo Scientific). High pH RP fractions were further fractionated using an Ultimate 3000 nano-LC system in line with an Orbitrap Fusion Tribrid mass spectrometer (Thermo Scientific). Peptides were ionized by nano-electrospray ionization at 2.0 kV using a stainless-steel emitter with an internal diameter of 30 µm (Thermo Scientific) and a capillary temperature of 275° C. All spectra were acquired using an Orbitrap Fusion Tribrid mass spectrometer controlled by Xcalibur 2.0 software (Thermo Scientific) and operated in data-dependent acquisition mode using an SPS-MS3 workflow. FTMS1 spectra were collected at a resolution of 120,000, with an automatic gain control (AGC) target of 200,000 and a max injection time of 50 ms. Precursors were filtered with an intensity threshold of 5000, according to charge state (to include charge states 2-7) and with monoisotopic precursor selection. Previously interrogated precursors were excluded using a dynamic window (60 s +/-10 part per million (ppm)). The MS2 precursors were isolated with a quadrupole mass filter set to a width of 1.2 m/z. ITMS2 spectra were collected with an AGC target of 10,000, max injection time of 70 ms and CID collision energy of 35%. For FTMS3 analysis, the Orbitrap was operated at 50,000 resolution with an AGC target of 50,000 and a max injection time of 105 ms. Precursors were fragmented by high energy collision dissociation (HCD) at a normalised collision energy of 60% to ensure maximal TMT reporter ion yield. Synchronous Precursor Selection (SPS) was enabled to include up to 5 MS2 fragment ions in the FTMS3 scan.

Condition	**Repeat**	**Tag**
Mock	1	126
Mock	2	127N
DV2	1	127C
DV2	2	128N
DV2	3	128C
iDV2	1	129N
iDV2	2	129C
iDV2	3	130N

Rep	1	130C
Rep	2	131N
Rep	3	131C

Table 2. 6. WCL conditions, repeats and tags.

Condition	**Repeat**	**Tag**
Mock	1	126
Mock	2	127N
DV2	1	127C
DV2	2	128N
DV2	3	128C
iDV2	1	129N
iDV2	2	129C
iDV2	3	130N
Rep	1	130C
Rep	2	131N
Rep	3	131C

Table 2. 7. 16K Conditions, repeats, and tags

2.5.3 Raw Data Analysis

The raw data files were processed and quantified using Proteome Discoverer software v2.1 (Thermo Scientific) and searched against the UniProt Human database (downloaded September 2017: 140000 entries) plus a bespoke list of proteins encoded by DENV-2 strain using the SEQUEST algorithm. Peptide precursor mass tolerance was set at 10 ppm, and MS/MS tolerance was set at 0.6 Daltons (Da). Search criteria included oxidation of methionine (+15.9949) as a variable modification and carbamidomethylation of cysteine (+57.0214) and the addition of the TMT mass tag (+229.163) to peptide N-termini and lysine as fixed modifications. Searches were performed with full tryptic digestion and a maximum of 2 missed cleavages were allowed. The reverse database search option was enabled, and all data were filtered to satisfy a false discovery rate (FDR) of 5%. Protein abundances were normalised to total peptide amount. The protein grouping from the proteome discoverer analysis was taken, and the master protein selection improved using an in-house method

that maintains ID quality but improves protein annotation. The normalised abundances were $\log_2$ transformed to bring the data closer to a normal distribution. Statistical significance was calculated using a Welch's T-Test and corrected for multiple testing using the Benjamini-Hochberg FDR method. Due to the variations in the powers of t-tests between different sample sizes, FDR-adjustment using the Benjamini-Hochberg method was only performed on proteins that had been quantified in all samples. The raw data processing was done by Dr Kate Heesom and Dr Phil Lewis in the Proteomics Facility and the data provided for this project as Excel spreadsheets.

2.5.4 Data Handling in Excel, Perseus, and Prism

In Excel, true/false formulas were applied to the WCL and 16K data sets to determine if a protein hit was significantly altered by at least 1.5-fold or 2.0-fold with a p-value of >0.05. These were carried out on (but not limited to) dengue virus infected Huh-7 cells (DENV-2) compared to Mock infected, DENV-2 compared to iDV2, and Huh-7 replicon cells (Rep) compared to Mock.

Then, the Excel documents were saved as .txt files and imported into the bioinformatic analysis software Perseus v1.6.6.0 (Tyanova, S. *et al.,* 2016) to enable further statistical analysis of the data. Principle component analysis (PCA), histograms, multiple scatter plots and volcano plots were made using the normalized $\log_2$ abundance values for each protein.

Multiple scatter plots comparing each replicate of each condition to each other were made using the default settings, and R^2 correlation was applied. Histograms of each repeat were made, also using the default settings. To perform PCA analysis, the matrix was cloned, and the proteins were filtered to contain only those that were identified in each repeat of each condition. PCA was performed using the default settings in Perseus v1.6.6.0 and the groups were colour coded.

Even though the preliminary data handling by Phil Lewis had removed non-human proteins and contaminants from the data set, the original matrix containing all the protein hits was filtered again in Perseus to remove any that might be left as a precaution. Then, the repeats of each condition were each grouped together, and the matrices filtered based on the true/false formulas applied in Excel to produce lists of significantly changed proteins.

The raw numbers of proteins altered significantly ($p < 0.05$) in abundance were added to Prism v9.6.0. Figure 2.1 below is schematic of the process described above.

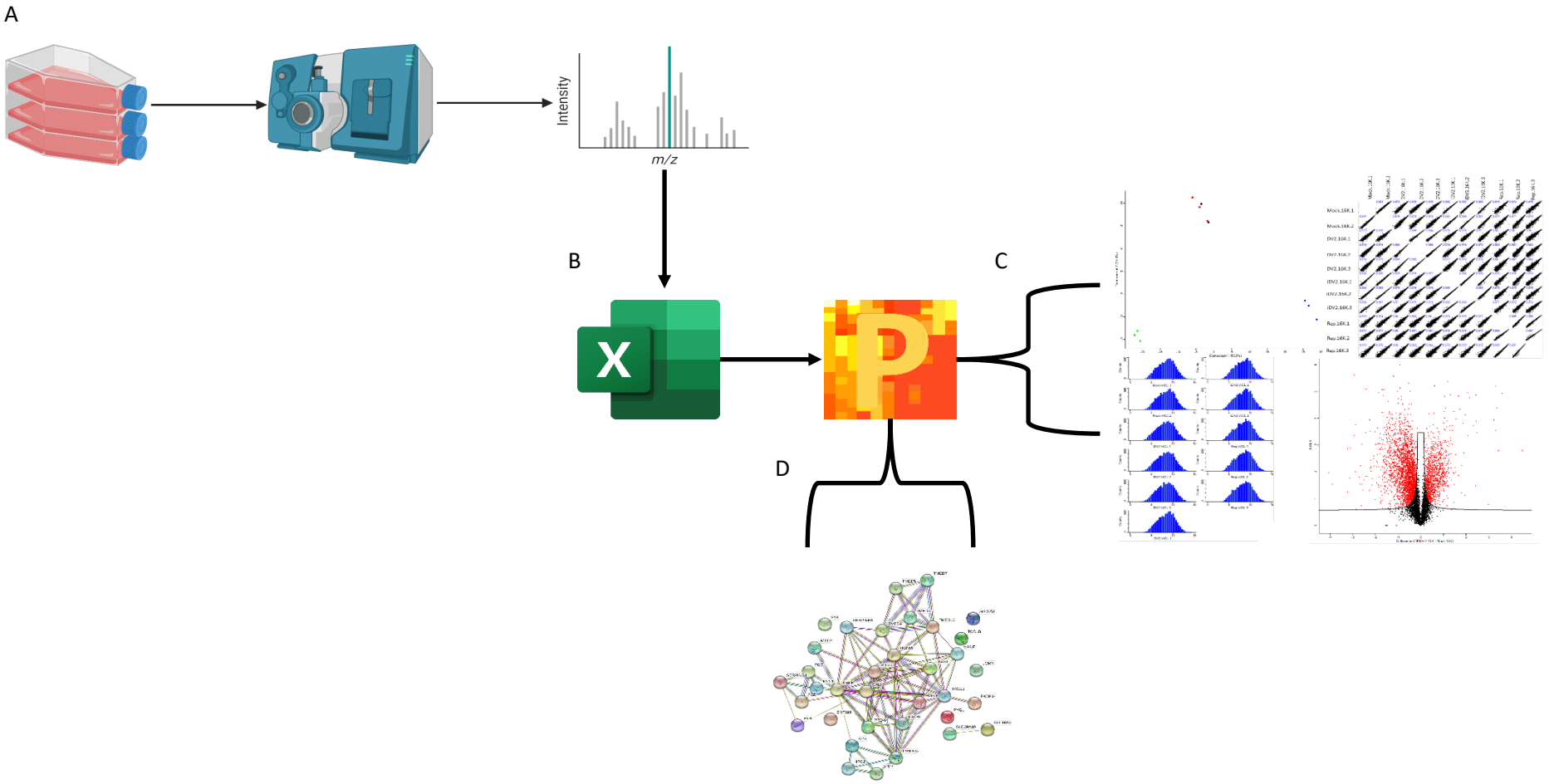

Figure 2. 1. Workflow of bioinformatics carried out during this present study. A) Sample preparation, TMT and data preparation performed by Dr Maia Kavanagh Williamson, Dr Kate Heesom and Dr Phil Lewis respectively (Dr Kate Heesom performed both the TMT and data preparation). B) Once the data was provided by Dr Phil Lewis it was formatted in Excel and transferred to Perseus. C) Initial data analysis was performed in Perseus, including PCA, multi-scatter plots, histograms and volcano plots for each data set and condition. D) Lists of significantly altered proteins were exported and ran through PANTHER v16, DAVID v6.8, STRING v11.0/v11.0b/v11.5, and FunRich v3.1.3, represented by an example STRING network (Szklarczyk et al., 2019). Figure made in BioRender.com and Microsoft Powerpoint. Thumbnails for Excel and Perseus taken from program icon.

2.5.5 Downstream Analysis

The downstream analysis programs used for Gene Ontology (GO) enrichment analysis were DAVID v6.8 (Huang, *et al*., (2009), FunRich v3.1.3 (Fonseka, *et al.* 2021), PANTHER v16.0 (Mi, *et al.* 2021), and STRING v11 and v11.5 (Szklarczyk, *et al.* 2019). Uniprot accession numbers were copied from the protein lists in Perseus and added to all downstream analysis programs.

Uniprot accession numbers were supplied to DAVID (Database for Annotation, Visualisation, and Integrated Discovery) v6.8 as a gene list and functional enrichment was carried versus the default human proteome. DAVID v6.8 provides functional annotation clustering data, a functional annotation chart and a functional annotation table. Classification stringency was set to "Medium", and the EASE Score threshold was set to 1.0.

STRING (Search Tool for the Retrieval of Interacting Genes/Proteins) analysis was then performed using a minimum required interaction score of "Medium Confidence (0.4)" to generate functional protein association networks generating GO terms enriched within these lists of Uniprot accession numbers. Versions 11.0 and 11.5 were all used at different points during this study.

Uniprot accession numbers of significantly changed proteins were entered into the PANTHER (Protein ANalysis THrough Evolutionary Relationships) v17.0 Online Classification System software and using the default settings Functional Classification of GO:slim terms were produced as bar charts and a table.

Uniprot accession numbers were added to FunRich v3.1.3 and Venn diagrams were made comparing compositions of the lists, and functional enrichment analysis of the cellular components was performed against the Uniprot protein database, and the top five enriched terms were exported as an automatically generated graph.

Chapter 3: Proteomics of DENV-2 Replication in Huh-7 Cells

3.1 Introduction

Bioinformatics has been used to study and learn about the interaction between DENV and the host in a variety of ways. These include metabolomic analysis of human sera and urine, metabolites in humanised mice (known as humice), as well as a plethora of *in vitro* proteomic and transcriptomic studies.

The *in vitro* studies have been performed using a range of cell lines, including hepatic cells which are and biologically relevant for DENV infection (Clyde et al., 2006). Through mass spectrometry, metabolomic and lipidomic analyses of the sera of patients with a range of dengue disease severities have been studied. Overall, the findings show liver dysfunction, and perturbations in the pathways of fatty acid β-oxidation, phospholipid catabolism, and amino acid and nucleotide metabolism (Cui et al., 2013, 2018). Other analysis of the urine of dengue positive patients also showed alterations in the levels of a range of metabolites, including citrate, further supporting the idea that a range of metabolic pathways are affected by DENV infection (El-Bacha et al., 2016). Mice are not normally a good model for DENV infection, as they are not a natural host, but humice have been used for sera metabolomic analysis. This study showed that although they do not develop a viraemia like humans, humice are a relatively good model to use as they share a lot of the same metabolite alterations as humans infected with DENV (Cui et al., 2017).

A 2014 study of DENV infected Huh-7 cells using label free liquid chromatography mass spectrometry (LC-MS) identified 2300 proteins and found 155 proteins that were altered at least two-fold in amount in infected cells – 41% were increased (Pando-Robles et al., 2014). The top enriched Kyoto Encyclopaedia of Genes and Genomes (KEGG) pathways from the analysis were related to metabolism, including the TCA cycle and glycolysis (Pando-Robles et al., 2014). A SILAC-based LC-MS proteomic study of DENV infected A549 cells published in 2014 provided similar results. In this study the DENV-2 and mock infected A549 cells were fractionated into nuclear and cytoplasmic portions using centrifugation steps, leading to the reliable identification of 2115 and 3098 proteins in each fraction respectively (Chiu et al., 2014). The gene enrichment analysis performed on proteins found to be increased in amount in DENV-2 infected cells compared to mock cells identified terms related to the interferon response and the ER and

ER membrane, while proteins that were decreased were associated with terms linked to the electron transport chain and fatty acid biosynthesis pathways (Chiu et al., 2014).

More recently, a phosphorylation-based approach to proteomics identified 2263 host proteins and 799 host phosphoproteins using LC and tandem mass spectrometry (together referred to as LC-MS/MS) altered in K652 cells during DENV infection (Miao et al., 2019). This study found several ribosomal proteins and translation factors that were altered during DENV infection, as well as several RNA splicing proteins (Miao et al., 2019). This study highlights the ever-expanding power of proteomics by showing that new questions that can be asked of big data and that more proteins can be found using these techniques.

In this study a downstream bioinformatic analysis of proteomic data produced using DENV-2 infected Huh-7 cells was performed. The proteomic data was produced by analysis of Huh-7 cells infected with DENV-2 and of Huh-7 replicon cells compared to the Mock infected Huh-7 cells (see section 2.5 for details). Proteins in each fraction were then identified and quantitated using Tandem Mass Tagging (TMT) and mass spectrometry. TMT can be used to identify and quantify proteins of multiple samples simultaneously. In this case, 11 samples were analysed. The identities of the proteins were matched to their measured abundances, and these data were the starting point for the bioinformatic analysis described below.

The results of the t tests were used in formulas to create lists of proteins significantly altered in abundance in each comparison. The data was imported into Perseus v1.6.6.0 where preliminary statistical analysis could be performed to assess the data, including, but not limited to, histograms and scatter plots. Then the protein hits were filtered to produce more easily manageable lists of proteins altered in abundance and the protein's UniProt accession numbers were then analysed using downstream (DS) analysis programs.

Functional enrichment analysis using downstream analysis programs was the basis for choosing a set of candidates for siRNA mediated knockdown and analysis on their importance on the DENV-2 life cycle – primarily DENV-2 replication (described in Chapter 4).

The inclusion of the replicon data sets was done to better understand whether a replicon system was a suitable surrogate to study DENV-2 genome replication. It has been shown DENV replicon systems respond to antivirals the same way DENV-2 does in infected cells (Massé et al., 2010), and so it was important to find out if the replicon impacts cellular protein levels in the same way as the functional virus.

3.2 Results

3.2.1 Initial Statistical Interrogation

Initially, principal component analysis (PCA) was performed (section 2.5.5) to visualise the variance between the proteomic datasets from each of the repeat experiments. Each repeat is represented by a point on the graph. The more closely positioned the points of the replicates, the higher the correlation between, and so the more reliable the data. As expected, the PCA plot (Figure 3.1) showed there was minimal variance between the replicates belonging to the DENV2, iDV2, and Mock conditions. However, the repeats belonging to the replicon cells showed that while two of the repeats (Rep.16K.1 and Rep.16K.2) are similar, the third (Rep.16K.3) was an outlier.

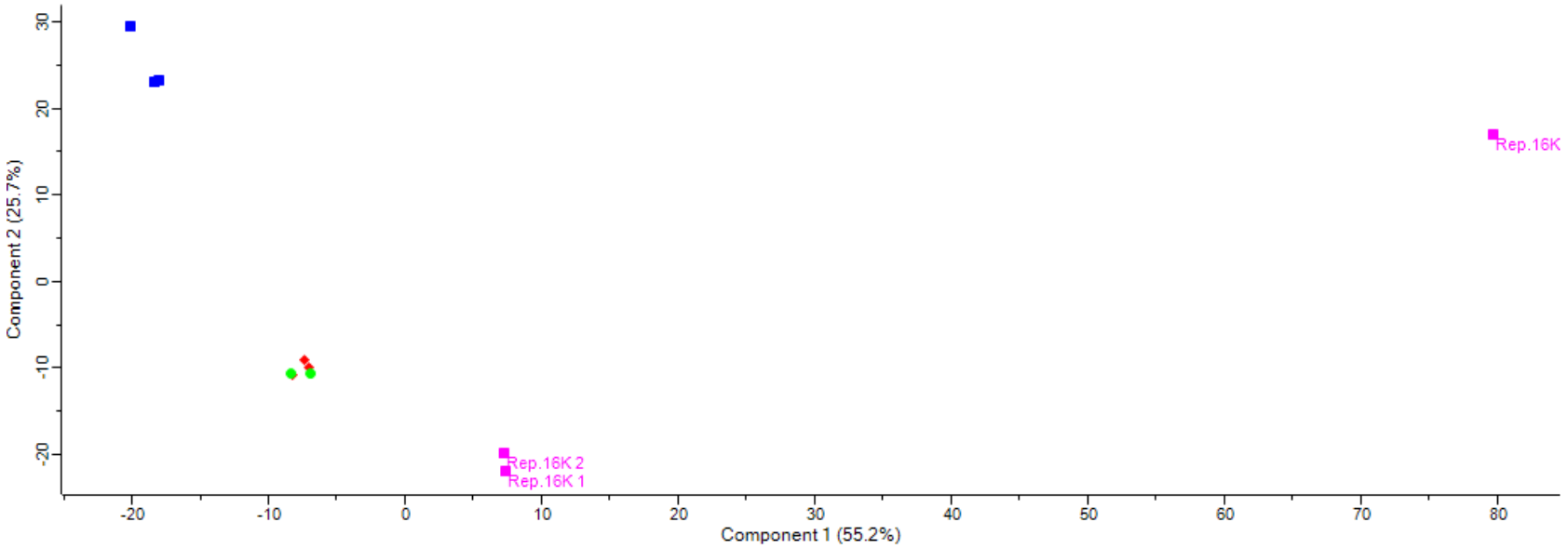

Figure 3. 1 PCA plot of the repeat data sets for each condition, made in Perseus v1.6.6.0. Blue – DENV-2, Red – iDV2, Green – Mock, Pink – Rep cells. Note the outlier Rep.16K.3 on the right-hand side of the plot.

Following PCA, histogram plots of the data sets were made to visualise the distribution of the data (Figure 3.2). Each histogram shows a normal distribution of the data, and the repeats of each of the conditions showed the same distribution, aside from the Rep.16K.3 data set.

Multiple scatter plots (Figure 3.3) of all the data sets were made to show correlations between them using Pearson's correlation coefficient. The Pearson's correlation coefficient is shown in blue in the top left-hand corner of each plot – the closer the value is to 1 the better the correlation between the two conditions. The analysis also reflects the strong correlation between the repeats. The multiple scatter plots show some slight deviation between the conditions but all the R^2 values are greater than 0.9. Although the correlation between the Rep.16K.1 and Rep.16K.2 data sets is very high (R^2 of 0.993), the Rep.16K.1 and Rep.16K.3 and Rep.16K.2 and Rep.16K.3 data sets correlated less well with R^2 values of 0.765 and 0.77 respectively. The correlation between the mock and iDV2 data sets is also very strong, all the R^2 values are above 0.991, Mock.16K.1 and iDV2.16K.2 has an R^2 of 0.997.

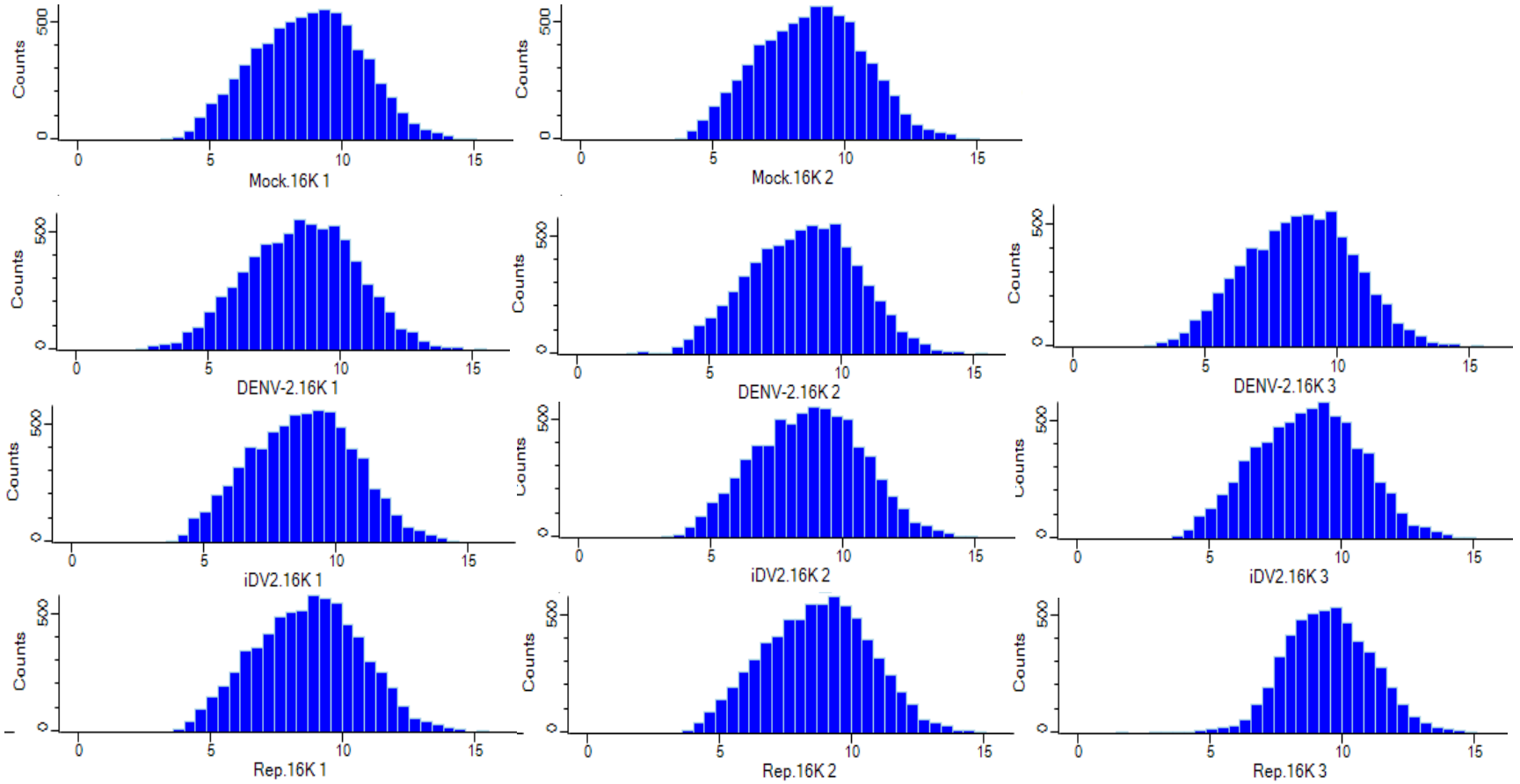

Figure 3. 2. Multiple histograms showing the distribution of data in each of the repeat data sets for each experimental condition, made using Perseus v1.6.6.0. Mock (top); DENV-2 infected cells (DV2) (second from the top); iDV2 infected cells (iDV2) (second from the bottom) and Rep cells (Rep) (bottom).

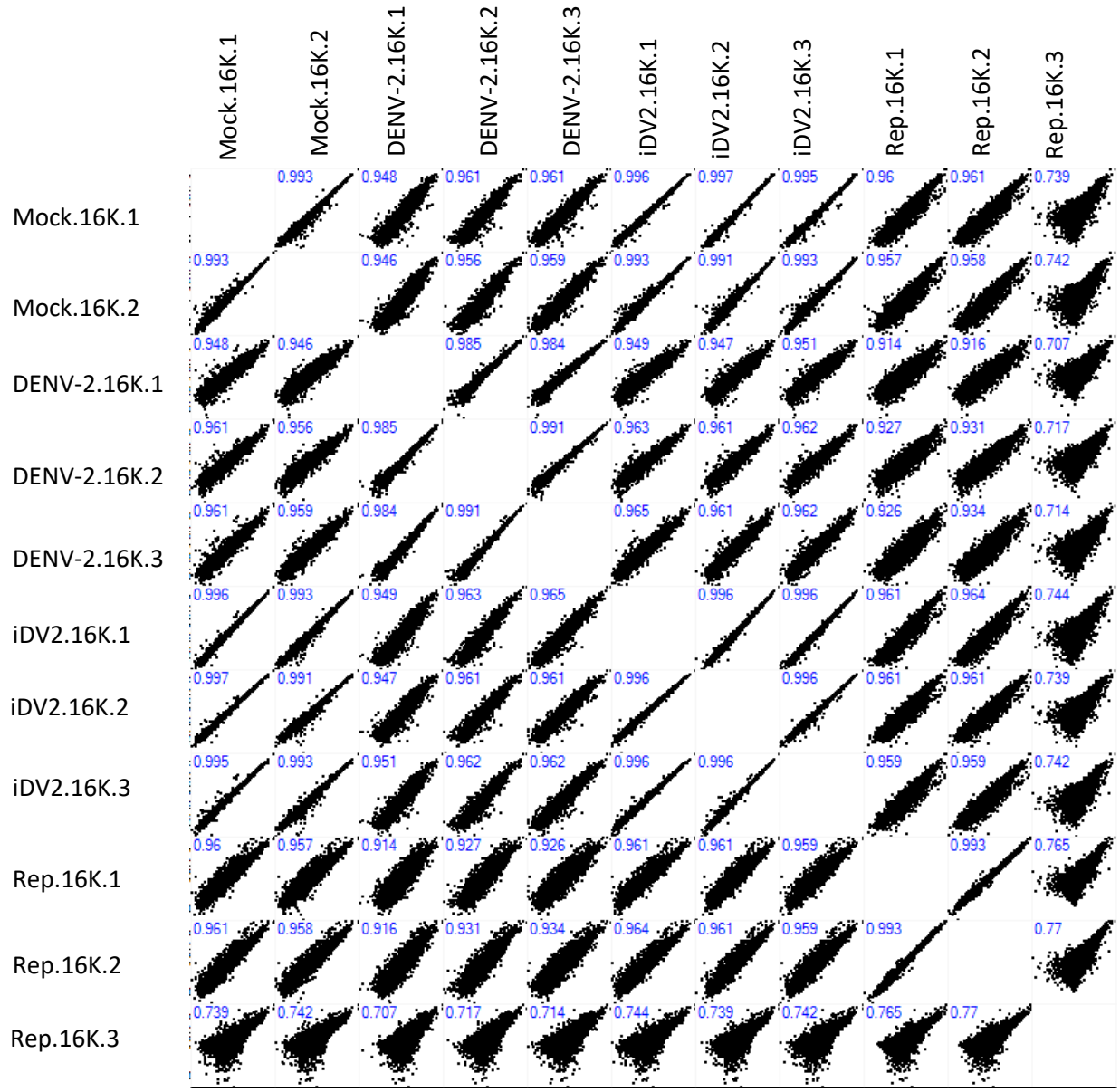

Figure 3. 3. Multiple scatter plots of each repeat from each condition plotted against each other, with the correlation of the plot described using the Pearson's correlation in blue in the top left of each graph, made using Perseus v1.6.6.0. Data sets derived from mock infected cells (Mock); DENV-2 infected cells (DENV-2); iDV2 infected cells (iDV2) and replicon cells (Rep).

Overall, the PCA, histogram and scatterplots showed that the replicate data sets were reliable except for the Rep.16K.3 data set which showed some variation from the Rep.16K.1 and Rep.16K.2. The Rep.16K.3 data set could have been left out, and only the Rep.16K.1 and Rep.16K.2 data sets included in the downstream analysis (there were only two mock infection data sets). However, a decision was made to retain the Rep.16K.3 data set in the downstream analysis for completeness of data. If the experiment was repeated, more data sets from replicon cells could be included.

3.2.2 Statistically Significant Proteins

To examine changes in the host proteome in response to different stimuli, downstream proteomic analysis typically focuses on proteins that have a statistically significant fold change in abundance between two different conditions. In this analysis, the significance was set as p-value of less than 0.05 and an increase or decrease in abundance of either 1.5- or 2.0-fold or more compared to the control examined as threshold cutoff values. The threshold values were arbitrary; previous DENV-host cell proteomic studies have used 1.3-fold (Yousef, 2016) and 2.0-fold (Pando-Robles et al., 2014). Initially, a cutoff threshold of 1.5-fold change was used, but as the total number of proteins in the DENV-2/Mock data sets was large, the second stricter cutoff threshold of 2.0-fold change was used to provide more stringency in the bioinformatic analysis.

As significance and fold change values were already present in the supplied Excel data sets, the next step was to use Perseus to apply filters to select significantly altered proteins with the different fold-change thresholds between conditions. Table 3.1 and Figures 3.4 and 3.5 below show the numbers of proteins in comparison, and their proportion to the rest of the data set and to the other significantly altered proteins.

There was a total of 7247 reliably identified human proteins in the 16K fraction. There were 2.3 times more proteins statistically significantly altered in abundance at least 1.5-fold in the DENV-2 infected cells compared to mock than the replicon cells compared to the mock. In the DENV-2 data, many more proteins were calculated to be decreased in amount than increased compared to the mock infected cells, but this was the other way round in the replicon data sets – more proteins were increased in amount than decreased.

Ratio of conditions	**FC**	**Number of proteins increased (% of total)**	**Number of proteins decreased (% of total)**	**Total number of proteins significantly changed (% of total)**
DENV-2/Mock	1.5	400 (5.52)	961 (13.26)	1361 (18.78)
DENV-2/Mock	2.0	120 (1.66)	383 (5.28)	503 (6.94)
Rep/Mock	1.5	320 (4.42)	263 (3.63)	583 (8.04)
Rep/Mock	2.0	185 (2.55)	87 (1.20)	272 (3.75)

Table 3. 1. The numbers of significantly ($p < 0.05$) altered proteins in the 16K fraction from DENV-2 infected and replicon cells compared to mock with fold change (FC) cutoffs of 2 and 1.5.

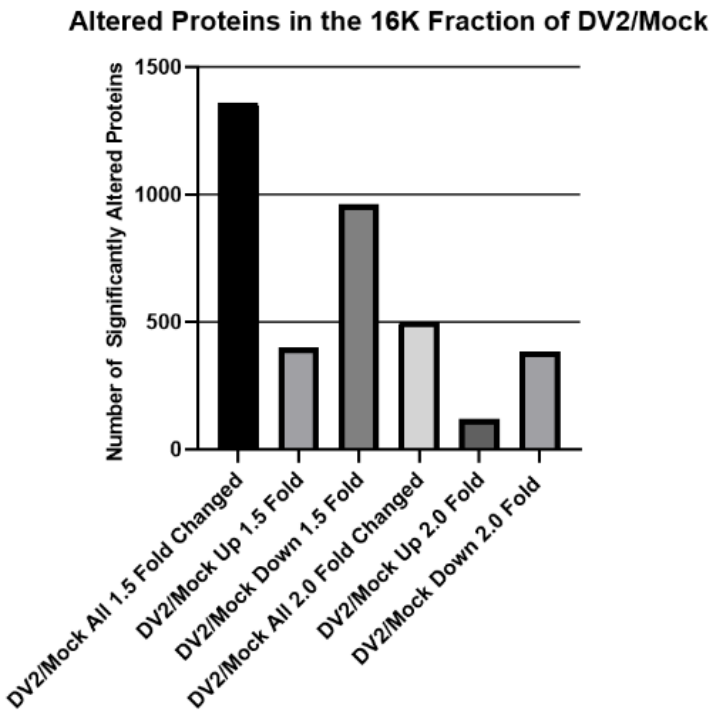

Figure 3. 4. Numbers of significantly altered proteins in the 16K fraction of DENV-2 infected Huh-7 cells (DV2) compared to the mock-infected cells.

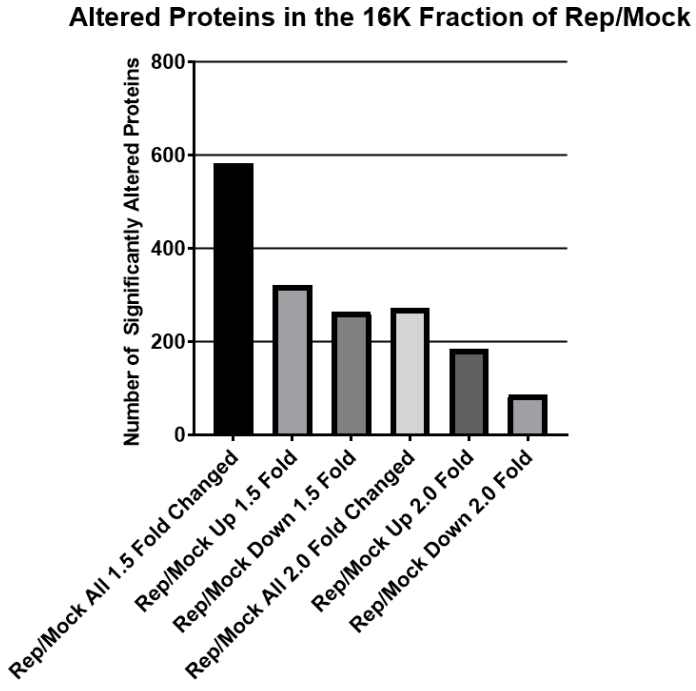

Figure 3. 5. Numbers of significantly altered proteins in the 16K fraction of Huh-7 replicon cells (Rep) compared to the mock-infected cells.

Comparing the proteins in the 16K fraction isolated from DENV-2 infected cells with those from cells incubated with iDV2 would be a more biologically relevant comparison than comparing to proteins in the 16K fraction isolated from mock infected cells, as well as more statistically robust, as there were three replicates of the iDV2 data and only two of the mock data. However, a Welch's t-test had not been calculated comparing the replicon data with the iDV2 treated Huh-7 cells, so for consistency the mock data sets were used for comparison against both DENV-2 infected and replicon containing cells. Comparative analysis of the iDV2 and mock data sets supported this decision, as described below in section 3.2.8.

To better visualise the significantly altered proteins, volcano plots were made for the proteins detected in the 16K fraction of DENV-2 infected and replicon cells compared to mock infected cells (Figures 3.6 and 3.7 respectively). The plot made with the DENV-2/mock data (Figure 3.6) shows that there is a skew in the distribution of the protein population to the left, indicating there are more proteins decreased than increased in abundance in DENV-2 infected cells compared to mock. Indeed, this was confirmed by analysis of the raw numbers of proteins altered (Table 3.1). The number of significantly decreased and increased proteins was 961 and 400 respectively.

The volcano plot of the replicon data compare to the mock-infected data (Figure 3.7) shows no obvious skew in the number of significantly altered proteins in each group. This is reflected in the raw numbers of proteins altered; 320 increased and 263 decreased (significantly) (Table 3.1). However, the plot does have a wider spread of data points in the increased (right hand) portion of the graph.

Volcano plots can used be as a way of identifying significantly altered proteins for downstream analysis, but they were not utilized in this manner in the present study. Perseus v1.6.6.0 is a powerful tool for bioinformatics, but the volcano plot function does not have the sensitivity to produce lists of proteins that were increased or decreased. Furthermore, the t-tests were more stringent and proved easier to handle in Excel.

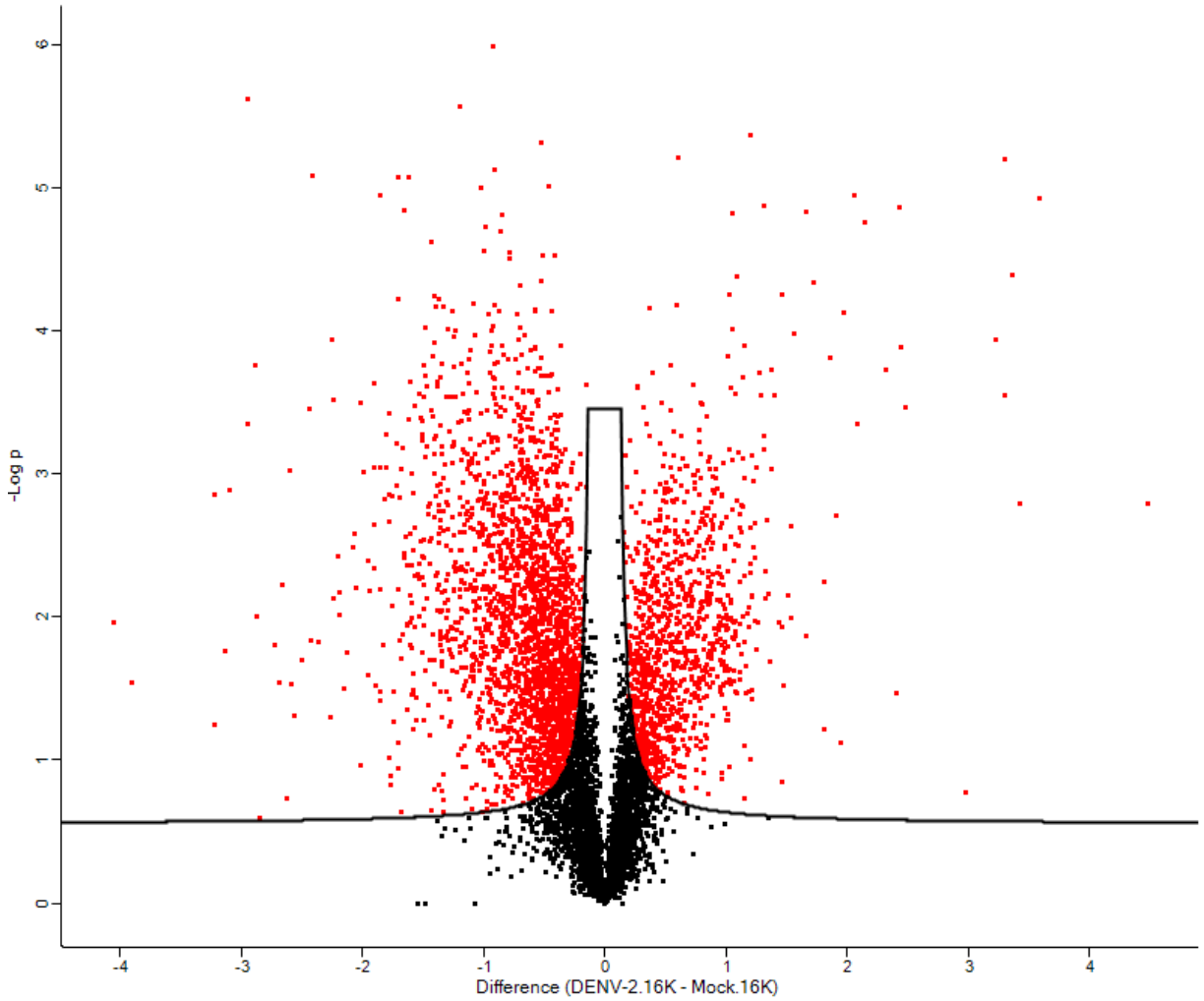

Figure 3. 6. Volcano plot made in Perseus v1.6.6.0 showing the distribution of proteins significantly altered in abundance in the 16K fraction from DENV-2 infected cells compared to mock infected cells (shown above the curve as red squares)

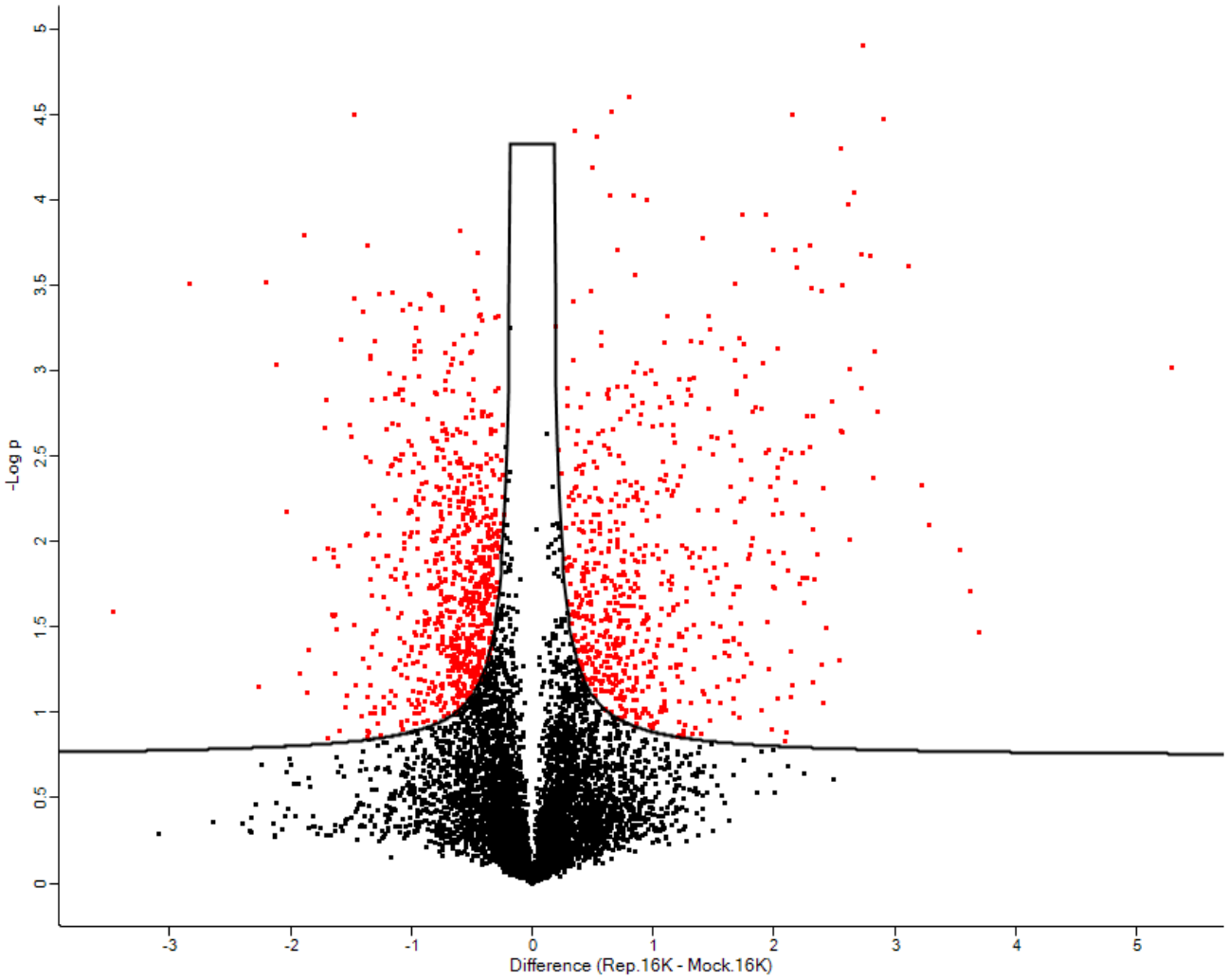

Figure 3. 7. Volcano plot made in Perseus v1.6.6.0 showing the distribution of proteins significantly altered in abundance in the 16K fraction from replicon containing cells compared to the mock infected cells (shown above the curve as red squares).

3.2.3 Downstream Analysis of 16K Data

Initial downstream analysis of the proteins significantly altered in amount in the 16K fractions from DENV-2 and replicon cells compared to mock cells was carried out using PANTHER v16.0, FunRich v3.1.3, STRING v11.0 and DAVID v6.8. The initial analysis was to gain a broad understanding of the Gene Ontology (GO) terms associated with proteins that were significantly changed in abundance either at least 1.5- or 2.0-fold in DENV-2 or replicon cells compared to the mock-infected cells.

PANTHER v16.0 was used to provide a broad overview of the GO enrichment in the protein lists by reducing the annotations into GO:slim terms, making it easier to see trends in the lists of significantly altered proteins. FunRich v3.1.3 was used to make quantitative Venn diagrams comparing the proteins in different conditions, and to provide figures of cellular compartment enrichment analysis (defined below).

STRING v11.0 was used initially (and v11.5 for some of the analysis later in the study) and has many uses, including making protein-protein interaction networks and general GO enrichment information, but in this study, STRING was used to identify the Reactome pathway, cellular compartment and biological process terms most significantly associated with the altered proteins. The protein-protein interaction network is built on “nodes” of identified proteins and their theoretical and experimental interaction evidence (Szklarczyk et al., 2019). Finally, DAVID v6.8 was used to provide detail on the most enriched GO terms and then to focus on specific pathways and sets of proteins for further investigation.

The UniProt accession numbers of significantly altered protein lists were imported into each of the programs listed above. Some of the accession numbers were not recognised by the downstream analysis software and so there was some discrepancy between the number of input proteins and output hits.

Four GO terms will be used throughout the following proteomic analysis: molecular function, biological process, cellular compartment and Reactome pathway. Molecular function defines the action or activity at the molecular level of a specific gene product. Biological process refers to a large order process completed by multiple molecular events. The cellular compartment is the location in the cell in which a protein has been identified (Ashburner et al., 2000; Carbon et al., 2021). Reactome is a database of pathways and reactions, and so a highly enriched Reactome pathway is likely to be altered in the same way as proteins contributing to that term (Gillespie et al., 2022).

Significance of the enrichment by FunRich v3.1.3 was measured by p-value, and the top cellular compartment terms were ranked by p-value. Enrichment terms generated by PANTHER v16 analysis

were ranked by number of proteins contributing to that term as a percentage of the total number of proteins that make up that term. STRING (both v11.0 and v11.5) produced multiple functional enrichments, which were all ranked by false discovery rate (FDR). DAVID v6.8 ranks annotation clusters based on their calculated enrichment score (EASE score) which is the $-\log_{10}$ of the mean of the p-values of terms making up that cluster – thus a larger EASE score indicates greater enrichment.

3.2.3.1 Proteomic Changes in Huh-7 Cells After Dengue Virus Infection

3.2.3.1.1 All 1.5-Fold Changed Proteins in DENV-2/Mock

There were 1361 proteins that were significantly increased or decreased by ≥1.5-fold in the 16K fraction from DENV-2 infected cells compared to mock infected cells. This list of proteins was imported into PANTHER v16.0 and a list of the top GO:slim terms was produced (multiple GO:terms into one GO:slim to provide an overview of the functional enrichment).

Of the 1361 proteins imported, there were 1219 recognised and 857 functional hits. The top two molecular function terms were: Catalytic Activity (28.2%), Binding (26.3%) – table 3.2.

Category name (Accession)	**Number of proteins**	**Percent of proteins in the category vs total number of proteins in the dataset.**
Catalytic activity (GO:0003824)	344	28.20%
Binding (GO:0005488)	321	26.30%
Molecular function regulator (GO:0098772)	68	5.60%
Transporter activity (GO:0005215)	50	4.10%
Structural molecule activity (GO:0005198)	28	2.30%

Table 3. 2. Top five molecular function GO:slim terms of the proteins altered ≥ 1.5-Fold as assigned by PANTHER v16

The Uniprot accessions were added to FunRich v3.1.3 and cellular compartment enrichment analysis was performed. A graph was made showing percentage of proteins associated and the $-\log_{10}$ p-value of each term (Figure 3.8). The top five cellular compartment terms (as ranked by p-value) are shown. Almost 25% of the proteins identified were associated with the term mitochondria, and around 15% were associated with nucleolus.

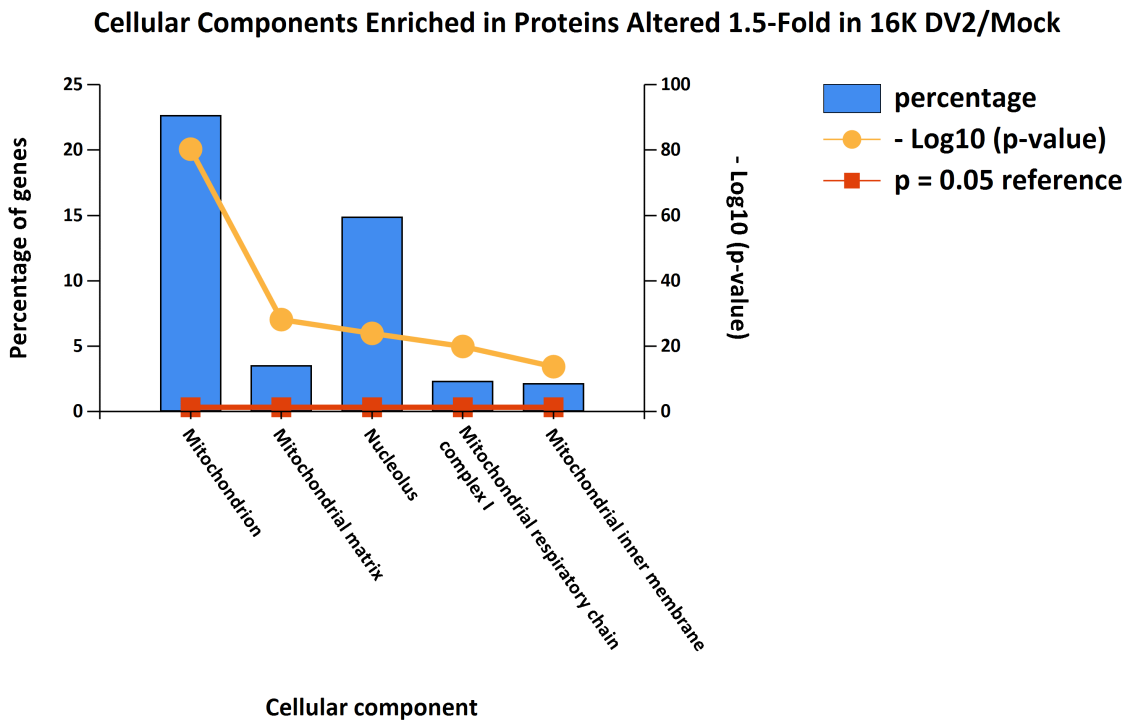

Figure 3. 8. Graph showing cellular compartment enrichment of proteins changed ≥ 1.5-fold in the 16K of DENV-2 infected cells, made in FunRich v3.1.3.

The list of proteins significantly altered 1.5-fold or more in the 16K fraction from DENV-2 infected cells compared to mock infected cells was imported into STRING v11.0, which produced 1261 nodes. The top Reactome pathway of these proteins (shown in Table 3.3) were metabolism (3.31×10^{-36}), the TCA cycle and respiratory electron transport (1.19×10^{-27}), respiratory electron transport, ATP synthesis by chemiosmotic coupling, and heat production by uncoupling proteins (4.21×10^{-22}) and respiratory electron transport (2.49×10^{-17}).

Due to the reductive nature of functional annotations these are repeated, further investigation of the proteins by DAVID 6.8 was necessary. These data gave an indication of the types of cellular pathways affected by DENV-2 infection.

Term ID	Term Description	Observed	Background	FDR
HSA-1430728	Metabolism	300	2032	$3.31x10^{-36}$
HSA-1428517	The citric acid (TCA) cycle and respiratory electron transport	72	173	$1.19x10^{-27}$
HSA-163200	Respiratory electron transport, ATP synthesis by chemiosmotic coupling, and heat production by uncoupling proteins.	55	123	$4.21x10^{-22}$
HSA-611105	Respiratory electron transport	44	100	$2.49x10^{-17}$
HSA-156827	L13a-mediated translational silencing of Ceruloplasmin expression	43	107	$7.30x10^{-16}$

Table 3. 3. Top Reactome pathways for the proteins significantly altered ≥ 1.5-fold in the 16K fraction from DENV-2 infected cells compared to mock infected cells as assigned by STRING v11.0.

Of the 1361 proteins imported into DAVID 6.8, 1280 proteins were identified. Forty-one proteins contributed to the top Annotation Cluster (Table 3.4), which clearly identified mitochondrial respiration as a key process altered by DENV-2 infection.

Annotation Cluster 1	**Enrichment Score: 20.58**			
Category	**Term**	**Count**	**%**	**p-value**
UP_KEYWORDS	Respiratory chain	34	2.66	$1.32x10^{-23}$
GOTERM_BP_DIRECT	GO:0032981~Mitochondrial respiratory chain complex I assembly	35	2.73	$4.65x10^{-23}$
GOTERM_CC_DIRECT	GO:0005747~Mitochondrial respiratory chain complex I	29	2.27	$1.70x10^{-20}$
GOTERM_BP_DIRECT	GO:0006120~Mitochondrial electron transport, NADH to ubiquinone	29	2.27	$3.89x10^{-20}$
GOTERM_MF_DIRECT	GO:0008137~NADH dehydrogenase (ubiquinone) activity	28	2.19	$2.99x10^{-19}$

Table 3. 4. Most enriched functional annotation cluster of proteins altered in abundance ≥ 1.5-fold in the 16K fraction from DENV-2 infected cells compared to mock infected, assigned by DAVID v6.8.

3.2.3.1.2 All 2.0-Fold Changed Proteins in DENV-2/Mock

Five hundred and three proteins were either increased or decreased in abundance 2-fold or more in the 16K fraction of Huh-7 cells infected with DENV-2 compared to mock infected cells. Analysis using PANTHER v16 categorised these proteins into GO:slim terms and provided a list of the most enriched molecular function terms. The top 3 most enriched molecular function terms of these 503 proteins were: Catalytic Activity (27.4%), Binding (25.1%) and Transporter Activity (4.8%). The top five are shown in Table 3.5.

Category name (Accession)	**Number of Proteins**	**Percent of Proteins in the Category vs Total Number of Proteins in the Dataset.**
Catalytic activity (GO:0003824)	121	27.40%
Binding (GO:0005488)	111	25.10%
Transporter activity (GO:0005215)	21	4.80%
Molecular function regulator (GO:0098772)	19	4.30%
Molecular transducer activity (GO:0060089)	16	3.60%

Table 3. 5. Top five most enriched molecular function terms of all proteins altered ≥ 2.0-Fold in the 16K fraction from DENV-2 infected cells compared to mock infected cells as assigned by PANTHER v16

After adding the Uniprot accessions to FunRich v3.1.3, the top five cellular compartment (as ranked by p-value) were graphed (Figure 3.9). The graph shows that over 25% of proteins are related to the term mitochondrion, and a further 10% of proteins are related to mitochondria in some way. All the terms had a p-value of less than 0.05.

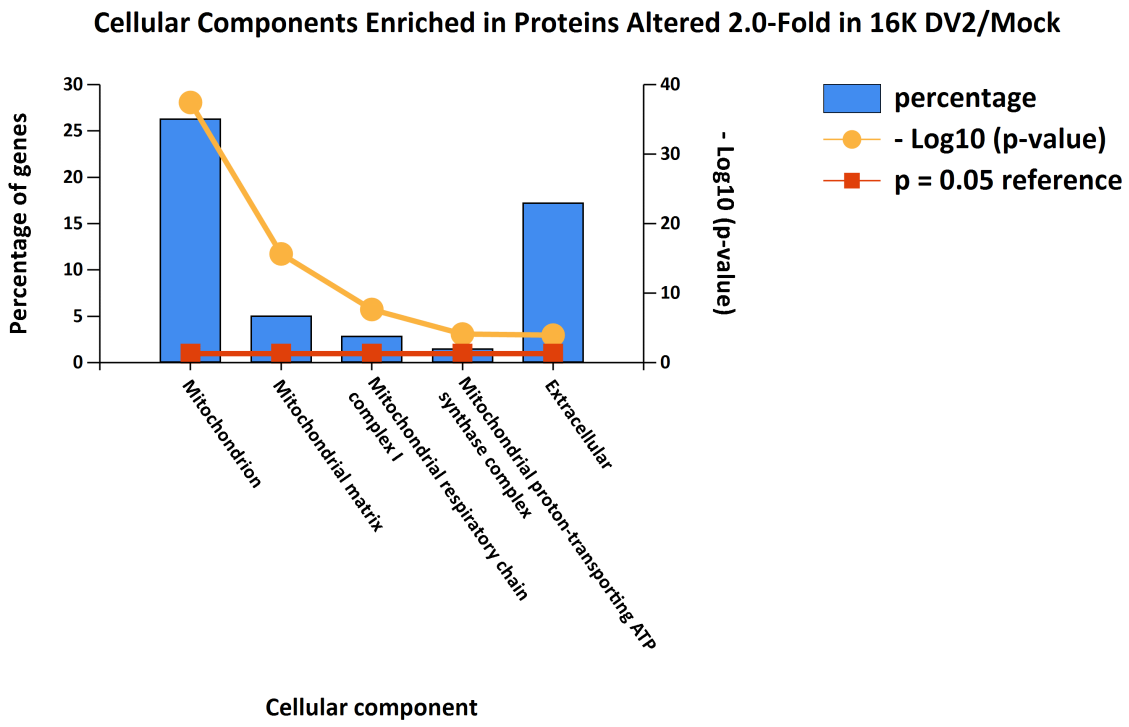

Figure 3. 9. Graph showing cellular compartment enrichment in proteins changed ≥ 2.0-fold in the 16K fraction from DENV-2 infected cells compared to mock infected cells, made in FunRich v3.1.3.

Of the 503 proteins imported into STRING 11.0, 462 proteins were assigned nodes. STRING provides a list of enriched Reactome pathways, and while there is some overlap between terms, the "Citric Acid Cycle" and "Respiratory Electron Transport" are the most highly enriched Reactome pathways in the 2.0-fold changed proteins. This shows that there is a strong enrichment of proteins related to mitochondrial ATP production in the 2.0-fold changed data set. Table 3.6 shows the top five most enriched Reactome pathways.

Term ID	term description	Observed	Background	FDR
HSA-1428517	The citric acid (TCA) cycle and respiratory electron transport	38	173	3.38×10^{-20}
HSA-163200	Respiratory electron transport, ATP synthesis by chemiosmotic coupling, and heat production by uncoupling proteins.	30	123	5.68×10^{-17}

HSA-1430728	Metabolism	116	2032	$1.93x10^{-16}$
HSA-611105	Respiratory electron transport	23	100	$1.58x10^{-12}$
HSA-6799198	Complex I biogenesis	15	55	$8.16x10^{-09}$

Table 3. 6. Top Reactome pathway enriched in the proteins altered ≥ 2.0-Fold in the 16K fraction from DENV-2 infected cells compared to mock infected cells, as assigned by STRING v11.0

Functional annotation was performed using DAVID 6.8. Of the 503 proteins imported into DAVID 6.8, 472 were identified. Using medium stringency, the most enriched cluster (based on Fisher's Exact test) is shown in Table 3.7. One hundred and sixty-eight proteins were attributed to this cluster (33.4% of the total number of 2.0-fold altered proteins) and are associated with the term Mitochondria.

Annotation Cluster 1	**Enrichment Score: 43.98**			
Category	**Term**	**Count**	**%**	**p-value**
UP_KEYWORDS	Mitochondrion	135	28.60	$3.93x10^{-60}$
UP_KEYWORDS	Transit peptide	94	19.92	$5.49x10^{-55}$
UP_SEQ_FEATURE	Transit peptide:Mitochondrion	84	17.80	$3.99x10^{-48}$
GOTERM_CC_DIRECT	GO:0005759~Mitochondrial matrix	73	15.47	$5.12x10^{-47}$
GOTERM_CC_DIRECT	GO:0005739~Mitochondrion	133	28.18	$7.76x10^{-45}$
KEGG_PATHWAY	hsa01100:Metabolic pathways	84	17.80	$3.79x10^{-13}$

Table 3. 7. Most enriched functional annotation cluster of all proteins changed ≥ 2.0-fold in the 16K fraction from DENV-2 infected cells compared to mock infected cells, made in DAVID v6.8

Taken together, these results clearly indicate a disturbance in mitochondrial proteins – and possibly mitochondrial function. The idea that DENV-2 infection altered the abundance of specific mitochondrial proteins and hence affected the cellular pathways in which the proteins were involved was further investigated by downstream bioinformatic analysis to identify the most interesting proteins for further validation and analysis.

3.2.3.1.3 DENV-2/Mock 1.5-Fold Increased

Initially, the 400 proteins that increased 1.5-fold in the 16K fraction of DENV-2 infected cells compared to mock-infected cells were imported into STRING, which identified 366 nodes. The most enriched cellular compartment GO term was "mitochondrial membrane" (GO:0031966), with 136 proteins assigned to that group, (FDR = $1.01x10^{-91}$) (Table 3.8). To further understand what kind of mitochondrial membrane proteins were increased, this protein list was exported and re-run in STRING resulting in the identification of three Reactome pathways (Table 3.9).

Term ID	**Term Description**	**Observed**	**Background**	**FDR**
GO:0031966	Mitochondrial membrane	136	679	$1.03x10^{-91}$
GO:0005740	Mitochondrial envelope	137	722	$4.75x10^{-90}$
GO:0005743	Mitochondrial inner membrane	112	456	$1.89x10^{-82}$
GO:0019866	Organelle inner membrane	114	513	$4.96x10^{-80}$
GO:0031967	Organelle envelope	145	1146	$9.05x10^{-75}$

Table 3. 8. The top five cellular components enriched in the proteins increased ≥ 1.5-fold in the DENV-2 infected cells compared to mock infected cells, generated in STRING v11.0.

Term ID	**Term Description**	**Observed**	**Background**	**FDR**
HSA-163200	Respiratory electron transport, ATP synthesis by chemiosmotic coupling, and heat production by uncoupling proteins.	51	123	$3.00x10^{-69}$
HSA-1428517	The citric acid (TCA) cycle and respiratory electron transport	54	173	$2.08x10^{-68}$
HSA-611105	Respiratory electron transport	40	100	$2.94x10^{-53}$

Table 3. 9. Top three Reactome pathways enriched in the 136 proteins re-run through STRING v11.0.

A comparison of the Reactome pathways unsurprisingly showed an involvement of respiratory electron transport. Alterations to mitochondrial function and ATP production was a common outcome in this downstream analysis and has been reported before in DENV-2 infection studies (Byers et al., 2019; Fernandes-Siqueira et al., 2018; Neufeldt et al., 2018). However, molecular function enrichment (also

carried out using STRING v11.0) assigned 44 proteins to the term "transporter activity" (data not shown). Included in this term were 12 members of the SLC25A family (SLC25A3, SLC25A4, SLC25A5, SLC25A6, SLC25A10, SLC25A11, SLC25A12, SLC25A13, SLC25A15, SLC25A20, SLC25A22 SLC25A24) and VDAC1 and VDAC3, (which have also been associated with DENV infection before (Jitobaom et al., 2016). More information on each transporter can be found in Section 3.6.

The list of 400 proteins that increased ≥1.5-fold in DENV-2 infected compared to mock infected cells was imported into DAVID 6.8, enrichment analysis was performed, and annotation clusters were produced. The EASE scores of Clusters 1 and 2 were 88.17 and 53.98, respectively. Both clusters corroborated with the STRING analysis and included terms such as mitochondrial inner membrane and mitochondrion (Tables 3.10 and 3.11 respectively).

Annotation Cluster 1	**Enrichment Score: 88.17**			
Category	**Term**	**Count**	**%**	**p-value**
GOTERM_CC_DIRECT	GO:0005743~Mitochondrial inner membrane	117	30.31	4.62×10^{-98}
UP_KW_CELLULAR_COMPONENT	KW-0999~Mitochondrion inner membrane	107	27.72	7.11×10^{-98}
UP_KW_CELLULAR_COMPONENT	KW-0496~Mitochondrion	160	41.48	2.94×10^{-83}
GOTERM_CC_DIRECT	GO:0005739~mitochondrion	154	39.89	2.23×10^{-76}

Table 3. 10. Functional annotation cluster 1 of proteins increased ≥ 1.5-fold in the DENV-2 infected cells compared to mock infected cells, generated in DAVID v6.8.

Annotation Cluster 2	**Enrichment Score: 53.98**			
Category	**Term**	**Count**	**%**	**p-value**
GOTERM_CC_DIRECT	GO:0005743~mitochondrial inner membrane	117	30.31	4.62×10^{-98}
UP_SEQ_FEATURE	TRANSIT:Mitochondrion	65	16.83	3.87×10^{-33}
UP_KW_DOMAIN	KW-0809~Transit peptide	67	17.35	6.53×10^{-33}

Table 3. 11. Functional annotation cluster 2 of proteins increased ≥ 1.5-fold in the DENV-2 infected cells compared to mock infected cells, generated in DAVID v6.8.

3.2.3.1.4 DENV-2/Mock 2.0-Fold Increased

There were 120 proteins increased ≥2-fold in the 16K fraction of DENV-2 infected cells compared to mock infected cells. One hundred and 10 protein Uniprot accessions were recognised by STRING v11.0, and unsurprisingly the top Reactome pathways identified were mitochondrial ATP producing pathways (Table 3.12). Proteins associated with these pathways included members of Respiratory Complex 1, ATP synthase, Cytochrome 1 and Electron Transfer Flavoprotein Dehydrogenase. The term "Metabolism" was the fifth most enriched Reactome pathway (39 proteins with an FDR of $2.19x10^{-9}$).

The top five biological processes, gathered in STRING (Table 3.13), were all associated with mitochondria – including oxidative phosphorylation (FDR=$9.35x10^{-26}$) and terms related to ATP processes. The cellular compartment enrichment data generated through STRING (table 3.14) showed the proteins identified were indicated to be heavily part of the mitochondrial structure.

Term ID	**Term Description**	**Observed**	**Background**	**FDR**
HSA-163200	Respiratory electron transport, ATP synthesis by chemiosmotic coupling, and heat production by uncoupling proteins.	26	125	$1.63x10^{-28}$
HSA-611105	Respiratory electron transport	19	101	$8.34x10^{-20}$
HSA-6799198	Complex I biogenesis	13	55	$3.31x10^{-14}$
HSA-8949613	Cristae formation	10	31	$8.27x10^{-12}$
HSA-1430728	Metabolism	39	2089	$2.19x10^{-09}$

Table 3. 12. Top five most enriched Reactome pathway of proteins increased ≥ 2-fold in DENV-2 infected cells compared to mock infected cells, as assigned by STRING v11.0.

Term ID	**Term Description**	**Observed**	**Background**	**FDR**
GO:0006119	Oxidative phosphorylation	23	100	$9.35x10^{-26}$
GO:0046034	ATP metabolic process	25	190	$3.84x10^{-23}$
GO:0009167	Purine ribonucleoside monophosphate metabolic process	26	230	$8.39x10^{-23}$

GO:0009205	Purine ribonucleoside triphosphate metabolic process	25	221	$3.94x10^{-22}$
GO:0007005	Mitochondrion organization	29	424	$1.42x10^{-20}$

Table 3. 8. Top five most enriched biological process of proteins increased increased ≥ 2-fold in DENV-2 infected cells compared to mock infected cells, as assigned by STRING v11.0

Term ID	**Term Description**	**Observed**	**Background**	**FDR**
GO:0098800	Inner mitochondrial membrane protein complex	29	128	$7.14x10^{-34}$
GO:0005743	Mitochondrial inner membrane	40	456	$1.61x10^{-33}$
GO:0019866	Organelle inner membrane	41	513	$3.98x10^{-33}$
GO:0005740	Mitochondrial envelope	45	722	$1.68x10^{-32}$
GO:0031966	Mitochondrial membrane	44	679	$1.91x10^{-32}$

Table 3. 14. Top five enriched cellular compartment of proteins increased increased ≥ 2-fold in DENV-2 infected cells compared to mock infected cells, as assigned by STRING v11.0.

Analysis using DAVID 6.8 yielded similar results as the STRING analysis. However, within this group was the term "transport" (Table 3.15). This was associated with a range of proteins, including members of Respiratory Complex 1, but also SCL25A11, SLC25A12 and SLC25A13. These proteins function as oxoglutarate/malate and calcium dependant glutamate/aspartate transporters, respectively. As these proteins were elevated in abundance 2.0-fold or more, they are strong candidates for further study of the role of mitochondrial proteins in DENV-2 infection.

Annotation Cluster 1	**Enrichment Score: 18.93**			
Category	**Term**	**Count**	**%**	**p-value**
UP_KEYWORDS	Transport	40	35.71	$2.06x10^{-13}$

Table 3. 9. Transport term identified in DAVID v6.8 analysis.

3.2.3.1.5 DENV-2/Mock 1.5-Fold Decreased

The same analysis process carried out on proteins that were increased was done on proteins that decreased in the 16K fraction of DENV-2 infected cells compared to mock infected cells. Initially 961 proteins that decreased ≥ 1.5-fold in abundance were imported into PANTHER and the GO:slim

enrichment analysed. 871 proteins were assigned to gene names. The top 3 GO:slim terms were; catalytic activity (30.1%), binding (27.6%) and molecular function (6.0%).

STRING analysis of the data set identified 895 nodes. The top five enriched Reactome pathways are shown in Table 3.16. Interestingly, they include terms related to translation, however, the 196 proteins that belong to the "metabolism" term were investigated further.

These 196 proteins were re-run in STRING. The Reactome pathways enriched included (but was not limited to) "Metabolism of lipids" (FDR=$1.84x10^{-97}$) and "Mitochondrial Fatty Acid Beta-Oxidation" (FDR=$3.59x10^{-18}$) (see Table 3.17). There were 12 proteins assigned to Mitochondrial Fatty Acid Beta-Oxidation (FDR=$3.59x10^{-18}$).

Term ID	Term Description	Observed	Background	FDR
HSA-156827	L13a-mediated translational silencing of Ceruloplasmin expression	43	107	$1.37x10^{-20}$
HSA-72706	GTP hydrolysis and joining of the 60S ribosomal subunit	43	108	$1.37x10^{-20}$
HSA-1430728	Metabolism	196	2032	$4.46x10^{-20}$
HSA-72613	Eukaryotic Translation Initiation	43	115	$4.46x10^{-20}$
HSA-72649	Translation initiation complex formation	33	55	$4.46x10^{-20}$

Table 3. 106. Top Reactome pathways enriched in the proteins decreased ≥ 1.5-fold in the DENV-2 infected cells compared to mock infected cells, as assigned by STRING v11.0.

Term ID	Term Description	Observed	Background	FDR
HSA-556833	Metabolism of lipids	70	721	$1.84x10^{-97}$
HSA-8978868	Fatty acid metabolism	24	171	$2.59x10^{-29}$
HSA-1989781	PPARA activates gene expression	19	114	$3.17x^{-24}$
HSA-77289	Mitochondrial Fatty Acid Beta-Oxidation	12	37	$3.59x10^{-18}$

HSA-8957322	Metabolism of steroids	15	146	$3.04x10^{-16}$

Table 3. 117. Top Reactome pathway enriched in the 196 metabolism proteins of the proteins decreased ≥1.5-Fold, as assigned by STRING v11.0.

Functional annotation clustering was carried out in DAVID 6.8. The two Clusters with highest EASE scores contained terms associated with ATP binding and Ribosomal proteins (9.7 and 7.9, respectively) (data not shown), but the next cluster was of more interest, given the context of the other bioinformatic results detailed above. The 12 genes in this cluster belong to 7 proteins: Fumarate hydratase, subunits of isocitrate dehydrogenase, subunits of succinate-CoA ligase, malate dehydrogenase, pyruvate carboxylase, aconitate hydratase, citrate synthase (Table 3.18).

Annotation Cluster 3	**Enrichment Score: 6.65**			
Category	**Term**	**Count**	**%**	**p-value**
UP_KEYWORDS	Tricarboxylic acid cycle	11	1.21	$2.85x10^{-8}$
KEGG_PATHWAY	hsa00020:Citrate cycle (TCA cycle)	12	1.32	$5.34x10^{-7}$
GOTERM_BP_DIRECT	GO:0006099~tricarboxylic acid cycle	11	1.21	$7.16x10^{-7}$

Table 3. 128. Annotation Cluster 3 (as ranked by Enrichment score) carried out by DAVID v6.8 analysis.

3.2.3.1.6 DENV-2/Mock 2.0-Fold Decreased

The 383 proteins that decreased ≥ 2-fold in abundance in the 16K fraction of DENV-2 infected cells compared to mock infected cells were then analysed. This list was imported into STRING which produced 352 nodes. The top four enriched Reactome pathways are shown in Table 3.19 and included the term "Citric acid cycle (TCA cycle) (FDR=$7.90x10^{-6}$). The eight proteins included in the TCA cycle term are: aconitate hydratase, four subunits of isocitrate dehydrogenase, malate dehydrogenase and two subunits of succinate-CoA ligase.

Term ID	**Term Description**	**Observed**	**Background**	**FDR**
has-1430728	Metabolism	77	2032	$2.77x10^{-7}$
HSA-381426	Regulation of Insulin-like Growth Factor (IGF) transport and uptake by Insulin-like Growth Factor Binding Proteins (IGFBPs)	15	123	$7.90x10^{-6}$

HSA-70895	Branched-chain amino acid catabolism	8	23	$7.90x10^{-6}$
HSA-71403	Citric acid cycle (TCA cycle)	8	22	$7.90x10^{-6}$

Table 3. 13. Top 4 most enriched Reactome pathways of proteins decreased ≥ 2.0-Fold in the DENV-2 infected cells compared to mock infected cells, generated through STRING v11.0 analysis.

Functional annotation clusters were produced using DAVID 6.8, and the top cluster is shown in Table 3.20. The eight proteins identified are Malate dehydrogenase, subunits of Isocitrate dehydrogenase, subunits of succinate Co-A ligase and Aconitate hydratase.

Annotation Cluster 1	**Enrichment Score: 6.08**			
Category	**Term**	**Count**	**%**	**p-value**
UP_KEYWORDS	Tricarboxylic acid cycle	8	2.22	$1.24x10^{-7}$
GOTERM_BP_DIRECT	GO:0006099~Tricarboxylic acid cycle	8	2.22	$1.08x10^{-6}$
KEGG_PATHWAY	hsa00020:Citrate cycle (TCA cycle)	8	2.22	$4.19x10^{-6}$

Table 3. 14. Functional Annotation Cluster 1 of proteins decreased ≥ 2.0-Fold in the DENV-2 infected cells compared to mock infected cells, generated by STRING v11.0.

Originally, experiments were planned to examine the role these enzymes in the DENV-2 lifecycle. However, as DENV is categorised as a BSL3 pathogen, performing metabolic analysis on infected cells proved too difficult logistically and these plans were changed to focus on the transporter and metabolic proteins increased in amount, which is detailed above.

3.2.4.1 Proteomic Changes in Huh-7 Cells Stably Expressing a DENV-2 Replicon.

3.2.4.1.1 Rep/Mock 1.5-Fold Change Proteins

The 583 proteins that increased or decreased ≥ 1.5-fold in abundance in the 16K fraction from the Rep cells compared to the mock cells were analysed using STRING v11.5 and DAVID 6.8 for GO analysis and Funrich v.3.1.3 for GO:slim. The top five cellular components (as ranked by p-value) identified by FunRich analysis are shown in Figure 3.10. The graph shows that over 25% of proteins are associated with the term “lysosome” and around 20% with the term “endoplasmic reticulum”. All the terms had a p-value of < 0.05.

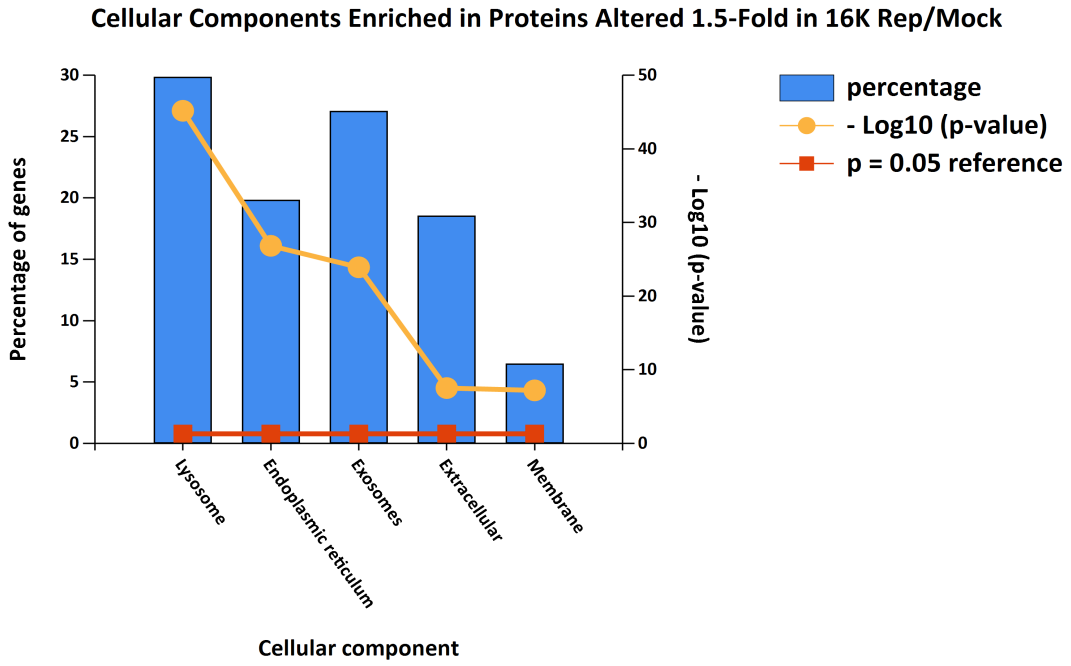

Figure 3. 10. Top five cellular compartment terms associated with proteins altered ≥ 1.5-fold in in the Rep cells compared to the mock cells. FunRich v3.1.3 was used for the enrichment analysis.

STRING analysis of the same protein data set produced 545 nodes and revealed an enrichment of GO terms associated with membrane-bound organelles like the "endomembrane system" (FDR=2.20×10^{-47}) and "vesicle" (FDR=8.68×10^{-31}) (as shown by four of the five cellular compartment terms being ER related and one of the five being "vesicle" itself), as shown in Table 3.21. Additionally, the proteins in the data set were associated with enriched terms related to membrane bound organelles like "vesicle mediated transport" (FDR=1.62×10^{-18}) and regulated exocytosis (FDR=1.48×10^{-16}) as shown in Table 3.22.

Table 3.23 details the top five most enriched Reactome pathways. These include immune pathways, (with a bias towards innate immunity) and metabolism. Interestingly, the fifth Reactome pathway most enriched in this data set was metabolism of lipids (FDR=2.67×10^{-8}) with 56 of the proteins in this set associated with this term.

Term ID	Term Description	Observed Gene Count	Background Gene Count	FDR
GO:0012505	Endomembrane system	291	4542	2.20×10^{-47}
GO:0005783	Endoplasmic reticulum	140	1438	8.17×10^{-35}

GO:0031982	Vesicle	234	3879	$8.68x10^{-31}$
GO:0005788	Endoplasmic reticulum lumen	63	308	$1.77x10^{-29}$
GO:0070062	Extracellular exosome	156	2099	$4.10x10^{-27}$

Table 3. 15. Top five enriched cellular compartment of proteins altered ≥1.5-Fold in the Rep cells compared to the mock cells, generated in STRING v11.5

Term ID	**Term Description**	**Observed Gene Count**	**Background Gene Count**	**FDR**
GO:0016192	Vesicle-mediated transport	129	1805	$1.62x10^{-18}$
GO:0045055	Regulated exocytosis	72	697	$1.48x10^{-16}$
GO:0051234	Establishment of localisation	219	4479	$2.56x10^{-15}$
GO:0006810	Transport	214	4353	$3.58x10^{-15}$
GO:0043312	Neutrophil degranulation	57	484	$3.58x10^{-15}$

Table 3. 16. Top five enriched biological process of proteins altered ≥1.5-Fold in the Rep cells compared to the mock cells, generated in STRING v11.5

Term ID	**Term Description**	**Observed Gene Count**	**Background Gene Count**	**FDR**
HSA-6798695	Neutrophil degranulation	56	473	$4.64x10^{-15}$
HSA-168249	Innate Immune System	79	1025	$2.16x10^{-12}$
HSA-168256	Immune System	109	1956	$3.86x10^{-9}$
HSA-1430728	Metabolism	111	2089	$2.67x10^{-8}$

HSA-556833	Metabolism of lipids	56	733	$2.67x10^{-8}$

Table 3. 17. Top five enriched Reactome pathway of proteins altered ≥1.5-Fold in the Rep cells compared to the mock cells, generated in STRING v11.5

DAVID analysis of the data set identified a top enrichment cluster (with an EASE score of 13.82) that contained four terms related to the lysosome including the lysosomal lumen (FDR=$8.90x10^{-13}$) and the lysosome (FDR=$1.52x10^{-11}$), shown in Table 3.24.

Annotation Cluster 1	**Enrichment Score: 13.82**		
Category	**Term**	**Count**	**p-value**
KEGG_PATHWAY	hsa04142:Lysosome	33	$1.21x10^{-17}$
GOTERM_CC_DIRECT	GO:0043202~Lysosomal lumen	23	$1.19x10^{-14}$
GOTERM_CC_DIRECT	GO:0005764~Lysosome	37	$2.71x10^{-13}$
UP_KW_CELLULAR_COMPONENT	KW-0458~Lysosome	42	$1.34x10^{-12}$

Table 3. 18. Top enriched functional annotation cluster of proteins altered ≥1.5-Fold in the Rep cells compared to the mock cells, generated in DAVID v6.8.

3.2.4.1.2 Rep/Mock 2.0-Fold Changed Proteins

There were 272 proteins that increased or decreased ≥ 2-fold in abundance in the 16K fraction from the Rep cells compared to the mock cells that were analysed as described above.

Analysis of the data set using FunRich identified the top five cellular compartments (as ranked by p-value) shown in Figure 3.11. The analysis revealed that over 30% of proteins were associated with the term lysosome, and a further 25% of proteins with the term endoplasmic reticulum. Thirty percent of the proteins were associated with the term exosomes and 25% with the term extracellular. All the terms had a p-value of less than 0.05.

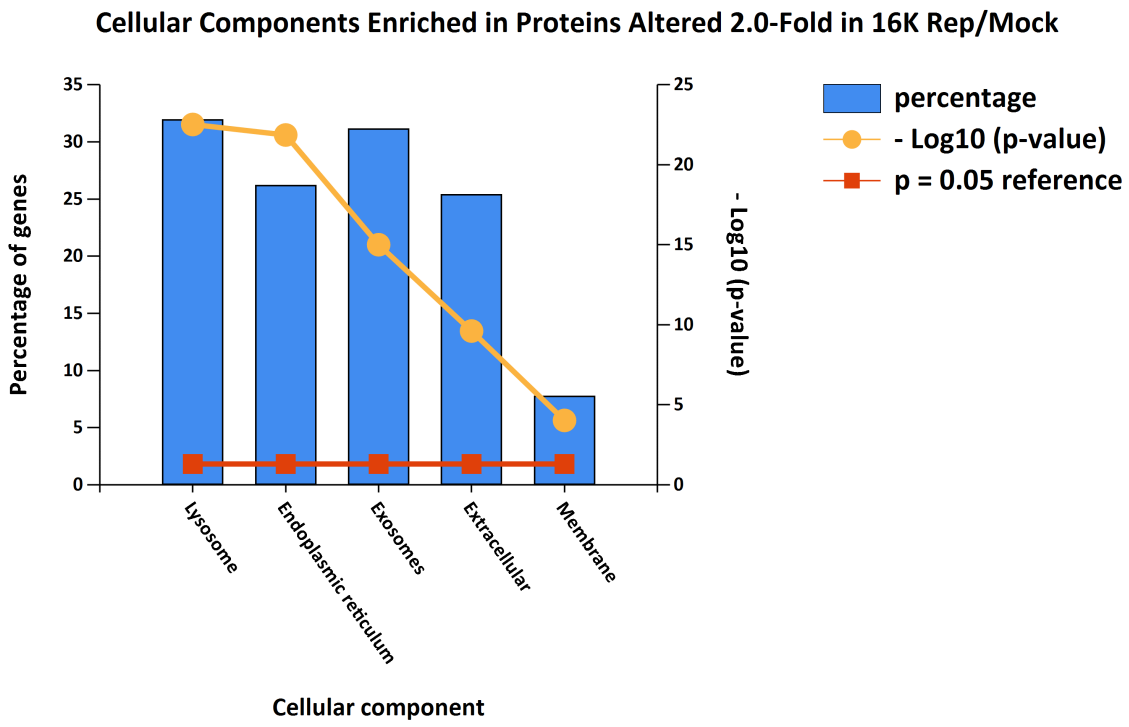

Figure 3. 11. Top five enriched cellular compartment of proteins altered in abundance ≥ 2.0-Fold in the Rep cells compared to the mock cells, made in FunRich v.3.1.3.

Analysis of the data set using STRING produced 250 nodes. The top five enriched cellular compartment and biological process terms are shown below in Tables 3.25 and 3.26 respectively. The Reactome pathways identified to be enriched were not significant and not analysed further.

Similarly, to the proteins increased or decreased ≥ 1.5-fold in abundance in the 16K fraction from the Rep cells compared to the mock cells, the cellular compartment analysis (shown in Table 3.25) revealed an enrichment of proteins associated with terms related to the ER – with three of the five terms being directly mentioned ("ER Lumen", "endoplasmic reticulum" and "endomembrane system" (FDRs=$3.38\text{x}10^{-40}$, $1.60\text{x}10^{-30}$, and $1.49\text{x}10^{-27}$, respectively)), and the final two terms related to extracellular proteins ("extracellular space", "extracellular vesicle" (FDRs=$4.99\text{x}10^{-23}$ and $7.29\text{x}10^{-21}$, respectively)). The biological process terms that were most enriched all related to release of a substance from a cell, including "regulated exocytosis" and "neutrophil degranulation" (FDRs=$7.84\text{x}10^{-09}$ and $1.67\text{x}10^{-7}$, respectively) – shown in table 3.26.

The top enrichment cluster identified using DAVID v6.8 also supported proteins associated with the ER (Table 3.27). Two of the terms were "endoplasmic reticulum lumen" and "endoplasmic reticulum" (FDRs=$7.25\text{x}10^{-45}$ and $1.57\text{x}10^{-22}$, respectively), the other being "prevents secretion from ER"

(FDR=2.18x10^{-37}). The Uniprot accession numbers associated with this term were re-run in STRING v11.5 to possibly characterize how they prevent ER secretion and Table 3.28 below shows the top five most highly enriched biological process terms generated. The enriched terms associated with these proteins are related to ER protein folding and cell redox homeostasis.

Term ID	**Term Description**	**Observed Gene Count**	**Background Gene Count**	**FDR**
GO:0005788	Endoplasmic reticulum lumen	55	308	3.38x10^{-40}
GO:0005783	Endoplasmic reticulum	85	1438	1.60x10^{-30}
GO:0012505	Endomembrane system	143	4542	1.49x10^{-27}
GO:0005615	Extracellular space	112	3195	4.99x10^{-23}
GO:1903561	Extracellular vesicle	87	2121	7.29X10^{-21}

Table 3. 19. Top five enriched cellular compartment, as ranked by FDR, of proteins altered ≥ 2.0-Fold in the Rep cells compared to the mock cells, gathered in STRING v11.5.

Term ID	**Term Description**	**Observed Gene Count**	**Background Gene Count**	**FDR**
GO:0045055	Regulated exocytosis	37	697	7.84X10^{-9}
GO:0032940	Secretion by cell	43	979	1.86X10^{-8}
GO:0140352	Export from cell	44	1028	1.86X10^{-8}
GO:0046903	Secretion	44	1097	7.19X10^{-8}
GO:0043312	Neutrophil degranulation	28	484	1.67X10^{-7}

Table 3. 20. Top five enriched biological process ranked by FDR of proteins altered ≥ 2.0-Fold in the Rep cells compared to the mock cells, gathered in STRING v11.5.

Annotation Cluster 1	**Enrichment Score: 36.56**		
Category	**Term**	**Count**	**p Value**
GOTERM_CC_DIRECT	GO:0005788~Endoplasmic reticulum lumen	56	2.65X10^{-47}

UP_SEQ_FEATURE	MOTIF:Prevents secretion from ER	30	$1.73X10^{-40}$
UP_KW_CELLULAR_COMPONENT	KW-0256~Endoplasmic reticulum	73	$4.50X10^{-24}$

Table 3. 21. Top enriched annotation cluster of proteins altered ≥ 2.0-Fold in the Rep cells compared to the mock cells, gathered in DAVID v6.8.

Term ID	**Term Description**	**Observed Gene Count**	**Background Gene Count**	**FDR**
GO:0006457	Protein folding	13	213	$1.01X10^{-14}$
GO:0034976	Response to endoplasmic reticulum stress	11	256	$1.69X10^{-10}$
GO:0034975	Protein folding in endoplasmic reticulum	5	10	$4.28X10^{-8}$
GO:0035966	Response to topologically incorrect protein	8	188	$5.27X10^{-7}$
GO:0045454	Cell redox homeostasis	6	60	$8.33X10^{-7}$

Table 3. 22. Top five enriched biological process assigned to the proteins associated with the term "prevents secretion from ER", gathered using STRING v11.5.

3.2.4.1.3 Rep/Mock 1.5-Fold Increased Proteins

There were 320 proteins that increased ≥ 1.5-fold in abundance in the 16K fraction from the Rep cells compared to the mock cells that were analysed using STRING v11.5 and DAVID v6.8. STRING analysis produced 302 nodes. GO enrichment analysis showed that four of the five most enriched biological process terms (Table 3.29) were broad metabolic terms, which were hard to interpret without further investigation. However, the fourth most enriched term was "regulated exocytosis" (FDR=$6.16X10^{-12}$). This also tied in with the enriched cellular compartment terms (table 3.30), as two of the five are ER related terms, and the remaining three are terms related to extracellular components. This also links in with the enriched Reactome pathway, two of which are extracellular ("neutrophil degranulation" and "extracellular organisation"). Interestingly, the fourth most enriched Reactome pathway is "metabolism of lipids" (FDR=$3.39X10^{-7}$), shown in Table 3.31. Lipid metabolism is highly linked to DENV replication as

autophagy is upregulated in infection and β-oxidation is favoured in DENV infected cells (Fernandes-Siqueira et al., 2018; Heaton et al., 2010b; Heaton & Randall, 2010).

The top enrichment cluster identified using DAVID 6.8 (Table 3.32) correlated with the extracellular nature of the cellular compartment and Reactome pathway terms as the three terms are "extracellular region", "extracellular space" and "secreted" (FDRs=8.53X10^{-20}, 1.10x10^{-13}, and 2.85x10^{-07}, respectively).

Term ID	Term Description	Observed Gene Count	Background Gene Count	FDR
GO:0008152	Metabolic process	202	8298	2.01x10^{-13}
GO:0044238	Primary metabolic process	184	7332	1.20x10^{-12}
GO:0071704	Organic substance metabolic process	191	7755	1.20x10^{-12}
GO:0045055	Regulated exocytosis	45	697	6.16x10^{-12}
GO:1901564	Organonitrogen compound metabolic process	144	5244	3.41x10^{-11}

Table 3. 23. Top five enriched biological process of proteins increased ≥ 1.5-Fold in the Rep cells compared to the mock cells, gathered in STRING v11.5.

Term ID	Term Description	Observed Gene Count	Background Gene Count	FDR
GO:0005788	Endoplasmic reticulum lumen	60	308	4.36x10^{-41}
GO:0005783	Endoplasmic reticulum	95	1438	4.57x10^{-31}
GO:0005615	Extracellular space	135	3195	1.32x10^{-27}
GO:1903561	Extracellular vesicle	107	2121	2.17x10^{-26}
GO:0070062	Extracellular exosome	106	2099	2.72x10^{-26}

Table 3. 24. Top five enriched cellular compartment of proteins increased ≥ 1.5-Fold in the Rep cells compared to the mock cells, gathered in STRING v11.5.

Term ID	Term Description	Observed Gene Count	Background Gene Count	FDR
HSA-168249	Innate Immune System	53	1025	$5.98x10^{-11}$
HSA-6798695	Neutrophil degranulation	33	473	$2.24x10^{-9}$
HSA-1474244	Extracellular matrix organization	24	301	$1.45x10^{-7}$
HSA-556833	Metabolism of lipids	37	733	$3.39x10^{-7}$
HSA-1430728	Metabolism	69	2089	$5.99x10^{-7}$

Table 3. 25. Top five enriched Reactome pathway of proteins increased ≥ 1.5-Fold in the Rep cells compared to the mock cells, gathered in STRING v11.5.

Annotation Cluster 1	Enrichment Score: 14.40		
Category	**Term**	**Count**	**P-value**
GOTERM_CC_DIRECT	GO:0005576~Extracellular region	94	$1.10x10^{-21}$
GOTERM_CC_DIRECT	GO:0005615~Extracellular space	78	$2.48x10^{-15}$
UP_KW_CELLULAR_COMPONENT	KW-0964~Secreted	71	$2.31x10^{-8}$

Table 3. 26. Top enriched functional annotation cluster of proteins increased ≥ 1.5-Fold in the Rep cells compared to the mock cells, gathered in DAVID v6.8.

3.2.4.1.4 Rep/Mock 2.0-Fold Increased Proteins

The 185 proteins increased ≥ 2-fold in abundance in the 16K fraction from the Rep cells compared to the mock cells were analysed by STRING with 173 nodes produced. The top five enriched cellular compartment terms identified by GO analysis are shown in Table 3.34.

Term ID	Term Description	Observed Gene Count	Background Gene Count	FDR
GO:0005788	Endoplasmic reticulum lumen	53	299	$2.69x10^{-48}$
GO:0005783	Endoplasmic reticulum	74	1796	$8.84x10^{-29}$
GO:0012505	Endomembrane system	105	4347	$3.69x10^{-25}$

GO:0005576	Extracellular region	77	2505	$1.97x10^{-22}$
GO:0005615	Extracellular space	44	1134	$4.54x10^{-15}$

Table 3. 27. Top five enriched cellular compartment of proteins increased ≥ 2.0-Fold, gathered in STRING v11.5.

The term "endomembrane system" includes structures such as the Golgi apparatus, the Endoplasmic Reticulum and Transport Vesicles. As some of these structures have a key role in the DENV life cycle, namely genomic replication, protein expression and virion trafficking (Byk & Gamarnik, 2016; Ma et al., 2004; Nasar et al., 2020; Norazharuddin & Lai, 2018), the 105 proteins assigned to this term were exported and re-run in the same program. Four of the results deemed as the most biologically relevant based on the current literature are shown below in Table 3.34.

Rank	**Term ID**	**Term Description**	**Observed Gene Count**	**Background Gene Count**	**FDR**
2	GO:0032940	Secretion by cell	31	959	$4.47x10^{-13}$
6	GO:0016192	Vesicle-mediated transport	35	1699	$4.48x10^{-10}$
14	GO:0034976	Response to endoplasmic reticulum stress	13	240	$7.55x10^{-8}$
15	GO:0006986	Response to unfolded protein	11	153	$9.43x10^{-8}$

Table 3. 28. Four of the top 15 enriched biological process as ranked by FDR, shown here in relevance to the current literature, of proteins increased ≥ 2.0-Fold in the Rep cells compared to the mock cells, gathered in STRING v11.5.

3.2.4.1.5 Rep/Mock 1.5-Fold Decreased Proteins

The 263 proteins increased ≥ 1.5-fold in abundance in the 16K fraction from the Rep cells compared to the mock cells were analysed by STRING with 244 nodes produced. The top five biological process, cellular compartment and Reactome pathways identified by GO analysis using STRING v11.5 are shown below in Tables 3.35, 3.36, and 3.37 respectively, along with the top enriched cluster from DAVID v6.8 (Table 3.38).

The top five biological process terms relate to transport and localisation including "transport" (FDR=$5.93x10^{-12}$) and "localisation" (FDR=$2.07x10^{-10}$). The cellular compartment terms enriched are Membrane and ER related (including "membrane" (FDR=$3.35x10^{-26}$) and "endomembrane system" (FDR=$4.84x10^{-24}$). The Reactome pathway enriched using the protein data set included two Clathrin-

mediated endocytosis terms ("cargo recognition for clathrin-mediated endocytosis" and "clathrin-mediated endocytosis" (FDRs=$4.62x10^{-6}$ and $4.77x10^{-6}$, respectively) as well as trafficking and transport terms.

The top enrichment cluster identified using DAVID v6.8 (Table 3.38) suggested many of the proteins were transmembrane proteins, which is likely given the strong bias towards membranous structures in the 16K fraction.

Term ID	**Term Description**	**Observed Gene Count**	**Background Gene Count**	**FDR**
GO:0006810	Transport	112	4353	$5.93x10^{-12}$
GO:0051234	Establishment of localisation	113	4479	$8.31x10^{-12}$
GO:0051179	Localisation	126	5591	$2.07x10^{-10}$
GO:0016192	Vesicle-mediated transport	62	1805	$7.47x10^{-10}$
GO:0071702	Organic substance transport	64	2173	$1.59x10^{-7}$

Table 3. 29. Top five enriched biological process of proteins decreased ≥ 1.5-Fold in the Rep cells compared to the mock cells, gathered in STRING v11.5.

Term ID	**Term Description**	**Observed Gene Count**	**Background Gene Count**	**FDR**
GO:0016020	Membrane	199	9072	$3.35x10^{-26}$
GO:0031090	Organelle membrane	122	3548	$3.80x10^{-26}$
GO:0012505	Endomembrane system	135	4542	$4.84x10^{-24}$
GO:0098805	Whole membrane	74	1715	$7.56x10^{-19}$
GO:0098588	Bounding membrane of organelle	82	2107	$1.02x10^{-18}$

Table 3. 30. Top five enriched cellular compartment of proteins decreased ≥ 1.5-Fold in the Rep cells compared to the mock cells, gathered in STRING v11.5.

Term ID	**Term Description**	**Observed Gene Count**	**Background Gene Count**	**FDR**
HSA-199991	Membrane Trafficking	29	622	$4.62x10^{-6}$

HSA-382551	Transport of small molecules	31	721	$4.62x10^{-6}$
HSA-5653656	Vesicle-mediated transport	30	660	$4.62x10^{-6}$
HSA-8856825	Cargo recognition for clathrin-mediated endocytosis	13	105	$4.62x10^{-6}$
HSA-8856828	Clathrin-mediated endocytosis	14	145	$4.77x10^{-6}$

Table 3. 31. Top five enriched Reactome pathways of proteins decreased ≥ 1.5-Fold in the Rep cells compared to the mock cells, gathered in STRING v11.5.

Annotation Cluster 1	**Enrichment Score: 18.23**		
Category	**Term**	**Count**	**p-value**
UP_KW_CELLULAR_COMPONENT	KW-0472~Membrane	184	$1.71x10^{-21}$
UP_SEQ_FEATURE	TRANSMEM:Helical	136	$3.97x10^{-21}$
GOTERM_CC_DIRECT	GO:0016021~integral component of membrane	132	$6.50x10^{-19}$
UP_KW_DOMAIN	KW-1133~Transmembrane helix	142	$1.07x10^{-18}$
UP_KW_DOMAIN	KW-0812~Transmembrane	142	$3.63x10^{-18}$
UP_SEQ_FEATURE	TOPO_DOM:Cytoplasmic	101	$2.39x10^{-15}$

Table 3. 32. Top enriched functional annotation cluster of proteins decreased ≥ 1.5-Fold in the Rep cells compared to the mock cells, gathered in DAVID v6.8

3.2.4.1.6 Rep/Mock 2.0-Fold Decreased Proteins

There were 87 proteins that decreased ≥ 2-fold in abundance in the 16K fraction from the Rep cells compared to the mock cells that were analysed using STRING v11.5 and DAVID v6.8. STRING analysis produced 77 nodes. Only three cellular compartment terms were listed because their FDR values were small enough to be significant (Table 3.39). As there are few proteins in this data set, STRING could not perform functional enrichment analysis of biological process and Reactome pathways, so the top two functional enrichment clusters identified using DAVID v6.8 were. Cluster 1 (Table 3.40) reflected the transmembrane properties of proteins in the data set (also shown in the cellular compartment data generated in STRING v11.5), and cluster two (Table 3.41) described their localisation in the cell, within the endomembrane system.

Term ID	Term Description	Observed Gene Count	Background Gene Count	FDR
GO:0016020	Membrane	66	9072	$1.43x10^{-9}$
GO:0016021	Integral component of membrane	50	5181	$1.43x10^{-9}$
GO:0031224	Intrinsic component of membrane	51	5345	$1.43x10^{-9}$

Table 3. 339. Top three enriched cellular compartment of proteins decreased ≥ 2.0-Fold in the Rep cells compared to the mock cells, gathered in STRING v11.5.

Annotation Cluster 1	**Enrichment Score: 8.68**		
Category	**Term**	**Count**	**p-value**
UP_SEQ_FEATURE	TRANSMEM:Helical	53	$2.79x10^{-13}$
GOTERM_CC_DIRECT	GO:0016021~Integral component of membrane	49	$2.49x10^{-10}$
UP_KW_DOMAIN	KW-1133~Transmembrane helix	53	$9.51x10^{-9}$
UP_KW_DOMAIN	KW-0812~Transmembrane	53	$1.53x10^{-8}$
UP_KW_CELLULAR_COMPONENT	KW-0472~Membrane	61	$4.68x10^{-8}$
UP_SEQ_FEATURE	TOPO_DOM:Cytoplasmic	36	$1.86x10^{-7}$

Table 3. 34. Top enriched functional annotation cluster of proteins decreased ≥ 2.0-Fold in the Rep cells compared to the mock cells, gathered in DAVID v6.8.

Annotation Cluster 2	**Enrichment Score: 3.62**		
Category	**Term**	**Count**	**p-value**
GOTERM_CC_DIRECT	GO:0005789~Endoplasmic reticulum membrane	17	$2.55x10^{-6}$
GOTERM_CC_DIRECT	GO:0005783~Endoplasmic reticulum	14	$4.56x10^{-4}$
UP_KW_CELLULAR_COMPONENT	KW-0256~Endoplasmic reticulum	13	0.011887

Table 3. 35. Second most enriched functional annotation cluster of proteins decreased ≥ 2.0-Fold in the Rep cells compared to the mock cells, gathered in DAVID v6.8.

3.2.3 Choosing Targets

As described at the beginning of this chapter, the bioinformatic analysis of the proteomes of heavy membrane fractions from infected Huh-7 cells and Huh-7 replicon containing cells was performed to identify host factors potentially required by the virus or the replicon for intracellular replication, which was evaluated by an siRNA screen. Using only the results from the enrichment analysis of the proteins increased in abundance, the terms with the highest enrichment were taken and ranked by fold change when compared to the mock. The proteins with the greatest fold change were used preferentially. If the protein identified was a member of a complex, it was not chosen for further knockdown. Knocking down subunits of complexes was avoided for simplicities sake. Knockdown of a subunit may have an unpredictable effect on the function or formation of its complex, ignoring these reduced any variability in the siRNA system that was used.

The complete target lists for both DENV-2 infection and replicon cells were added to FunRich v3.1.3 and a Venn diagram was made comparing the two (not shown). The seven overlapping proteins were then cross referenced to the list of targets, and if the protein was not already in the target list, it was added; B4E2P4 (cDNA FLJ58474, highly similar to Xaa-Pro aminopeptidase 1) was not included as it is not a confirmed protein.

Originally, based on the results of previous proteomic analyses conducted in the laboratory, this project was planning to determine the role of the TMED proteins 2, 5, 7, 9, and 10 in DENV-2 replication and replicon expression in more detail. Although these proteins were not found to be altered significantly in the proteomic datasets analysed in this study they were included for interest. Details on each protein target for the DENV-2 infected and Huh-7 replicon cells can be found in Tables S.17 and S.18 respectively.

3.2.3.1 Potential Host Factors for Dengue Virus 2 Replication

Using filtered data sets containing proteins that increased by at least 1.5-fold or 2.0-fold in DENV-2 infected cells compared to mock, 41 potential targets were identified. Mitochondrial transporter proteins were highly enriched in the DENV-2 infected cells and as mitochondrial activity is known to be affected in infection (El-Bacha et al., 2007; El-Bacha & Da Poian, 2013) it was deemed prudent to include proteins from this term. This included members of the inner mitochondrial membrane (IMM) transporter family Solute Carrier 25 (SLC25A), other IMM transporters, and outer mitochondrial membrane (OMM) transporters.

Eleven SLC25A family members and 10 other mitochondrial transporters were included. From the 39 metabolic proteins increased in abundance 2.0-fold, 11 members were taken and considered as possible host factors. There were four proteins that were shared with the replicon dataset (shown in Figure 3.12) that were not already in the list of targets, and so were added. The lists of protein targets for DENV-2 infected cells can be found in Table S.17.

Ten of the twelve SLC25A family members were included in the candidate protein shortlist – SLC25A4 and 5 (isoforms of each other) (Palmieri, 2013) were discarded and replaced with SLC25A1 (a mitochondrial citrate carrier, which is key component of fatty acid synthesis (Yang et al., 2021)), alongside the remaining 10 transporters that were not members of complexes.

3.2.3.2 Potential Host Factors for DENV-2 Replicon Expression

Using the proteins that were increased 2.0-fold or more in replicon containing cells compared to mock, 35 potential host factors were identified. The cellular compartment endomembrane system (Table 3.34) was taken for further investigation, and four of the most biologically relevant biological processes were exported and ranked by FDR (see Table 3.35). These include secretion by cell, vesicle-mediated transport, response to endoplasmic reticulum stress, and response to unfolded protein (FDRs=4.47×10^{-13}, 4.48×10^{-10}, 7.55×10^{-8}, and 9.43×10^{-8}, respectively).

The proteins that were assigned to each term were ranked by fold change; if they were repeated in other terms, they were ignored. This left nine proteins assigned to the term secretion by cell, seven assigned to vesicle mediated transport, six to response to endoplasmic stress, three to response to unfolded protein. Five proteins overlapped with the DENV-2 versus Mock data that were not already in the host factor lists, and finally the five TMED proteins were included as mentioned in section 3.4.1.

The protein target list is below in Table S.18. Note, SLC1A3 (Excitatory Amino Acid Transporter 1) is included in GO term “secretion by cell” in later versions of STRING but not the version used to generate these data – it was included anyway.

3.2.4 Overlapping Proteins

The proteins increased 2.0-Fold in both the DENV-2/Mock and Rep/Mock datasets were added to FunRich v3.1.3 and a Venn diagram was made to show the overlapping proteins (Figure 3.12). Seven proteins were shared between the two groups (Table 3.42).

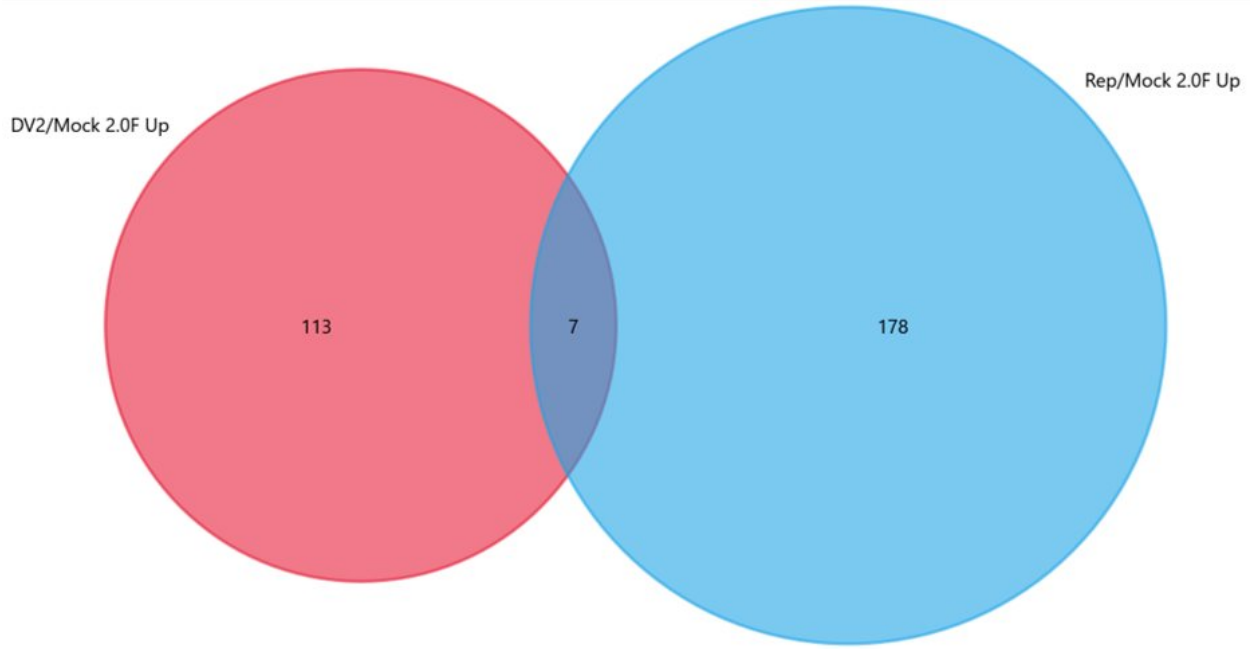

Figure 3. 12. Venn diagram produced in FunRich v3.1.3 showing the overlap between the proteins increased ≥ 2.0-fold in both the DENV-2 and Replicon containing cells compared to the mock.

UniProt Accession	Gene Name	Gene Product Name
B4E2P4	XPNPEP1	cDNA FLJ58474, highly similar to Xaa-Pro aminopeptidase 1
O95425	SVIL	Supervillin
P11021	HSPA5	Endoplasmic reticulum chaperone BiP
Q99538	LGMN	Legumain
Q9BZV2	SLC19A3	Thiamine Transporter 2
Q9P2F9	ZNF319	ZNF319
Q9ULF5	SLC39A10	Zinc Transporter ZIP10

Table 3. 36. Proteins overlapping between the ≥ 2.0-Fold increased protein lists identified by using FunRich v3.1.3.

The list was taken from FunRich and crossed referenced with the proteins already identified as possible targets. If they were already chosen as part of the list they were discarded, if they were not, they were added for further study. Four and five proteins were included in the DENV-2 and replicon candidates, respectively. “cDNA FLJ58474, highly similar to Xaa-Pro aminopeptidase 1” was discarded as it is an unreviewed protein.

3.2.5 Proteomics of the Whole Cell Lysate

The whole cell lysate (WCL) is different to the 16K lysate fractions analysed as described in Sections 3.3 – 3.4. The 16K fraction, as described in section 2.5.1 and Chapter 3, is the membranous portion of the cell that is produced after centrifuging the cells at $1.6x10^4$ x *g* for 15 minutes. In contrast, the WCL is the yield of a series of cell lysis procedures to disrupt and break apart the structural integrity of the cell. As such, the WCL will contain proteins found throughout the cell, which of course will include those also found in the 16K fraction, as well as nuclear and cytosolic proteins. The proteomic data described in this chapter, gathered from analysing the WCL, is important to consider as it contains a broader range of information on changes in the entire cellular environment. Additionally, the WCL data can be used with the 16K data set to show if a protein accumulates in the 16K fraction, the site of DENV-2 replication, but does not increase overall in the cell. However, these data were not a focus of this project and so is more briefly described than the sections on the 16K proteome analysis.

As with the 16K data set, the WCL proteomes derived from lysates of Huh-7 cells either infected with DENV-2, inactivated DENV-2, cells stably expressing a self-replicating non-infectious sub-genomic DENV-2 replicon or mock infected were analysed using TMT labelling in combination with LC-MS/MS. Eleven samples were analysed, and in the same way as the 16K data, the identities of the proteins were matched to their measured abundances. These data were the starting point for the bioinformatic analysis described below.

Unlike the 16K data, none of the results here were used to choose candidate proteins to knockdown using siRNA (Chapter 4) but were used to provide more detail on the changes to the proteome of Huh-7 cells in general, and whether a protein was altered in abundance only in the 16K fraction containing the replication complex or more broadly throughout the cell.

3.2.5.1 Statistical Interrogation

The PCA plot (Figure S.1) shows that the replicate datasets for each condition cluster together showing that the variability between the replicates is low. Also, the datasets for each condition were also separated, apart from the iDV2 and mock data sets, which clustered together as expected.

Following the PCA, histogram plots of each replicate were made (section 2.5.4) to visualise the distribution of the data (Figure S.2). Each histogram shows a normal distribution with a left-hand skew. Multiple scatter plots were then made (section 2.5.4) with a Pearson's correlation coefficient (R^2) applied to each plot. The plots (Figure S.3) for each replicate in each condition correlated well, as all the R^2 values within each condition were greater than 0.97. Additionally, the R^2 values for the plots

comparing replicates to other conditions were all greater than or equal to 0.96. Overall, these analyses showed that there were no outliers in the datasets with good reproducibility between the replicate datasets.

3.2.5.2 Statistically Significant Proteins

There was a total of 8200 human proteins identified in the WCL data set. The numbers of proteins significantly ($p < 0.05$) increased and decreased in amount greater than or equal to 2-fold or 1.5-fold in DENV-2 infected and replicon containing cells compared to the mock infected cells were plotted to allow for easier visualisation of the proportions of proteins in each group (Figures S.4 and S.5). There were 534 and 476 proteins significantly altered greater than or equal to 1.5-fold in amount in the DENV-2 infected and replicon containing cells compared to the mock cells, respectively. There were far fewer dysregulated proteins compared to the corresponding analysis of the 16K datasets. More proteins were decreased in amount than increased (1.5-fold and 2.0-fold) in DENV-2 infected cells compared to mock, which was the opposite for the proteins identified in replicon containing cells compared to mock. The numbers of proteins altered are summarised in Table S.1.

Volcano plots were made in Perseus v1.6.6.0 (section 2.5.4) to visualise the significantly altered proteins. The plot of the proteins significantly altered in amount in DENV-2 infected cells compared to the mock infected cells shows a skew towards the left, indicating that more proteins were decreased than increased (Figure S.6). The volcano plot of the proteins from the replicon containing cells compared to the mock infected cells had a much more central distribution, showing less bias towards an increase or decrease in the abundance of the significantly altered proteins (Figure S.7).

3.2.5.3 Downstream Analysis of the Whole Cell Lysate Data

Proteins identified to be significantly increased 1.5-fold or 2.0-fold in the DENV-2 infected cells compared to mock cells were not used for DS analysis as the numbers of proteins identified was too low (only 63 and 19 respectively), so meaningful enrichment could not be carried out. When the UniProt accession numbers of proteins in these categories were uploaded to STRING v11.5 or DAVID v6.8 no functional annotation clusters were identified within the cut offs defined above, thus no meaningful enrichment analysis could be performed. However, the proteins that were decreased significantly and the total list of significantly altered proteins were analysed successfully.

Additionally, the numbers of proteins identified to be increased 1.5-fold or more in the proteomes of replicon containing cells compared to mock infected cells were too low to produce much useful functional enrichment, the analysis produced that fell within the cut offs described above was included.

Furthermore, the analysis of the proteins increased 2.0-fold in the same comparison did not yield any enrichment information that was within the defined cut offs.

3.2.5.3.1 Functional Enrichment of the Proteomes DENV-2 Infected and Replicon Containing Huh-7 Cells

3.2.5.3.1.1 All Proteins Altered in Abundance at Least 1.5-Fold in DENV-2 Infected Cells

Five hundred and thirty-four proteins were identified which significantly changed in abundance by greater than 1.5-fold in DENV-2 infected cells compared to the mock. The proteins were analysed using their Uniprot accession numbers by FunRich v3.1.3 and the terms describing the cellular component enrichment are shown in Figure 3.13. Among the five most significantly enriched cellular component categories, four were directly associated with the term extracellular space (accumulating to around 35% of the total), with a smaller set of proteins associated with the term spherical high-density lipoprotein particle. All the terms had a p-value of less than 0.05.

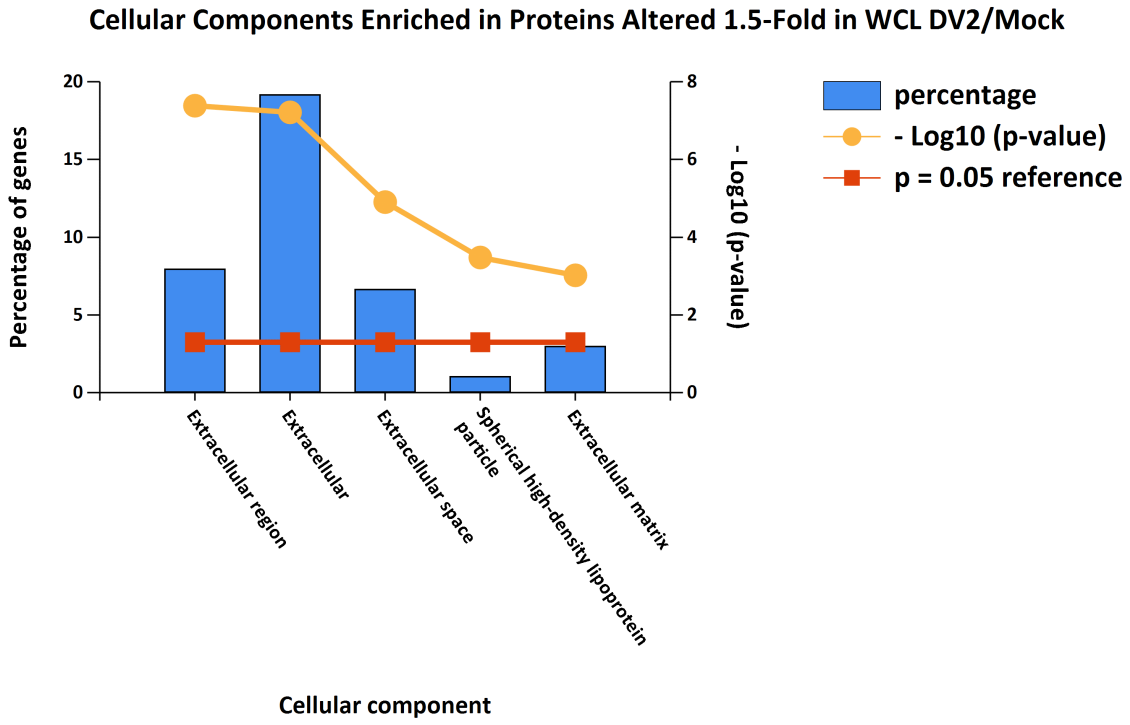

Figure 3. 13. Cellular components enriched in proteins altered ≥ 1.5-Fold in abundance of the WCL of DENV-2 infected cells compared to the mock condition.

The same set of proteins was analysed by STRING v11.5 resulting in the identification of 480 nodes. Functional enrichment networks were created and the top five most enriched biological processes, cellular components, and Reactome pathways as ranked by FDR, are shown below (Tables 3.43, 3.44, and 3.45, respectively).

Four of the top five biological processes are cell cycle related but contain some redundancy ("mitotic cell cycle process" and "mitotic cell cycle" for example (FDR=$6.83x10^{-11}$ and $8.07x10^{-11}$, respectively)) even across GO terms as one of the Reactome pathways is "cell cycle" (FDR=$1.68x10^{-6}$), see tables 3.43 and 3.45.

In contrast to the FunRich v3.1.3 cellular component enrichment analysis, the same analysis from STRING v11.5 contained a wider range of terms, (Table 3.44). These include cytoplasmic, organellular, and extracellular terms ("cytoplasm", "organelle" and "blood microparticle" (FDR=$1.63x10^{-15}$, $7.68x10^{-11}$, and $1.68x10^{-11}$, respectively)). The Reactome pathways enriched (Table 3.45) in these proteins were varied and included terms related to protein phosphorylation and the cell cycle (FDRs=$1.62x10^{-11}$ and $1.68x10^{-06}$, respectively).

The 534 proteins were also analysed by DAVID v6.8, and the top enrichment cluster that was generated (Table 3.46) was also related to the cell cycle and mitosis.

Term ID	**Term Description**	**Observed Gene Count**	**Background Gene Count**	**FDR**
GO:1903047	Mitotic cell cycle process	54	616	$6.83x10^{-11}$
GO:0000278	Mitotic cell cycle	57	695	$8.07x10^{-11}$
GO:0048518	Positive regulation of biological process	227	6112	$1.35x10^{-09}$
GO:0022402	Cell cycle process	66	976	$1.39x10^{-09}$
GO:0007049	Cell cycle	77	1313	$9.14x10^{-09}$

Table 3. 37. Top five enriched biological process, as ranked by FDR, assigned to proteins altered ≥ 1.5-Fold in abundance of the WCL of DENV-2 infected cells compared to the mock condition, identified by STRING v11.5 analysis.

Term ID	**Term Description**	**Observed Gene Count**	**Background Gene Count**	**FDR**
GO:0005737	Cytoplasm	373	11428	$1.63x10^{-15}$
GO:0005622	Intracellular	424	14276	$2.59x10^{-13}$
GO:0072562	Blood microparticle	24	115	$1.68x10^{-11}$
GO:0043229	Intracellular organelle	383	12528	$3.15x10^{-11}$

GO:0043226	Organelle	402	13515	$7.68x10^{-11}$

Table 3. 38. Top five enriched cellular components, as ranked by FDR, assigned to proteins altered ≥ 1.5-Fold in abundance of the WCL of DENV-2 infected cells compared to the mock condition, identified by STRING v11.5 analysis.

Term ID	**Term Description**	**Observed Gene Count**	**Background Gene Count**	**FDR**
HSA-8957275	Post-translational protein phosphorylation	24	107	$1.62x10^{-11}$
HSA-381426	Regulation of Insulin-like Growth Factor (IGF) transport and uptake by Insulin-like Growth Factor Binding Proteins (IGFBPs)	25	124	$1.85x10^{-11}$
HSA-114608	Platelet degranulation	19	127	$1.53x10^{-06}$
HSA-140877	Formation of Fibrin Clot (Clotting Cascade)	12	39	$1.53x10^{-06}$
HSA-1640170	Cell cycle	44	647	$1.68x10^{-06}$

Table 3. 39. Top five enriched Reactome pathways assigned to proteins altered ≥ 1.5-Fold in abundance of the WCL of DENV-2 infected cells compared to the mock condition, identified by STRING v11.5 analysis.

Annotation Cluster 1	**Enrichment Score: 8.01**		
Category	**Term**	**Count**	**p-value**
UP_KW_BIOLOGICAL_PROCESS	KW-0131~Cell cycle	50	$6.10x10^{-10}$
UP_KW_BIOLOGICAL_PROCESS	KW-0132~Cell division	36	$3.46x10^{-9}$
GOTERM_BP_DIRECT	GO:0051301~Cell division	32	$1.01x10^{-8}$
UP_KW_BIOLOGICAL_PROCESS	KW-0498~Mitosis	26	$4.12x10^{-7}$

Table 3. 40. Top enriched functional annotation cluster of proteins altered ≥ 1.5-Fold in abundance of the WCL of DENV-2 infected cells compared to the mock condition, identified by DAVID v6.8 analysis.

3.2.5.3.1.2 All Proteins Altered in Abundance at least 1.5-Fold in Replicon Cells

There were 476 proteins identified to have significantly changed in abundance by at least 1.5-fold when comparing the proteome of replicon containing and mock infected cells. The proteins were initially analysed by FunRich v3.1.3 and the top five cellular component terms enriched (as ranked by p-value)

are shown in Figure 3.14. Around 40% of the proteins identified belong to the CC term “cytoplasm”, and approximately 30% belong to terms related to extracellular spaces (“exosomes” and “extracellular matrix”). Around 60% of the proteins make up the term’s lysosome and cytoplasm (20-25% and 40% respectively). All these terms had a p-value of less than 0.05.

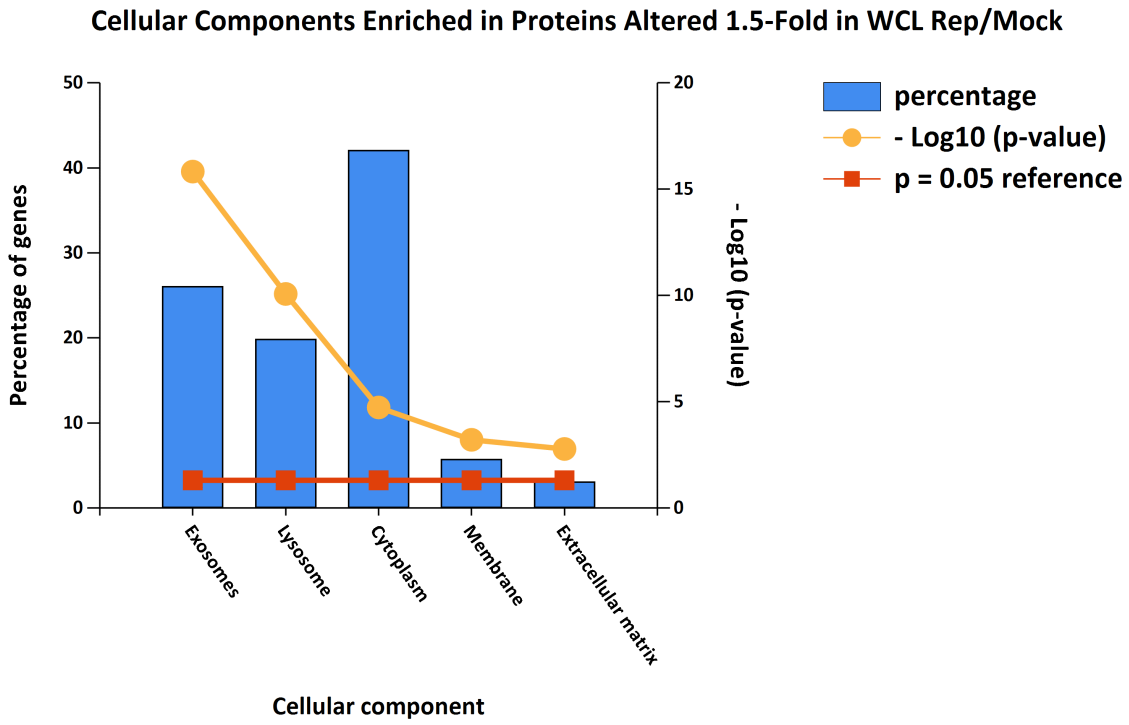

Figure 3. 14. Cellular Components Enriched in Proteins Altered ≥ 1.5-Fold in the WCL of Replicon Containing Cells Compared to the Mock Infected.

The proteins were analysed by STRING v11.5 resulting in the identification of 426 nodes. The DAVID v6.8 analysis was not used as the top enrichment cluster score was less than 3.

The top five biological processes, cellular components and top two Reactome pathways were ranked by FDR and are shown in Tables 3.47, 3.48, and 3.49, respectively. Metabolic processes are highly enriched in the biological process enrichment table, cytoplasmic and extracellular terms are enriched in the cellular component enrichment table (including “cytoplasm” and “extracellular organelle” (FDRs=1.19×10^{-19} and 9.01×10^{-14}, respectively)).

The two Reactome pathways (all the other Reactome pathways enriched had an FDR greater than 1.0×10^{-5} and so were excluded) are metabolic processes – “metabolism” (FDR=1.24×10^{-16}) and “metabolism of lipids” (FDR=4.79×10^{-7}).

Term ID	Term Description	Observed Gene Count	Background Gene Count	FDR
GO:0044281	Small molecule metabolic process	103	1684	$3.33x10^{-17}$
GO:0019752	Carboxylic acid metabolic process	65	853	$6.82x10^{-14}$
GO:0043436	Oxoacid metabolic process	67	944	$3.92x10^{-13}$
GO:0044283	Small molecule biosynthetic process	51	572	$4.68x10^{-13}$
GO:0032787	Monocarboxylic acid metabolic process	44	515	$1.76x10^{-10}$

Table 3. 41. Top five enriched biological process terms of proteins altered ≥ 1.5-Fold in abundance of the WCL of replicon containing cells compared to the mock condition, identified by STRING v11.5 analysis.

Term ID	Term Description	Observed Gene Count	Background Gene Count	FDR
GO:0005737	Cytoplasm	345	11428	$1.19x0^{-19}$
GO:0043230	Extracellular organelle	108	2126	$9.01x10^{-14}$
GO:1903561	Extracellular vesicle	107	2121	$1.39x10^{-13}$
GO:0070062	Extracellular exosome	106	2099	$1.41x10^{-13}$
GO:0005829	Cytosol	178	5193	$4.25x10^{-9}$

Table 3. 42. Top five enriched cellular component terms of proteins altered ≥ 1.5-Fold, identified by STRING v11.5 analysis.

Term ID	Term Description	Observed Gene Count	Background Gene Count	FDR
HSA-1430728	Metabolism	114	2089	$1.24x10^{-16}$
HSA-556833	Metabolism of lipids	46	733	$4.79x10^{-7}$

Table 3. 43. Top two enriched Reactome pathway terms of proteins altered ≥ 1.5-Fold in abundance of the WCL of replicon containing cells compared to the mock condition, identified by STRING v11.5 analysis.

3.2.6 A Comparison of the WCL and 16K Data Sets of DENV-2 Infected Cells

Much of the focus of this chapter has been to understand the changes in the proteins in the 16K fraction of infected and replicon containing cells through GO enrichment analysis. Here, we briefly explore the 16K fraction data in the context of the WCL.

Firstly, the overlap between proteins identified in both conditions was assessed. As previously shown, 8200 and 7247 proteins were identified in the WCL and 16K fraction, respectively. The protein accession numbers were added to FunRich v3.1.3 and a Venn diagram of these two data sets was made – see Figure 3.15. Six thousand and sixty-six proteins were shared between the two data sets. This leaves 1933 and 980 proteins only identified in the WCL and 16K fraction data sets, respectively. Brief enrichment analysis of these two lists does not reveal any insight into the proteomes of DENV-2 infected cells not already described throughout this chapter so the results have not been included.

Next, proteins altered in abundance at least 1.5-fold in either the WCL or 16K fractions of DENV-2 infected compared to mock infected cells were compared. Another Venn diagram was made using the proteins altered in abundance at least 1.5-fold (Figure 3.15). One hundred and ninety-seven proteins were altered significantly in both data sets and 1164 proteins were altered in just the 16K fraction data. Functional enrichment of these proteins was performed using STRING v11.0 but is not shown below as the enrichment analysis generated was largely the same as the results described in section 3.2.3.1.3. This is most likely because the numbers of proteins are very similar to the original data set of proteins measured to be increased or decreased 1.5-fold in the 16K fraction of DENV-2 infected cells.

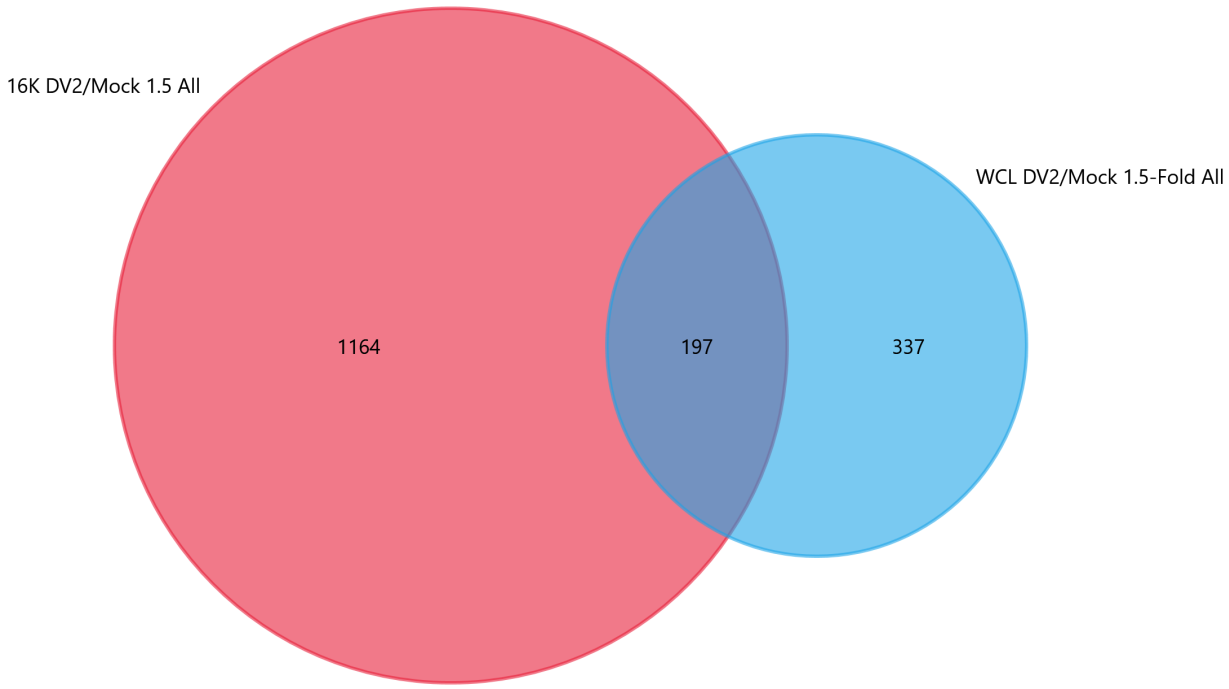

Figure 3. 15. Venn Diagram showing all the proteins altered in abundance ≥ 1.5-fold in the 16K DENV-2 infected data set compared to all the proteins identified in the WCL data set. Made in FunRich v3.1.3.

To identify if there was any interesting functional enrichment of the proteins only altered in abundance in the 16K fraction, but still identified in the WCL data set, another Venn diagram was made (Figure 3.16) with the accessions of the shared proteins and of the proteins altered 1.5-fold in the 16K and WCL data sets. This potentially would also reveal if proteins were sequestered to the 16K fraction from the WCL.

There were 168 proteins altered in abundance at least 1.5-fold only in the 16K fraction of DENV-2 infected or replicon containing cells compared to mock. The accession numbers of these proteins were added to DAVID v6.8. The top enrichment cluster (Table 3.49) reveals that most of these proteins are either transmembrane proteins or proteins associated with membranes which is unsurprising as the 16K fraction is made up of protein rich membranous structures like the Golgi, ER, and mitochondria. The analysis did not reveal any enrichment of proteins or pathways not expected to be seen in the 16K, such as those shown in section 3.2.3.1.1.

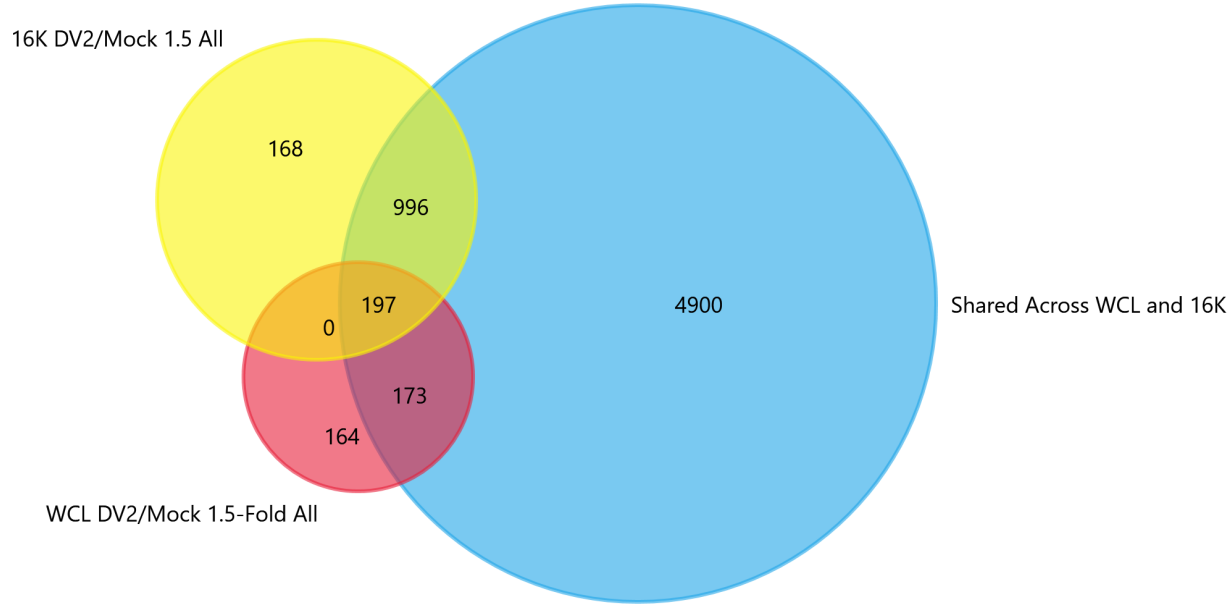

Figure 3. 16. Venn diagram showing the overlap between proteins shared between the different data sets. Made in FunRich v3.1.3.

Annotation Cluster 1	**Enrichment Score: 5.19**		
Category	**Term**	**Count**	**p-value**
UP_SEQ_FEATURE	TOPO_DOM:Cytoplasmic	54	3.85E-06
UP_SEQ_FEATURE	TRANSMEM:Helical	68	4.42E-06
GOTERM_CC_DIRECT	GO:0016021~Integral component of membrane	68	5.58E-06
UP_KW_DOMAIN	KW-0812~Transmembrane	77	6.25E-06
UP_KW_DOMAIN	KW-1133~Transmembrane helix	76	8.30E-06
UP_KW_CELLULAR_COMPONENT	KW-0472~Membrane	93	1.42E-05

Table 3. 44. Top functional annotation cluster of the proteins that were not increased in the WCL of DENV-2 infected Huh-7 cells compared to mock, gathered in DAVID 6.8.

3.2.7 A Comparison of the WCL and 16K Data Sets in Replicon Containing Cells

The process described above in section 3.2.6 was repeated, but using the proteins identified in the replicon data sets. There were 114 proteins identified to be altered in abundance in both the 16K and WCL replicon containing cells at least 1.5-fold when compared to the mock data set (Figure 3.17). They share 114 proteins, and so functional enrichment of the proteins only found in the different fractions subsets does not yield new information not described in sections 3.2.4.1 and 3.2.5.3.1.2 (16K and WCL replicon data respectively). This data was not included in the thesis.

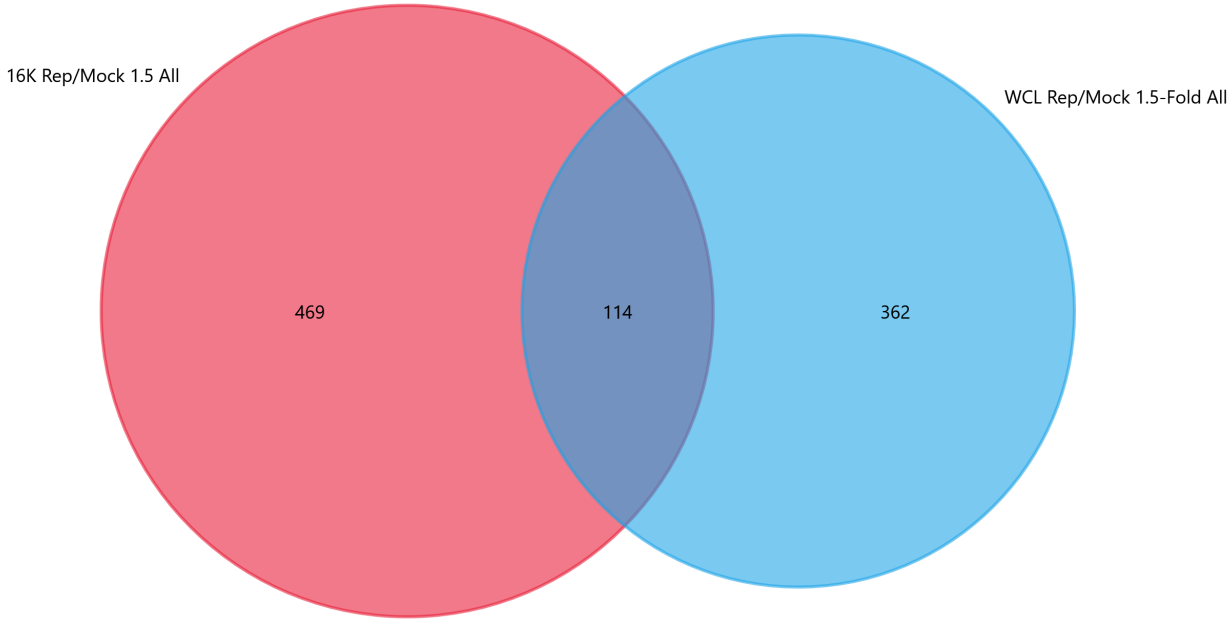

Figure 3. 17. Venn diagram showing the overlap between the proteins altered in abundance ≥ 1.5-fold in the 16K and WCL fractions of replicon cells compared to the mock conditions. Made in FunRich v3.1.3.

Following this, another Venn diagram was made using the proteins identified in both the WCL and 16K fractions, as well as the proteins altered ≥1.5-fold in both (Figure 3.18). Three hundred and eighty-nine proteins were found in both subsets but only increased in the 16K data. The accession numbers of these proteins were analysed using DAVID v6.8 and the functional annotation clustering was examined. The data are not shown here as it does not provide any new information not already shown.

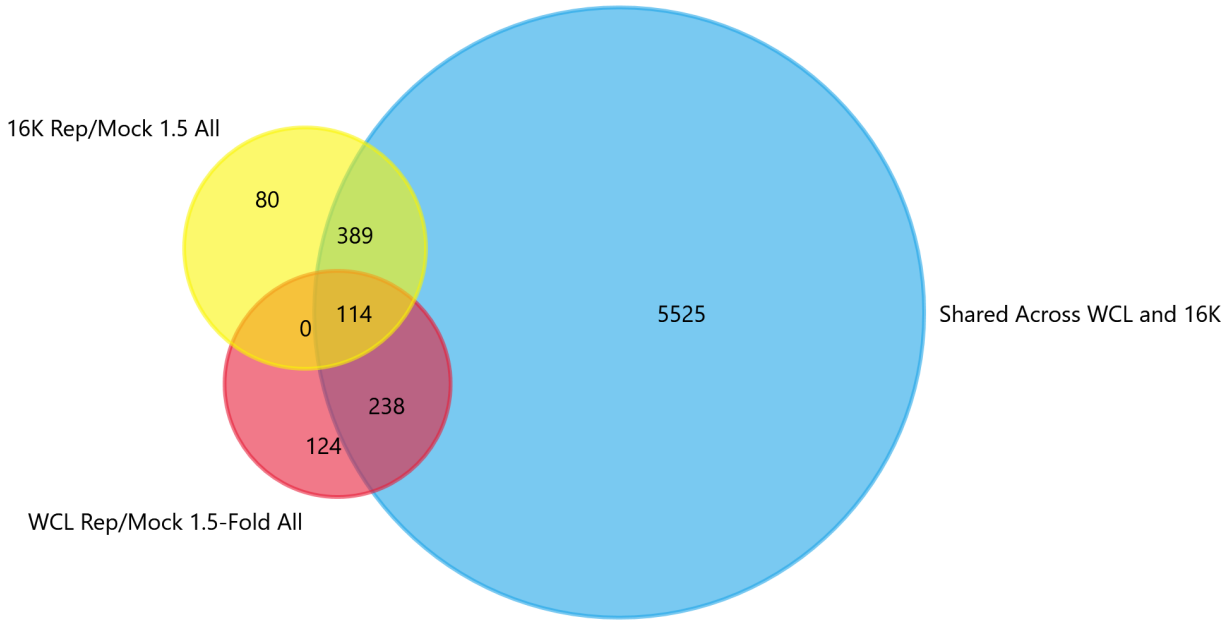

Figure 3. 18. Venn diagram showing the overlap between the different data sets. Made in FunRich v3.1.3.

3.2.8 Mock and Inactivated DENV-2 Infection as Controls

Bioinformatic analysis was performed to explore the changes to the proteomes of Huh-7 cells either infected with DENV-2 or stably expressing the replicon, the results of which have been described above. The proteomic analysis was performed by comparing the altered proteins against the mock infection condition.

This section describes the rationale for the use of the mock infected cell lysate data instead of the corresponding data from lysates of cells treated with inactivated DENV-2.

Firstly, the PCA plotted from both the 16K (Figure 3.1) and WCL (Figure S.1) data show low variation between the identified protein abundances in the iDV2 and mock infected cells. Secondly, although the iDV2 control was a suitable comparator for the data produced using DENV-2 infected cells this was not the case for data produced using replicon containing cells. Therefore the decision was made to use the data from the mock infected cells as the comparator for all analysis for consistency.

As iDV2 may have been a better comparator to use for the infected cells, a brief analysis comparing the results of DV2/Mock and DV2/iDV2 in the 16K and WCL conditions was performed. Only the proteins altered 2.0-fold or more were included in the GO enrichment, but the proteins changed 1.5-fold in abundance are included in the Venn diagrams. Additionally, the proteins chosen for siRNA knockdown (based on the DENV-2 infected and Mock infected data) were cross referenced with the DV2/iDV2 data.

3.2.8.1 16K Fraction

Taking the proteins altered in abundance ≥ 1.5-Fold, there were 1361 and 1412 in the DENV-2 versus mock and DENV-2 versus iDV2 conditions respectively. The UniProt accession numbers of each hit from these two protein lists were added to FunRich v3.1.3 and a quantitative Venn diagram was made (Figure 3.19). These two data sets shared a total of 1193 proteins, with 168 and 219 unique to mock and iDV2, respectively.

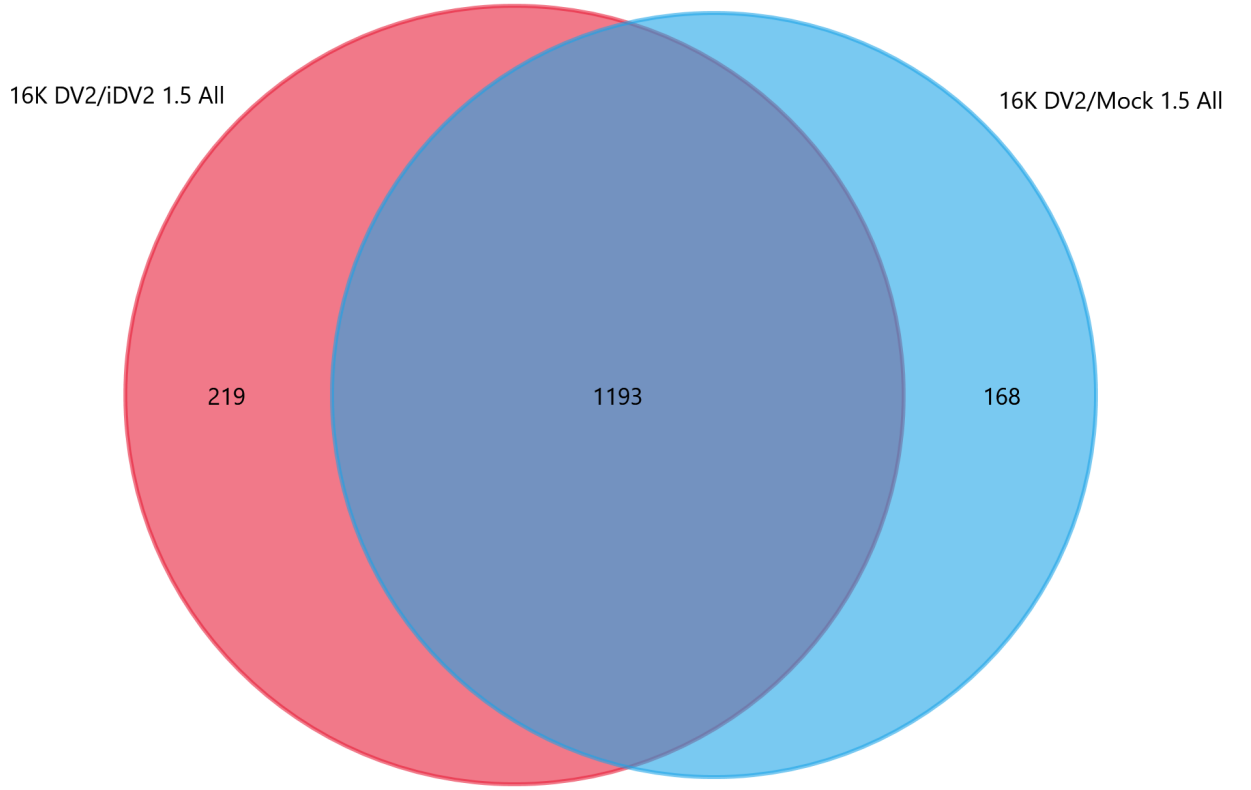

Figure 3. 19. Venn diagram made in FunRich v3.1.3 showing the overlap of proteins altered ≥ 1.5-Fold in abundance in the DENV-2 infected compared to either the iDV2 or Mock infected cells.

In contrast, the differences between the 2.0-Fold altered protein data sets DV2 versus Mock and DV2 versus iDV2 were much smaller (Figure 3.20). There were 503 and 500 significantly changed in abundance 2.0-fold or more in the groups DV2 versus Mock and DV2 versus iDV2, respectively. When compared, these two data sets shared a total of 439 proteins, with only 64 and 61 unique to mock and iDV2, respectively.

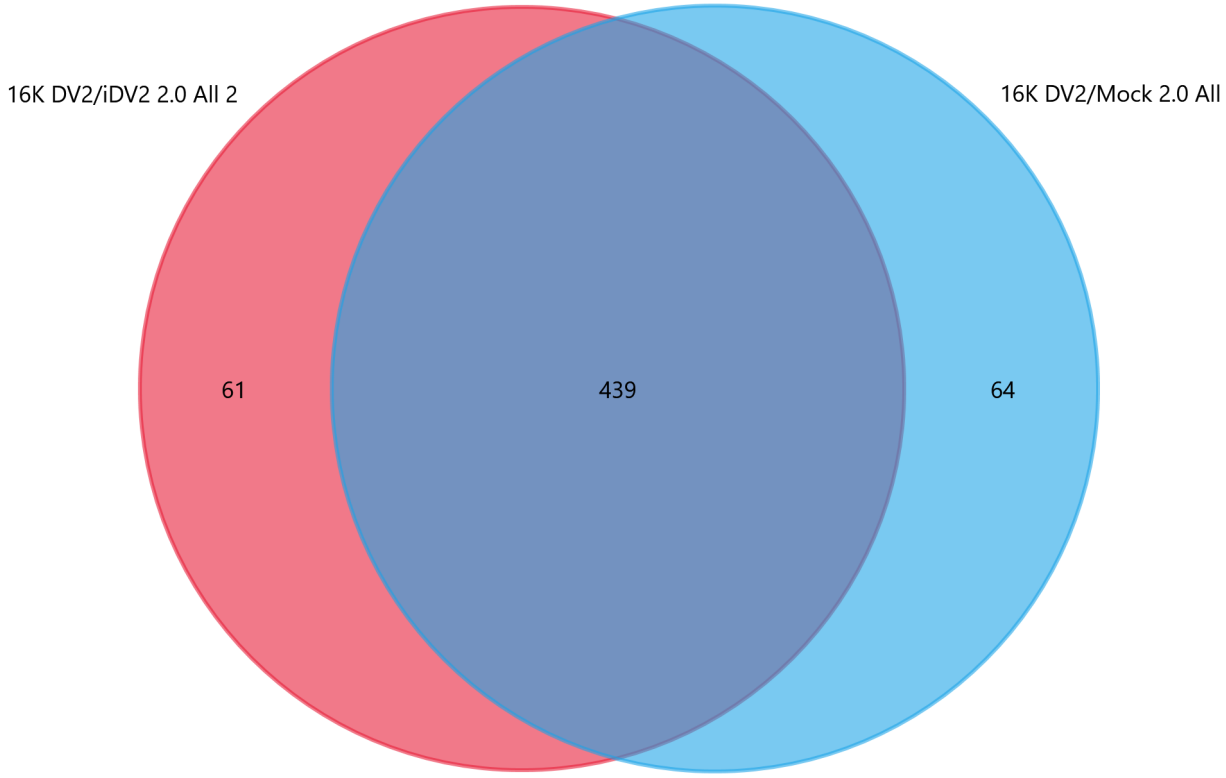

Figure 3. 20. Venn diagram made in FunRich v3.1.3 showing the overlap of proteins altered ≥ 2.0-Fold in amount in the DENV-2 infected compared to either the iDV2 or Mock infected cells.

To understand if there is a difference in functional enrichment when mock and iDV2 were used as comparators, downstream analysis was performed on the proteins significantly altered in DENV-2 infected cells compared to the iDV2 treated cells. STRING version v11.5 were used to produce protein-protein interaction networks and from that, enrichment analysis of the biological processes, cellular components, and the Reactome pathways associated with the proteins identified as significant.

3.2.8.1.1 All Proteins Altered ≥ 2.0-Fold in the 16K of DENV-2 Infected Cells Compared to iDV2 Treated Cells

Five hundred proteins were altered at least 2.0-fold in DENV-2 infected cells when compared to cells treated with iDV2, which is 3 fewer than the number of proteins altered when compared to the Mock infected. Of the 500 proteins identified, 456 nodes were made when the UniProt accessions were added to STRING v11.5.

The top five biological processes were all metabolic processes, for example “small molecule metabolic process” (FDR=3.23×10^{-23}) and “metabolic process” (FDR=9.53×10^{-16}) – shown in more detail in Table S.2. This term is associated with 289 proteins (62.7% of the total number of nodes made in STRING v11.5).

Four of the top five cellular components are related to mitochondria: including “mitochondrion”, “mitochondrial matrix”, and “mitochondrial membrane” (FDRs=$8.62x10^{-48}$, $4.36x10^{-45}$, and $6.95x10^{-12}$, respectively), which is shown in Table S.3. The remaining term is “cytoplasm” (FDR=$1.93x10^{17}$).

The top Reactome pathways are all related to metabolism. These included the “citric acid (TCA) cycle” and “respiratory electron transport”, “metabolism”, “respiratory electron transport” and “citric acid cycle (TCA cycle)” (FDRs=$6.72x10^{-18}$, $1.07x10^{-17}$, $1.63x10^{-8}$, and $6.09x10^{-7}$, respectively), shown in Table S.4.

3.2.8.1.2 All Proteins Inwcreased ≥ 2.0-Fold in the 16K of DENV-2 Infected Cells Compared to iDV2 Treated Cells

One hundred and ten proteins were increased in abundance at least 2.0-fold in DENV-2 infected cells versus those treated with inactivated DENV-2. When the UniProt accession numbers were pasted into STRING v11.5, 103 nodes were made.

The five biological processes with the smallest FDR values (Table S.5) they include metabolic and respiratory terms such as “oxidative phosphorylation”, “generation of precursor metabolites” and “energy and respiratory electron transport chain” (FDRs=$1.22x10^{-22}$, $1.11x10^{-14}$, and $1.11x10^{-14}$, respectively).

The cellular component terms with the greatest enrichment as determined by FDR are “mitochondrial and organellular”; “inner mitochondrial membrane protein complex”, “mitochondrial inner membrane”, and “organelle inner membrane” (FDRs=$3.52X10^{-24}$, $5.15X10^{-23}$, and $7.26X10^{-23}$, respectively) (Table S.6). The term “organelle inner membrane” is contributed to by mitochondrial proteins, such as those in respiratory complex one.

The top five Reactome pathways enriched in these proteins are also all mitochondrial (Table S.7). They include “respiratory electron transport”, “cristae formation”, “formation of ATP by chemiosmotic coupling”, and “complex I biogenesis” (FDR=$2.74X10^{-14}$, $1.25X10^{-8}$, $1.70X10^{-8}$, and $1.70X10^{-8}$, respectively).

3.2.8.1.3 All Proteins Decreased ≥ 2.0-Fold in the 16K Fraction of DENV-2 Infected Cells Compared to iDV2 Treated Cells

The 390 proteins that were decreased at least 2.0-fold in DENV-2 infected cells when compared to the inactivated DENV-2 treated cells. After adding the UniProt accessions to STRING v11.5, a protein-protein interaction network of 353 nodes was made.

The top enriched five enriched biological processes were all metabolic terms, including “carboxylic acid metabolic process”, “small molecule metabolic process”, and “oxoacid metabolic process” (FDR= $2.17X10^{-21}$, $2.79X10^{-21}$, and $7.80X10^{-21}$, respectively) (Table S.8). The top five enriched Cellular components (Table S.9) were mitochondrial, cytoplasmic and organellular, including “mitochondrion”, “cytoplasm”, and “intracellular organelle lumen” (FDR= $5.02X10^{-32}$, $2.82X10^{-10}$, and $3.75X10^{-10}$, respectively).

The Reactome pathway terms enriched were varied (Table S.10), and include metabolic, catabolic and phosphorylation related terms metabolism, branched-chain amino acid catabolism, and post-translational protein phosphorylation (FDR= $3.50X10^{-10}$, $2.02X10^{-5}$, and $9.18X10^{-5}$, respectively).

3.2.8.2 Whole Cell Lysate Fraction

More proteins were altered in abundance at least 1.5-fold in DENV-2 infected cells compared to iDV2 than compared to the mock infected (775 and 534 proteins respectively). The UniProt accession numbers were added to FunRich v3.1.3 and a Venn diagram was made, shown in Figure 3.21. When the two protein lists were compared, they shared a total of 495 proteins. 39 and 280 proteins were not shared between the two groups when mock and iDV2 was used, respectively.

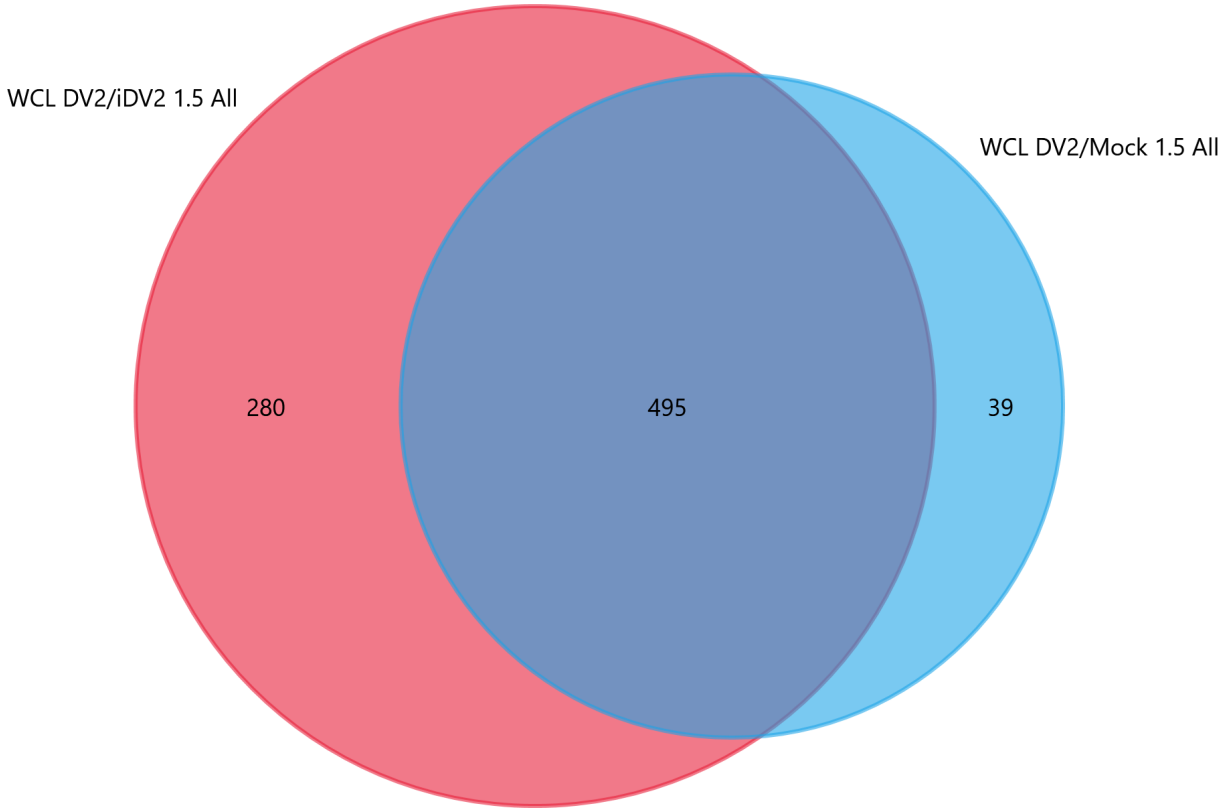

Figure 3. 21. Venn diagram made in FunRich v3.1.3 showing the overlap of proteins altered in abundance ≥ 1.5-Fold in DENV-2 infected cells compared to either iDV2 or mock infected cells.

The UniProt accession numbers of the proteins altered in abundance at least 2.0-Fold were added to FunRich v3.1.3, and a Venn diagram was made (Figure 3.22). There were more proteins altered at least 2.0-Fold in abundance in the DENV-2 infected cells when compared to the iDV2 than mock infected at 398 and 219, respectively. When compared, these two data sets shared a total of 161 proteins, with 58 and 237 not being shared between them when mock or iDV2 were used as a comparator, respectively.

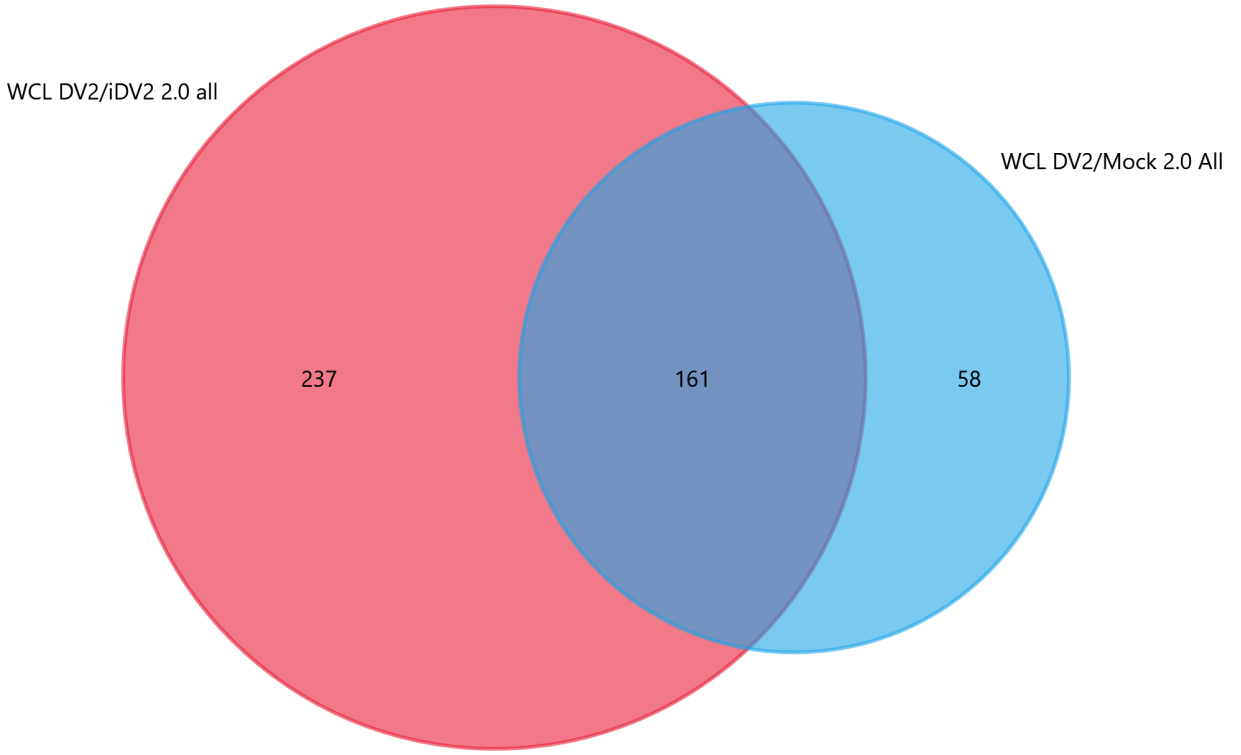

Figure 3. 22. Venn diagram made in FunRich v3.1.3 showing the overlap of the proteins altered in abundance ≥ 2.0-Fold in DENV-2 infected cells compared to either iDV2 or mock infected cells.

3.2.8.2.1 All Proteins Altered at Least 2.0-Fold in DENV-2 Infected Cells Compared to iDV2 Treated Cells

There were 398 proteins that were altered in abundance 2.0-fold or more in DENV-2 infected cells when compared to the iDV-2 treated cells. The UniProt accessions were added to STRING v11.5 where a protein-protein interaction network was made with 359 nodes.

As the top six enriched biological processes assigned to these proteins were related to negative regulation terms (e.g. “negative regulation of metabolic process”, FDR=2.00x10^{-6}) seven biological processes were exported to give a broader picture of the terms enriched. The seventh most enriched term was “mitotic cell cycle phase transition” (FDR=1.38x10^{-5}) (Table S.11).

The top five cellular components enriched in these proteins ranged from extracellular to cytoplasmic and organellular (“collagen-containing extracellular matrix”, “membrane bounded organelle”, and “cytoplasm” (FDR=4.24x10^{-14}, 6.56x10^{-12}, and 7.79x10^{-11}, respectively) (Table S.12).

Only three Reactome pathway terms were enriched with an FDR of less than 1.0x10^{-5}, these are: post-translational protein phosphorylation, regulation of Insulin-like Growth Factor (IGF) transport and uptake by Insulin-like Growth Factor Binding Proteins (IGFBPs) and platelet degranulation (FDR=1.99X10^{-7}, 7.72X10^{-7}, and 3.19X10^{-5}, respectively) (Table S.13).

3.2.8.2.2 All Proteins Increased ≥ 2.0-Fold in DENV-2 Infected Cells Compared to iDV2 Treated Cells

As only 26 proteins were increased 2.0-fold no significant enrichment was detected using STRING v11.5 nor DAVID v6.8 so no analysis was performed – which was also the case for the 2.0-fold increased proteins in the DENV-2 infected cells when compared to the mock infected cells.

3.2.8.2.3 All Proteins Decreased ≥ 2.0-Fold in DENV-2 Infected Cells Compared to iDV2 Treated Cells

There were 372 proteins that were decreased at least 2.0-fold in cells infected with DENV-2 when compared to the cells treated with inactivated DENV-2. The UniProt accession numbers were added to STRING v11.5 where a network with 338 nodes was made.

The top four biological processes were regulatory processes, three of which directly termed negative. The final term was "mitotic cell cycle phase transition" (FDR=6.30×10^{-6}) (Table S.14). The top five cellular components (Table S.15) were related to the extracellular matrix, and intracellular environment; "extracellular matrix", "intracellular", "membrane bounded organelle" (FDR=$9.42X10^{-11}$, $2.57X10^{-10}$, and $3.68X10^{-10}$, respectively).

Only three Reactome pathways were enriched with an FDR of less than 1.0×10^{-5}, these are the same terms as the 2.0-fold changed DENV-2 versus iDV2 data described above in section 3.2.8.2.1 (FDR=$6.68X10^{-7}$, $2.32X10^{-6}$, and $1.46X10^{-5}$, respectively) (Table S.16).

3.2.9 Cross Referencing

The UniProt accession numbers of the 1412 proteins 1.5-fold increased or decreased in the DENV-2 infected cells versus the mock infected were analysed using FunRich v3.1.3, 1379 accessions were recognized. The UniProt accession numbers of the proteins selected for siRNA knockdown were also analysed using FunRich v3.1.3 and a Venn diagram showing the overlap between the lists was made (Figure 3.22).

The eight proteins in the DENV-2 target list that lie outside the Venn are: citrate carrier (CiC), ornithine carrier (ORNT1), mitochondrial inner membrane protein (OXA1L), mitochondrial Pyruvate Carrier 2 (MPC2) and TMEDs 2, 5, 7 and 10 (detail of which is described in this section and included in Table 3.50). CiC is not expected to be in the list of significant proteins as the p-value was 0.048 and the fold change in DENV-2 infection versus mock infection was 1.36. CiC (aka SLC25A1) was chosen to be part of the target protein list because as so many of the SLC25A family were changed in abundance, it was thought that it may have a role in the potentially altered mitochondrial activity.

TMEDs 2, 5, 7 and 10 are expected to be outside of this list as they are not changed significantly in the DENV-2 versus mock data sets and were included in the siRNA knockdown screens to continue previous work. TMED7 was increased 1.59-fold, with a p-value of 0.0024 and so is a significantly altered protein. The targets chosen from the replicon versus mock data were not included in the Venn diagram (Figure 3.23) as there is no data comparing the replicon to the iDV2 treated cells.

Protein Name	**UniProt Accession Number**	**Gene Name**	**DV2/Mock Fold Change (log_2)**	**DV2/Mock p-value**	**DV2/iDV2 Fold Change (log_2)**	**DV2/iDV2 p-value**
Citrate Carrier (CiC)	P53007	SLC25A1	0.443	0.048*	0.472	0.049*
Ornithine Carrier (ORNT1)	Q9Y619	SLC25A15	0.723†	0.019*	0.566	0.025*
Mitochondrial inner membrane protein OXA1L	Q15070	OXA1L	0.633†	0.035*	0.515	0.036*
Mitochondrial Pyruvate Carrier 2	O95563	MPC2	0.587†	0.024*	0.563	0.026*
Transmembrane emp24 domain-containing protein 2	Q15363	TMED2	0.021	0.611	0.022	0.300
Transmembrane emp24 domain-containing protein 5	Q9Y3A6	TMED5	-0.008	0.832	0.022	0.305
Transmembrane emp24 domain-	Q9BVK6	TMED9	0.220	0.195	0.278	0.135

containing protein 9						
Transmembrane emp24 domain-containing protein 10	P49755	TMED10	0.341	0.011*	0.376	0.001*

*Table 3. 45. The 8 protein targets that were either non-significant or were not increased at least 1.5-Fold in DENV-2 infected cells compared to iDV2 treated cells. † Denotes significant fold change. * Denotes significant p-value.*

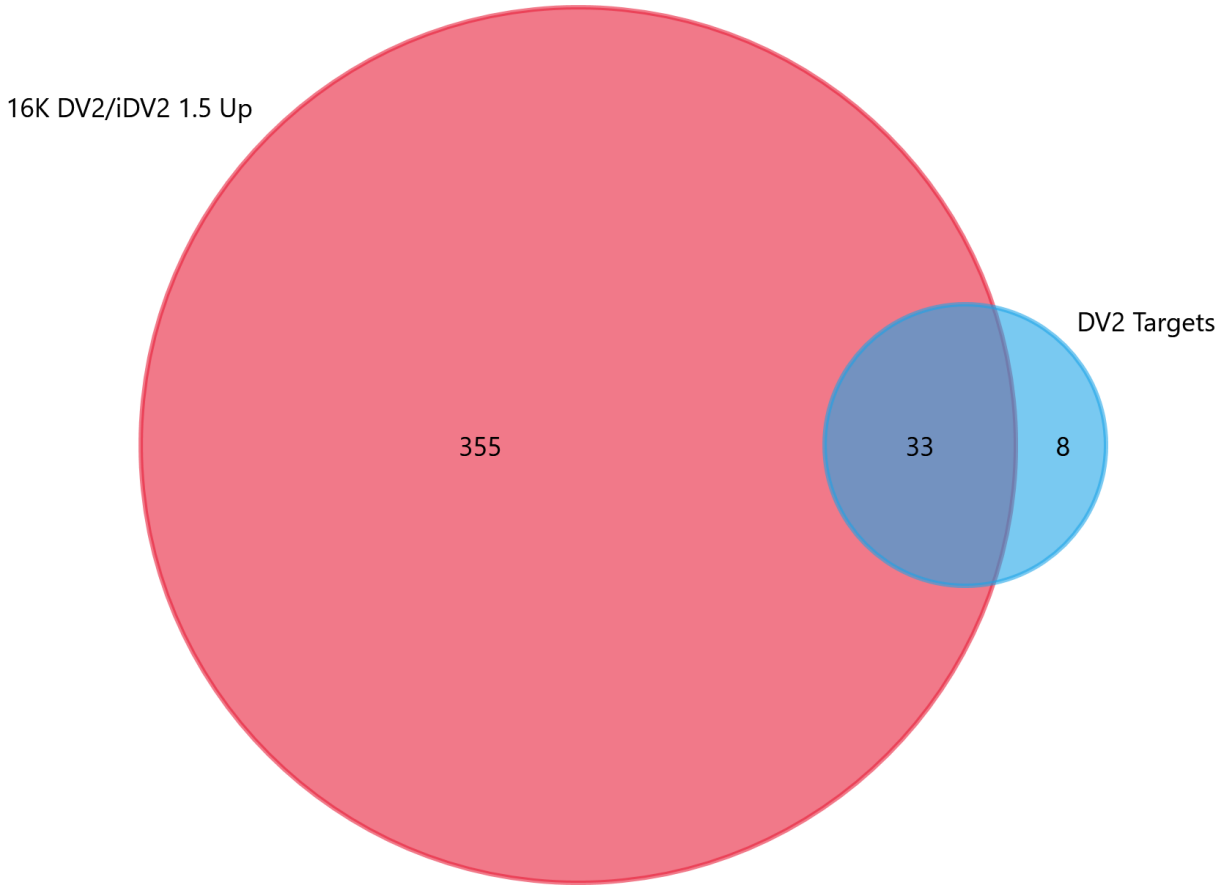

Figure 3. 23. Venn diagram made in FunRich v3.1.3 showing overlap between the proteins altered in abundance ≥ 1.5-Fold in DENV-2 infection when compared to the iDV2 treated cells and the 16K siRNA target proteins.

Chapter 4: siRNA Screening

4.1 Introduction

Large scale siRNA and other screening techniques, such as CRISPR Cas9, have been used since 2009 to identify HFs in dengue virus (DENV) infection. Silencing RNAs (siRNAs) are short RNA duplexes targeted to specific regions of an mRNA. The function of an siRNA is to transiently reduce the amount of protein in a cell, termed knockdown, by directing the mRNA for degradation before translation via the RNA-induced silencing complex (RISC) (Dana et al., 2017; Svoboda, 2020).

siRNAs take advantage of RNA interference (RNAi), a conserved mechanism which has many roles, including antiviral activity and regulation of endogenous gene expression (Svoboda, 2020). RNAi is the process by which trigger RNA (e.g. dsRNA) is processed to short interfering RNAs (also known as siRNAs). RNA-induced Silencing Complex (RISC) cleaves the target RNA and so it cannot be expressed (Svoboda, 2020). An siRNA skips the step of processing (mentioned above) and is loaded directly into RISC, once activated RISC can destroy the mRNA in a highly specific manner (Dana et al., 2017).

An early targeted siRNA screens of HFs required for DENV infection was in 2009, using A549 cells and focussed on knocking down proteins involved in cholesterol synthesis. Rothwell et al. (2009) showed that the cholesterol synthesis pathway was required for DENV-2 replication. A year later, an siRNA screen (based on reverse transfection) focussing on knocking down proteins with a role in trafficking and entry into a cell found that clathrin-mediated endocytosis was required for DENV entry into A549 cells, crucial facts in our understanding of DENV replication (Ang et al., 2010). More recently, an siRNA screen targeting kinases was performed using Huh-7 cells and identified a range of host sensitivity factors (HSFs) and host resistance factors (HRFs), indicating that DENV hijacks different cellular processes in different ways (Kwon et al., 2014).

A study published in 2016 that neatly used a cell line specific siRNA screen in combination with CRISPR/Cas9 and proteomics to unpick the HFs required for DENV and Zika virus (ZIKV) infection found that the endoplasmic reticulum membrane complex (EMC), in conjunction with the oligosaccharide-transferase complex (OST) and the translocon, was required by both viruses for effective replication (Savidis et al., 2016). Another parallel study published in 2016, showed that the OST complex was necessary for DENV infection but less crucial for Yellow Fever virus (YFV), West Nile virus (WNV), and ZIKV (Marceau et al., 2016).

More recently, a genome wide CRISPR/Cas9 knockout (KO) screen revealed that receptor for activated protein kinase 1 (RACK1) was required for ZIKV infection, and further experiments using siRNAs showed that it was also an HSF in DENV-2 infection (Shue et al., 2021). This is not an exhaustive list of the screens that have taken place but are described to demonstrate the power of this method of experiment at identifying HFs in DENV infection.

To try to understand the role of the proteins increased in the 16K fraction of DENV-2 infected cells compared to mock infected cells (described in Chapter 3), which are potentially required for DENV-2 replication, a siRNA screen was performed. Huh-7 cells have been used in a variety of capacities to study DENV infection as they are permissive and a biologically relevant model. A fairly recent RNAi screen using Huh-7 cells infected with either DENV or YFV in 384 well imaging plates revealed that multiple members of the EMC are required for virus infection (Barrows et al., 2019).

Huh-7 cells have also been used in antiviral drug assays. One publication documented the development of a small molecular inhibitor high throughput tool and the importance of the c-Src protein kinase in the replication cycle of DENV (Chu & Yang, 2007). A high throughput antiviral drug screen based on cytopathic effect (CPE), using natural compounds from the United States National Cancer Institute, was developed using Huh-7.5.1 cells. This screen identified four compounds with potent anti-DENV activity (Mccormick et al., 2012). Lastly, a 96-well antiviral screen was developed and validated in Huh-7 cells (as well as other cell lines) using both DENV and Zika virus (ZIKV) with a pan-flaviviral α-E monoclonal antibody. The system was designed to assay the effect of a drug on the initial infectivity and the infectivity of the secreted viruses from treated cells (Vicenti et al., 2020).

The proteomic analysis described in Chapter 3 identified several proteins that were dysregulated during DENV-2 infection, as well as Huh-7 cells expressing a DENV-2 replicon. A selection of these proteins were chosen as targets to examine further their relevance to the virus lifecycle, using a siRNA screen. the selected target proteins and information about them is shown in Tables S.17 and S.18. Before the screen could go ahead, the conditions had to be optimised. These included the amount of transfection reagent used (TFR), concentration of siRNA, initial seeding density, and length of transfection. The titre of the DENV-2 stock used was also determined using Huh-7 cells.

The method used for this siRNA screen (as it is a high throughput system) was reverse transfection. In this process, the cells are seeded into the wells of a plate (in this case a 96-well plate) where siRNAs and the reagents necessary for transfection are already present. As the cells adhere and grow, the specific transcripts targeted by the siRNAs are concurrently knocked down, resulting in depletion of the

corresponding proteins. After 72, hours the Huh-7 replicon cells were fixed with 8% PFA. The Huh-7 cells were infected with DENV-2 for a further 24 hours, and then fixed with 8% PFA. The straining protocol was adapted from a SARS-CoV-2 protocol, developed by Dr Kavanagh Williamson, and optimised for Huh-7 cells and DENV-2 infection.

A custom library of "On-Targetplus" siRNAs against target proteins identified through the proteomic analysis performed was used to test their role in DENV infection and replicon replication. Each siRNA has a pool of four siRNAs used in conjunction with each other in the transfections as a single reagent.

4.2 Establishment of Conditions for Silencing RNA Screening

Due to the number of target proteins in each data set, the only practical approach to performing the screen was to employ a reverse transfection method. Similar methods have been used in previous knockdown screens in Huh-7 cells, for both DENV and other flavivirus studies (Ang et al., 2010; Chu & Yang, 2007; Krishnan et al., 2008; Morchang et al., 2017).

Before high-throughput screening using the Dharmacon Cherry-Picked siRNA library could begin, the parameters for most efficient siRNA knockdown using Huh-7 cells needed to be evaluated.

First the initial cell seeding density needed to be optimised so at the time of analysis (72 hours post transfection (hpt) and 24 hours post-infection (hpi)) the monolayer of cells in the well would be around 80%. This maintains visual acuity of the cells and allows successful image analysis.

The TFR primarily recommended by Dharmacon for Huh-7 cells (and thus Huh-7 replicon cells) is DF4, this reagent has been used in previous flavivirus studies employing knockdown screens in Huh-7 cells (Ang et al., 2010; Chu & Yang, 2007; Krishnan et al., 2008; Morchang et al., 2017). The TFR facilitates the uptake of the siRNA into the cells. It is also important to optimise the amount of siRNA and transfection reagent. Low concentrations of siRNA in the transfection mix will not produce sufficient knockdown, excessive siRNA concentrations increase the risk of off-target effects, resulting in depletion of the wrong protein. Similarly, insufficient TFR reduces the uptake of the siRNA, resulting in inadequate knockdown. Too much TFR is likely to be cytotoxic and so the assay will be unsuccessful. Together, the siRNA and TFR are termed the transfection mix.

The duration of knockdown is tightly linked to the length of transfection. This is the time that the cells are left for the levels of protein to decrease. Dharmacon claim that a reduction of mRNA occurs between 24 and 48 hours after siRNA transfection with a subsequent reduction of protein levels

between 48- and 96-hpt (Horizon Discovery, 2022. "DharmaFECT™ Transfection Reagents—siRNA transfection protocol", Available at: https://horizondiscovery.com/-/media/Files/Horizon/resources/Protocols/basic-dharmafect-protocol.pdf (Accessed: 25th July 2022)). Based on this information, the assay was performed for a total of 72 hours for estimated maximal knockdown considering the conditions for cell growth and virus infection.

Finally, the last conditions that needed to be determined were reliability of Huh-7 replicon expression and subsequent fluorescence using the eGFP marker and the MOI to be used for DENV-2 infection of Huh-7 cells.

4.2.1 Optimal Cell Density, Transfection Reagent and Volume of Transfection Reagent

4.2.1.1 siGLO Green

siGLO Green is an RNA molecule that is not complementary to a cellular mRNA. It has a conjugated fluorophore (in this case green fluorescent protein (GFP)), and the fluorescence was used as a surrogate to measure siRNA uptake.

The first experiment performed was carried out to determine the best cell seeding densities, siGLO Green concentrations and volume of DF4 in the TFR. The GFP fluorescence of Huh-7 cells after siGLO transfection was measured with a Promega plate reader at 24 hpt in PBS, at which point they were fixed and the nuclei stained with DAPI for 60 minutes without cell permeabilisation and were imaged. The number of GFP positive cells and total number of cells were counted.

Cells were seeded at a range of densities and transfected with siGLO Green using a range of conditions; these were $2.5x10^3$ to $1x10^4$ cells per well, 25 nM to 100 nM siGLO and 0.1 µL to 0.4 µL DF4. Each condition had three repeats, the experiment was performed once. GFP fluorescence was measured, and the background removed by using the averaged un-transfected control readings. Increasing siGLO Green concentration, DF4 volume, and seeding density has a positive effect on the GFP fluorescence (Figure 4.1A). The condition with the most GFP fluorescence was $1.0x10^4$ cells seeded, with 100 nM siGLO Green, and 0.4 µL DF4.

However, $1.0x10^4$ cells per well was not a suitable seeding density as at 24 hpt, the confluency was already too high for the planned three- or four-day (Huh-7 replicon cells or Huh-7 cells respectively) siRNA screens. Figure 4.1B shows a representative image of $1.0x10^4$ cells transfected with 0.4 µL DF4 and 100 nM siGLO Green taken at 10x.

As $1.0x10^4$ Huh-7 cells was deemed too many, the uptake of siGLO Green in $5.0x10^3$ Huh-7 cells was examined. Corroborating with the GFP fluorescence data shown in Figure 4.1A, increasing the DF4 volume and the siGLO Green concentration increased the percentage of GFP positive cells. The difference between GFP positive cells using 0.1 µL and 0.2 µL DF4 was much greater than the difference between 0.2 µL and 0.4 µL DF4 at all concentrations of siGLO Green. The factor to consider next was cellular toxicity of DF4 and the siGLO Green, which is shown in Figure 4.1D as the relative number of cells as a percentage of the control wells. Both 0.1 µL and 0.4 µL had a negative effect on the number of cells at all three concentrations of siGLO Green, but strangely the number of cells transfected with 0.2 µL DF4 were greater at all three concentrations of siGLO Green. The reason for the higher number of cells is not immediately obvious, but it is most likely due to an error in seeding the cells at the start of the experiment rather than the DF4 having a positive effect on cell proliferation.

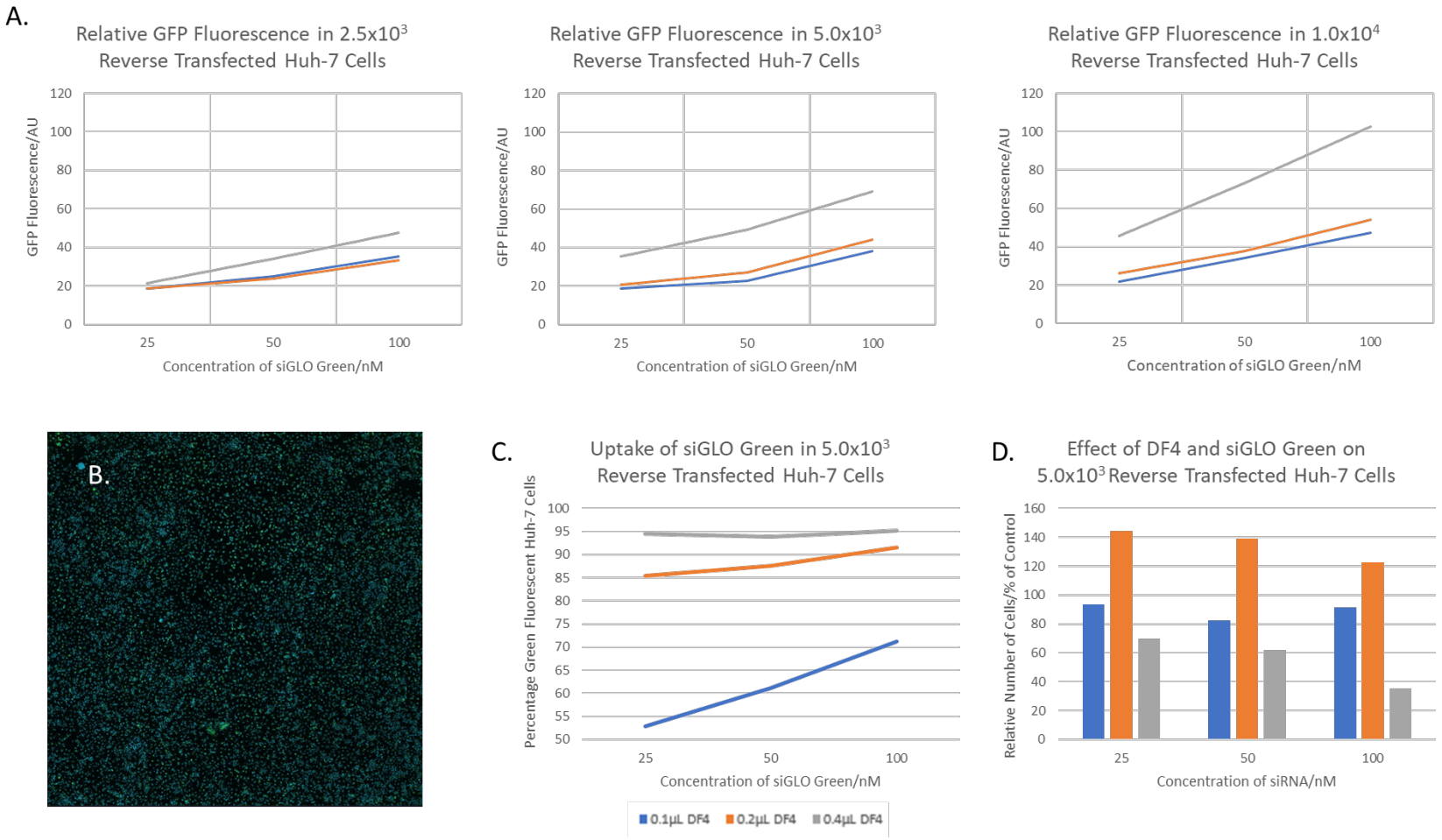

*Figure 4. 1. Huh-7 cells were reverse transfected in a 96-well imaging plate at a range of densities, from 2.5x10⁴ to 1.0x10⁵ cells/mL, with a range of volumes of DF4 (0.1µL to 0.4µL final volume per well) and a range of concentrations of siGLO Green (25nM to 100nM) made up to a total of 100µL CCM and left to transfect for 24 hours. At this point they were fixed with equal volumes 8% PFA for 15 minutes, and the PFA replaced with sterile PBS and read on a Promega GloMax. The nuclei of the cells were then stained with DAPI for 60 minutes without permeabilization, and the plate imaged. The total number of cells and GFP positive cells was counted. (**A**) Relative GFP fluorescence of 2.5x10³, 5.0x10³, and 1.0x10⁴ Huh-7 cells reverse transfected with a range of siGLO Green concentrations (25nM, 50nM, and 100nM) and DF4 volumes (0.1µL, 0.2µL, and 0.4µL). (**B**) Representative image of 1.0x10⁴ Huh-7 cells reverse transfected with 0.4µL DF4 and 100nM siGLO Green, taken at 10x. (**C**) Percentage of GFP positive cells at 24 hpt using 5.0x10³ Huh-7 cells. (**D**) Number of cells of each condition of 5.0x10³ Huh-7 cells displayed relative to the un-transfected control wells. Blue – 0.1µL DF4, orange – 0.2µL DF4, grey – 0.4µL.*

4.2.1.2 Using siRNAs with RISC activity

siGLO Green is an experimental surrogate for siRNA uptake as siGLO green has no effect on the RNAi pathway and does not engage the RISC - siGLO Green merely produces signal from the conjugated GFP. The next step in the optimisation pipeline was to use the parameters identified in the previous experiment ($5x10^3$ cells per well, 50 nM siRNA, 0.2 µL DF4, 24-hour transfection over 72 to 96 hours) as a guide to accurately determine the conditions for mRNA knockdown and protein depletion. Thus, subsequent experiments were conducted covering a range of concentrations of siRNA and time periods to determine an adequate set of conditions for the high-throughput screens.

Five thousand Huh-7 cells were reverse transfected with a variety of concentrations (ranging from 10 nM to 40 nM) of the siRNA controls provided by Dharmacon with the Cherry-Picked Libraries, and then stained and imaged following the IF protocol (detailed in section 2.3.1). These controls included siRNAs targeting glyceraldehyde 3-phosphate dehydrogenase (GAPDH) and Lamins A and C (Lamin A/C), as well as non-targeting siRNAs (siRNAs with a sequence that is not complementary to a cellular mRNA). A range of experimental durations were examined – including altering the initial transfection time and the entire duration of the experiment. The knockdown of GAPDH and Lamin A/C was measured by counting the number of cells positive for the antibody stain versus the control. However, the control knock-down experiments were inconsistent for a number of reasons.

First, knockdown of the control proteins was insufficient. Possibly, the concentrations of siRNA were too low. At first, the highest concentration of siRNA used was 40 nM. Even though the siGLO Green experiments indicated 50 nM worked well, it was reasoned that 40 nM might be sufficient to knockdown the proteins by around 70% and avoid cell toxicity – additionally, this spared reagent and so wastage of materials would to be minimized.

Second, transfecting the Huh-7 cells for longer than 24 hours (i.e. leaving the transfection mix on the cells) produced considerable cytotoxic effects. To avoid this, trials of transfections under 24 hours were performed, which were less toxic but did not knockdown GAPDH or Lamin A/C satisfactorily.

Third, the primary antibodies for GAPDH and Lamin A/C – while validated for IFA – did not provide precise enough staining for the analysis software to exactly measure the level of knockdown of these proteins. Deciding if a cell is “positive” or “negative” based on the intensity of signal was too complex for the built-in analysis software of the ImageExpressPico imaging platform. Possibly, it would have been better to transfect Huh-7 cells in a larger vessel, lyse and harvest the cells, perform a Western blot, and measure the intensity of the bands.

However, some conditions were chosen to move forward with and to refine. Huh-7 and Huh-7 replicon containing cells were transfected using 0.2 µL DF4, which performed best in the initial siGLO optimisation, in 100 µL of transfection mix for 24 hours. After this time, it was then replaced with 150 µL CCM then the cells fixed at 72 hpt for staining and image analysis. Finally, an siRNA targeting the protein KIF11 (impairment of expression of KIF11 is lethal to the cell (Zhou et al., 2019)) was used (instead of an siRNA targeting GAPDH or Lamin A/C) for a more easily quantifiable experimental readout.

KIF11 is a motor protein, its main role is during mitosis and knockdown, knockout or inhibition of this protein is lethal to dividing cells (Ang et al., 2010; Jungwirth et al., 2021). Thus, the knockdown of KIF11 via an siRNA would lead to a much easier experimental output – simply count the number of cells in the treated wells versus the cells in the non-transfected well and use as an illustration of protein knockdown.

4.2.2 KIF11 Knockdown

The first KIF11 knockdown screen used the basic reverse transfection protocol as described in the methods. Five thousand Huh-7 and five thousand Huh-7 replicon containing cells (in different wells of the same plate) were reverse transfected with 50 nM or 75 nM KIF11 siRNA or 50 nM or 75 nM non-targeting (NT) siRNA, 0.24 µL DF4, and incubated in a total of 100µL of transfection mix for 24 or 48 hours. Then the media was changed to 150 µL CCM and incubated for a further 48 hours. The cells were fixed with 8% PFA and the nuclei stained with DAPI, without permeabilising the cells, for one hour.

The volume of DF4 was increased as a previous study using a Reverse Transfection High-Throughput siRNA Knockdown screen on Huh-7 cells in 384-well plates used a proportion of the transfection mix that was equal to 0.24 µL when scaled up to a 96-well format (Ang et al., 2010).

There was no discernible difference in the cytotoxic effect of KIF11 versus NT between 50 nM and 75 nM of KIF11 at each time (not shown) and no apparent difference in number of cells treated with KIF11 versus NT siRNAs between 24 and 48 hpt (Figures 4.2a and 2b). The lowest concentrations of siRNAs and shorter transfection times were used in the next experiment to try to avoid non-RISC mediated cytotoxicity and off-target effects. Interestingly, there was considerable cell death in the cells treated with the non-targeting siRNA which had not been seen in previous experiments.

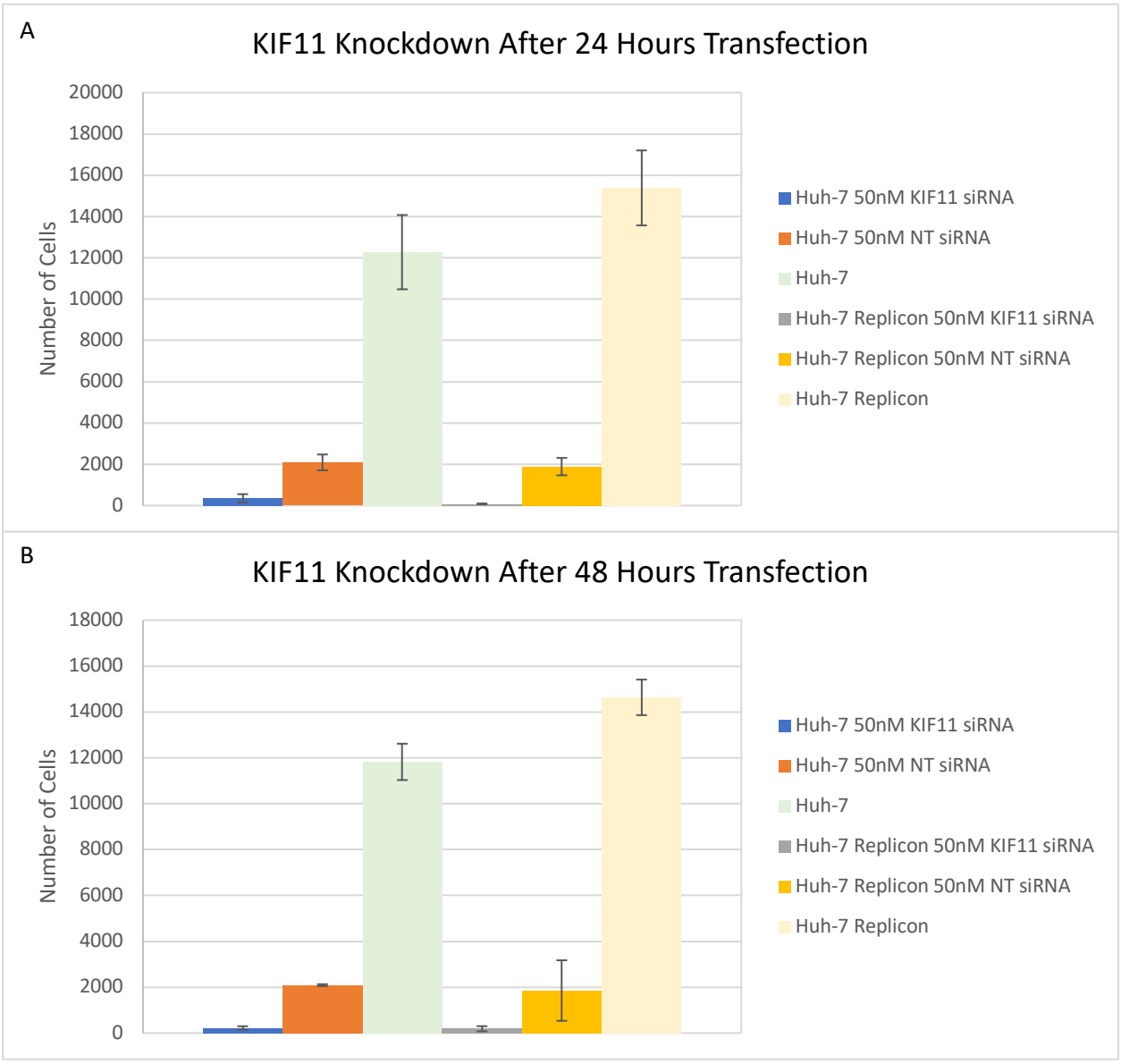

*Figure 4. 2. Bar charts showing numbers of Huh-7 and Huh-7 replicon containing cells remaining after treatment with 50nM KIF11 or 50nM NT siRNA's over (**A**) 24 or (**B**) 48 hours. Cells were transfected with 50nM siRNA and 0.24µL DF4 in a total of 100µL and left to transfect for either 24 or 48 hours, before the transfection mix was removed and replaced with 150 µL CCM and left for a total of 72 hours. After which time, the cells were fixed with equal volumes of 8% PFA for 15 minutes, and the nuclei of the cells stained with DAPI for 60 minutes without permeabilization. The number of cells was counted using the Pico ImageXpress and the graphs made using Microsoft Excel. Each condition was performed with 3 technical repeats, the experiment was performed once. The error bars represent standard deviation.*

The experiment described above was repeated but with a greater number of replicates. Five thousand cells per well were reverse transfected with 50 nM of either KIF11 or NT siRNA, 0.24 µL DF4 for 24 hours, then the transfection mix was replaced with 150 µL CCM and incubated for a further 48 hours.

The results of this test are shown below in Figure 4.3. Fifty nanomolar of siRNA targeting KIF11 produced similar cytotoxic effects in both the Huh-7 and Huh-7 replicon cells, and the NT siRNA had very little cytotoxic effect which was reassuring based on the results of the previous experiment. The unexpected cell death in the NT conditions previously may have resulted from a mistake in preparing the siRNA and DF4 master mix or possibly from an error in seeding the cells. Nevertheless, the desired effect of knocking down KIF11 via siRNA (≥80% cytotoxicity) had not been achieved in either the Huh-7 or the replicon containing cell conditions.

Due to time constraints, the high throughput screen was carried out regardless of the optimisation experiment results. The final conditions chosen were: 50 nM siRNA, 0.2 µL DF4 and 24-hour transfection then a further 48-hour incubation in CCM before fixing or infection.

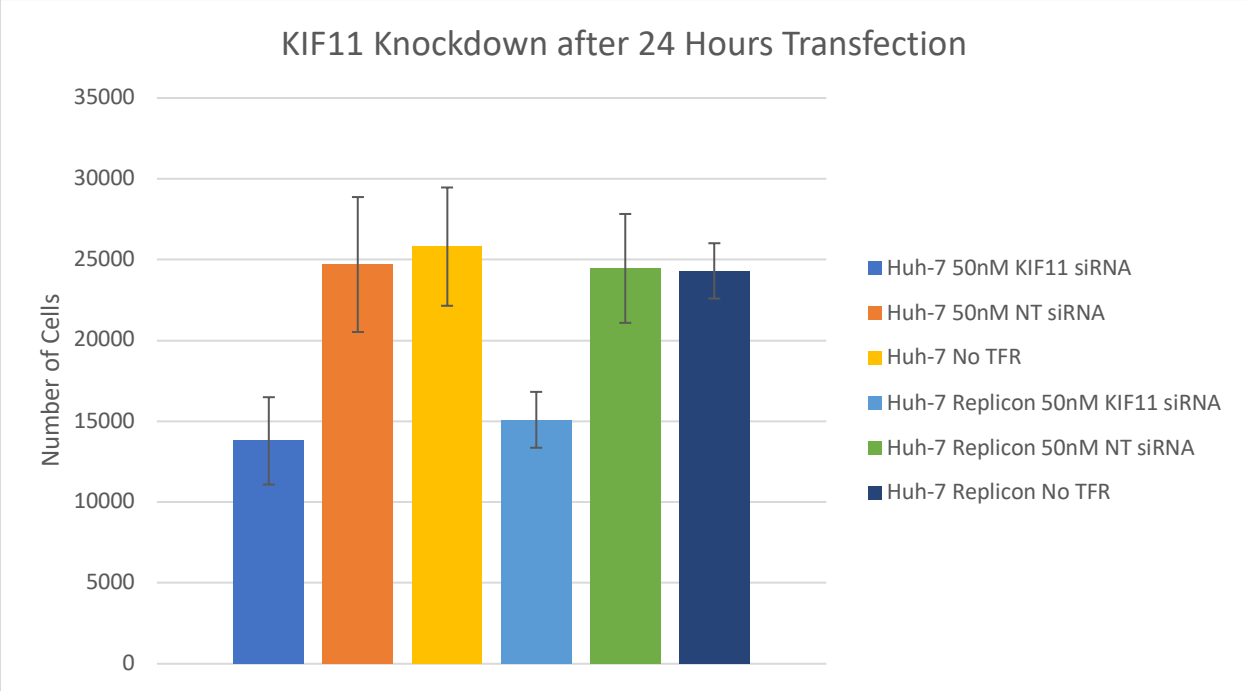

Figure 4. 3. Bar chart showing the number of Huh-7 and Huh-7 replicon containing cells remaining after treatment with 50nM KIF11 or 50nM NT siRNAs over a total of 72 hours. Cells were transfected with 50nM siRNA and 0.24µL DF4 in a total of 100µL and left to transfect for 24, before the transfection mix was removed and replaced with 150 µL CCM and left for 48 hours, to a total of 72 hours. After which time, the cells were fixed with equal volumes of 8% PFA for 15 minutes, and the nuclei of the cells stained with DAPI for 60 minutes without permeabilization. The number of cells was counted using the PicoImageXpress and the graphs made using Microsoft Excel. Each condition was performed with 6 technical repeats, the experiment was performed only once. The error bars represent standard deviation.

4.2.3 Confirming replicon Expression

Before siRNA knockdown screens could be performed targeting proteins dysregulated in Huh-7 replicon containing cells, the presence and expression of the replicon needed to be assessed. Additionally, the efficacy of antibodies that could potentially be used in the screening process required testing including α-GFP, α-double stranded RNA (dsRNA), α-NS1, and α-NS5.

The DENV replicon is known to be stably maintained in Huh-7 cells during passaging but populations of GFP positive cells can decline over time as the GFP-puromycin resistance fusion protein gene can be lost. Therefore, it was important to determine if the proportion of replicon containing cells could be increased by selecting the cell population with puromycin. The images of non-selected and puromycin selected cells were compared visually and the differences in expression of the replicon judged qualitatively.

Fifty thousand or one hundred thousand unselected Huh-7 replicon containing cells in 0.5 mL CCM were seeded per well of a 24-well imaging plate and left overnight. They were fixed for 15 minutes, then they were stained following the staining protocol (section 2.3.2) with volumes adjusted for the larger wells of the 24-well plate. The cells were stained with α-GFP and α-dsRNA. GFP signal was not seen in all cells, unlike dsRNA (Figure 4.4). An initial seeding density of $5x10^4$ cells per well resulted in approximately 80% confluency whereas as the cells initially seeded at $1x10^5$ cells/well were overconfluent (images are not shown).

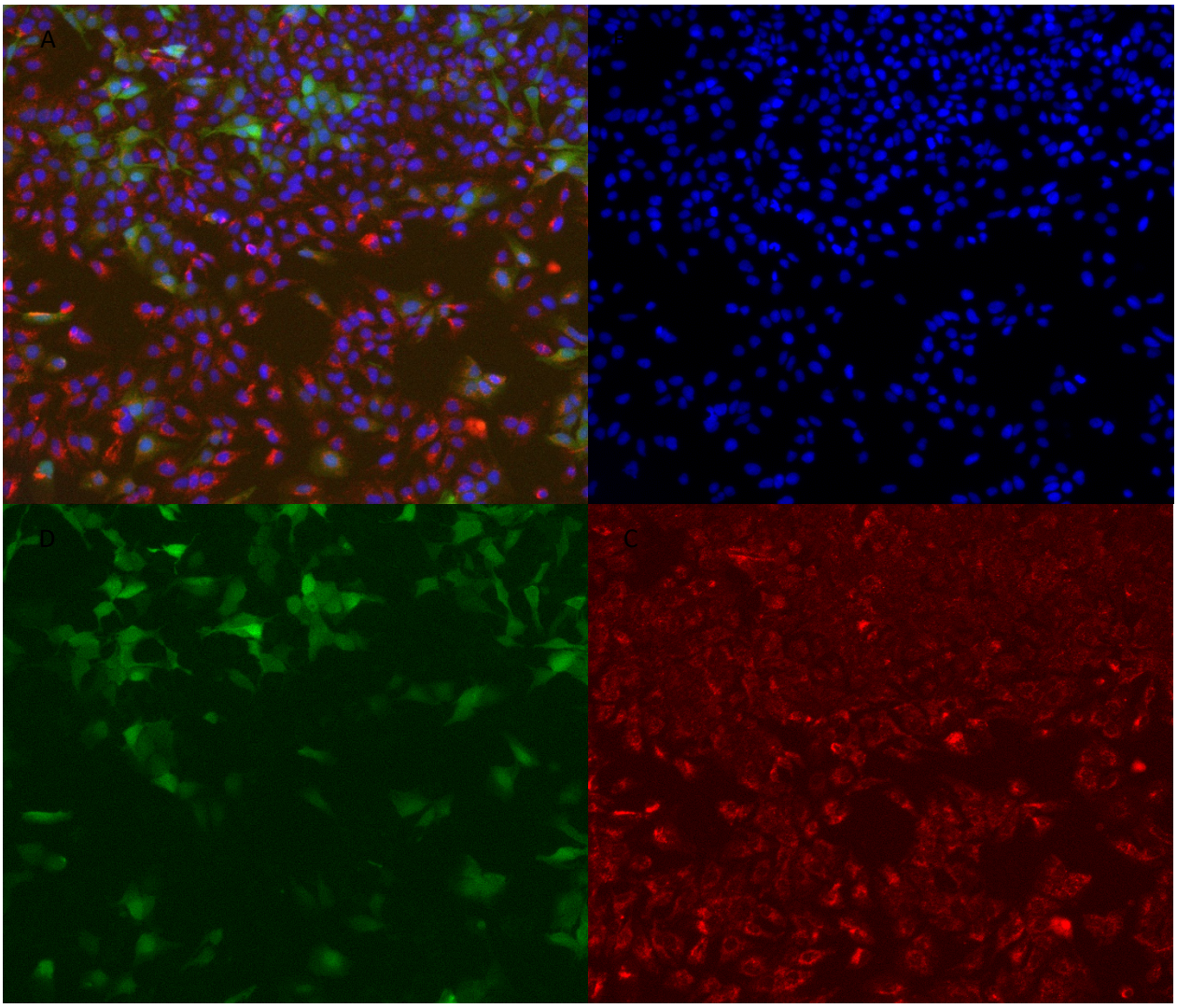

*Figure 4. 4. Representative image taken at 10x of 5x10^4 unselected Huh-7 replicon containing cells grown in a 24 well imaging plate overnight, fixed with equal volumes 8% PFA as CCM for 15 minutes and then stained with DAPI (blue), α-dsRNA (red), and showing expressed GFP (green). (**A**) Merged channels showing cells expressing GFP and stained with DAPI and dsRNA. (**B**) Nuclei stained with DAPI. (**C**) Cells stained with α-dsRNA showing replication of the DENV replicon. (**D**) GFP expression from the GFP-puromycin resistance gene.*

The same experiment was repeated after selecting the Huh-7 replicon containing cells with 4.5 µg/mL puromycin for two passages. Fifty thousand Huh-7 replicon containing cells were used for initial seeding as they had the more optimal confluency after 24 hours and stained with a combination of α-GFP and α-dsRNA, α-NS5 or α-NS1. All cells were stained with DAPI (Figures 4.5A-D, 4.6A-D, 4.7A-D respectively). Even though the replicon encodes GFP, an antibody specific for GFP was included to boost the GFP signal.

After selection with 4.5 µg/mL puromycin for two passages prior to seeding and staining with DAPI and α-GFP, the replicon was judged qualitatively to be expressed in 90% or more of the Huh-7 replicon containing cells (Figure 4.5) – as compared visually to non-replicon Huh-7 cells (images not shown).

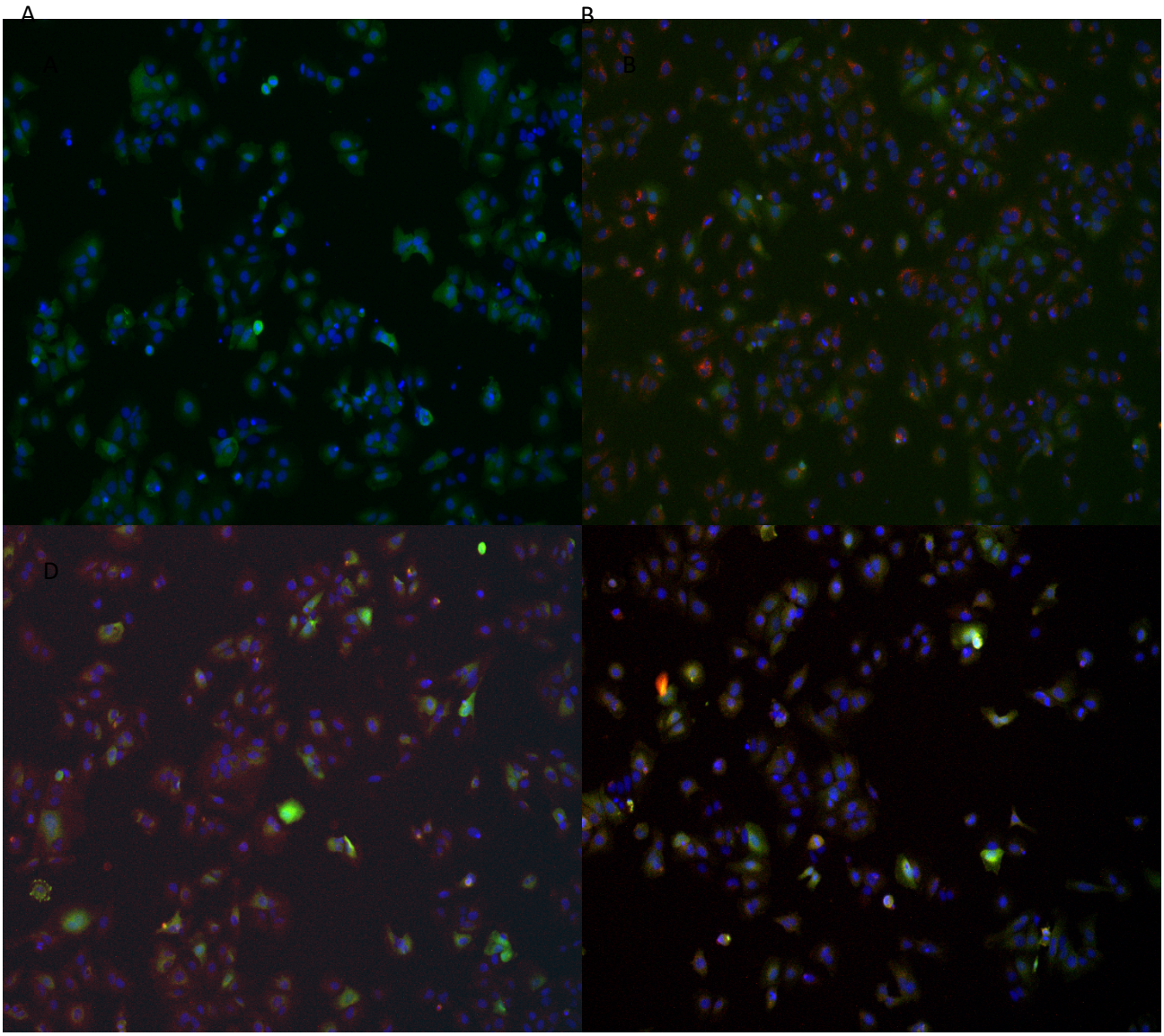

Figure 4. 5. Representative images of wells taken at 10x seeded with 5x10^4 Huh-7 replicon containing cells selected with 4.5ug/mL puromycin for two passages prior to seeding. 24 hours after seeding, the cells were fixed with an equal volume of 8% PFA to the CCM for 15 minutes, then the cells were stained with DAPI and different combinations of α-GFP, α-NS1, and α-NS5. A. α-GFP (Green) and DAPI (Blue). B. α-GFP (Green), α-dsRNA (Red) and DAPI (Blue). C. α-GFP (Green), α-NS5 (Red) and DAPI (Blue). D. α-GFP (Green), α-NS1 (Red) and DAPI (Blue).

The replicon can be seen to be expressed in 90% or more cells as shown in Figures 4.5A-D by qualitative assessment of the GFP staining. Figure 4.5B shows most cells are positive for dsRNA, as the non-selected cells did (Figure 4.4). Antibodies specific for NS5 and NS1 did not show as good a signal as those raised against dsRNA (figures 4.5C and 4.5D, respectively). The NS1 and NS5 antibodies were examined in more detail and the results shown in Figures 4.6 and 4.7.

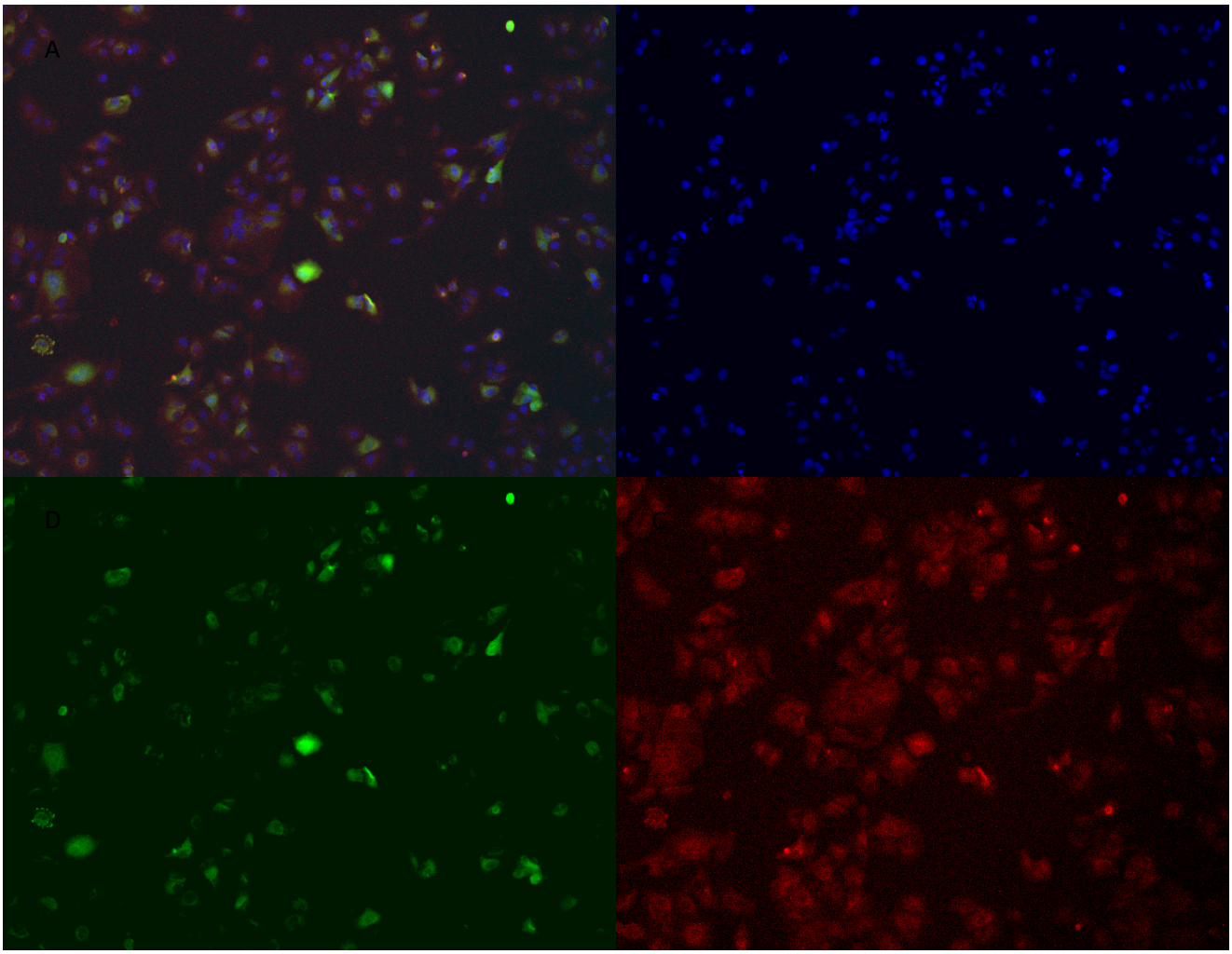

Figure 4. 6. Representative images of wells taken at 10x seeded with $5x10^4$ Huh-7 replicon containing cells selected with 4.5ug/mL puromycin for two passages prior to seeding. After leaving to grow overnight, the cells were fixed with an equal volume of 8% PFA to the CCM for 15 minutes, then the cells were stained with DAPI (blue), α-GFP (green), and α-NS1 (red). A. Merged. B. DAPI nuclear stain. C. α-NS1. D. α-GFP (Green).

Figure 4.6 is a representative image of selected Huh-7 replicon containing cells stained with DAPI, α-GFP and α-dsNS1. Figure 4.6D shows high levels of expression of GFP, in contrast to this Figure 4.6C which shows moderate signal after boosting in Image-J.

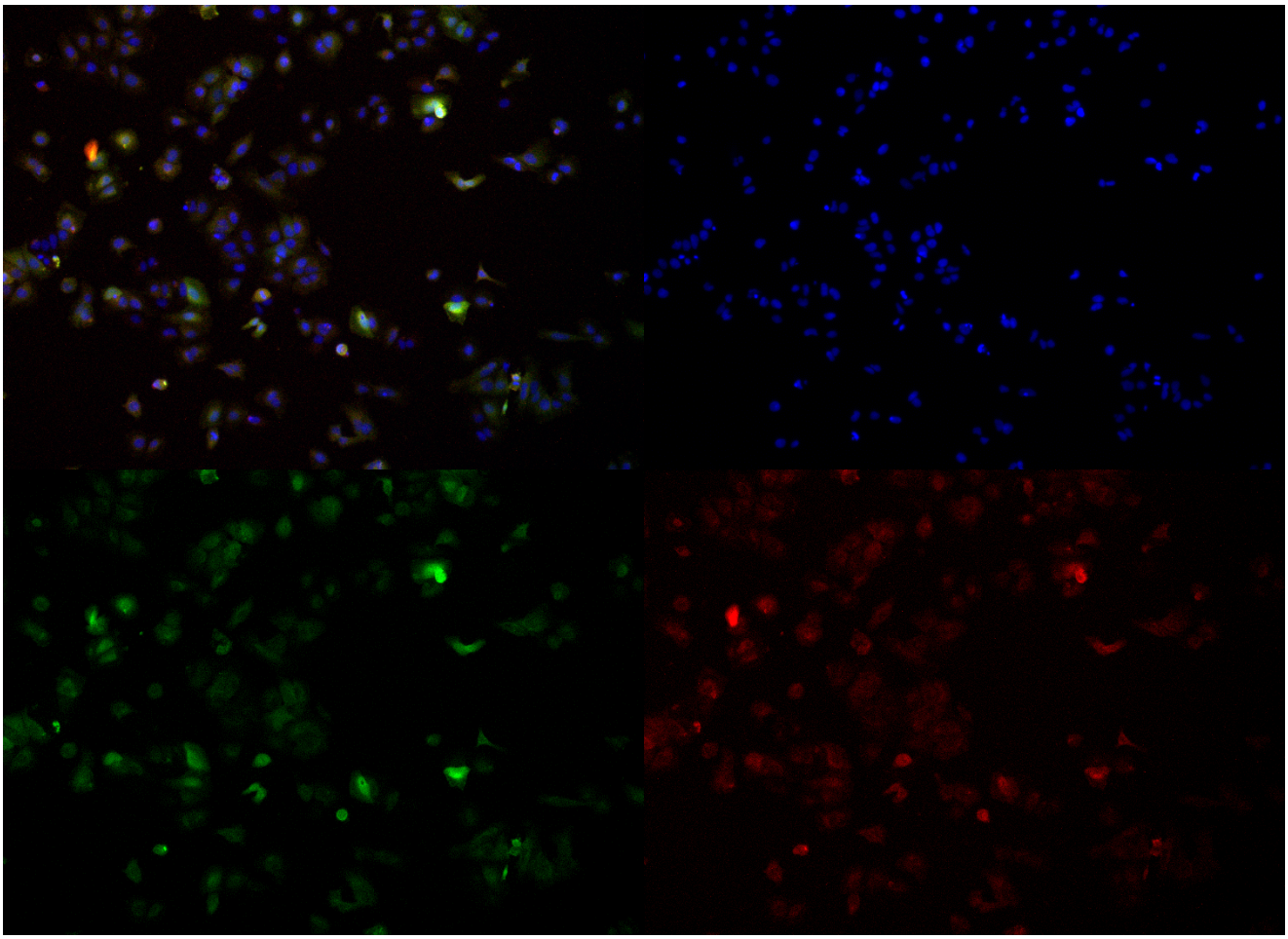

Figure 4. 7. Representative images of wells taken at 10x seeded with 5x10⁴ Huh-7 replicon containing cells selected with 4.5ug/mL puromycin for two passages prior to seeding. 24 hours after seeding, the cells were fixed with an equal volume of 8% PFA to the CCM for 15 minutes, then the cells were stained with DAPI (blue), anti-GFP (green), and anti-NS5 (red). A. Merged. B. DAPI nuclear stain. C. anti-NS5. D. α-GFP (Green).

Figure 4.7A-D is a representative image of Huh-7 replicon containing cells after selection for two passages before seeding, stained with DAPI, α-GFP and α-NS5. As judged visually, most cells are positive for GFP, and many cells are positive for NS5. The staining is much weaker than the signal from the GFP channel and so has been boosted in Image-J.

After selection, the Huh-7 replicon containing cells expressed more GFP than those that were un-selected. Staining for dsRNA produced similar results in both experiments. The presence of NS1 and NS5 was not examined in the unselected cells but from the second part of the experiment NS1 produced a better signal.

From these images, it is clear that the Huh-7 replicon containing cells should be selected for at least 2 passages prior to the siRNA knockdown screens and α-GFP and α-dsRNA could be considered to be used in analysing the effects of the siRNA screen on replicon expression in Huh-7 cells.

4.2.4 Titration of DENV-2 Stocks in Huh-7 Cells

To accurately determine the number of infectious particles in a given volume of the DENV-2 viral stock a titration must be performed. From this, the volume of the viral stock needed to make an inoculum that yields a specific multiplicity of infection (MOI) at a specific cell density can be calculated. Different viruses and different cell types produce different titres, so it is critically important to establish the titre of the DENV-2 stock in Huh-7 cells. Previously, the titre of the DENV-2 stocks was calculated using a plaque assay. However, a method using IFA was developed to calculate the titre more quickly by staining for DENV-2 infected Huh-7 cells, counting the number of infected cells and using that to calculate the infectious dose.

A two-fold serial dilution of the DENV-2 stock in MEM supplemented with 2% FCS and non-essential amino acids (termed Viral Assay Media (VAM)) was carried out and 60 μL of the inoculum was used to infect Huh-7 cells for 24 hours; each dilution was performed in triplicate. After 24 hours, the cells were fixed PFA (section 2.2.2), and the cells stained for DENV envelope protein (E) (section 2.3.2). The number of infected cells were counted and then used to calculate the number of infectious viral particles per millilitre and thus calculate the amount of virus required at the chosen cell density and MOI.

Using an inbuilt analysis program in the Pico ImageXpress software the number of Huh-7 cells infected with DENV-2 was counted in each well. From this, a graph of the average number of infected cells was plotted against the volume of DENV-2 added (Figure 4.8A). Figure 4.8A has a non-linear shape, at low doses of DENV-2 the number and percentage of infected cells increases quickly with a small increase in the volume of DENV-2 added. At higher doses, the number of infected cells and percentage infection increases at a slower rate than in the linear part of the curve. Figure 4.8A plateaus and declines at the highest dose. This may be because DENV-2 at that high a dose causes some cytotoxicity. Figure 4.8B is a table of data taken from Figure 4.8A that was used to calculate the titre.

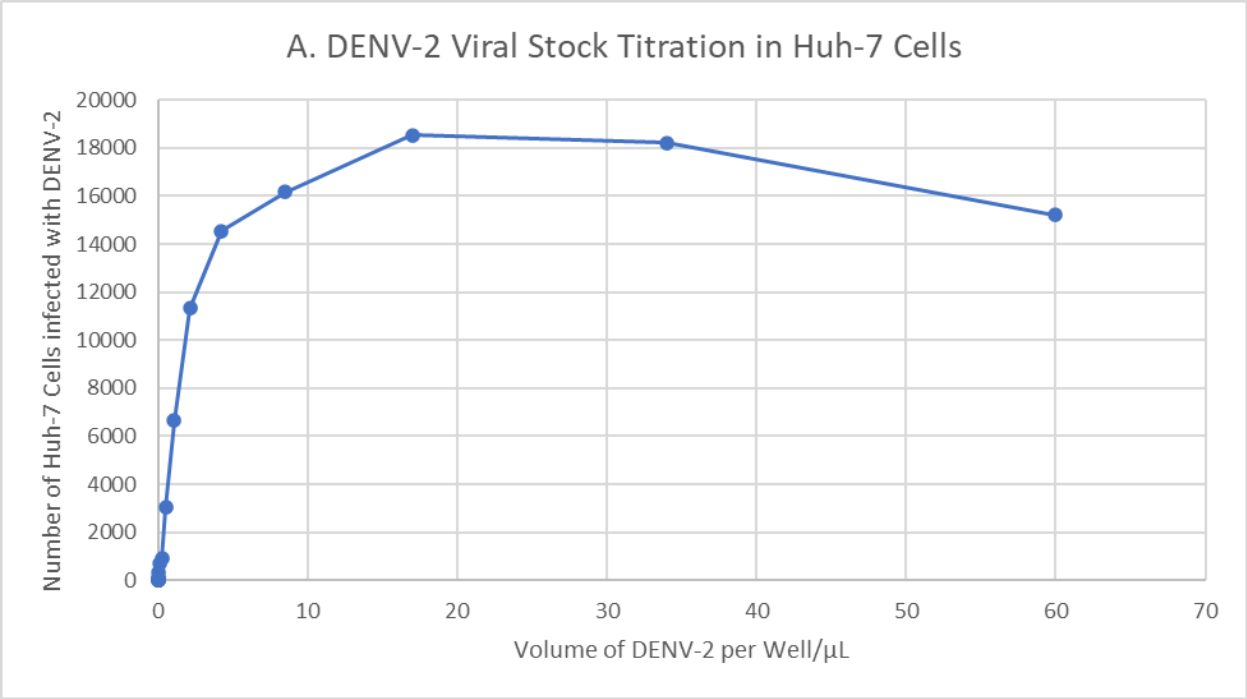

B.

Number of Infected Cells	Volume DENV2/µL	Number of Infected Cells/Volume of DENV-2(µL)	Average	Infectious Units/µL
11406	3.125	3650		
6832	1.25	5466	5170	$1.x10^4$
3198	0.5	6396		

Figure 4. ***A.*** *Graph of DENV-2 titration in Huh-7 cells. A 96-well imaging plate was seeded with $5.0x10^3$ Huh-7 cells per well the day before. The media was removed and 60 µL of the virus inoculum was added to nearly each well but avoiding some wells which only contained VAM. The plate was left for 24 hours and then each well was fixed and stained with an anti-E antibody (section 2.3.2). The plate was imaged, and the number of infected cells plotted against the volume of DENV-2 stock in each well of the plate, then the titre of the stocks was calculated.* ***B.*** *Table showing the data taken from the graph (**A**) and used to calculate the titre, shown here in Infectious Units per µL, values were rounded to the nearest whole number.*

To calculate the titre, the three doses of DENV-2 that span the 50% infection mark are used. The number of infected cells is divided by their relevant doses and averaged, then scaled into infectious units (IFU) per millilitre. The titre of the DENV stocks used in the siRNA screens was $1.0x10^4$ IFU/µL, or $1.0x10^7$ IFU/mL.

4.3 Silencing RNA Screening and the Effects on Dengue Virus Replication

The effects of siRNA mediated depletion of proteins on DENV replication was assessed by IFA. The protein targets that were selected were chosen based on the proteomic analysis in Chapter 3. The effect

on replication was assessed by measuring the expression of DENV-2 proteins after 24 hours of infection. The assay was performed twice with each condition repeated in triplicate.

Huh-7 cells were reverse transfected in 96-well plates for a total of 72 hours, using conditions described above in section 4.2.2, followed by an infection that lasted 24 hours.

Multiple controls were used in each plate. These included a positive control of transfection, siRNA targeting KIF11, a non-targeting (NT) negative control, siRNA non-complementary to a cellular mRNA, transfection reagent only (DF4), to account for transfection reagent cytotoxicity, and a non-transfected control.

Cells were transfected per the methods section (section 2.4.3) for 24 hours with 100 µL transfection mix, which was then replaced with 150 µL CCM for the remaining 48 hours of the 3-day transfection. At which point 60 µL of DENV inoculum at an MOI of 5 was added and allowed to infect for 90 minutes at 37° C, then replaced with 150 µL VAM for 24 hours.

The cells were fixed 8% PFA for one hour. In the first assay the cells were stained with anti-E and DAPI, in the second assay the cells were stained with anti-prM. The plates were imaged with PicoImageReporterXpress software using the Viral Infectivity analysis pipeline to determine the number of cells expressing E/prM and DAPI and the number of cells expressing DAPI alone. This gives the total cell number and number of DENV positive (presence of DENV protein) or negative (absence of DENV protein) cells.

4.3.1 Screening

For the first attempt, $5x10^3$ Huh-7 cells were reverse transfected. This led to over-crowding of the well after 96 hours of growth. This should have been anticipated as all the optimisation experiments had only been up to 72 hours. The cells were stained with anti-DENV-2 E but the images were too poor to analyse due to the overcrowding. The non-infected and infected controls also had similar measured levels of infection and so as the experimental controls did not work, it was decided that a repeat would be performed with fewer cells and a different primary antibody.

During the second repeat of the assay the seeding density was reduced to $4x10^3$ cells to try to negate the over confluency. The other change to the protocol was using an anti-prM primary antibody. Regrettably, the control conditions did not work; the non-infected wells showed some infection, and the KIF11 transfection did not provide sufficient transfection efficiency.

The method must be changed to produce valid results. The concentration of siRNA needs to be much higher – possibly 100 nM or even greater – but it is important to ensure there are no off-target effects from the high concentrations of siRNA. Fewer cells should be seeded at the start, possibly 2500 per well. Additionally, the Huh-7 cells need to be more carefully prepared to avoid multi-cellular lumps.

4.4 Silencing RNA Screening and the Effects on Replicon Expression

To explore the role of proteins shown to be increased in amount in Huh-7 cells expressing a DENV-2 replicon (section 3.3.2), immunofluorescence assays were performed on Huh-7 replicon containing cells after siRNA mediated knockdown. Measuring the reduction of GFP expression was used as a way of examining the role of the proteins in the DENV replication cycle. If the siRNA's chosen using the replicon data reduced GFP expression sufficiently, then the siRNA chosen using the DENV-2 data sets could be tested against the replicon containing cells to see if there was crossover.

Huh-7 replicon containing cells were selected with 4.5 µg/mL puromycin for two passages prior to transfection. Four thousand Huh-7 cells were reverse transfected with 50 nM siRNA and 0.2 µL DF4 in a total of 100 µL transfection mix. NT and KIF11 siRNAs were used as negative and positive controls respectively, alongside non-siRNA treated Huh-7 replicon and Huh-7 cells. The cells were left for 24 hours in the transfection mix, after which the media was changed for 150 µL CCM and left for a further 48 hours.

The cells were fixed with 150 µL 8% PFA for 15 minutes, then they were stained for GFP and DAPI. GFP fluorescence was used as the basis for the analysis. The number of cells positive for a nuclear stain and GFP signal were counted and used to calculate the percentage of replicon positive cells, the ratio of replicon positive cells versus non-transfected Huh-7 replicon containing cells and raw number of cells per condition were plotted.

Compared to the non-transfected cells and cells transfected with NT siRNAs there was some reduction in GFP expression in siRNA transfected cells except for siRNAs targeting TMED10, TXNDC5 and ZNF319. However, it is worth noting that the number of cells in the death control versus NT was less than 20% lower in plates 1 and 2 and even approximately 10% higher in plate 3. Clearly, transfection efficiency was sub-optimal, and the conditions need to be altered to provide much better efficiency.

Some basic changes to the method would include increasing the concentration of siRNA, lowering starting seeding density, or preparing cell line siRNA plates one at a time to lose possible drop off in complex formation. Re-optimising the method would be a good next step, increasing the concentration

of siRNA as high as possible (whilst avoiding off target effects and general cell toxicity) with a different transfection reagent. For example Chu & Yang (2007) used 200 nM and 300 nM with HiPerfect (Qiagen, Valencia, CA).

Chapter 5: Discussion

5.1 Proteomics

High throughput analysis of the proteomes of virus infected cells can provide a broad and quantitative insight into host-virus interactions. This has been reported for a range of viruses, including DENV infection of Huh-7 cells (Pando-Robles et al., 2014).

The aim of the present study was to use a high throughput approach to identify new HRFs or HSFs required for DENV infection of Huh-7 cells. Huh-7 replicon containing cells were included in the proteomic analysis to try to increase understanding of the role of structural proteins in the lifecycle of DENV in Huh-7 cells and to evaluate the effectiveness of the replicon system as a surrogate for DENV infection, and subsequently to evaluate the usefulness of siRNAs in this system.

A PCA was performed on the 16K and WCL datasets. They showed good grouping of all replicates – excluding Rep.16K.3. Both the histograms and the multiple scatter plots of proteins in the 16K and WCL fractions show good distribution of data and reproducibility between them – again, except for Rep.16K.3.

The abnormal repeat identified (Rep.16K.3) is likely to result from sample preparation error, but as this cannot be shown conclusively it was included in the analysis. If the experiment was repeated, more replicates could be included.

There were 8200 and 7247 proteins were identified using LC-MS/MS in the WCL and 16K fractions respectively. In the 16K fraction, 503 and 272 proteins were altered in abundance at least 2-fold in the DV2/Mock and Rep/Mock comparisons, respectively. In the WCL dataset, 219 and 144 proteins were altered at least 2-fold in the DV2/Mock and Rep/Mock comparisons respectively. A previous study by Pando-Robles et al. (2014) using label free LC-MS to analyse Huh-7 cells infected with DENV-2 identified 155 proteins that were changed 2-fold in amount compared to mock infected cells, showing that this present study potentially has more power to identify host factors than previous work.

Interestingly, in both the 16K and WCL data sets there were more proteins significantly decreased than increased in abundance during DENV-2 infection, but more proteins were increased in abundance than decreased in the replicon containing cells. Details on exact numbers of proteins in each condition can be found in Tables 3.1 and S.1 respectively. From this present study it is not clear why this was the case, though it is possibly through an activity of the structural proteins.

From this information, the question of whether the replicon is a good surrogate for DENV-2 infection arises. The replicon responds to ribavirin in the same way as DENV-2 and also produces similar ultrastructural changes to the cell as in DENV-2 infection (Ng et al., 2007). However, the trends in functional enrichment results of the replicon containing cells must be compared to DENV-2 infected cells to further understand the differences. The targets for siRNA mediated knockdown in DENV-2 infection were also to be targeted in replicon containing cells to see if there is an overlap in the role of these proteins, even if they were not identified to be altered in abundance in replicon containing cells, but unfortunately the screen could not be optimised in time.

No data was presented here that showed a conformation of fractionation or DENV-2 infection. This would have been as simple as performing a Western blot on some remaining lysate and probing for a subcellular region-specific protein or DENV protein. However, these lysates were not available. An alternative to this could be searching for a marker in the proteomic data, such as one that has been documented in the literature to be increased in the regions analysed, or for a DENV protein. Not demonstrating this does limit the validity of these results, and this would be taken into account if this type of study was repeated.

The analysis of the proteomes of DENV-2 infected Huh-7 cells and Huh-7 replicon containing cells compared to mock infected are discussed below, alongside the effectiveness of using the mock data in the DENV-2 proteomic analysis as opposed to the iDV2 data set.

5.1.1 DENV-2 Infected Cells Compared to Mock Treated Cells

The results of the comparison of DENV-2 infection of Huh-7 cells with mock infected cells in both the 16K and WCL fractions are discussed here. In brief, the 16K fraction of DENV-2 infected Huh-7 cells showed significant levels of enrichment of proteins associated with mitochondria– reflected in the differences in the abundance of proteins involved in the TCA cycle, transport proteins, and the electron transport chain. Analysis of the WCL data tells a slightly different story. The proteomes of the WCL of DENV-2 infected cells have greater levels of enrichment of cell cycle proteins and proteins related to platelet degranulation compared to mock infected cells.

Over 20% of the proteins altered at least 1.5-fold in the 16K data set were assigned the term ‘mitochondrion’ by FunRich v.3.1.3 and only one of the top five terms from FunRich was not related to mitochondria; the most enriched term of the top annotation cluster of these proteins was ‘respiratory chain,’ indicating that the metabolism of DENV-2 infected Huh-7 cells may be different to uninfected cells. Indeed, it has been known for some time that mitochondrial function and structure are both

affected by DENV infection to different extents in different cell lines. Yu et al. (2015) demonstrated that mitochondrial membrane potential (MMP) and fusion were disrupted in A549 cells infected with DENV-2, whereas Barbier et al. (2017) showed that mitochondrial respiration was increased in Huh-7 cells.

In the proteins that were altered 2-fold or more in the 16K dataset, 38 were assigned to the TCA cycle and respiratory transport by STRING v11.0. This indicates that the metabolic balance is affected in some way, indeed, in proteins decreased 2.0-Fold, eight proteins are assigned to the TCA cycle term in STRING v11.0. It is impossible to tell if this means that the TCA cycle is influenced in infected cells (as the scope of the proteomic data does not stretch that far), but as fatty acids are the main source of energy in DENV-2 infected Huh-7 cells and β-oxidation is required for viral replication and has been shown to feed the TCA cycle, further experiments examining the role of the TCA cycle in DENV infection are needed (Fernandes-Siqueira et al., 2018).

However, it is intriguing to see that of the proteins decreased 1.5-fold or more in DENV-2 infected compared to mock infected cells, 196 were assigned to metabolism and further investigation of this term showed that the metabolism of lipids, metabolism of fatty acids, and mitochondrial fatty acid beta-oxidation were three of the top four terms. Given that β-oxidation and lipid metabolism are so tightly linked with DENV-2 infection, these data suggests that DENV infection may alter lipid metabolism by changing the balance in specific enzymes in these pathways – and that this could be cell line dependent (Chiu et al., 2014; Fernandes-Siqueira et al., 2018; Heaton et al., 2010a; Jiménez de Oya et al., 2018, 2019).

There were 400 proteins increased at least 1.5-fold in abundance in the 16K fraction of DENV-2 infected Huh-7 cells compared to mock infected cells. The enrichment analysis of these proteins revealed that mitochondrial pathways such as the TCA cycle and respiratory electron transport were. Additionally, 44 proteins with ‘transporter activity’ were identified. These included 12 members of the SLC25A family and additionally VDAC1 and 3, non-specific outer mitochondrial membrane (OMM) transporters.

Proteins belonging to the SLC25A family are inner mitochondrial membrane transporters and are crucial to the function of mitochondria, as they transport metabolites and small molecules necessary for the reactions that take place in the matrix (Kunji et al., 2020; Ruprecht & Kunji, 2020).

It is likely that the altered balance of reactions would require a change in the distribution of the transporters. Therefore, the reliance on mitochondrial metabolism for DENV infection would have been tested by the knockdown of the SLC25A and other mitochondrial transport proteins, however the siRNA screen failed. Possibly the increased amount of these proteins in DENV-2 infected cells is a response to a

greater metabolic pressure on the mitochondria, but this remains to be seen. Figure 5.1 shows the roles of the SLC25A transporters, with those chosen as targets highlighted in green.

The SCL25A family members are described in more detail in Table S.17 but selected proteins and their possible role in mitochondrial metabolism in DENV infection will be discussed here. Firstly, the carnititine/acyl-carnitine carrier (CAC) was detected to be 1.6-fold greater in DENV infected cells compared to the mock infection. CAC is transporter for acyl-carnitine and carnitine, bringing fatty acids into the matrix in a chain length dependent manner (Palmieri, 2013). Additionally, citrate carrier (CiC), which was increased 1.3-fold in DENV infected cells but included in the target proteins based on a potential role in infection, transports citrate out of the matrix in exchange for malate (Catalina-Rodriguez et al., 2012). With TCA enzymes decreased in abundance in DENV infected cells and β-oxidation increased in infected cells (Fernandes-Siqueira et al., 2018), it is plausible that these two carriers could work in tandem to provide a more metabolically favourable environment for DENV within the mitochondria.

Additionally, Ca^{2+}-sensitive mitochondrial carrier (AGC1/2), oxoglutarate carrier (OGC), and dicarboxylate carrier (DIC) all transport metabolites of the TCA cycle and so could contribute to the altered metabolic state of mitochondria with dysregulated TCA enzyme levels.

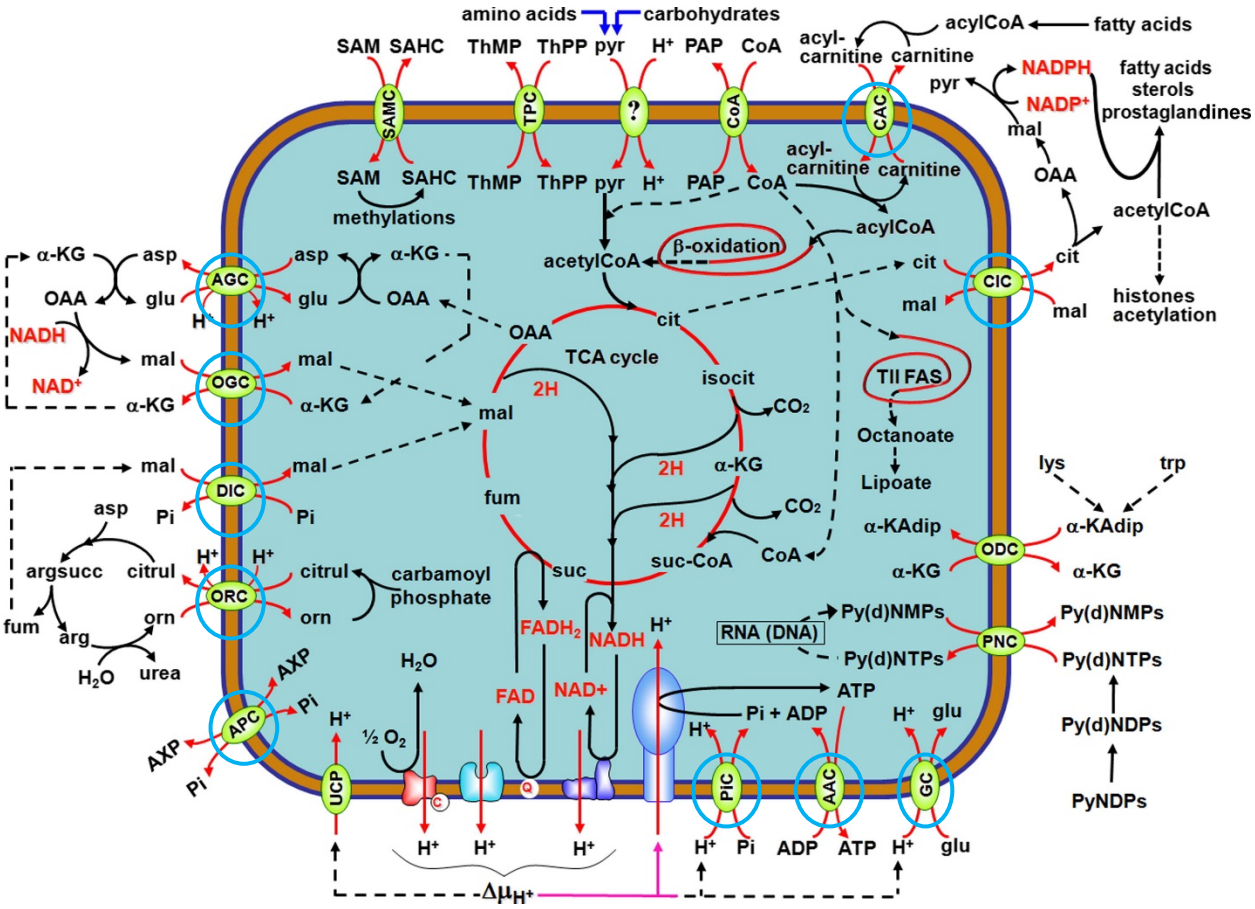

Figure 5. 1. Diagram showing the roles of the SLC25A transporter families including the reactions prior to the transport of metabolite, in addition to the reactions of the metabolite once inside the matrix. SLC25A protein family members chosen for siRNA knockdown are highlighted in blue. Adapted from Palmieri (2013).

Surprisingly, for proteins altered greater than 1.5-fold in amount in the 16K fraction of DENV-2 infected cells compared to the mock cells, the third most enriched cellular component term was “nucleolus” – around 15% of proteins were assigned to this term as produced by FunRich v3.1.3. However, there is very little other enrichment data supporting a significant involvement of nuclear proteins. This may indicate the level of redundancy in functional enrichment software or that there could be a nuclear contamination in the 16K fraction, although this might be supported in other enrichment data.

Some of the proteins chosen for siRNA knockdown were associated with the term ‘metabolism,’ assigned to proteins increased in abundance 2.0-fold. One protein, increased 2.3-fold in DENV infection, is cystathionine gamma-lyase. This is the enzyme responsible for catalysing the last step of a pathway generating cysteine (Sagong et al., 2020). It is not known if this pathway is crucial to DENV infection, but inhibition has been shown to increase respiratory syncytial virus (RSV) replication (Pal et al., 2018). While RSV and DENV are unrelated viruses, it is possible this is a common pathway in viral infections. As

a lot of the enrichment in this data set showed enrichment of members of the respiratory electron chain. Electron transfer flavoprotein-ubiquinone oxidoreductase (ETFDH) was chosen as a target in this process. This protein accepts electrons during the electron chain process, so would have a role in the increased ATP production in DENV infected liver cells (El-Bacha et al., 2007).

The GO enrichment analysis of the WCL data shows a different story. More proteins were identified in the WCL, but the number of statistically significantly altered hits was much lower. Therefore, the enrichment analysis was much less convincing.

As the vast majority of the proteins found to be changed significantly in the WCL would be decreased in abundance, the 534 proteins altered 1.5-fold in abundance were analysed. Four of the top five cellular components assigned to these proteins in FunRich were explicitly extracellular, and one was a spherical high-density lipoprotein particle found in the blood.

After using FunRich, these same proteins were analysed using STRING. The top five biological processes returned were related to the cell cycle. This is unsurprising as a previous proteomic analysis also found a link between proteins decreased in abundance and terms related to the cell cycle (Chiu et al., 2014). However, this study was performed using A549 cells, not Huh-7 cells and other previous work has shown a cell line dependent relationship between the cell cycle and DENV-2 infection, so further investigation into the role of the cell cycle in DENV-2 infection should be undertaken (Pattanakitsakul et al., 2007; Phoolcharoen & Smith, 2004).

5.1.2 Replicon Expressing Cells Compared to Mock Treated Cells

The DENV replicon is a useful tool to study DENV-2 infection. It has already been shown to respond to antivirals targeting replication like DENV-2 itself (Massé et al., 2010b; Ng et al., 2007b), but its effectiveness as a BSL-2 surrogate for understanding the biology of DENV-2 infection has not been fully established. The proteomic analysis of the replicon containing cells was performed to try to uncover information on the role of the NS proteins in Huh-7 cells and to establish if there is a difference in the interaction of the cell with a stably expressed replicon compared to DENV-2 infection.

In contrast to the Huh-7 cells infected with DENV-2, proteins enriched in abundance in the 16K fraction of Huh-7 cells containing the replicon were much more skewed towards proteins involved in membranous structures rather than simply the mitochondria. For proteins altered in abundance 1.5-fold compared to mock cells (according to STRING v11.5) the top three enriched terms related to cell compartments included the endomembrane system and extracellular vesicles, and the top biological

process related term for these proteins was vesicle mediated transport, clearly showing the important role of members of the secretory pathway in the replicon replication cycle. Indeed, 143 of the 272 proteins altered in abundance 2.0-fold or more are associated with the endomembrane system – 105 of the proteins increased in abundance 2.0-fold in replicon cells compared to mock cells are also found in this term. It is interesting to see the term 'extracellular vesicles' in this analysis no virions would be released from transfected cells but possibly it reflects the release of NS1. DENV infection is known to cause massive membrane reorganisation within infected cells through development of the RC, reviewed in 2021 by Van Den Elsen et al. (2021).

As the NS proteins induce the membrane changes required for DENV RC formation, it is expected that the replicon would make ER modifications similar to those made during DENV infection. Examination of the 16K data revealed the top annotation cluster generated by DAVID using the proteins altered in abundance 2.0-fold contained the term 'prevents secretion from the ER'. The 30 proteins associated with this term were reanalysed in STRING and the top biological processes were exported. These included proteins involved in protein folding and response to ER stress. The most enriched terms for the proteins increased or decreased significantly in amount (rather than just altered) did not reveal any more information. However, given that the unfolded protein response (UPR) is hijacked in DENV infection to provide a more pro-viral state (Perera et al., 2017), the replicon could potentially be used to unpick some of the HFs involved in DENV infection.

The proteomic analysis of the DENV infected Huh-7 cells showed that mitochondrial proteins and pathways were significantly enriched in the 16K fraction compared to mock infected cells. Analysis of the proteins increased in the 16K fraction of replicon cells showed a slightly different story. Proteins associated with 4 of the top 15 most enriched biological processes were targeted for siRNA knockdown. These included proteins associated with secretory terms, responses to ER stress and the unfolded protein response. The siRNA knockdown was unsuccessful but could have uncovered novel HFs in replicon containing cells which could have been used to investigate DENV infection. Additionally, there were 37 proteins that were associated with the Reactome pathway - metabolism of lipids, which is unsurprising as NS3 is known to interact and stimulate fatty acid synthase (FASN) in Huh-7.5 cells (Heaton et al., 2010a).

The proteins which decreased a minimum of 1.5-fold in the 16K fraction of replicon containing cells had a variety of different enrichments, including members of membrane trafficking and vesicle-mediated transport pathways, but the most interesting proteins were involved in clathrin-mediated endocytosis

pathways. It is known that DENV enters human target cells by clathrin-mediated endocytosis (Cruz-Oliveira et al., 2015), so it might be expected that these proteins would be increased in abundance – until the location of these proteins is considered. It is possible during the replication of the replicon that these proteins are sequestered elsewhere in the cell, and so were not identified in the 16K fraction.

The proteome of the WCL from replicon containing Huh-7 cells was also analysed. This analysis was much briefer than that of the corresponding 16K fraction, as the HF required for the RC was the focus of this study. However, the 476 proteins found to be altered in amount 1.5-fold or more were analysed by STRING. The BPs identified were very general and included terms related to metabolism and biosynthesis. The RPs associated with these proteins were 'metabolism' – another general term – and 'metabolism of lipids,' which was identified frequently throughout this analysis.

More of the proteins chosen for siRNA knockdown in the replicon containing cells have evidence of a role in DENV and viral infection. Details of the full list of proteins can be found in Table S.18. Whilst one of the aims of this study was to find novel HFs in DENV infection, some of these protein targets were included as a way of testing the usefulness of the replicon as a surrogate in a biochemical test. Some of these proteins will be discussed here.

'Vesicle-mediated transport' was the first term used to identify targets. Calreticulin, the ER resident calcium binding chaperone, was measured to be 6.3-fold higher in replicon containing cells than mock cells. This protein would likely have a role in DENV protein folding and thus replicon expression, given the interplay between the UPR and DENV protein expression (Perera et al., 2017) and indeed it has been shown to localise with viral dsRNA and DENV NS3 and NS5 during infection (Dalrymple & Mackow, 2012). Another ER chaperone found in this data set was hypoxia up-regulated protein 1 that was 7.1-fold greater in replicon containing cells. This has also been found to be increased in abundance during DENV infection (Chiu et al., 2014), which is a good marker for the effectiveness of this bioinformatic approach.

Proteins associated with the term 'response to endoplasmic stress' were also used to generate targets. Of the six proteins associated with this term, one had clear previous evidence of a role in DENV infection. Protein disulfide-isomerase A3 (PDIA3) has been found to be increased in abundance during infection, and knockdown by RNAi decreased levels of intracellular virus (Mishra et al., 2012). Other targets belonging to this term with a documented involvement in viral infections include PDIA1, PDIA4, and UDP-glucose:glycoprotein glucosyltransferase 1 (UGGT1). These enable HIV entry to cells, are involved in astrovirus entry to Caco-2 cells, and evidence of overexpression increases enterovirus growth rates, respectively (Aguilar-Hernández et al., 2021; Bi et al., 2011; P. N. Huang et al., 2017).

Comparing the functional enrichment of proteomes of DENV infected and replicon containing Huh-7 cells yielded some similar results, but with a few key differences. DENV infection seems to impact the amounts of mitochondrial proteins detected, where the replicon had no such effect. However, both analyses identified lipid metabolism as a pathway associated with these proteins.

5.1.3 Mock versus iDV2 as controls

The analysis here was based on the differences in the proteomes of DENV-2 infected and replicon containing Huh-7 cells compared to a control. The control used throughout the analysis was a mock infection, although data from an additional control using treatment with inactivated DENV was included in the dataset. To demonstrate that there is no discernible difference between using the mock infection to the inactivated DENV-2 infection a comparison was performed. However, this was not performed with the replicon as there was no data comparing the replicon and the iDV2 data set. For consistency, both the DENV-2 data and the replicon data were compared to the Mock – the most biologically relevant controls for both.

Considering the 16K data set, from DENV-2 infected cells there are 110 proteins increased 2.0-fold when using iDV2 as a comparator, and 120 when the mock is used. There is also a similar difference in the number of proteins decreased in abundance when these two comparators are used – 390 to 383 when iDV2 and mock are used, respectively. Enrichment analysis performed on these data provided very similar results. The themes of mitochondria and TCA are heavily enriched. When the protein targets were cross referenced, there were only eight that were not increased in abundance at least 1.5-fold in the DV2/iDV2 data. Four belonged to the TMED family (TMED2, 5, 9, 10 – the five chosen from the DV2/mock did not change significantly), and the remaining 4 were transport proteins – one target (CiC) was not increased significantly in the DV2/mock data set but still included for biological relevance. This brief analysis shows that there would have been very little difference in the results if iDV2 had been used as a comparator.

If iDV2 had been used when the proteomic analyses of the WCL data was performed, the results would also have been broadly similar, 534 were changed when the mock was used and 775 proteins were changed at least 2.0-fold in the DV2/iDV2 data. The vast majority were decreased in abundance, as only 26 were increased 2.0-fold (not enough to perform meaningful downstream analysis). Just like in the 16K data, there was very little difference in the results of the enrichment analysis of the DV2/iDV2 and the DV2/mock. The BPs included terms related to regulation and negative regulation of processes, and mitotic cell cycle phase transition.

5.2 Silencing RNA Screens

The aim of this study was to identify potential HFs in DENV infection, find any differences in the host proteome when comparing DENV infected to replicon containing cells, and to unpick the role of these HFs. A good way to do this is to perform loss of function studies, for which custom libraries of siRNAs are a relatively easy method. Other methods include CRISPR or dominant negative mutations – the former being more much more expensive, and the latter being too labour intensive for a high throughput method.

The siRNA screens were unsuccessful, for which there were several potential explanations. Initially seeding the cells at too high a concentration, so when they grow out the image is too crowded. The knockdown was far too inefficient, this would probably be explained by the transfection mix – a previous siRNA screen in Huh-7 cells have used 200 nM or 300 nM (Chu & Yang, 2007), much higher than the 50 nM that was used here. The MOI of five chosen for the infection was much too high, this amount of virus would have massively saturated the cells, and so any effect the siRNA's may have had on reducing DENV-2 replication would have been lost. The amount of virus used should have been a tenth less to provide a better representation of infection.

5.3 Concluding Remarks

Overall, this present study has shown that a detailed and broad proteomic analysis of TMT mass spectrometry data sets can identify proteins modulated after DENV infection in different fractions of Huh-7 cells. An IFA based approach to titrate DENV stock was shown to be successful, and while the siRNA screens were not successful, they provide a good basis to be repeated and optimised in future.

Appendix

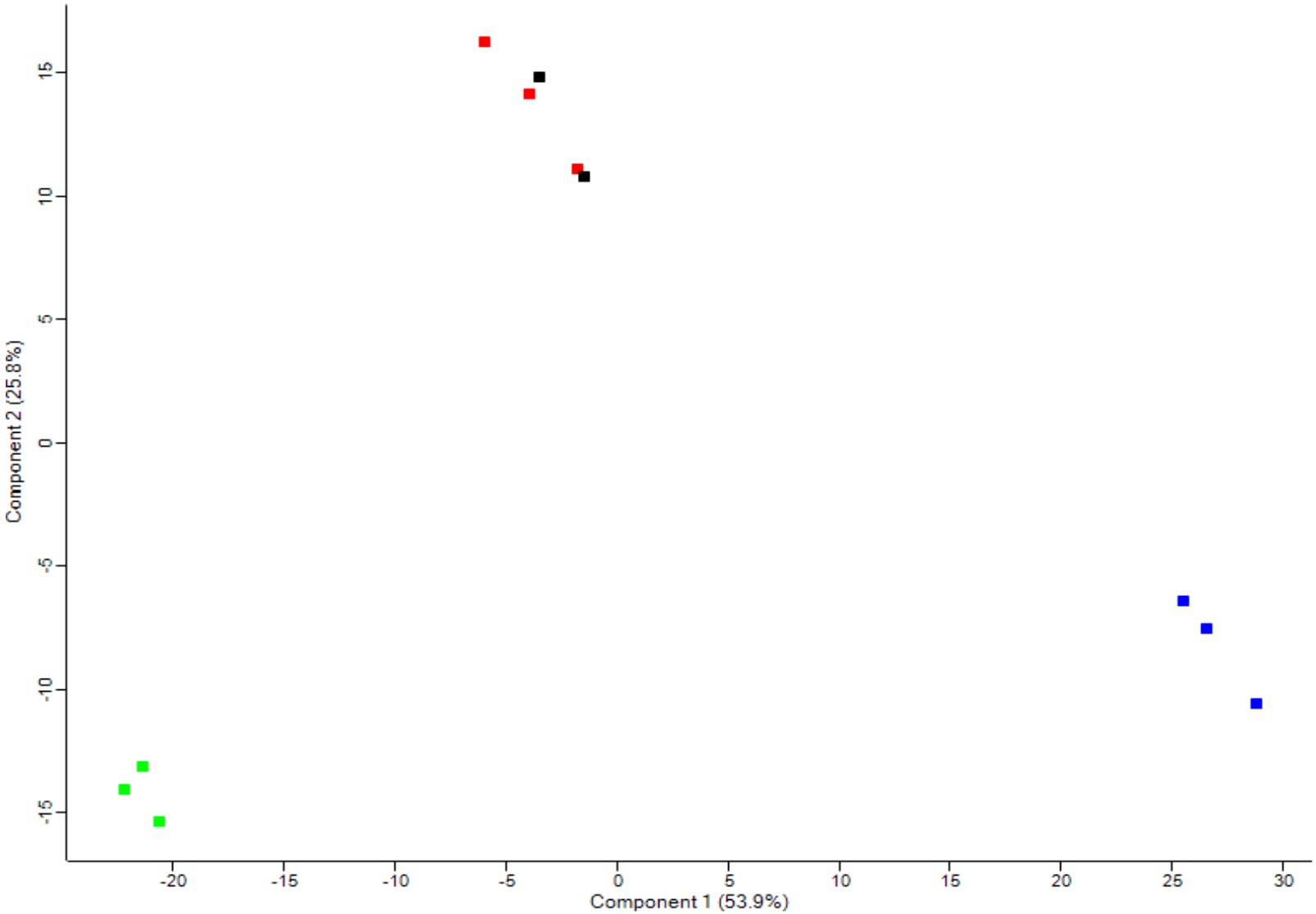

Figure S. 1. PCA plot of the replicates of the WCL datasets, made using Perseus v1.6.6.0. Mock infected (black), DENV-2 infected (blue), iDV2 treated (red) and replicon cells (green).

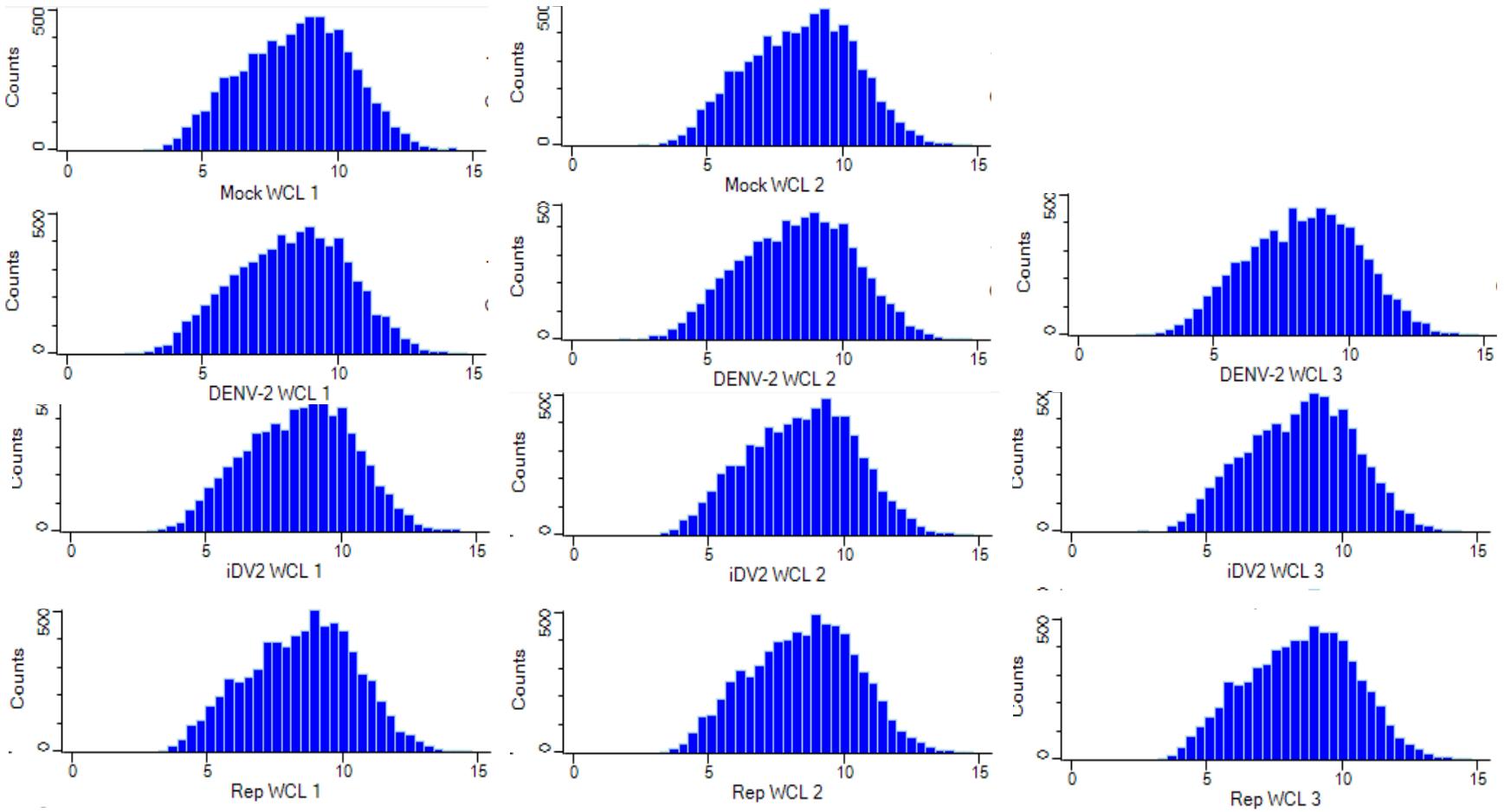

Figure S. 2. Multiple histograms showing the distribution of data in each of the repeat datasets for each experimental condition, made using Perseus v1.6.6.0. Mock (top), DENV-2 infected (DENV-2) (second from the top), iDENV-2 treated (iDV2) (second from the bottom) and replicon cells (Rep) (bottom).

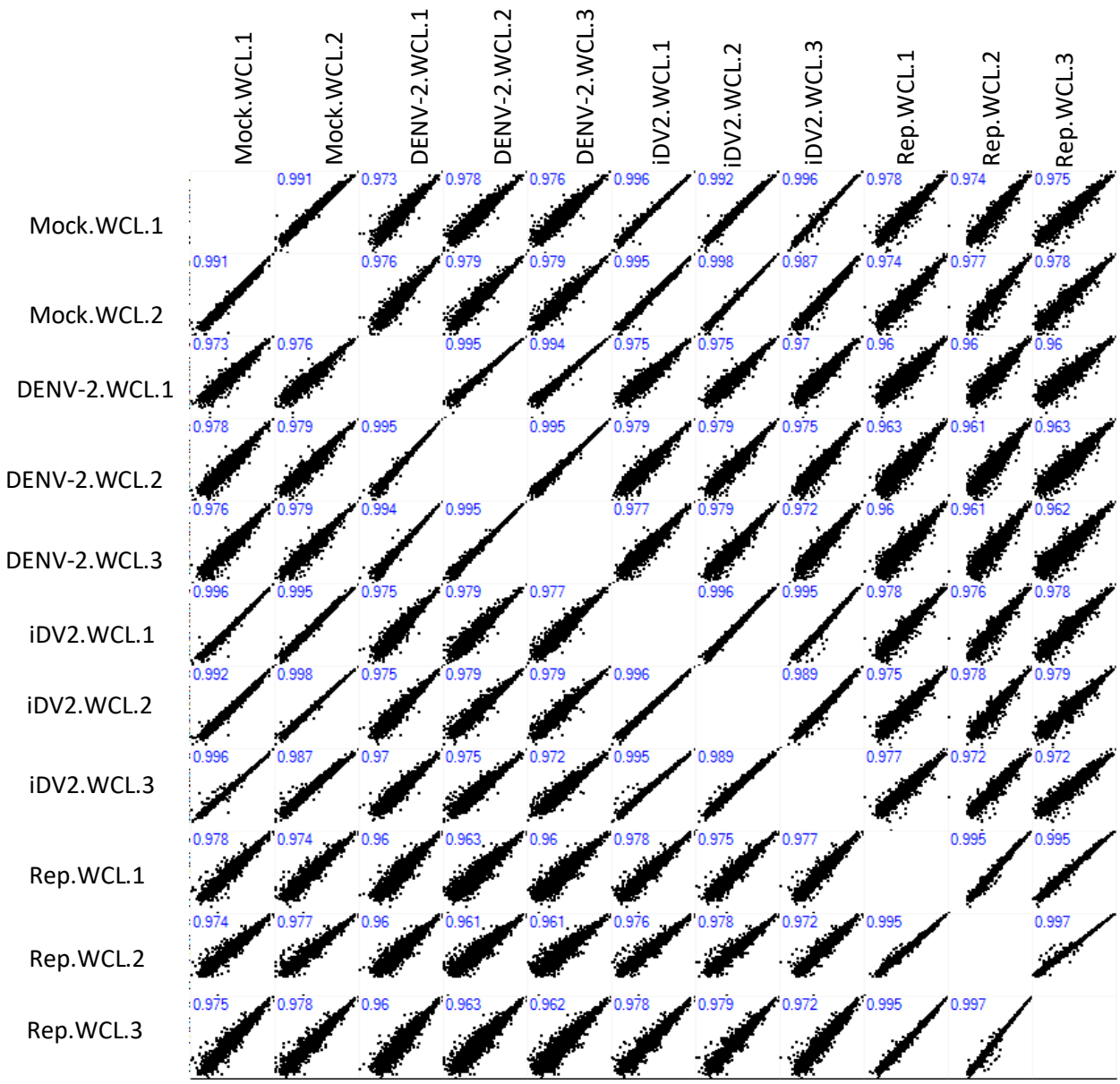

Figure S. 3. Multiple scatter plots of each repeat from each condition plotted against each other, with the correlation of the plot described using the Pearson's correlation in blue in the top left of each graph, made using Perseus v1.6.6.0. Datasets derived from mock infected cells (Mock); DENV-2 infected cells (DENV-2); iDV2 infected cells (iDV2) and replicon cells (Rep).

Comparison	Fold Change Cut-off	Number of Proteins Increased (% of Total)	Number of Proteins Decreased (% of Total)	Total Number of Proteins Significantly Changed (% of Total)
DV2/Mock	1.5	63 (0.77)	471 (5.74)	534 (6.51)
DV2/Mock	2.0	19 (0.23)	200 (2.44)	219 (2.67)
Replicon/Mock	1.5	250 (3.05)	226 (2.76)	476 (5.8)
Replicon/Mock	2.0	73 (0.89)	71 (0.87)	144 (1.76)

Table S. 1. The numbers of significantly ($p < 0.05$) altered proteins in the WCL from DENV-2 infected and replicon cells compared to mock with fold change (FC) cut-offs of 2 and 1.5.

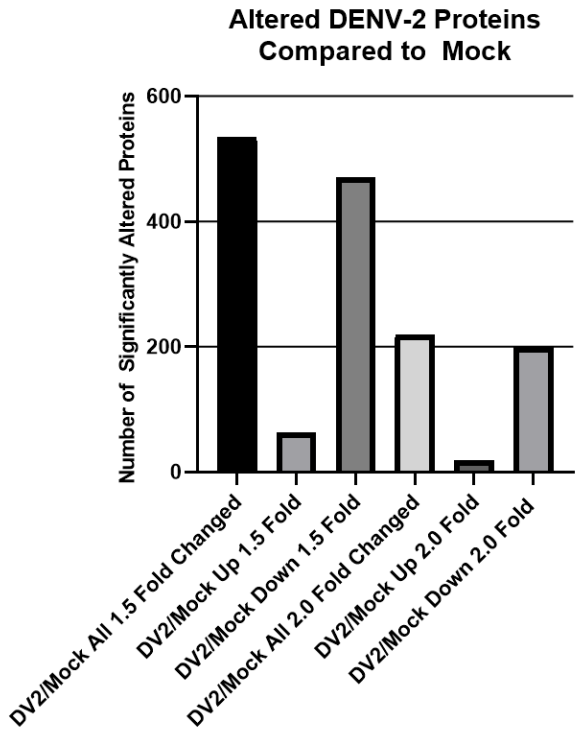

Figure S. 4.Bar chart made in GraphPad Prism v9.6.0 showing numbers of significantly ($p < 0.05$) increased and decreased (2-fold and 1.5-fold) proteins in the WCL fraction of DENV-2 infected cells compared to mock.

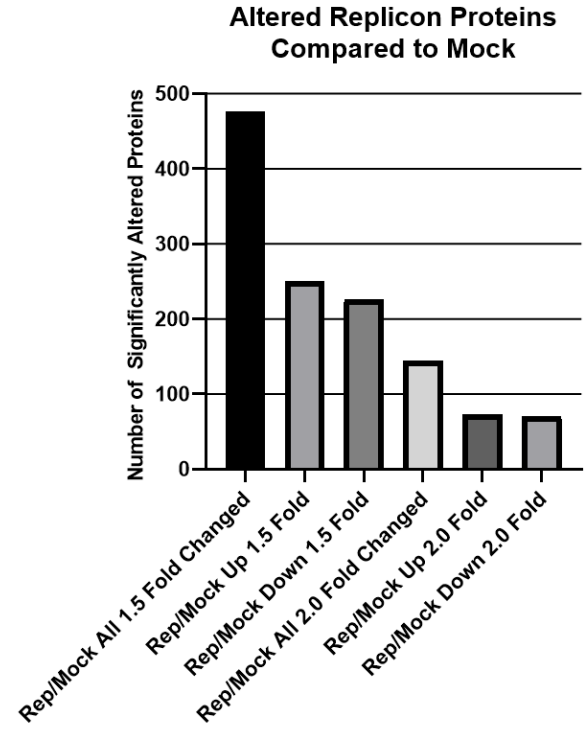

Figure S. 5. Bar chart made in GraphPad Prism v9.6.0 showing numbers of significantly ($p < 0.05$) increased and decreased (2-fold and 1.5-fold) proteins in the WCL fraction of replicon cells compared to mock.

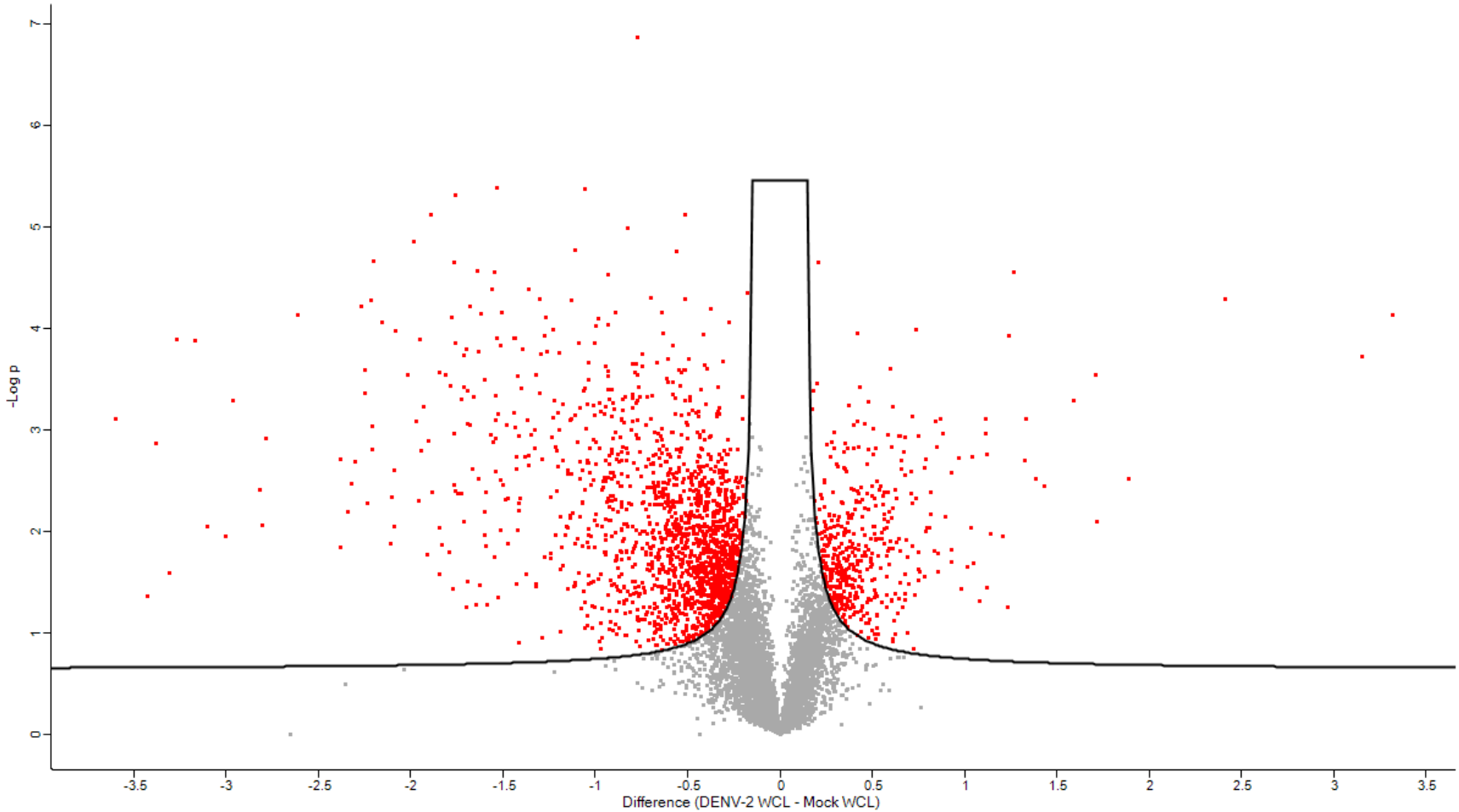

Figure S. 6. Volcano plot made in Perseus v1.6.6.0 showing the distribution of proteins significantly altered in abundance of the DENV-2 infected proteomes compared to the mock infected proteomes (shown above the curve as red squares)

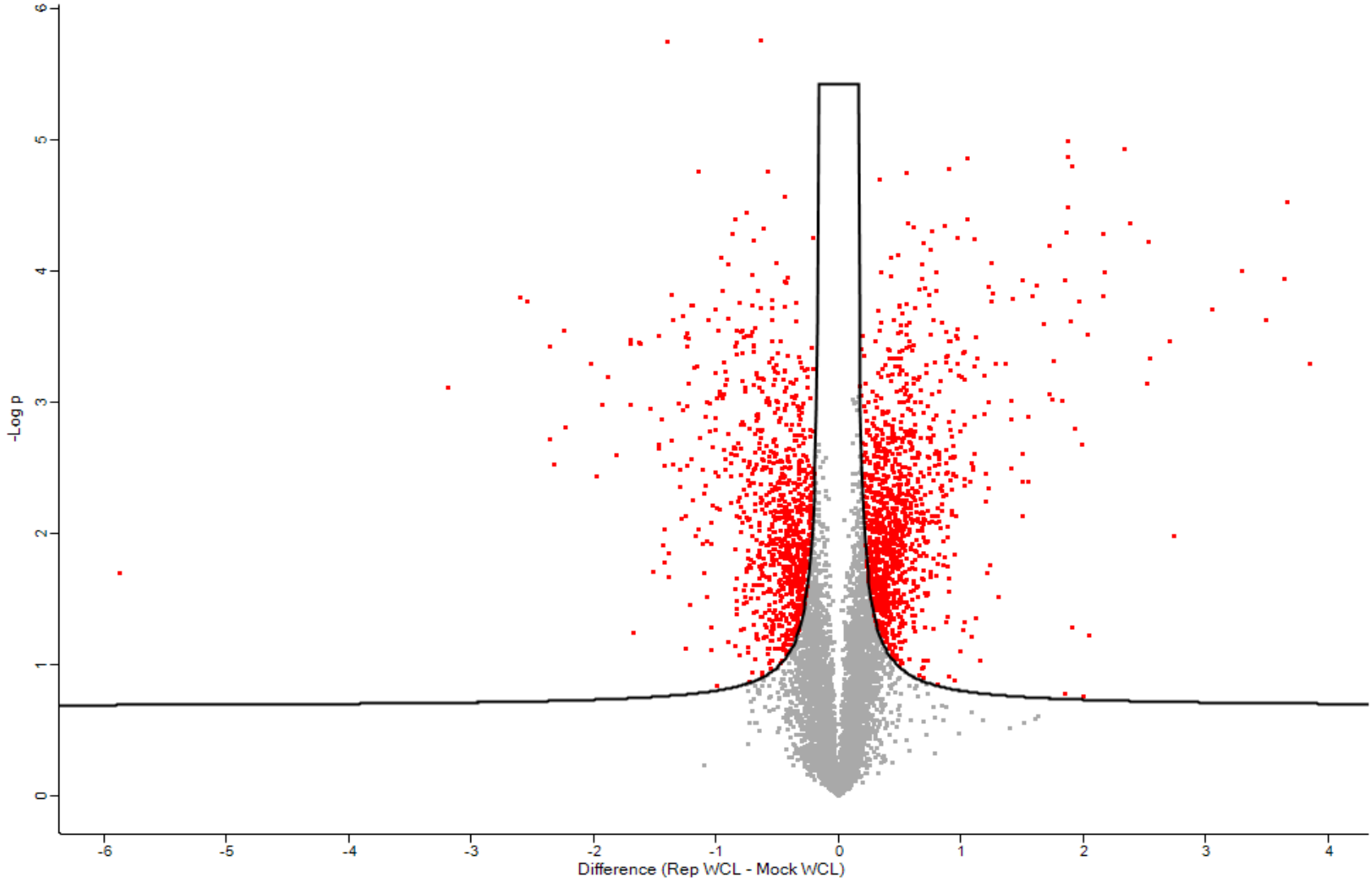

Figure S. 7. Volcano plot made in Perseus v1.6.6.0 showing the distribution of proteins significantly altered in abundance of the replicon transfected Huh-7 proteomes compared to the mock infected proteomes (shown above the curve as red squares)

Term ID	Term Description	Observed Gene Count	Background Gene Count	FDR
GO:0044281	Small molecule metabolic process	119	1684	$3.23X10^{-23}$
GO:0019752	Carboxylic acid metabolic process	75	853	$3.34X10^{-18}$
GO:0043436	Oxoacid metabolic process	78	944	$9.92X10^{-18}$
GO:0044237	Cellular metabolic process	276	7513	$1.07X10^{-17}$
GO:0008152	Metabolic process	289	8298	$9.53X10^{-16}$

Table S. 2. Top five biological processes of proteins altered ≥ 2.0-Fold in 16K DENV-2 versus iDV2, generated by STRING v11.5 as ranked by FDR.

Term ID	Term Description	Observed Gene Count	Background Gene Count	FDR
GO:0005739	Mitochondrion	153	1611	$8.62X10^{-48}$
GO:0005759	Mitochondrial matrix	88	479	$4.36X10^{-45}$
GO:0005737	Cytoplasm	360	11428	$1.93X10^{-17}$
GO:0005740	Mitochondrial envelope	58	766	$6.95X10^{-12}$
GO:0031966	Mitochondrial membrane	56	722	$6.95X10^{-12}$

Table S. 3. Top five Cellular components of proteins altered ≥ 2.0-Fold in 16K DENV-2 versus iDV2, generated by STRING v11.5 as ranked by FDR.

Term ID	Term Description	Observed Gene Count	Background Gene Count	FDR
HSA-1428517	The citric acid (TCA) cycle and respiratory electron transport	36	176	$6.72X10^{-18}$
HSA-1430728	Metabolism	121	2089	$1.07X10^{-17}$
HSA-163200	Respiratory electron transport, ATP synthesis by chemiosmotic coupling, and heat production by uncoupling proteins.	26	125	$5.80X10^{13}$

HSA-611105	Respiratory electron transport	19	101	$1.63X10^{-8}$
HSA-71403	Citric acid cycle (TCA cycle)	10	22	$6.09X10^{-7}$

Table S. 4. Top five Reactome pathways of proteins altered ≥ 2.0-Fold in 16K DENV-2 versus iDV2, generated by STRING v11.5 as ranked by FDR.

Term ID	Term Description	Observed Gene Count	Background Gene Count	FDR
GO:0006119	Oxidative phosphorylation	22	118	$1.22X10^{-22}$
GO:0046034	ATP metabolic process	25	204	$1.93X10^{-22}$
GO:0006091	Generation of precursor metabolites and energy	24	405	$1.11X10^{-14}$
GO:0022904	Respiratory electron transport chain	16	107	$1.11X10^{-14}$
GO:0045333	Cellular respiration	17	158	$9.48X10^{-14}$

Table S. 5. Top five biological processes of proteins increased ≥ 2.0-Fold in 16K DENV-2 versus iDV2, generated by STRING v11.5 as ranked by FDR.

Term ID	Term Description	Observed Gene Count	Background Gene Count	FDR
GO:0098800	Inner mitochondrial membrane protein complex	23	131	$3.52X10^{-24}$
GO:0005743	Mitochondrial inner membrane	32	480	$5.15X10^{-23}$
GO:0019866	Organelle inner membrane	33	541	$7.26X10^{-23}$
GO:0005740	Mitochondrial envelope	37	766	$7.79X10^{-23}$
GO:0031966	Mitochondrial membrane	36	722	$1.18X10^{-22}$

Table S. 6. Top five Cellular components of proteins increased ≥ 2.0-Fold in 16K DENV-2 versus iDV2, generated by STRING v11.5 as ranked by FDR.

Term ID	Term Description	Observed Gene Count	Background Gene Count	FDR

HSA-163200	Respiratory electron transport, ATP synthesis by chemiosmotic coupling, and heat production by uncoupling proteins.	22	125	$6.43X10^{-23}$
HSA-611105	Respiratory electron transport	15	101	$2.74X10^{-14}$
HSA-8949613	Cristae formation	8	31	$1.25X10^{-8}$
HSA-163210	Formation of ATP by chemiosmotic coupling	7	18	$1.70X10^{-8}$
HSA-6799198	Complex I biogenesis	9	55	$1.70X10^{-8}$

Table S. 7. Top five Reactome pathways of proteins increased ≥ 2.0-Fold in 16K DENV-2 versus iDV2, generated by STRING v11.5 as ranked by FDR.

Term ID	Term Description	Observed Gene Count	Background Gene Count	FDR
GO:0019752	Carboxylic acid metabolic process	70	853	$2.17X10^{-21}$
GO:0044281	Small molecule metabolic process	98	1684	$2.79X10^{-21}$
GO:0043436	Oxoacid metabolic process	72	944	$7.80X10^{-21}$
GO:0006520	Cellular amino acid metabolic process	34	278	$5.93X10^{-14}$
GO:0044237	Cellular metabolic process	212	7513	$6.57X10^{-13}$

Table S. 8. Top five biological processes of proteins decreased ≥ 2.0-Fold in 16K DENV-2 versus iDV2, generated by STRING v11.5 as ranked by FDR.

Term ID	Term Description	Observed Gene Count	Background Gene Count	FDR
GO:0005759	Mitochondrial matrix	77	479	$2.74X10^{-13}$
GO:0005739	Mitochondrion	111	1611	$5.02X10^{-32}$
GO:0005737	Cytoplasm	271	11428	$2.82X10^{-10}$
GO:0070013	Intracellular organelle lumen	170	5857	$3.75X10^{-10}$
GO:0043231	Intracellular membranx10bounded organelle	254	10761	$1.52X10^{-8}$

Table S. 9. Top five Cellular components of proteins decreased ≥ 2.0-Fold in 16K DENV-2 versus iDV2, generated by STRING v11.5 as ranked by FDR.

Term ID	Term Description	Observed Gene Count	Background Gene Count	FDR
HSA-1430728	Metabolism	87	2089	$3.50X10^{-10}$
HSA-71403	Citric acid cycle (TCA cycle)	10	22	$1.33X10^{-7}$
HSA-70895	Branched-chain amino acid catabolism	8	21	$2.02X10^{-5}$
HSA-381426	Regulation of Insulin-like Growth Factor (IGF) transport and uptake by Insulin-like Growth Factor Binding Proteins (IGFBiological processes)	14	124	$9.18X10^{-5}$
HSA-8957275	Post-translational protein phosphorylation	13	107	$9.18X10^{-5}$

Table S. 10. Top five Reactome pathways of proteins decreased ≥ 2.0-Fold in 16K DENV-2 versus iDV2, generated by STRING v11.5 as ranked by FDR.

Term ID	Term Description	Observed Gene Count	Background Gene Count	FDR
GO:0009892	Negative regulation of metabolic process	105	3124	$2.00X10^{-6}$
GO:0010605	Negative regulation of macromolecule metabolic process	100	2875	$2.00X10^{-6}$
GO:0051172	Negative regulation of nitrogen compound metabolic process	88	2429	$2.00X10^{-6}$
GO:0031324	Negative regulation of cellular metabolic process	91	2630	$6.02X10^{-6}$
GO:0048523	Negative regulation of cellular process	140	4874	$9.71X10^{-6}$
GO:0051346	Negative regulation of hydrolase activity	30	450	$9.71X10^{-6}$
GO:0044772	Mitotic cell cycle phase transition	23	280	$1.38X10^{-5}$

Table S. 11. Top seven biological processes of proteins altered ≥ 2.0-Fold in the WCL of DENV-2 infected cells compared to iDV2 treated cells, generated by STRING v11.5 as ranked by FDR.

Term ID	Term Description	Observed Gene Count	Background Gene Count	FDR
GO:0062023	Collagen-containing extracellular matrix	40	396	$4.24X10^{-14}$
GO:0005622	Intracellular	322	14276	$5.71X10^{-12}$
GO:0043227	Membrane bounded organelle	295	12427	$6.56X10^{-12}$
GO:0031012	Extracellular matrix	41	527	$1.66X10^{-11}$
GO:0005737	Cytoplasm	276	11428	$7.79X10^{-11}$

Table S. 12. Top five Cellular components of proteins altered ≥ 2.0-Fold in the WCL of DENV-2 infected cells compared to iDV2 treated cells, generated by STRING v11.5 as ranked by FDR.

Term ID	Term Description	Observed Gene Count	Background Gene Count	FDR
HSA-8957275	Post-translational protein phosphorylation	17	107	$1.99X10^{-7}$
HSA-381426	Regulation of Insulin-like Growth Factor (IGF) transport and uptake by Insulin-like Growth Factor Binding Proteins (IGFBPs)	17	124	$7.72X10^{-7}$
HSA-114608	Platelet degranulation	15	127	$3.19X10^{-5}$

Table S. 13. Top three Reactome pathways of proteins altered ≥ 2.0-Fold in the WCL of DENV-2 infected cells compared to iDV2 treated cells, generated by STRING v11.5 as ranked by FDR.

Term ID	Term Description	Observed Gene Count	Background Gene Count	FDR
GO:0009892	Negative regulation of metabolic process	100	3124	$3.28X10^{-6}$
GO:0010605	Negative regulation of macromolecule metabolic process	95	2875	$3.28X10^{-6}$
GO:0051172	Negative regulation of nitrogen compound metabolic process	83	2429	$4.88X10^{-6}$
GO:0019222	Regulation of metabolic process	174	6948	$6.30X10^{-6}$
GO:0044772	Mitotic cell cycle phase transition	23	280	$6.30X10^{-6}$

Table S. 14. Top five biological processes of proteins decreased ≥ 2.0-Fold in DENV-2 infected cells compared to the iDV2 treated cells, generated by STRING v11.5 as ranked by FDR.

Term ID	Term Description	Observed Gene Count	Background Gene Count	FDR
GO:0062023	Collagen-containing extracellular matrix	38	396	$1.81X10^{-13}$
GO:0031012	Extracellular matrix	39	527	$9.42X10^{-11}$
GO:0005622	Intracellular	301	14276	$2.57X10^{-10}$
GO:0043227	Membrane bounded organelle	275	12427	$3.68X10^{-10}$
GO:0043226	Organelle	288	13515	$2.75X10^{-9}$

Table S. 15. Top five Cellular components of proteins decreased ≥ 2.0-Fold in DENV-2 infected cells compared to the iDV2 treated cells, generated by STRING v11.5 as ranked by FDR.

Term ID	Term Description	Observed Gene Count	Background Gene Count	FDR
HSA-8957275	Post-translational protein phosphorylation	16	107	$6.68X10^{-7}$
HSA-381426	Regulation of Insulin-like Growth Factor (IGF) transport and uptake by Insulin-like Growth Factor Binding Proteins (IGFBPs)	16	124	$2.32X10^{-6}$
HSA-114608	Platelet degranulation	15	127	$1.46X10^{-5}$

Table S. 16. Top three Cellular components of proteins decreased ≥ 2.0-Fold in DENV-2 infected cells compared to the iDV2 treated cells, generated by STRING v11.5 as ranked by FDR.

DENV-2 Protein Targets

Table S. 17. Targets for siRNA knockdown in Huh-7 cells to be infected

Gene Name	UniProt Accession Number	Protein Name	Description	Normalised Fold Change (log2)	p Value
SLC25A6	P12236	Adenine Nucleotide Translocases 3	Exchanges ADP from the cytosol with ATP generated in the matrix. ANTs are highly expressed on the IMM and can bind respiratory super-complexes and protein import machinery (Gutiérrez-Aguilar & Baines, 2013; Palmieri, 2013; Palmieri et al., 2020; Ruprecht & Kunji, 2020).	0.895	0.024
SLC25A12	O75746	Ca2+-Sensitive Mitochondrial Carrier (AGC1 aka Aralar)	Calcium ion sensitive Mitochondrial carriers. AGC1 and AGC2 mediate proton-coupled glutamate co-transport (Gutiérrez-Aguilar & Baines, 2013; Palmieri, 2013; Palmieri et al., 2020; Ruprecht & Kunji, 2020).	1.037	0.033
SLC25A13	Q9UJS0	Ca^{2+}-Sensitive Mitochondrial Carrier (AGC2 aka Citrin)	Calcium ion sensitive Mitochondrial carriers. AGC1 and AGC2 mediate proton-coupled glutamate co-transport (Gutiérrez-Aguilar & Baines, 2013; Palmieri, 2013; Palmieri et al., 2020; Ruprecht & Kunji, 2020).	1.046	0.007
SLC25A24	Q6NUK1	Ca2+-Sensitive Mitochondrial Carrier (APC1)	APC1 exchanges ATP and Magnesium ions for protons (Gutiérrez-Aguilar & Baines, 2013; Palmieri, 2013; Palmieri et al., 2020; Ruprecht & Kunji, 2020).	0.903	0.022

SLC25A20	O43772	Carnitine/Acyl-Carnitine Carrier (CAC)	Transports Carnitine in exchange for Acylcarnitine in an Acyl-chain-length-dependant-manner. Second transporter in the Carnitine Shuttle (after CPT1 on the OMM providing fatty acids for β-oxidation (Gutiérrez-Aguilar & Baines, 2013; Palmieri, 2013; Palmieri et al., 2020; Ruprecht & Kunji, 2020).	0.748	0.032
SLC25A1	P53007	Citrate Carrier (CiC)	Tricarboxylate Carrier, the main physiological role is to transport Citrate across the Mitochondrial Matrix (MM) in exchange for Malate. 1:1 process. Citrate is cleaved to Acetyl-CoA which is necessary for Fatty Acid Synthesis (Gutiérrez-Aguilar & Baines, 2013; Palmieri, 2013; Palmieri et al., 2020; Ruprecht & Kunji, 2020).	0.443	0.048
SLC25A10	Q9UBX3	Dicarboxylate Carrier (DIC)	Transports Malate (and Succinate) out of the Mitochondria in exchange for Phosphate (Gutiérrez-Aguilar & Baines, 2013; Palmieri, 2013; Palmieri et al., 2020; Ruprecht & Kunji, 2020).	0.600	0.042
SLC25A22	Q9H936	Glutamate Carrier (GC1)	Symporter of Glutamate and H+ ions. GC1 has a higher Km and Vmax than its isoform, GC2. The main role of GC1 is to ultimately provide substrates for the Urea cycle (Gutiérrez-Aguilar & Baines, 2013; Palmieri, 2013; Palmieri et al., 2020; Ruprecht & Kunji, 2020).	0.783	0.016
SLC25A15	Q9Y619	Ornithine Carrier (ORNT1)	Facilitate import of Ornithine into the matrix in exchange for Citrulline and H+ ion export. Necessary for the Urea cycle (Gutiérrez-Aguilar & Baines, 2013; Palmieri, 2013; Palmieri et al., 2020; Ruprecht & Kunji, 2020).	0.723	0.019

SLC25A11	Q02978	Oxoglutarate Carrier (OGC)	Facilitates Oxoglutarate export in exchange for dicarboxylate (usually Malate) import (Gutiérrez-Aguilar & Baines, 2013; Palmieri, 2013; Palmieri et al., 2020; Ruprecht & Kunji, 2020).	1.027	0.021
SLC25A3	Q00325	Phosphate Carrier (PiC)	Transports Phosphate into the Mitochondrial matrix either accompanied with an H+ ion or in exchange for an OH- ion (Gutiérrez-Aguilar & Baines, 2013; Palmieri, 2013; Palmieri et al., 2020; Ruprecht & Kunji, 2020).	0.850	0.036
MCU	Q8NE86	Calcium uniporter protein, mitochondrial	IMM calcium uniporter strongly dependent on mitochondrial membrane potential (Anand & Tikoo, 2013).	1.122	0.050
MRS2	Q9HD23	Magnesium transporter MRS2 homolog, mitochondrial	Magnesium transporter that mediates the influx of magnesium into the mitochondrial matrix (Zsurka et al., 2001).	0.966	0.015
OXA1L	Q15070	Mitochondrial inner membrane protein OXA1L	Insertion of integral membrane proteins into the mitochondrial inner membrane. Essential for the activity and assembly of cytochrome oxidase (Rötig et al., 1997).	0.633	0.035
LETM1	O95202	Mitochondrial proton/calcium exchanger protein	Mitochondrial calcium transporter, proton-dependant (Nakamura et al., 2020).	0.876	0.015

MPC2	O95563	Mitochondrial Pyruvate Carrier 2	Mediates the uptake of pyruvate into mitochondria (Nagampalli et al., 2018; Schell et al., 2014).	0.587	0.024
NNT	Q13423	NAD(P) transhydrogenase, mitochondrial	Catalyzes the generation of NADH using proton transport along the gradient (Ho et al., 2017).	0.869	0.023
SFXN1	Q9H9B4	Sideroflexin-1	Mitochondrial Serine transporter involved in one carbon metabolism. Shares high (~70%) sequence homology with SFXN-3 (Kory et al., 2018).	0.840	0.038
SFXN3	Q9BWM7	Sideroflexin-3	Mt Serine transporter, like SFXN1 (Rivell et al., 2019).	1.115	0.010
VDAC1	P21796	Voltage Dependent Anion-selective Channel Protein 1	Anion Selective OMM channel, expressed more widely than VDAC3. Evidence of no significant change in amount of VDAC1 expression during DENV infection, but evidence of localisation between GRP78 and DENV E (Camara et al., 2017; Jitobaom et al., 2016)	0.772	0.028
VDAC3	Q9Y277	Voltage Dependent Anion-selective Channel Protein 3	Isoform of VDAC1 (Camara et al., 2017).	0.733	0.021

TMED10	P49755	Transmembrane emp24 domain-containing protein 10	Multiple roles including intracellular transport, reviewed in Pastor-Cantizano et al., 2016 and Strating & Martens, 2009.	0.341	0.011
TMED2	Q15363	Transmembrane emp24 domain-containing protein 2	Multiple roles including intracellular transport, reviewed in Pastor-Cantizano et al., 2016 and Strating & Martens, 2009.	0.021	0.611
TMED5	Q9Y3A6	Transmembrane emp24 domain-containing protein 5	Multiple roles including intracellular transport, reviewed in Pastor-Cantizano et al., 2016 and Strating & Martens, 2009.	-0.008	0.832
TMED7	Q9Y3B3	Transmembrane emp24 domain-containing protein 7	Multiple roles including intracellular transport, reviewed in Pastor-Cantizano et al., 2016 and Strating & Martens, 2009.	0.611	0.006
TMED9	Q9BVK6	Transmembrane emp24 domain-containing protein 9	Multiple roles including intracellular transport, reviewed in Pastor-Cantizano et al., 2016 and Strating & Martens, 2009.	0.220	0.195

HPGD	P15428	15-hydroxyprostaglandin dehydrogenase [NAD(+)]	Inactivates catabolism of prostaglandin E2, contributes to the regulation of events that are under the control of prostaglandin levels (Kim et al., 2015).	2.479	0.007
ARSD	P51689	Arylsulfatase D	Isoform of Arylsulfatase A, expression of which is increased in type 2 diabetes (Montgomery et al., 2022; Urbitsch et al., 2004).	1.229	0.006
CTH	P32929	Cystathionine gamma-lyase	Catalyses last step in the pathway turning methionine to cysteine (Steegborn et al., 1999).	1.191	0.007
ETFDH	Q16134	Electron transfer flavoprotein-ubiquinone oxidoreductase, mitochondrial	Accepts electrons from ETF and reduces ubiquinone (Missaglia et al., 2018) .	1.057	0.013
EXT1	Q16394	Exostosin-1	Glycosyltransferase required for the biosynthesis of heparan-sulfate (Ropero et al., 2004).	1.128	0.011
LGMN	Q99538	Legumain	Cysteine endopeptidase, has a role in class II MHC presentation (Dall & Brandstetter, 2016).	1.318	0.011

AK2	F8VY04	Nucleoside-diphosphate kinase	Regulates homeostasis of adenine nucleotides in the mitochondria (Six et al., 2015).	2.083	0.018
PIK3C3	Q8NEB9	Phosphatidylinositol 3-kinase catalytic subunit type 3	Lipid kinase, involved in cargo sorting in lysosomes (Song et al., 2023).	1.104	0.040
PRKCA	P17252	Protein kinase C alpha type	Calcium-activated, diacylglycerol-dependent serine/threonine-protein kinase with a range of homeostatic functions (Okat, 2018).	1.049	0.001
SLC26A1	Q9H2B4	Sulphate Anion Transporter 2	Anion transporter across the cell membrane (Wu et al., 2016).	2.320	0.000
SLC19A3	Q9BZV2	Thiamine transporter 2	Thiamine transporter (Yamada et al., 2010).	3.365	0.000
HSPA5	P11021	Endoplasmic Reticulum Chaperone BiP	Also known as GRP78 and BiP, resides in the ER, key player in the UPR (T. Li et al., 2023).	1.255	0.003
SVIL	O95425	Supervillin	Membrane skeleton protein, regulates cellular motility (Fang et al., 2010).	1.113	0.024

ZNF319	Q9P2F9	Zinc Finger Protein 319	May be involved in transcriptional regulation and the cell cycle (L. Wang et al., 2022).	3.427	0.025
SLC39A10	Q9ULF5	Zinc Transporter ZIP10	Cell membrane zinc transporter (He et al., 2023).	1.097	0.011

Replicon Protein Targets

Table S. 18. Targets for siRNA knockdown in Huh-7 replicon cells

Gene Name	UniProt Accession Number	Protein Name	Description	Normalised Fold Change (log2)	p Value
CALR	P27797	Calreticulin	ER resident, protein chaperone, also regulates Ca^{2+} (Michalak et al., 1999).	2.667	0.000
HYOU1	Q9Y4L1	Hypoxia up-regulated protein 1	ER chaperone, probable role in the UPR (Ikeda et al., 1997).	2.831	0.009
MANF	P55145	Mesencephalic astrocyte-derived neurotrophic factor	ER chaperone, induced by stress (S. Xu et al., 2019).	2.159	0.000
NPC2	P61916	NPC intracellular cholesterol transporter 2	Role in cholesterol homeostasis, including intracellular sorting (Subramanian & Balch, 2008).	2.211	0.025
PRDX4	Q13162	Peroxiredoxin-4	Protects the cell against antioxidant stress, found in the ER (Jia et al., 2019).	2.803	0.000
SERPING1	P05155	Plasma protease C1 inhibitor	Serine protease, inhibits C1 of the complement cascade (Y. Y. Xu et al., 2020).	2.438	0.032

TXNDC5	Q8NBS9	Thioredoxin domain-containing protein 5	Rearranges sulphide bonds, has a role in protein folding (X. Wang et al., 2022).	2.274	0.005
ERO1A	Q96HE7	ERO1-like protein alpha	ER oxidoreductase, involved in ER-stress related apoptosis (Liu et al., 2022).	2.486	0.003
FKBP14	Q9NWM8	Peptidyl-prolyl cis-trans isomerase FKBP14	PPIase, speeds folding of proteins during protein synthesis (Baumann et al., 2012).	2.409	0.010
P4HB	P07237	Protein disulfide-isomerase	ER resident chaperone folding proteins in response to ER stress (Baumann et al., 2012)	2.066	0.010
PDIA3	P30101	Protein disulfide-isomerase A3	Folds proteins in ER, chaperone (Tu et al., 2022).	1.494	0.037
PDIA4	P13667	Protein disulfide-isomerase A4	Related to PDIA3, also folds proteins in ER (Kuo et al., 2017).	2.273	0.021
UGGT1	Q9NYU2	UDP-glucose:glycoprotein glucosyltransferase 1	Folding sensor in ER, glycoprotein quality control (W. Zhang et al., 2011).	1.667	0.024

HSPA5	P11021	Endoplasmic reticulum chaperone BiP	Molecular chaperone in ER lumen (Gething, 1999)	1.393	0.012
SERPINH1	P50454	Serpin H1	Binds specifically to collagen. Serine peptidase inhibitor (Y. Wang et al., 2022).	1.610	0.020
TOR1B	O14657	Torsin-1B	ATPase in the ER, could function as a chaperone (Nguyen et al., 2023).	1.687	0.015
TMED10	P49755	Transmembrane emp24 domain-containing protein 10	Multiple roles including intracellular transport, reviewed in Pastor-Cantizano et al., 2016 and Strating & Martens, 2009.	-0.510	0.113
TMED2	Q15363	Transmembrane emp24 domain-containing protein 2	Multiple roles including intracellular transport, reviewed in Pastor-Cantizano et al., 2016 and Strating & Martens, 2009.	-0.020	0.895
TMED5	Q9Y3A6	Transmembrane emp24 domain-containing protein 5	Multiple roles including intracellular transport, reviewed in Pastor-Cantizano et al., 2016 and Strating & Martens, 2009.	-0.439	0.222
TMED7	Q9Y3B3	Transmembrane emp24 domain-containing protein 7	Multiple roles including intracellular transport, reviewed in Pastor-Cantizano et al., 2016 and Strating & Martens, 2009.	-2.336	0.420

TMED9	Q9BVK6	Transmembrane emp24 domain-containing protein 9	Multiple roles including intracellular transport, reviewed in Pastor-Cantizano et al., 2016 and Strating & Martens, 2009.	-0.300	0.005
LGMN	Q99538	Legumain	See table S.17	1.631	0.046
SVIL	O95425	Supervillin	See table S.17	1.299	0.008
SLC19A3	Q9BZV2	Thiamine Transporter 2	See table S.17	2.245	0.027
ZNF319	Q9P2F9	Zinc Finger Protein 319	See table S.17	2.144	0.031
SLC39A10	Q9ULF5	Zinc Transporter ZIP10	See table S.17	1.236	0.015
DPP7	Q9UHL4	Dipeptidyl Peptidase 2	Intracellular protease (Maes et al., 2007).	2.091	0.010
SLC1A3	P43003	Excitatory Amino Acid Transporter 1	Glutamate transporter, mainly found in the central nervous system (Malik & Willnow, 2019).	2.026	0.012

FTH1	P026794	Ferritin heavy chain	Stores cellular iron in a soluble form. Important for iron homeostasis. Forms complex with the light chain (Tirinato et al., 2021).	1.731	0.037
FGB	P02675	Fibrinogen beta chain	Component of fibrinogen which has a key role in clotting (Weisel & Litvinov, 2017).	1.753	0.004
FGG	P02679	Fibrinogen gamma chain	Polymerizes with fibrinogen alpha and beta to form an insoluble fibrin matrix (Weisel & Litvinov, 2017).	1.645	0.024
PYGL	P06737	Glycogen Phosphorylase, liver form	Regulates glycogen mobilisation (Mathieu et al., 2017). b	1.511	0.034
KNG1	P01042	Kininogen-1	Glycoprotein, has a role in innate immunity (Köhler et al., 2020)	1.730	0.009
MTTP	P55157	Microsomal triglyceride transfer protein large subunit	Transfers lipids between membrane bound vesicles (Hussain et al., 2012)	2.568	0.004
AGA	P20933	N(4)-(beta-N-acetylglucosaminyl)-L-asparaginase	Glycosylates proteins, role in protein maturation (Fisher et al., 1990).	1.644	0.003

References

Aguilar-Hernández, N., Meyer, L., López, S., Dubois, R. M., & Arias, C. F. (2021). Protein disulfide isomerase a4 is involved in genome uncoating during human astrovirus cell entry. *Viruses*, *13*(1). https://doi.org/10.3390/v13010053

Aguirre, S., Luthra, P., Sanchez-Aparicio, M. T., Maestre, A. M., Patel, J., Lamothe, F., Fredericks, A. C., Tripathi, S., Zhu, T., Pintado-Silva, J., Webb, L. G., Bernal-Rubio, D., Solovyov, A., Greenbaum, B., Simon, V., Basler, C. F., Mulder, L. C. F., García-Sastre, A., & Fernandez-Sesma, A. (2017). Dengue virus NS2B protein targets cGAS for degradation and prevents mitochondrial DNA sensing during infection. *Nature Microbiology*, *2*(March), 1–11. https://doi.org/10.1038/nmicrobiol.2017.37

Aktepe, T. E., Liebscher, S., Prier, J. E., Simmons, C. P., & Mackenzie, J. M. (2017). The Host Protein Reticulon 3.1A Is Utilized by Flaviviruses to Facilitate Membrane Remodelling. *Cell Reports*, *21*(6), 1639–1654. https://doi.org/10.1016/j.celrep.2017.10.055

Anand, S. K., & Tikoo, S. K. (2013). Viruses as modulators of mitochondrial functions. In *Advances in Virology* (Vol. 2013, p. 17). Hindawi Limited. https://doi.org/10.1155/2013/738794

Ang, F., Wong, A. P. Y., Ng, M. M. L., & Chu, J. J. H. (2010). Small interference RNA profiling reveals the essential role of human membrane trafficking genes in mediating the infectious entry of dengue virus. *Virology Journal*, *7*(1), 24. https://doi.org/10.1186/1743-422X-7-24

Anton, A., Mazeaud, C., Freppel, W., Gilbert, C., Tremblay, N., Sow, A. A., Roy, M., Rodrigue-Gervais, I. G., & Chatel-Chaix, L. (2021). Valosin-containing protein ATPase activity regulates the morphogenesis of Zika virus replication organelles and virus-induced cell death. *Cellular Microbiology*, *23*(4). https://doi.org/10.1111/cmi.13302

Ashburner, M., Ball, C. A., Blake, J. A., Botstein, D., Butler, H., Cherry, J. M., Davis, A. P., Dolinski, K., Dwight, S. S., Eppig, J. T., Harris, M. A., Hill, D. P., Issel-Tarver, L., Kasarskis, A., Lewis, S., Matese, J. C., Richardson, J. E., Ringwald, M., Rubin, G. M., & Sherlock, G. (2000). Gene ontology: Tool for the unification of biology. *Nature Genetics*, *25*(1), 25–29. https://doi.org/10.1038/75556

Baggen, J., Vanstreels, E., Jansen, S., & Daelemans, D. (2021). Cellular host factors for SARS-CoV-2 infection. *Nature Microbiology*, *6*(10), 1219–1232. https://doi.org/10.1038/s41564-021-00958-0

Barrows, N. J., Anglero-Rodriguez, Y., Kim, B., Jamison, S. F., Le Sommer, C., McGee, C. E., Pearson, J. L., Dimopoulos, G., Ascano, M., Bradrick, S. S., & Garcia-Blanco, M. A. (2019). Dual roles for the

ER membrane protein complex in flavivirus infection: viral entry and protein biogenesis. *Scientific Reports 2019 9:1*, *9*(1), 1–16. https://doi.org/10.1038/s41598-019-45910-9

Baumann, M., Giunta, C., Krabichler, B., Rüschendorf, F., Zoppi, N., Colombi, M., Bittner, R. E., Quijano-Roy, S., Muntoni, F., Cirak, S., Schreiber, G., Zou, Y., Hu, Y., Romero, N. B., Carlier, R. Y., Amberger, A., Deutschmann, A., Straub, V., Rohrbach, M., … Fauth, C. (2012). Mutations in FKBP14 cause a variant of Ehlers-Danlos syndrome with progressive kyphoscoliosis, myopathy, and hearing loss. *American Journal of Human Genetics*, *90*(2), 201–216. https://doi.org/10.1016/j.ajhg.2011.12.004

Bhatnagar, P., Sreekanth, G. P., Murali-Krishna, K., Chandele, A., & Sitaraman, R. (2021). Dengue Virus Non-Structural Protein 5 as a Versatile, Multi-Functional Effector in Host–Pathogen Interactions. *Frontiers in Cellular and Infection Microbiology*, *11*, 169. https://doi.org/10.3389/FCIMB.2021.574067/BIBTEX

Bhatt, S., Gething, P. W., Brady, O. J., Messina, J. P., Farlow, A. W., Moyes, C. L., Drake, J. M., Brownstein, J. S., Hoen, A. G., Sankoh, O., Myers, M. F., George, D. B., Jaenisch, T., William Wint, G. R., Simmons, C. P., Scott, T. W., Farrar, J. J., & Hay, S. I. (2013). The global distribution and burden of dengue. *Nature*, *496*(7446), 504–507. https://doi.org/10.1038/nature12060

Bi, S., Hong, P. W., Lee, B., & Baum, L. G. (2011). Galectin-9 binding to cell surface protein disulfide isomerase regulates the redox environment to enhance T-cell migration and HIV entry. *Proceedings of the National Academy of Sciences of the United States of America*, *108*(26), 10650–10655. https://doi.org/10.1073/pnas.1017954108

Brady, O. J., Gething, P. W., Bhatt, S., Messina, J. P., Brownstein, J. S., Hoen, A. G., Moyes, C. L., Farlow, A. W., Scott, T. W., & Hay, S. I. (2012). Refining the Global Spatial Limits of Dengue Virus Transmission by Evidence-Based Consensus. *PLoS Neglected Tropical Diseases*, *6*(8). https://doi.org/10.1371/journal.pntd.0001760

Byers, N. M., Fleshman, A. C., Perera, R., & Molins, C. R. (2019). Metabolomic insights into human arboviral infections: Dengue, chikungunya, and zika viruses. In *Viruses* (Vol. 11, Issue 3). MDPI AG. https://doi.org/10.3390/v11030225

Byk, L. A., & Gamarnik, A. V. (2016). Properties and Functions of the Dengue Virus Capsid Protein. *Annual Review of Virology*, *3*, 263–281. https://doi.org/10.1146/annurev-virology-110615-042334

Camara, A. K. S., Zhou, Y. F., Wen, P. C., Tajkhorshid, E., & Kwok, W. M. (2017). Mitochondrial VDAC1: A key gatekeeper as potential therapeutic target. In *Frontiers in Physiology* (Vol. 8, Issue JUN, p. 460). Frontiers Media S.A. https://doi.org/10.3389/fphys.2017.00460

Carbaugh, D. L., & Lazear, H. M. (2020). Flavivirus Envelope Protein Glycosylation: Impacts on Viral Infection and Pathogenesis. *Journal of Virology*, *94*(11). https://doi.org/10.1128/jvi.00104-20

Carbon, S., Douglass, E., Good, B. M., Unni, D. R., Harris, N. L., Mungall, C. J., Basu, S., Chisholm, R. L., Dodson, R. J., Hartline, E., Fey, P., Thomas, P. D., Albou, L. P., Ebert, D., Kesling, M. J., Mi, H., Muruganujan, A., Huang, X., Mushayahama, T., … Elser, J. (2021). The Gene Ontology resource: Enriching a GOld mine. *Nucleic Acids Research*, *49*(D1), D325–D334. https://doi.org/10.1093/nar/gkaa1113

Carnec, X., Meertens, L., Dejarnac, O., Perera-Lecoin, M., Hafirassou, M. L., Kitaura, J., Ramdasi, R., Schwartz, O., & Amara, A. (2016). The Phosphatidylserine and Phosphatidylethanolamine Receptor CD300a Binds Dengue Virus and Enhances Infection. *Journal of Virology*, *90*(1), 92–102. https://doi.org/10.1128/jvi.01849-15

Catalina-Rodriguez, O., Kolukula, V. K., Tomita, Y., Preet, A., Palmieri, F., Wellstein, A., Byers, S., Giaccia, A. J., Glasgow, E., Albanese, C., & Avantaggiati, M. L. (2012). The mitochondrial citrate transporter, CiC, is essential for mitochondrial homeostasis. *Oncotarget*, *3*(10), 1220–1235. https://doi.org/10.18632/oncotarget.714

Chatel-Chaix, L., & Bartenschlager, R. (2014). Dengue Virus- and Hepatitis C Virus-Induced Replication and Assembly Compartments: the Enemy Inside—Caught in the Web. *Journal of Virology*, *88*(11), 5907–5911. https://doi.org/10.1128/jvi.03404-13

Chatel-Chaix, L., Cortese, M., Romero-Brey, I., Bender, S., Neufeldt, C. J., Fischl, W., Scaturro, P., Schieber, N., Schwab, Y., Fischer, B., Ruggieri, A., & Bartenschlager, R. (2016). Dengue Virus Perturbs Mitochondrial Morphodynamics to Dampen Innate Immune Responses. *Cell Host and Microbe*, *20*(3), 342–356. https://doi.org/10.1016/j.chom.2016.07.008

Chen, H. R., Lai, Y. C., & Yeh, T. M. (2018). Dengue virus non-structural protein 1: a pathogenic factor, therapeutic target, and vaccine candidate. *Journal of Biomedical Science 2018 25:1*, *25*(1), 1–11. https://doi.org/10.1186/S12929-018-0462-0

Chiu, H. C., Hannemann, H., Heesom, K. J., Matthews, D. A., & Davidson, A. D. (2014). High-throughput quantitative proteomic analysis of dengue virus type 2 infected A549 cells. *PLoS ONE*, *9*(3), e93305. https://doi.org/10.1371/journal.pone.0093305

Chong, H. Y., Leow, C. Y., Abdul Majeed, A. B., & Leow, C. H. (2019). Flavivirus infection—A review of immunopathogenesis, immunological response, and immunodiagnosis. *Virus Research*, *274*, 197770. https://doi.org/10.1016/j.virusres.2019.197770

Chu, J. J. H., & Yang, P. L. (2007). c-Src protein kinase inhibitors block assembly and maturation of dengue virus. *Proceedings of the National Academy of Sciences of the United States of America*, *104*(9), 3520–3525. https://doi.org/10.1073/pnas.0611681104

Clyde, K., Kyle, J. L., & Harris, E. (2006). Recent Advances in Deciphering Viral and Host Determinants of Dengue Virus Replication and Pathogenesis. *Journal of Virology*, *80*(23), 11418–11431. https://doi.org/10.1128/jvi.01257-06

Cruz-Oliveira, C., Freire, J. M., Conceição, T. M., Higa, L. M., Castanho, M. A. R. B., & Da Poian, A. T. (2015). Receptors and routes of dengue virus entry into the host cells. In *FEMS Microbiology Reviews* (Vol. 39, Issue 2, pp. 155–170). Oxford University Press. https://doi.org/10.1093/femsre/fuu004

Cui, L., Hou, J., Fang, J., Lee, Y. H., Costa, V. V., Wong, L. H., Chen, Q., Ooi, E. E., Tannenbaum, S. R., Chen, J., & Ong, C. N. (2017). Serum Metabolomics Investigation of Humanized Mouse Model of Dengue Virus Infection. *Journal of Virology*, *91*(14). https://doi.org/10.1128/jvi.00386-17

Cui, L., Lee, Y. H., Kumar, Y., Xu, F., Lu, K., Ooi, E. E., Tannenbaum, S. R., & Ong, C. N. (2013). Serum Metabolome and Lipidome Changes in Adult Patients with Primary Dengue Infection. *PLoS Neglected Tropical Diseases*, *7*(8), e2373. https://doi.org/10.1371/journal.pntd.0002373

Cui, L., Pang, J., Lee, Y. H., Ooi, E. E., Ong, C. N., Leo, Y. S., & Tannenbaum, S. R. (2018). Serum metabolome changes in adult patients with severe dengue in the critical and recovery phases of dengue infection. *PLoS Neglected Tropical Diseases*, *12*(1), 1–15. https://doi.org/10.1371/journal.pntd.0006217

Dall, E., & Brandstetter, H. (2016). Structure and function of legumain in health and disease. *Biochimie*, *122*, 126–150. https://doi.org/10.1016/j.biochi.2015.09.022

Dalrymple, N. A., & Mackow, E. R. (2012). Endothelial Cells Elicit Immune-Enhancing Responses to Dengue Virus Infection. *Journal of Virology*, *86*(12), 6408–6415. https://doi.org/10.1128/jvi.00213-12

Dana, H., Chalbatani, G. M., Mahmoodzadeh, H., Karimloo, R., Rezaiean, O., Moradzadeh, A., Mehmandoost, N., Moazzen, F., Mazraeh, A., Marmari, V., Ebrahimi, M., Rashno, M. M., Abadi, S. J., & Gharagouzlo, E. (2017). Molecular Mechanisms and Biological Functions of siRNA. In *International journal of biomedical science : IJBS* (Vol. 13, Issue 2). http://www.ncbi.nlm.nih.gov/pubmed/28824341%0Ahttp://www.pubmedcentral.nih.gov/articlerender.fcgi?artid=PMC5542916

Diaz, A., & Ahlquist, P. (2012). Role of host reticulon proteins in rearranging membranes for positive-strand RNA virus replication. In *Current Opinion in Microbiology* (Vol. 15, Issue 4, pp. 519–524). https://doi.org/10.1016/j.mib.2012.04.007

Donovan-Banfield, I. (2019). 'Dengue virus-host factor interactions in the secretory pathway'. MScR Thesis, University of Bristol. Bristol.

Du Toit, A. (2016). Viral infection: Dengue as mitochondrial landscapers. In *Nature Reviews Microbiology* (Vol. 14, Issue 10, p. 603). Nature Publishing Group. https://doi.org/10.1038/nrmicro.2016.132

El-Bacha, T., & Da Poian, A. T. (2013). Virus-induced changes in mitochondrial bioenergetics as potential targets for therapy. *International Journal of Biochemistry and Cell Biology*, *45*(1), 41–46. https://doi.org/10.1016/j.biocel.2012.09.021

El-Bacha, T., Midlej, V., Pereira da Silva, A. P., Silva da Costa, L., Benchimol, M., Galina, A., & Da Poian, A. T. (2007). Mitochondrial and bioenergetic dysfunction in human hepatic cells infected with dengue 2 virus. *Biochimica et Biophysica Acta - Molecular Basis of Disease*, *1772*(10), 1158–1166. https://doi.org/10.1016/j.bbadis.2007.08.003

El-Bacha, T., Struchiner, C. J., Cordeiro, M. T., Almeida, F. C. L., Marques, E. T., & Da Poian, A. T. (2016). 1 H Nuclear Magnetic Resonance Metabolomics of Plasma Unveils Liver Dysfunction in Dengue Patients . *Journal of Virology*, *90*(16), 7429–7443. https://doi.org/10.1128/jvi.00187-16

Fang, Z., Takizawa, N., Wilson, K. A., Smith, T. C., Delprato, A., Davidson, M. W., Lambright, D. G., & Luna, E. J. (2010). The Membrane-Associated Protein, Supervillin, Accelerates F-Actin-Dependent

Rapid Integrin Recycling and Cell Motility. *Traffic*, *11*(6), 782–799. https://doi.org/10.1111/J.1600-0854.2010.01062.X

Fernandes-Siqueira, L. O., Zeidler, J. D., Sousa, B. G., Ferreira, T., & Da Poian, A. T. (2018). Anaplerotic Role of Glucose in the Oxidation of Endogenous Fatty Acids during Dengue Virus Infection. *MSphere*, *3*(1). https://doi.org/10.1128/msphere.00458-17

Fischl, W., & Bartenschlager, R. (2011). Exploitation of cellular pathways by Dengue virus. *Current Opinion in Microbiology*, *14*(4), 470–475. https://doi.org/10.1016/j.mib.2011.07.012

Fishburn, A. T., Pham, O. H., Kenaston, M. W., Beesabathuni, N. S., & Shah, P. S. (2022). Let's Get Physical: Flavivirus-Host Protein–Protein Interactions in Replication and Pathogenesis. *Frontiers in Microbiology*, *13*, 447. https://doi.org/10.3389/FMICB.2022.847588/BIBTEX

Fisher, K. J., Tollersrud, O. K., & Aronson, N. N. (1990). Cloning and sequence analysis of a cDNA for human glycosylasparaginase. *FEBS Letters*, *269*(2), 440–444. https://doi.org/10.1016/0014-5793(90)81211-6

Fonseka, P., Pathan, M., Chitti, S. v., Kang, T., & Mathivanan, S. (2021). FunRich enables enrichment analysis of OMICs datasets. *Journal of Molecular Biology*, *433*(11). https://doi.org/10.1016/J.JMB.2020.166747

Fontaine, K. A., Sanchez, E. L., Camarda, R., & Lagunoff, M. (2015). Dengue Virus Induces and Requires Glycolysis for Optimal Replication. *Journal of Virology*, *89*(4), 2358–2366. https://doi.org/10.1128/jvi.02309-14

Gething, M. J. (1999). Role and regulation of the ER chaperone BiP. *Seminars in Cell & Developmental Biology*, *10*(5), 465–472. https://doi.org/10.1006/SCDB.1999.0318

Gillespie, M., Jassal, B., Stephan, R., Milacic, M., Rothfels, K., Senff-Ribeiro, A., Griss, J., Sevilla, C., Matthews, L., Gong, C., Deng, C., Varusai, T., Ragueneau, E., Haider, Y., May, B., Shamovsky, V., Weiser, J., Brunson, T., Sanati, N., … D'Eustachio, P. (2022). The reactome pathway knowledgebase 2022. *Nucleic Acids Research*, *50*(D1), D687–D692. https://doi.org/10.1093/nar/gkab1028

Gopala Reddy, S. B., Chin, W. X., & Shivananju, N. S. (2018). Dengue virus NS2 and NS4: Minor proteins, mammoth roles. *Biochemical Pharmacology*, *154*, 54–63. https://doi.org/10.1016/J.BCP.2018.04.008

Gualano, R. C., Pryor, M. J., Cauchi, M. R., Wright, P. J., & Davidson, A. D. (1998). Identification of a major determinant of mouse neurovirulence of dengue virus type 2 using stably cloned genomic-length cDNA. *Journal of General Virology*, *79*(3), 437–446. https://doi.org/10.1099/0022-1317-79-3-437/CITE/REFWORKS

Gutiérrez-Aguilar, M., & Baines, C. P. (2013). Physiological and pathological roles of mitochondrial SLC25 carriers. In *Biochemical Journal* (Vol. 454, Issue 3, pp. 371–386). NIH Public Access. https://doi.org/10.1042/BJ20121753

Haas, A. K., Fuchs, E., Kopajtich, R., & Barr, F. A. (2005). A GTPase-activating protein controls Rab5 function in endocytic trafficking. *Nature Cell Biology*, *7*(9), 887–893. https://doi.org/10.1038/ncb1290

Harapan, H., Michie, A., Sasmono, R. T., & Imrie, A. (2020). Dengue: A minireview. In *Viruses* (Vol. 12, Issue 8). MDPI AG. https://doi.org/10.3390/v12080829

He, X., Ge, C., Xia, J., Xia, Z., Zhao, L., Huang, S., Wang, R., Pan, J., Cheng, T., Xu, P. F., Wang, F., & Min, J. (2023). The Zinc Transporter SLC39A10 Plays an Essential Role in Embryonic Hematopoiesis. *Advanced Science*, *10*(17), 1–17. https://doi.org/10.1002/advs.202205345

Heaton, N. S., Perera, R., Berger, K. L., Khadka, S., LaCount, D. J., Kuhn, R. J., & Randall, G. (2010a). Dengue virus nonstructural protein 3 redistributes fatty acid synthase to sites of viral replication and increases cellular fatty acid synthesis. *Proceedings of the National Academy of Sciences of the United States of America*, *107*(40), 17345–17350. https://doi.org/10.1073/pnas.1010811107

Heaton, N. S., Perera, R., Berger, K. L., Khadka, S., LaCount, D. J., Kuhn, R. J., & Randall, G. (2010b). Dengue virus nonstructural protein 3 redistributes fatty acid synthase to sites of viral replication and increases cellular fatty acid synthesis. *Proceedings of the National Academy of Sciences of the United States of America*, *107*(40), 17345–17350. https://doi.org/10.1073/PNAS.1010811107/SUPPL_FILE/PNAS.201010811SI.PDF

Heaton, N. S., & Randall, G. (2010). Dengue virus-induced autophagy regulates lipid metabolism. *Cell Host and Microbe*, *8*(5), 422–432. https://doi.org/10.1016/j.chom.2010.10.006

Ho, H. Y., Lin, Y. T., Lin, G., Wu, P. R., & Cheng, M. L. (2017). Nicotinamide nucleotide transhydrogenase (NNT) deficiency dysregulates mitochondrial retrograde signaling and impedes proliferation. *Redox Biology*, *12*, 916–928. https://doi.org/10.1016/j.redox.2017.04.035

Huang, P. N., Jheng, J. R., Arnold, J. J., Wang, J. R., Cameron, C. E., & Shih, S. R. (2017). UGGT1 enhances enterovirus 71 pathogenicity by promoting viral RNA synthesis and viral replication. *PLoS Pathogens*, *13*(5), e1006375. https://doi.org/10.1371/journal.ppat.1006375

Huang, P. yan, Wu, J. guo, Gu, J., Zhang, T. qi, Li, L. feng, Wang, S. qun, & Wang, M. (2021). Bioinformatics analysis of miRNA and mRNA expression profiles to reveal the key miRNAs and genes in osteoarthritis. *Journal of Orthopaedic Surgery and Research*, *16*(1). https://doi.org/10.1186/s13018-021-02201-2

Husain, M. (2020). Host factors involved in influenza virus infection. In *Emerging Topics in Life Sciences* (Vol. 4, Issue 4, pp. 401–410). Portland Press. https://doi.org/10.1042/ETLS20200232

Hussain, M. M., Rava, P., Walsh, M., Rana, M., & Iqbal, J. (2012). Multiple functions of microsomal triglyceride transfer protein. *Nutrition and Metabolism*, *9*, 1–16. https://doi.org/10.1186/1743-7075-9-14

Ikeda, J., Kaneda, S., Kuwabara, K., Ogawa, S., Kobayashi, T., Matsumoto, M., Yura, T., & Yanagi, H. (1997). Cloning and expression of cDNA encoding the human 150 kDa oxygen-regulated protein, ORP150. *Biochemical and Biophysical Research Communications*, *230*(1), 94–99. https://doi.org/10.1006/bbrc.1996.5890

Izmirly, A. M., Alturki, S. O., Alturki, S. O., Connors, J., & Haddad, E. K. (2020). Challenges in Dengue Vaccines Development: Pre-existing Infections and Cross-Reactivity. *Frontiers in Immunology*, *11*, 1055. https://doi.org/10.3389/fimmu.2020.01055

Jia, W., Chen, P., & Cheng, Y. (2019). PRDX4 and Its Roles in Various Cancers. *Technology in Cancer Research and Treatment*, *18*, 1–10. https://doi.org/10.1177/1533033819864313

Jiménez de Oya, N., Blázquez, A.-B., Casas, J., Saiz, J.-C., & Martín-Acebes, M. A. (2018). Direct Activation of Adenosine Monophosphate-Activated Protein Kinase (AMPK) by PF-06409577 Inhibits Flavivirus Infection through Modification of Host Cell Lipid Metabolism. *Antimicrobial Agents and Chemotherapy*, *62*(7). https://doi.org/10.1128/aac.00360-18

Jiménez de Oya, N., Esler, W. P., Huard, K., El-Kattan, A. F., Karamanlidis, G., Blázquez, A. B., Ramos-Ibeas, P., Escribano-Romero, E., Louloudes-Lázaro, A., Casas, J., Sobrino, F., Hoehn, K., James, D. E., Gutiérrez-Adán, A., Saiz, J. C., & Martín-Acebes, M. A. (2019). Targeting host metabolism by inhibition of acetyl-Coenzyme A carboxylase reduces flavivirus infection in mouse

models. *Emerging Microbes and Infections*, *8*(1), 624–636. https://doi.org/10.1080/22221751.2019.1604084

Jitobaom, K., Tongluan, N., & Smith, D. R. (2016). Involvement of voltage-dependent anion channel (VDAC) in dengue infection. *Scientific Reports*, *6*(1), 1–12. https://doi.org/10.1038/srep35753

Jungwirth, G., Yu, T., Cao, J., Eddine, M. A., Moustafa, M., Warta, R., Debus, J., Unterberg, A., Abdollahi, A., & Herold-Mende, C. (2021). KIF11 inhibitors filanesib and ispinesib inhibit meningioma growth in vitro and in vivo. *Cancer Letters*, *506*, 1–10. https://doi.org/10.1016/j.canlet.2021.02.016

Katzelnick, L. C., Gresh, L., Halloran, M. E., Mercado, J. C., Kuan, G., Gordon, A., Balmaseda, A., & Harris, E. (2017). Antibody-dependent enhancement of severe dengue disease in humans. *Science*, *358*(6365), 929–932. https://doi.org/10.1126/science.aan6836

Kaufmann, B., & Rossmann, M. G. (2011). Molecular mechanisms involved in the early steps of flavivirus cell entry. In *Microbes and Infection* (Vol. 13, Issue 1, pp. 1–9). NIH Public Access. https://doi.org/10.1016/j.micinf.2010.09.005

Kim, H. J., Lee, S., Lee, H. Y., Won, H., Chang, S. H., & Nah, S. S. (2015). 15-Hydroxyprostaglandin dehydrogenase is upregulated by hydroxychloroquine in rheumatoid arthritis fibroblast-like synoviocytes. *Molecular Medicine Reports*, *12*(3), 4141–4148. https://doi.org/10.3892/mmr.2015.3931

Klein, D. E., Choi, J. L., & Harrison, S. C. (2013). Structure of a Dengue Virus Envelope Protein Late-Stage Fusion Intermediate. *Journal of Virology*, *87*(4), 2287–2293. https://doi.org/10.1128/jvi.02957-12

Köhler, J., Maletzki, C., Koczan, D., Frank, M., Springer, A., Steffen, C., Revenko, A. S., MacLeod, A. R., Mikkat, S., Kreikemeyer, B., & Oehmcke-Hecht, S. (2020). Kininogen supports inflammation and bacterial spreading during Streptococccus Pyogenes Sepsis. *EBioMedicine*, *58*, 102908. https://doi.org/10.1016/J.EBIOM.2020.102908

Kory, N., Wyant, G. A., Prakash, G., De Bos, J. uit, Bottanelli, F., Pacold, M. E., Chan, S. H., Lewis, C. A., Wang, T., Keys, H. R., Guo, Y. E., & Sabatini, D. M. (2018). SFXN1 is a mitochondrial serine transporter required for one-carbon metabolism. *Science*, *362*(6416). https://doi.org/10.1126/science.aat9528

Krishnan, M. N., Ng, A., Sukumaran, B., Gilfoy, F. D., Uchil, P. D., Sultana, H., Brass, A. L., Adametz, R., Tsui, M., Qian, F., Montgomery, R. R., Lev, S., Mason, P. W., Koski, R. A., Elledge, S. J., Xavier, R. J., Agaisse, H., & Fikrig, E. (2008). RNA interference screen for human genes associated with West Nile virus infection. *Nature*, *455*(7210), 242. https://doi.org/10.1038/NATURE07207

Krishnan, M. N., Sukumaran, B., Pal, U., Agaisse, H., Murray, J. L., Hodge, T. W., & Fikrig, E. (2007). Rab 5 Is Required for the Cellular Entry of Dengue and West Nile Viruses. *Journal of Virology*, *81*(9), 4881–4885. https://doi.org/10.1128/jvi.02210-06

Kunji, E. R. S., King, M. S., Ruprecht, J. J., & Thangaratnarajah, C. (2020). The SLC25 carrier family: Important transport proteins in mitochondrial physiology and pathology. *Physiology*, *35*(5), 302–327. https://doi.org/10.1152/physiol.00009.2020

Kuo, T. F., Chen, T. Y., Jiang, S. T., Chen, K. W., Chiang, Y. M., Hsu, Y. J., Liu, Y. J., Chen, H. M., Yokoyama, K. K., Tsai, K. C., Yeh, H. H., Chen, Y. R., Yang, M. T., Yang, C. Y., & Yang, W. C. (2017). Protein disulfide isomerase a4 acts as a novel regulator of cancer growth through the procaspase pathway. *Oncogene*, *36*(39), 5484–5496. https://doi.org/10.1038/onc.2017.156

Kwon, Y. J., Heo, J., Wong, H. E. E., Cruz, D. J. M., Velumani, S., Da Silva, C. T., Mosimann, A. L. P., Duarte Dos Santos, C. N., Freitas-Junior, L. H., & Fink, K. (2014). Kinome siRNA screen identifies novel cell-type specific dengue host target genes. *Antiviral Research*, *110*(1), 20–30. https://doi.org/10.1016/j.antiviral.2014.07.006

Lee, Y. R., Lei, H. Y., Liu, M. T., Wang, J. R., Chen, S. H., Jiang-Shieh, Y. F., Lin, Y. S., Yeh, T. M., Liu, C. C., & Liu, H. S. (2008). Autophagic machinery activated by dengue virus enhances virus replication. *Virology*, *374*(2), 240–248. https://doi.org/10.1016/j.virol.2008.02.016

Lescar, J., Soh, S., Lee, L. T., Vasudevan, S. G., Kang, C., & Lim, S. P. (2018). The dengue virus replication complex: From RNA replication to protein-protein interactions to evasion of innate immunity. In *Advances in Experimental Medicine and Biology* (Vol. 1062, pp. 115–129). Springer New York LLC. https://doi.org/10.1007/978-981-10-8727-1_9

Li, M., Wang, P., Zheng, Z., Hu, K., Zhang, M., Guan, X., Fu, M., Zhang, D., Wang, W., Xiao, G., Hu, Q., & Liu, Y. (2017). Japanese encephalitis virus counteracts BST2 restriction via its envelope protein E. *Virology*, *510*, 67–75. https://doi.org/10.1016/j.virol.2017.07.008

Li, T., Fu, J., Cheng, J., Elfiky, A. A., Wei, C., & Fu, J. (2023). New progresses on cell surface protein HSPA5/BiP/GRP78 in cancers and COVID-19. *Frontiers in Immunology*, *14*(May), 1–9. https://doi.org/10.3389/fimmu.2023.1166680

Liu, L., Li, S., Qu, Y., Wang, J., Fei, K., Wang, C., Zhang, X., Ma, Z., Bai, H., & Wang, J. (2022). Tumour ERO1A instigates T cell dysfunction by transmission of endoplasmic reticulum stress. *Journal of Clinical Oncology*, *40*(16_suppl), e14533–e14533. https://doi.org/10.1200/JCO.2022.40.16_suppl.e14533

Ma, L., Jones, C. T., Groesch, T. D., Kuhn, R. J., & Post, C. B. (2004). Solution structure of dengue virus capsid protein reveals another fold. *Proceedings of the National Academy of Sciences of the United States of America*, *101*(10), 3414–3419. https://doi.org/10.1073/pnas.0305892101

Maes, M. B., Scharpé, S., & De Meester, I. (2007). Dipeptidyl peptidase II (DPPII), a review. *Clinica Chimica Acta*, *380*(1–2), 31–49. https://doi.org/10.1016/J.CCA.2007.01.024

Malik, A. R., & Willnow, T. E. (2019). Excitatory amino acid transporters in physiology and disorders of the central nervous system. *International Journal of Molecular Sciences*, *20*(22), 1–37. https://doi.org/10.3390/ijms20225671

Marceau, C. D., Puschnik, A. S., Majzoub, K., Ooi, Y. S., Brewer, S. M., Fuchs, G., Swaminathan, K., Mata, M. A., Elias, J. E., Sarnow, P., & Carette, J. E. (2016). Genetic dissection of Flaviviridae host factors through genome-scale CRISPR screens. *Nature*, *535*(7610), 159–163. https://doi.org/10.1038/nature18631

Markoff, L., Falgout, B., & Chang, A. (1997). A conserved internal hydrophobic domain mediates the stable membrane integration of the dengue virus capsid protein. *Virology*, *233*(1), 105–117. https://doi.org/10.1006/viro.1997.8608

Massé, N., Davidson, A., Ferron, F., Alvarez, K., Jacobs, M., Romette, J. L., Canard, B., & Guillemot, J. C. (2010a). Dengue virus replicons: Production of an interserotypic chimera and cell lines from different species, and establishment of a cell-based fluorescent assay to screen inhibitors, validated by the evaluation of ribavirin's activity. *Antiviral Research*, *86*(3), 296–305. https://doi.org/10.1016/j.antiviral.2010.03.010

Massé, N., Davidson, A., Ferron, F., Alvarez, K., Jacobs, M., Romette, J. L., Canard, B., & Guillemot, J. C. (2010b). Dengue virus replicons: Production of an interserotypic chimera and cell lines from different species, and establishment of a cell-based fluorescent assay to screen inhibitors,

validated by the evaluation of ribavirin's activity. *Antiviral Research*, *86*(3), 296–305. https://doi.org/10.1016/j.antiviral.2010.03.010

Mathieu, C., Dupret, J. M., & Rodrigues Lima, F. (2017). The structure of brain glycogen phosphorylase—from allosteric regulation mechanisms to clinical perspectives. *The FEBS Journal*, *284*(4), 546–554. https://doi.org/10.1111/FEBS.13937

Mccormick, K. D., Liu, S., Jacobs, J. L., Marques, E. T. A., Sluis-Cremer, N., & Wang, T. (2012). Development of a Robust Cytopathic Effect-Based High-Throughput Screening Assay To Identify Novel Inhibitors of Dengue Virus. *Antimicrobial Agents and Chemotherapy*, *56*(6), 3399–3401. https://doi.org/10.1128/AAC.06425-11

Miao, M., Yu, F., Wang, D., Tong, Y., Yang, L., Xu, J., Qiu, Y., Zhou, X., & Zhao, X. (2019). Proteomics Profiling of Host Cell Response via Protein Expression and Phosphorylation upon Dengue Virus Infection. *Virologica Sinica*, *34*(5), 549–562. https://doi.org/10.1007/s12250-019-00131-2

Michalak, M., Corbett, E. F., Mesaeli, N., Nakamura, K., & Opas, M. (1999). Calreticulin: One protein, one gene, many functions. *Biochemical Journal*, *344*(2), 281–292. https://doi.org/10.1042/0264-6021:3440281

Mishra, K. P., Shweta, Diwaker, D., & Ganju, L. (2012). Dengue virus infection induces upregulation of hn RNP-H and PDIA3 for its multiplication in the host cell. *Virus Research*, *163*(2), 573–579. https://doi.org/10.1016/j.virusres.2011.12.010

Missaglia, S., Tavian, D., Moro, L., & Angelini, C. (2018). Characterization of two ETFDH mutations in a novel case of riboflavin-responsive multiple acyl-CoA dehydrogenase deficiency. *Lipids in Health and Disease*, *17*(1), 1–8. https://doi.org/10.1186/s12944-018-0903-5

Montgomery, M. K., Bayliss, J., Nie, S., De Nardo, W., Keenan, S. N., Miotto, P. M., Karimkhanloo, H., Huang, C., Schittenhelm, R. B., Don, A. S., Ryan, A., Williamson, N. A., Ooi, G. J., Brown, W. A., Burton, P. R., Parker, B. L., & Watt, M. J. (2022). Deep proteomic profiling unveils arylsulfatase A as a non-alcoholic steatohepatitis inducible hepatokine and regulator of glycemic control. *Nature Communications 2022 13:1*, *13*(1), 1–18. https://doi.org/10.1038/s41467-022-28889-2

Morchang, A., Lee, R. C. H., Yenchitsomanus, P. T., Sreekanth, G. P., Noisakran, S., Chu, J. J. H., & Limjindaporn, T. (2017). RNAi screen reveals a role of SPHK2 in dengue virus–mediated apoptosis in hepatic cell lines. *PLoS ONE*, *12*(11). https://doi.org/10.1371/JOURNAL.PONE.0188121

Mukhopadhyay, S., Kuhn, R. J., & Rossmann, M. G. (2005). A structural perspective of the Flavivirus life cycle. In *Nature Reviews Microbiology* (Vol. 3, Issue 1, pp. 13–22). Nature Publishing Group. https://doi.org/10.1038/nrmicro1067

Murray, N. E. A., Quam, M. B., & Wilder-Smith, A. (2013). Epidemiology of dengue: Past, present and future prospects. In *Clinical Epidemiology* (Vol. 5, Issue 1, pp. 299–309). https://doi.org/10.2147/CLEP.S34440

Nagampalli, R. S. K., Quesnãy, J. E. N., Adamoski, D., Islam, Z., Birch, J., Sebinelli, H. G., Girard, R. M. B. M., Ascencõ, C. F. R., Fala, A. M., Pauletti, B. A., Consonni, S. R., De Oliveira, J. F., Silva, A. C. T., Franchini, K. G., Leme, A. F. P., Silber, A. M., Ciancaglini, P., Moraes, I., Dias, S. M. G., & Ambrosio, A. L. B. (2018). Human mitochondrial pyruvate carrier 2 as an autonomous membrane transporter. *Scientific Reports*, *8*(1), 1–13. https://doi.org/10.1038/s41598-018-21740-z

Nakamura, S., Matsui, A., Akabane, S., Tamura, Y., Hatano, A., Miyano, Y., Omote, H., Kajikawa, M., Maenaka, K., Moriyama, Y., Endo, T., & Oka, T. (2020). The mitochondrial inner membrane protein LETM1 modulates cristae organization through its LETM domain. *Communications Biology*, *3*(1), 1–11. https://doi.org/10.1038/s42003-020-0832-5

Nanaware, N., Banerjee, A., Bagchi, S. M., Bagchi, P., & Mukherjee, A. (2021). Dengue virus infection: A tale of viral exploitations and host responses. *Viruses*, *13*(10). https://doi.org/10.3390/v13101967

Nasar, S., Rashid, N., & Iftikhar, S. (2020). Dengue proteins with their role in pathogenesis, and strategies for developing an effective anti-dengue treatment: A review. *Journal of Medical Virology*, *92*(8), 941–955. https://doi.org/10.1002/jmv.25646

Neufeldt, C. J., Cortese, M., Acosta, E. G., & Bartenschlager, R. (2018). Rewiring cellular networks by members of the Flaviviridae family. In *Nature Reviews Microbiology* (Vol. 16, Issue 3, pp. 125–142). Nature Publishing Group. https://doi.org/10.1038/nrmicro.2017.170

Ng, C. Y., Gu, F., Phong, W. Y., Chen, Y. L., Lim, S. P., Davidson, A., & Vasudevan, S. G. (2007a). Construction and characterization of a stable subgenomic dengue virus type 2 replicon system for antiviral compound and siRNA testing. *Antiviral Research*, *76*(3), 222–231. https://doi.org/10.1016/j.antiviral.2007.06.007

Ng, C. Y., Gu, F., Phong, W. Y., Chen, Y. L., Lim, S. P., Davidson, A., & Vasudevan, S. G. (2007b). Construction and characterization of a stable subgenomic dengue virus type 2 replicon system for

antiviral compound and siRNA testing. *Antiviral Research*, *76*(3), 222–231. https://doi.org/10.1016/j.antiviral.2007.06.007

Nguyen, M. N., Akter, S., Akhter, H., Ansary, S., Han, S., Shin, Y., Ha, J., Kang, I., Kim, S. S., & Choi, T. G. (2023). TOR1B: a predictor of bone metastasis in breast cancer patients. *Scientific Reports*, *13*(1), 1–10. https://doi.org/10.1038/s41598-023-28140-y

Norazharuddin, H., & Lai, N. S. (2018). Roles and prospects of dengue virus nonstructural proteins as antiviral targets: An easy digest. *Malaysian Journal of Medical Sciences*, *25*(5), 6–15. https://doi.org/10.21315/mjms2018.25.5.2

Okat, Z. (2018). The molecular functions of protein kinase C (PKC) isoforms. *International Physical Medicine & Rehabilitation Journal*, *3*(6), 540–544. https://doi.org/10.15406/ipmrj.2018.03.00161

Pal, V. K., Bandyopadhyay, P., & Singh, A. (2018). Hydrogen Sulfide in Physiology and Pathogenesis of Bacteria and Viruses. *IUBMB Life*, *70*(5), 393. https://doi.org/10.1002/IUB.1740

Palmieri, F. (2013). The mitochondrial transporter family SLC25: Identification, properties and physiopathology. *Molecular Aspects of Medicine*, *34*(2–3), 465–484. https://doi.org/10.1016/j.mam.2012.05.005

Palmieri, F., Scarcia, P., & Monné, M. (2020). Diseases caused by mutations in mitochondrial carrier genes SLC25: A review. In *Biomolecules* (Vol. 10, Issue 4). MDPI AG. https://doi.org/10.3390/biom10040655

Pan, X. Ben, Han, J. C., Cong, X., & Wei, L. (2012). BST2/Tetherin Inhibits Dengue Virus Release from Human Hepatoma Cells. *PLoS ONE*, *7*(12). https://doi.org/10.1371/JOURNAL.PONE.0051033

Pan, P., Zhang, Q., Liu, W., Wang, W., Lao, Z., Zhang, W., Shen, M., Wan, P., Xiao, F., Liu, F., Zhang, W., Tan, Q., Liu, X., Wu, K., Liu, Y., Li, G., & Wu, J. (2019). Dengue Virus M Protein Promotes NLRP3 Inflammasome Activation To Induce Vascular Leakage in Mice. *Journal of Virology*, *93*(21). https://doi.org/10.1128/jvi.00996-19

Pando-Robles, V., Oses-Prieto, J. A., Rodríguez-Gandarilla, M., Meneses-Romero, E., Burlingame, A. L., & Batista, C. V. F. (2014). Quantitative proteomic analysis of Huh-7 cells infected with Dengue virus by label-free LC-MS. *Journal of Proteomics*, *111*, 16–29. https://doi.org/10.1016/j.jprot.2014.06.029

Pastor-Cantizano, N., Montesinos, J. C., Bernat-Silvestre, C., Marcote, M. J., & Aniento, F. (2016). P24 Family Proteins: Key Players in the Regulation of Trafficking Along the Secretory Pathway. In *Protoplasma* (Vol. 253, Issue 4, pp. 967–985). https://doi.org/10.1007/s00709-015-0858-6

Pattanakitsakul, S. N., Rungrojcharoenkit, K., Kanlaya, R., Sinchaikul, S., Noisakran, S., Chen, S. T., Malasit, P., & Thongboonkerd, V. (2007). Proteomic analysis of host responses in HepG2 cells during dengue virus infection. *Journal of Proteome Research*, *6*(12), 4592–4600. https://doi.org/10.1021/pr070366b

Paul, D., & Bartenschlager, R. (2015). Flaviviridae Replication Organelles: Oh, What a Tangled Web We Weave. *Annual Review of Virology*, *2*(1), 289–310. https://doi.org/10.1146/annurev-virology-100114-055007

Perera, N., Miller, J. L., & Zitzmann, N. (2017). The role of the unfolded protein response in dengue virus pathogenesis. *Cellular Microbiology*, *19*(5), 1–9. https://doi.org/10.1111/cmi.12734

Phoolcharoen, W., & Smith, D. R. (2004). Internalization of the dengue virus is cell cycle modulated in HepG2, but not Vero cells. *Journal of Medical Virology*, *74*(3), 434–441. https://doi.org/10.1002/jmv.20195

Płaszczyca, A., Scaturroid, P., Neufeldtid, C. J., Corteseid, M., Cerikan, B., Ferla, S., Brancale, A., Pichlmair, A., & Bartenschlager, R. (2019). A novel interaction between dengue virus nonstructural protein 1 and the NS4A-2K-4B precursor is required for viral RNA replication but not for formation of the membranous replication organelle. *PLoS Pathogens*, *15*(5). https://doi.org/10.1371/journal.ppat.1007736

Ramnarayan, V. R., Hein, Z., Janßen, L., Lis, N., Ghanwat, S., & Springer, S. (2018). Cytomegalovirus gp40/m152 Uses TMED10 as ER Anchor to Retain MHC Class I. *Cell Reports*, *23*(10), 3068–3077. https://doi.org/10.1016/j.celrep.2018.05.017

Reyes-del Valle, J., Salas-Benito, J., Soto-Acosta, R., & del Angel, R. M. (2014). Dengue Virus Cellular Receptors and Tropism. In *Current Tropical Medicine Reports* (Vol. 1, Issue 1, pp. 36–43). https://doi.org/10.1007/s40475-013-0002-7

Rivell, A., Petralia, R. S., Wang, Y. X., Mattson, M. P., & Yao, P. J. (2019). Sideroflexin 3 is a Mitochondrial Protein Enriched in Neurons. *NeuroMolecular Medicine*, *21*(3), 314–321. https://doi.org/10.1007/s12017-019-08553-7

Ropero, S., Setien, F., Espada, J., Fraga, M. F., Herranz, M., Asp, J., Benassi, M. S., Franchi, A., Patiño, A., Ward, L. S., Bovee, J., Cigudosa, J. C., Wim, W., & Esteller, M. (2004). Epigenetic loss of the familial tumor-suppressor gene exostosin-1 (EXT1) disrupts heparan sulfate synthesis in cancer cells. *Human Molecular Genetics*, *13*(22), 2753–2765. https://doi.org/10.1093/hmg/ddh298

Rothwell, C., LeBreton, A., Young Ng, C., Lim, J. Y. H., Liu, W., Vasudevan, S., Labow, M., Gu, F., & Gaither, L. A. (2009). Cholesterol biosynthesis modulation regulates dengue viral replication. *Virology*, *389*(1–2), 8–19. https://doi.org/10.1016/j.virol.2009.03.025

Rötig, A., Parfait, B., Heidet, L., Dujardin, G., Rustin, P., & Munnich, A. (1997). Sequence and structure of the human OXA1L gene and its upstream elements. *Biochimica et Biophysica Acta (BBA) - Molecular Basis of Disease*, *1361*(1), 6–10. https://doi.org/10.1016/S0925-4439(97)00031-8

Ruprecht, J. J., & Kunji, E. R. S. (2020). The SLC25 Mitochondrial Carrier Family: Structure and Mechanism. In *Trends in Biochemical Sciences* (Vol. 45, Issue 3, pp. 244–258). Elsevier Ltd. https://doi.org/10.1016/j.tibs.2019.11.001

Sagong, H. Y., Kim, B., Joo, S., & Kim, K. J. (2020). Structural and Functional Characterization of Cystathionine γ-lyase from Bacillus cereus ATCC 14579. *Journal of Agricultural and Food Chemistry*, *68*(51), 15267–15274. https://doi.org/10.1021/acs.jafc.0c06503

Samsa, M. M., Mondotte, J. A., Iglesias, N. G., Assunção-Miranda, I., Barbosa-Lima, G., Da Poian, A. T., Bozza, P. T., & Gamarnik, A. V. (2009). Dengue virus capsid protein usurps lipid droplets for viral particle formation. *PLoS Pathogens*, *5*(10), e1000632. https://doi.org/10.1371/journal.ppat.1000632

Savidis, G., McDougall, W. M., Meraner, P., Perreira, J. M., Portmann, J. M., Trincucci, G., John, S. P., Aker, A. M., Renzette, N., Robbins, D. R., Guo, Z., Green, S., Kowalik, T. F., & Brass, A. L. (2016). Identification of Zika Virus and Dengue Virus Dependency Factors using Functional Genomics. *Cell Reports*, *16*(1), 232–246. https://doi.org/10.1016/j.celrep.2016.06.028

Schell, J. C., Olson, K. A., Jiang, L., Hawkins, A. J., VanVranken, J. G., Xie, J., Egnatchik, R. A., Earl, E. G., DeBerardinis, R. J., & Rutter, J. (2014). A role for the mitochondrial pyruvate carrier as a repressor of the warburg effect and colon cancer cell growth. *Molecular Cell*, *56*(3), 400–413. https://doi.org/10.1016/j.molcel.2014.09.026

Screaton, G., Mongkolsapaya, J., Yacoub, S., & Roberts, C. (2015). New insights into the immunopathology and control of dengue virus infection. *Nature Reviews Immunology*, *15*(12), 745–759. https://doi.org/10.1038/nri3916

Shah, P. S., Link, N., Jang, G. M., Sharp, P. P., Zhu, T., Swaney, D. L., Johnson, J. R., Von Dollen, J., Ramage, H. R., Satkamp, L., Newton, B., Hüttenhain, R., Petit, M. J., Baum, T., Everitt, A., Laufman, O., Tassetto, M., Shales, M., Stevenson, E., … Krogan, N. J. (2018). Comparative Flavivirus-Host Protein Interaction Mapping Reveals Mechanisms of Dengue and Zika Virus Pathogenesis. *Cell*, *175*(7), 1931-1945.e18. https://doi.org/10.1016/j.cell.2018.11.028

Shahfiza, N., Osman, H., Hock, T. T., & Abdel-Hamid, A.-H. Z. (2017). Metabolomics approach for multibiomarkers determination to investigate dengue virus infection in human patients. *Acta Biochimica Polonica*, *64*(2). https://doi.org/10.18388/abp.2015_1224

Sherman, B. T., Hao, M., Qiu, J., Jiao, X., Baseler, M. W., Lane, H. C., Imamichi, T., & Chang, W. (2022). DAVID: a web server for functional enrichment analysis and functional annotation of gene lists (2021 update). *Nucleic Acids Research*, *50*(W1), W216–W221. https://doi.org/10.1093/NAR/GKAC194

Shirasago, Y., Sekizuka, T., Saito, K., Suzuki, T., Wakita, T., Hanada, K., Kuroda, M., Abe, R., & Fukasawa, M. (2014). Isolation and Characterization of an Huh.7.5.1-Derived Cell Clone Highly Permissive to Hepatitis C Virus. *Jpn. J. Infect. Dis*, *68*, 81–88. https://doi.org/10.7883/yoken.JJID.2014.231

Shue, B., Chiramel, A. I., Cerikan, B., To, T.-H., Frölich, S., Pederson, S. M., Kirby, E. N., Eyre, N. S., Bartenschlager, R. F. W., Best, S. M., & Beard, M. R. (2021). Genome-Wide CRISPR Screen Identifies RACK1 as a Critical Host Factor for Flavivirus Replication. *Journal of Virology*, *95*(24). https://doi.org/10.1128/jvi.00596-21

Six, E., Lagresle-Peyrou, C., Susini, S., De Chappedelaine, C., Sigrist, N., Sadek, H., Chouteau, M., Cagnard, N., Fontenay, M., Hermine, O., Chomienne, C., Reynier, P., Fischer, A., André-Schmutz, I., Ueguen, N., & Cavazzana, M. (2015). AK2 deficiency compromises the mitochondrial energy metabolism required for differentiation of human neutrophil and lymphoid lineages. *Cell Death and Disease*, *6*(8). https://doi.org/10.1038/cddis.2015.211

Song, W., Postoak, J. L., Yang, G., Guo, X., Pua, H. H., Bader, J., Rathmell, J. C., Kobayashi, H., Haase, V. H., Leaptrot, K. L., Schrimpe-Rutledge, A. C., Sherrod, S. D., McLean, J. A., Zhang, J., Wu, L., & Van

Kaer, L. (2023). Lipid kinase PIK3C3 maintains healthy brown and white adipose tissues to prevent metabolic diseases. *Proceedings of the National Academy of Sciences of the United States of America*, *120*(1), e2214874120. https://doi.org/10.1073/pnas.2214874120

Steegborn, C., Clausen, T., Sondermann, P., Jacob, U., Worbs, M., Marinkovic, S., Huber, R., & Wahl, M. C. (1999). Kinetics and inhibition of recombinant human cystathionine γ-lyase: Toward the rational control of transsulfuration. *Journal of Biological Chemistry*, *274*(18), 12675–12684. https://doi.org/10.1074/jbc.274.18.12675

Strating, J. R. P. M., & Martens, G. J. M. (2009). The p24 family and selective transport processes at the ER-Golgi interface. *Biology of the Cell*, *101*(9), 495–509. https://doi.org/10.1042/bc20080233

Strating, J. R. P. M., Van Bakel, N. H. M., Leunissen, J. A. M., & Martens, G. J. M. (2009). A comprehensive overview of the vertebrate p24 family: Identification of a novel tissue-specifically expressed member. *Molecular Biology and Evolution*, *26*(8), 1707–1714. https://doi.org/10.1093/molbev/msp099

Subramanian, K., & Balch, W. E. (2008). NPC1/NPC2 function as a tag team duo to mobilize cholesterol. *Proceedings of the National Academy of Sciences of the United States of America*, *105*(40), 15223–15224. https://doi.org/10.1073/pnas.0808256105

Sun, M. S., Zhang, J., Jiang, L. Q., Pan, Y. X., Tan, J. Y., Yu, F., Guo, L., Yin, L., Shen, C., Shu, H. B., & Liu, Y. (2018). TMED2 Potentiates Cellular IFN Responses to DNA Viruses by Reinforcing MITA Dimerization and Facilitating Its Trafficking. *Cell Reports*, *25*(11), 3086-3098.e3. https://doi.org/10.1016/j.celrep.2018.11.048

Svoboda, P. (2020). Key Mechanistic Principles and Considerations Concerning RNA Interference. *Frontiers in Plant Science*, *11*, 1237. https://doi.org/10.3389/fpls.2020.01237

Swarbrick, C. M. D., Basavannacharya, C., Chan, K. W. K., Chan, S. A., Singh, D., Wei, N., Phoo, W. W., Luo, D., Lescar, J., & Vasudevan, S. G. (2017). NS3 helicase from dengue virus specifically recognizes viral RNA sequence to ensure optimal replication. *Nucleic Acids Research*, *45*(22), 12904. https://doi.org/10.1093/NAR/GKX1127

Szklarczyk, D., Gable, A. L., Lyon, D., Junge, A., Wyder, S., Huerta-Cepas, J., Simonovic, M., Doncheva, N. T., Morris, J. H., Bork, P., Jensen, L. J., & von Mering, C. (2019). STRING v11: protein-protein association networks with increased coverage, supporting functional discovery in genome-

wide experimental datasets. *Nucleic Acids Research*, *47*(D1), D607–D613. https://doi.org/10.1093/NAR/GKY1131

Thomas, S. J. (2023). Is new dengue vaccine efficacy data a relief or cause for concern? *NPJ Vaccines*, *8*(1), 55. https://doi.org/10.1038/s41541-023-00658-2

Tirinato, L., Marafioti, M. G., Pagliari, F., Jansen, J., Aversa, I., Hanley, R., Nisticò, C., Garcia-Calderón, D., Genard, G., Guerreiro, J. F., Costanzo, F. S., & Seco, J. (2021). Lipid droplets and ferritin heavy chain: A devilish liaison in human cancer cell radioresistance. *ELife*, *10*, 1–17. https://doi.org/10.7554/eLife.72943

Tremblay, N., Freppel, W., Sow, A. A., & Chatel-Chaix, L. (2019). The interplay between dengue virus and the human innate immune system: A game of hide and seek. In *Vaccines* (Vol. 7, Issue 4). MDPI AG. https://doi.org/10.3390/vaccines7040145

Tu, Z., Ouyang, Q., Long, X., Wu, L., Li, J., Zhu, X., & Huang, K. (2022). Protein Disulfide-Isomerase A3 Is a Robust Prognostic Biomarker for Cancers and Predicts the Immunotherapy Response Effectively. *Frontiers in Immunology*, *13*(March), 1–16. https://doi.org/10.3389/fimmu.2022.837512

Tyanova, S., Temu, T., Sinitcyn, P., Carlson, A., Hein, M. Y., Geiger, T., Mann, M., & Cox, J. (2016). The Perseus computational platform for comprehensive analysis of (prote)omics data. *Nature Methods 2016 13:9*, *13*(9), 731–740. https://doi.org/10.1038/nmeth.3901

Umareddy, I., Pluquet, O., Wang, Q. Y., Vasudevan, S. G., Chevet, E., & Gu, F. (2007). Dengue virus serotype infection specifies the activation of the unfolded protein response. *Virology Journal*, *4*(1), 1–10. https://doi.org/10.1186/1743-422X-4-91/FIGURES/6

Urbitsch, P., Salzer, M. J., Hirschmann, P., & Vogt, P. H. (2004). Arylsulfatase D Gene in Xp22.3 Encodes Two Protein Isoforms. *Https://Home.Liebertpub.Com/Dna*, *19*(12), 765–773. https://doi.org/10.1089/104454900750058125

Utarini, A., Indriani, C., Ahmad, R. A., Tantowijoyo, W., Arguni, E., Ansari, M. R., Supriyati, E., Wardana, D. S., Meitika, Y., Ernesia, I., Nurhayati, I., Prabowo, E., Andari, B., Green, B. R., Hodgson, L., Cutcher, Z., Rancès, E., Ryan, P. A., O'Neill, S. L., … Simmons, C. P. (2021). Efficacy of Wolbachia-Infected Mosquito Deployments for the Control of Dengue. *New England Journal of Medicine*, *384*(23), 2177–2186. https://doi.org/10.1056/nejmoa2030243

Van Bergen En Henegouwen, P. M. P. (2009). Eps15: A multifunctional adaptor protein regulating intracellular trafficking. *Cell Communication and Signaling*, *7*, 24. https://doi.org/10.1186/1478-811X-7-24

Van Den Elsen, K., Quek, J. P., & Luo, D. (2021). Molecular Insights into the Flavivirus Replication Complex. *Viruses*, *13*(6). https://doi.org/10.3390/V13060956

Vicenti, I., Dragoni, F., Giannini, A., Giammarino, F., Spinicci, M., Saladini, F., Boccuto, A., & Zazzi, M. (2020). Development of a Cell-Based Immunodetection Assay for Simultaneous Screening of Antiviral Compounds Inhibiting Zika and Dengue Virus Replication. *SLAS Discovery*, *25*(5), 506–514. https://doi.org/10.1177/2472555220911456

Walker, T., Johnson, P. H., Moreira, L. A., Iturbe-Ormaetxe, I., Frentiu, F. D., McMeniman, C. J., Leong, Y. S., Dong, Y., Axford, J., Kriesner, P., Lloyd, A. L., Ritchie, S. A., O'Neill, S. L., & Hoffmann, A. A. (2011). The wMel Wolbachia strain blocks dengue and invades caged Aedes aegypti populations. *Nature*, *476*(7361), 450–455. https://doi.org/10.1038/nature10355

Wang, L., Zhou, L., Li, M., Zhao, J., Liu, Y., Chen, Y., Qin, X., Wang, S., Chen, H., Piao, Y., Xiang, R., Li, J., & Shi, Y. (2022). Genome-wide CRISPR/Cas9 knockout screening uncovers ZNF319 as a novel tumor suppressor critical for breast cancer metastasis. *Biochemical and Biophysical Research Communications*, *589*, 107–115. https://doi.org/10.1016/j.bbrc.2021.12.023

Wang, X., Li, H., & Chang, X. (2022). The role and mechanism of TXNDC5 in diseases. *European Journal of Medical Research*, *27*(1), 1–10. https://doi.org/10.1186/s40001-022-00770-4

Wang, Y., Gu, W., Wen, W., & Zhang, X. (2022). SERPINH1 is a Potential Prognostic Biomarker and Correlated With Immune Infiltration: A Pan-Cancer Analysis. *Frontiers in Genetics*, *12*, 756094. https://doi.org/10.3389/FGENE.2021.756094/BIBTEX

Wang, Y., & Zhang, P. (2017). Recent advances in the identification of the host factors involved in dengue virus replication. *Virologica Sinica*, *32*(1), 23–31. https://doi.org/10.1007/s12250-016-3902-6

Weisel, J. W., & Litvinov, R. I. (2017). Fibrin formation, structure and properties. In *Sub-Cellular Biochemistry* (Vol. 82). https://doi.org/10.1007/978-3-319-49674-0_13

Wong, S. S., Haqshenas, G., Gowans, E. J., & MacKenzie, J. (2012). The dengue virus M protein localises to the endoplasmic reticulum and forms oligomers. *FEBS Letters*, *586*(7), 1032–1037. https://doi.org/10.1016/j.febslet.2012.02.047

Wu, M., Heneghan, J. F., Vandorpe, D. H., Escobar, L. I., Wu, B. L., & Alper, S. L. (2016). Extracellular Cl− regulates human SO42−/anion exchanger SLC26A1 by altering pH sensitivity of anion transport. *Pflugers Archiv European Journal of Physiology*, *468*(8), 1311–1332. https://doi.org/10.1007/s00424-016-1823-8

Xu, S., Di, Z., He, Y., Wang, R., Ma, Y., Sun, R., Li, J., Wang, T., Shen, Y., Fang, S., Feng, L., & Shen, Y. (2019). Mesencephalic astrocyte-derived neurotrophic factor (MANF) protects against Aβ toxicity via attenuating Aβ-induced endoplasmic reticulum stress. *Journal of Neuroinflammation*, *16*(1), 1–14. https://doi.org/10.1186/s12974-019-1429-0

Xu, Y. Y., Gu, J. Q., & Zhi, Y. X. (2020). Hereditary angioedema caused by a premature stop codon mutation in the SERPING1 gene. *Clinical and Translational Allergy*, *10*(1), 1–5. https://doi.org/10.1186/s13601-020-00360-9

Yamada, K., Miura, K., Hara, K., Suzuki, M., Nakanishi, K., Kumagai, T., Ishihara, N., Yamada, Y., Kuwano, R., Tsuji, S., & Wakamatsu, N. (2010). A wide spectrum of clinical and brain MRI findings in patients with SLC19A3 mutations. *BMC Medical Genetics*, *11*(1). https://doi.org/10.1186/1471-2350-11-171

Yang, Y., He, J., Zhang, B., Zhang, Z., Jia, G., Liu, S., Wu, T., He, X., & Wang, N. (2021). SLC25A1 promotes tumor growth and survival by reprogramming energy metabolism in colorectal cancer. *Cell Death and Disease*, *12*(12), 1–9. https://doi.org/10.1038/s41419-021-04411-2

Yousuf, A. (2016). 'High-throughput quantitative proteomic analysis of host proteins interacting with dengue virus replication complex.' PhD Thesis, University of Bristol. Bristol.

Zanini, F., Pu, S. Y., Bekerman, E., Einav, S., & Quake, S. R. (2018). Single-cell transcriptional dynamics of flavivirus infection. *ELife*, *7*. https://doi.org/10.7554/eLife.32942

Zeng, Z., Shi, J., Guo, X., Mo, L., Hu, N., Sun, J., Wu, M., Zhou, H., & Hu, Y. (2018). Full-length genome and molecular characterization of dengue virus serotype 2 isolated from an imported patient from Myanmar. *Virology Journal*, *15*(1), 131. https://doi.org/10.1186/s12985-018-1043-2

Zhang, H., & Lui, R. (2020). Releasing Wolbachia-infected Aedes aegypti to prevent the spread of dengue virus: A mathematical study. *Infectious Disease Modelling*, *5*, 142–160. https://doi.org/10.1016/j.idm.2019.12.004

Zhang, Q., Hunke, C., Yau, Y. H., Seow, V., Lee, S., Tanner, L. B., Guan, X. L., Wenk, M. R., Fibriansah, G., Chew, P. L., Kukkaro, P., Biuković, G., Shi, P. Y., Shochat, S. G., Grüber, G., & Lok, S. M. (2012). The stem region of premembrane protein plays an important role in the virus surface protein rearrangement during dengue maturation. *Journal of Biological Chemistry*, *287*(48), 40525–40534. https://doi.org/10.1074/jbc.M112.384446

Zhang, W., Wearsch, P. A., Zhu, Y., Leonhardt, R. M., & Cresswell, P. (2011). A role for UDP-glucose glycoprotein glucosyltransferase in expression and quality control of MHC class I molecules. *Proceedings of the National Academy of Sciences of the United States of America*, *108*(12), 4956–4961. https://doi.org/10.1073/pnas.1102527108

Zhou, J., Chen, W. R., Yang, L. C., Wang, J., Sun, J. Y., Zhang, W. W., He, Z. Y., & Wu, S. G. (2019). KIF11 functions as an oncogene and is associated with poor outcomes from breast cancer. *Cancer Research and Treatment*, *51*(3), 1207–1221. https://doi.org/10.4143/crt.2018.460

Zsurka, G., Gregǎ, J., & Schweyen, R. J. (2001). The Human Mitochondrial Mrs2 Protein Functionally Substitutes for Its Yeast Homologue, A Candidate Magnesium Transporter. *Genomics*, *72*(2), 158–168. https://doi.org/10.1006/GENO.2000.6407